ANALYSIS OF PROPELLANT FEEDLINE DYNAMICS

by

J. L. Holster

W. J. Astleford

C. R. Gerlach

FINAL REPORT

Contract No. NAS8-25919

Control No. DCN 1-1-75-10051 (1F)

SwRI Project No. 02-2889

Prepared for

National Aeronautics and Space Administration

George C. Marshall Space Flight Center

Marshall Space Flight Center, Alabama 35812

May 1973

SOUTHWEST RESEARCH INSTITUTE

SAN ANTONIO   CORPUS CHRISTI   HOUSTON

SOUTHWEST RESEARCH INSTITUTE
Post Office Drawer 28510, 8500 Culebra Road
San Antonio, Texas 78284

ANALYSIS OF PROPELLANT FEEDLINE DYNAMICS
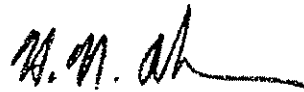
by

J. L. Holster

W. J. Astleford

C. R. Gerlach

FINAL REPORT

Contract No. NAS8-25919

Control No. DCN 1-1-75-10051 (1F)

SwRI Project No. 02-2889

Prepared for

National Aeronautics and Space Administration

George C. Marshall Space Flight Center

Marshall Space Flight Center, Alabama 35812

May 1973

Approved:

H. Norman Abramson

Technical Vice-President

FOREWORD

This report summarizes all work performed by Southwest Research Institute during the past two years, under Contract No. NAS8-25919, "Analysis of Propellant Feedline Dynamics." This study was performed for the George C. Marshall Space Flight Center of the National Aeronautics and Space Administration, and was administered technically by Messrs. Larry Kiefling and Gary Muller of the Aero-Astrodynamics Laboratory.

ACKNOWLEDGMENTS

TABLE OF CONTENTS

Table of Contents (Cont'd) -   <u>Page</u>

LIST OF SYMBOLS

A =   cross-sectional area

A_b =   cross-sectional area of the side branch

A_x =   Laplace transform of the axial acceleration

A_o =   Orifice area

$a_i(s)$ =   Laplace transform of the applied structural acceleration

$a_\ell(s)$ =   Laplace transform of the resultant line acceleration

$\underline{B}_j$ =   column matrix of one of the $\underline{C}_i$ matrices premultiplied by one or more $\underline{D}$ matrices

b =   coefficient of damping

b_{ij} =   elements of matrix $\underline{B}_j$

C =   compliance of a fluid element; also a constant

$\underline{C}_i$ =   column matrix, present only if the particular line component·is externally excited

C_p =   specific heat at constant pressure

c =   phase velocity corrected for wall elasticity effects

c_g =   speed of sound in a pure gas

c_ℓ =   speed of sound in a pure liquid

c_o =   speed of sound in the fluid medium

c_w =   speed of sound in the feedline wall

$\underline{D}$ = 2×2 square matrix characteristic of each line element

D_1 =   thermal diffusivity of the entrained gas·

D_n =   damping number

d =   line diameter

d_b =   side branch diameter

d_{ij} =   elements of the matrix $\underline{D}$

E_t =   elastic modulus

$F; F_x$ =   externally applied forces; body force

$F(\rho V_x^2, G)$ =   loss factor due to bellows or PVC joint

$$f = \frac{2J_1(\xi r_o)}{\xi r_o J_o(\xi r_o)} \; ; \; \text{also used as excitation frequency}$$

f_o	=	resonant frequency
G	=	bellows geometry factor
G(s)	=	lag caused by PVC joint; also transfer function relating structural velocities at each end of a line
g_o	=	acceleration due to gravity
h	=	feedline wall thickness
I	=	line inertance, $\rho_o L/A$
J_o, J_1	=	zero and first order Bessel functions of the first kind
K	=	Laplace transform of an external forcing function
K_b	=	volume change constant for a bellows
K_c	=	PVC volume compensation constant
k	=	spring constant; also bubble stiffness term, $\gamma P_o/V_o$
k_d	=	orifice discharge coefficient
L	=	length of a line element
L_{ij}	=	elements of the matrix for an accelerated line
M	=	mass
MW	=	gas molecular weight
M_g	=	mass of the gas
M_ℓ	=	mass of the liquid
m_2	=	equivalent mass term, $\rho_\ell/4\pi R_o$
N_R	=	Reynolds number
P(s)	=	Laplace transform of p(t), often written as P
P_o, p_o	=	mean pressures
P_t	=	terminal pressure perturbation amplitude
p(t)	=	perturbation pressure, often written as p
Q_d	=	side branch pulser flow perturbation amplitude
Q(s)	=	Laplace transform of the volume flow, q(t)
q(t)	=	volume flow perturbation, often written as q
R	=	resistance; also gas constant
R_o	=	mean radius of a gas bubble
r	=	radial coordinate, measured from centerline
r_o	=	line internal radius

s	=	Laplace variable, $\sqrt{-1}\,\omega$; also entropy
T	=	temperature
TDT	=	turbulent dissipation terms
t	=	time
U	=	$V + \dfrac{1}{\rho_o s}\,\dfrac{\partial \bar{P}}{\partial x}$
V_g	=	volume of the gas
V_ℓ	=	volume of the liquid
V_o	=	steady state or mean bubble volume, also written as V_{BUB}
$Vol(s)$	=	apparent volume production (in Laplace domain)
V_x	=	Laplace transform of v_x
v	=	amplitude of bubble volume pulsations; also specific volume
$\bar{v}$	=	dynamic velocity perturbation
v_B	=	relative bubble velocity
v_{BR}	=	bubble rate of rise
v_f	=	specific volume of the liquid
v_g	=	specific volume of the gas
v_o	=	mean velocity component
v_r	=	radial velocity component
v_t	=	turbulent velocity component
v_x	=	perturbation velocity component in the axial direction
W_g	=	measured gas weight flow
X	=	Laplace transform of the axial displacement
X_o	=	actuator stroke
x	=	axial coordinate
Y	=	Laplace transform of $y\,(x,t)$
y	=	axial displacement of a point in the wall
Z_c	=	characteristic impedance
Z_{c2}	=	characteristic impedance of the horizontal line segment 1 to 2 of Figure 19.

Z_i = impedance at the tank outlet

Z_s = structural impedance

Z_t = terminal impedance of the line

α = spatial attenuation factor; also volume ratio

β = separation constant

Γ_c = turbulent attenuation contribution to the propagation operator for a line of length L.

Γ_L = laminar propagation operator for a line of length L

Γ_{L_i} = imaginary part of the laminar propagation operator for a line of length L

Γ_{L_r} = real part of the laminar propagation operator for a line of length L

Γ_t = turbulent propagation operator for a line of length L

γ = propagation operator; also ratio of specific heats for a gas

γ_{lam} = laminar propagation operator

γ_r = spatial attenuation factor

δ = damping constant

ζ_{cn} = constants in rational approximate model, n=0, 1, 2, ...

ζ_{sn} = constants in rational approximate model, n=0, 1, 2, ...

η = polytropic exponent

$\varkappa$ = liquid bulk modulus

λ = separation constant

μ = dynamic viscosity

ξ = $\sqrt{-s/\nu}$

ν = kinematic viscosity

ρ = density of the fluid medium

ρ_g = density of the gas

ρ_ℓ = density of the liquid

ρ_o = mean density (steady state value)

ρ_t = density of feedline wall material

τ = time constant

Φ = mass ratio, mass of gas/mass of liquid

ϕ = phase angle

χ = mixture quality

Ω = dimensionless frequency

ω = angular frequency, radian/sec

ω_{cn} = constant in rational approximate model, n = 0, 1, 2, ...

ω_{o} = natural frequency, radian/sec

ω_{sn} = constant in rational approximate model, n = 0, 1, 2, ...

LIST OF FIGURES

LIST OF FIGURES (Cont'd.)

xiii

xiv

LIST OF FIGURES (Cont'd.)

I. INTRODUCTION

I. 1.   Background and Objectives

At least three classes of feed system instabilities have been identified for liquid propellant rockets [1,2,3,4]*. In each case, the dynamic behavior of the feed line plays a major role in the instability. Probably the best known problem[1,2] involves a closed-loop coupling of the vehicle longitudinal structural modes, the feed system and the engine. A second problem[3] showed up on Saturn flight AS-504 when the S-II center engine displayed severe pressure and thrust oscillations rather late in the stage burn. In this case, the problem was localized, involving a closed-loop instability of the engine support structure, the feed system, and the engine. A third type of problem which can exist[4] involves only the feed system, the inducer-pump combination and the engine. This instability is traceable directly to the inducer dynamics, with the feed system and engine providing an impedance loading which governs the resultant oscillation frequency.

All of the above instabilities pose a threat to the success of a mission. For simulation purposes, it is readily recognized that adequate modeling procedures are needed for each portion of the vehicle involved in a given instability. The objective of this study was to develop an analytical method, and its corresponding computer program, to allow the study of disturbances of liquid propellants in typical engine feedline systems. This method was to include (1) the effect of steady flow, (2) the influence of distributed compliances and axial wall stiffness, (3) the effects of local compliances, such as vapor bubbles, and (4) various factors causing coupled responses between the line and structure, i. e. , bends, mounting stiffness, forced changes in line length, and bellows and PVC couplings.

An additional objective of this program was to construct a basic test apparatus to simulate a feedline system, consisting of an upper reservoir, a feedline, a terminational resistance (impedance), a lower reservoir, and a circulation pump; this test facility was to be used to experimentally verify many of the various effects discussed above on the frequency response of a feedline. In general, the experimental program was to provide a check-out or verification of the analytical model and computer program.

---

* Superscript numbers in the text refer to References presented on page 148 of this report.

In all respects, this objective has been satisfied. This report summarizes the modeling results for each item defined above, and presents a generalized computer program which allows the user to easily determine dynamic performance of a line containing any number of elemental components. Use of this computer program is illustrated by way of a detailed set of instructions contained in Appendix D, plus a presentation of several example problems.

I. 2.   General Feedline Problem

The problem of modeling a given feedline can best be illustrated by an example. Figure 1 shows a hypothetical case involving a propellant tank, a feedline, a pump and an engine. In general, each element of the model is elastically supported and can experience some motion relative to a frame of reference on the vehicle. These accelerations, plus pressure oscillations in the engine combustion chamber and cavitating inducer instabilities, represent disturbance inputs to the feed system which can cause flow and pressure oscillations. These flow disturbances may, in turn, couple back with the engine and/or structure to produce a large amplitude, closed-loop instability. The modeling problem, with respect to the feed system, is to describe analytically the dynamic pressure and flow at an arbitrary point in the system, with proper treatment of the end conditions, the acceleration inputs and the flexible supports.

Generally, a feedline may be regarded as a series of elements, such as lengths of line, bends, bellows PVC coupling, etc. Therefore, it is necessary to describe each element individually, and then define means for mathematically combining these elements so as to produce the proper overall system mode. In this report, each element is basically defined by a four-terminal representation in the Laplace domain. Overall system model formulation is also achieved in the Laplace or operator domain. Where problem solution is required only in the frequency domain, this Laplace formulation is the one to use, and the present computer program is set up on this basis. For problem solution in the time domain, the Laplace operator formulation must be converted to an equivalent time domain formulation (rational approximate model). The procedure for accomplishing this conversion is described herein.

2

- a_1, a_2, a_3 are axial accelerations
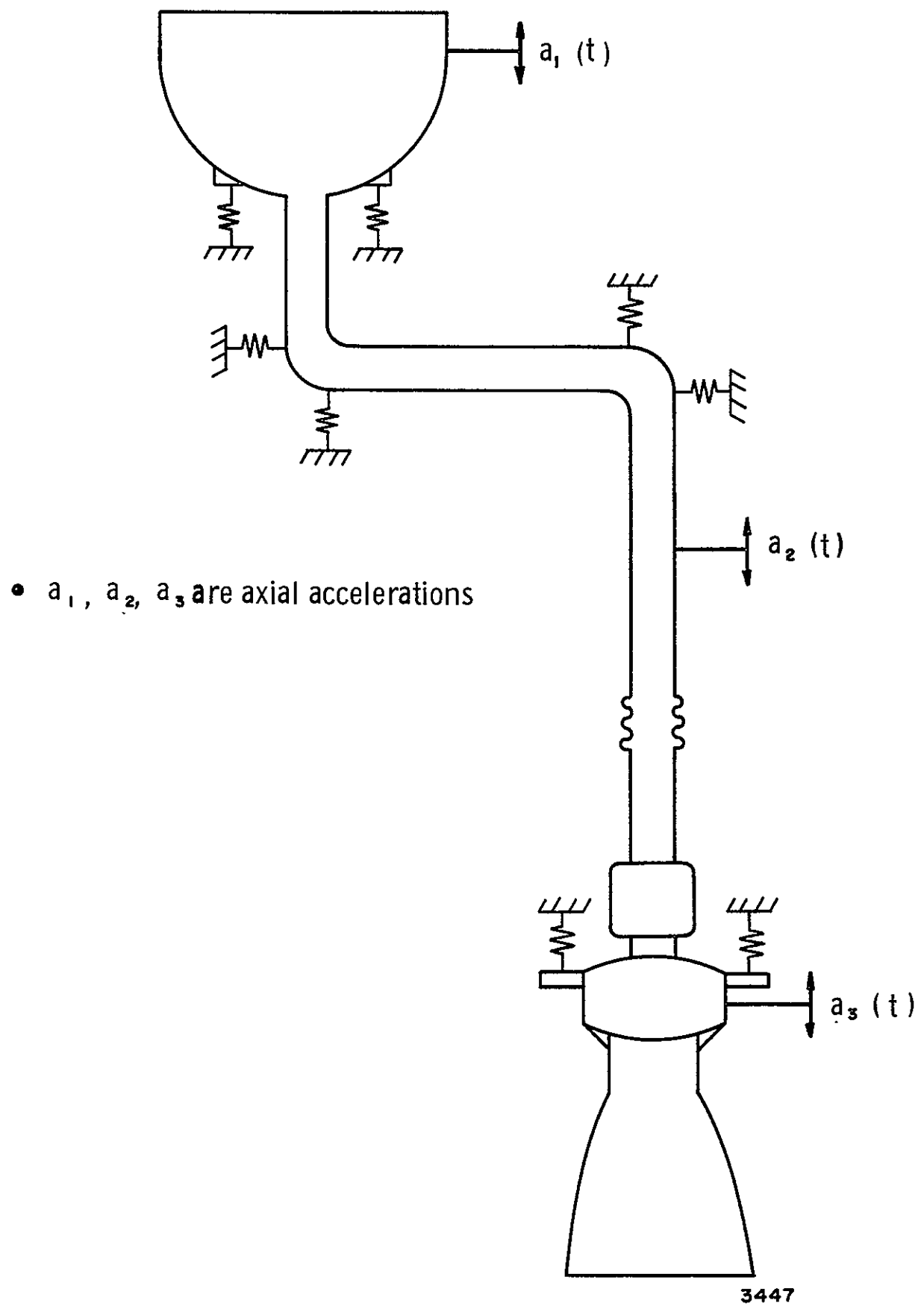
Figure 1. Hypothetical Feed System And Engine

3

II. GENERAL LINE MODEL WITH MEAN FLOW

II. 1.   Physical Picture and Requirements

An illustration of the physical picture of the flow behavior in a feedline is given in Figure 2. For the present, only the fluid dynamic effects in a line, assumed cylindrical, straight, and with infinitely stiff walls, will be considered.

The line shown in Figure 2 is assumed to contain a turbulently flowing viscous liquid. The mean vector velocity is represented by $\bar{v}_0$, which contains only the axial component, $v_0(r)$. Superimposed on this mean flow are two dynamic velocity perturbation quantities, $\bar{v}$ and $\bar{v}_t$. The velocity component $\bar{v}$ represents the dynamic velocity perturbation of interest, and $\bar{v}_t$ represents the turbulent velocity fluctuations. Similarly, the total pressure is the sum of a mean quantity, p_0, a dynamic-perturbation part, p, and a turbulent part, p_t.

By substitution of the assumed summation forms for velocity into the Navier-Stokes equations[5], and short-time averaging of the turbulence quantities, the following form results:

$$\frac{\partial \bar{v}}{\partial t} + v_0 \frac{\partial \bar{v}}{\partial x} = -\frac{\nabla p}{\rho_0} + \nu \left\{ \frac{4}{3} \nabla(\nabla \cdot \bar{v}) - \nabla \times (\nabla \times \bar{v}) \right\} + \text{TDT} \tag{1}$$

In addition, we may complete our description of the dynamic fluid behavior with a continuity equation:

$$\frac{\partial \rho}{\partial t} + \rho_0 \nabla \cdot \bar{v} + v_0 \frac{\partial \rho}{\partial x} = 0 \tag{2}$$

and a liquid equation of state:

$$dp = \varkappa \frac{d\rho}{\rho_0} \tag{3}$$

Equation (1) is a first-order form of the Navier-Stokes equations, including turbulent dissipation terms (TDT). Similarly, Equation (2) is a first-order continuity expression relating the dynamic velocity perturbation to density perturbations (ρ_0 is the mean density).

Examination of Equations (1) and (2) shows that the presence of a mean turbulent flow has two possible effects. First, the
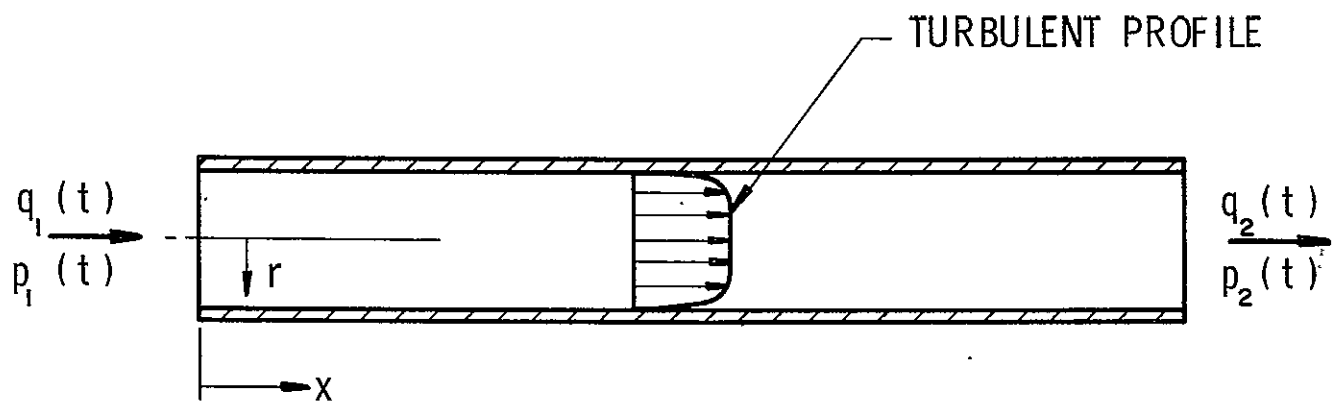
$$\overline{V}_T(r,x,t) \equiv \text{vector total velocity}$$

$$\overline{V}_T = \overline{V}_0 + \overline{V} + \overline{V}_t$$

$\overline{V}_0 = $ time invariant mean flow

$\overline{V} = $ dynamic perturbation of interest

$\overline{V}_t = $ turbulent fluctuations

$$P_T = P_0 + P + P_t$$

2747

Figure 2. General Physical Picture Of Flow Behavior In Feed Line

turbulent dissipation terms introduce damping in addition to the conventional "laminar" damping accounted for by the terms in brackets on the right side of Equation (1). Second, the mean flow introduces a "convective" effect represented by the terms $v_o\, \partial\bar{v}/\partial x$ and $v_o\, \partial\rho/\partial x$ in Equations (1) and (2) respectively.

The requirements for a dynamic feedline model with a mean flow are that (1) the attenuation effects of the turbulent flow be properly treated and (2) the possible convective influences be examined and included if necessary. The following sections treat these two topics. In general, the feedline model presented will be an extension of an existing distributed parameter model which exactly accounts for laminar viscous effects, but negligible mean flow. This existing model, which is discussed in References 5 and 6, may be given in the following form:

$$P_2(s) = P_1(s)\ \cosh \gamma L - Z_c A^{-1} Q_1(s)\ \sinh \gamma L$$

$$Q_2(s) = Q_1(s)\ \cosh \gamma L - Z_c^{-1} A P_1(s)\ \sinh \gamma L \tag{4}$$

The laminar propagation operator takes the familiar form

$$\gamma_{lam} = \frac{s}{c} \left[1 - \frac{2 J_1(\xi r_o)}{\xi r_o J_o(\xi r_o)} \right]^{-\frac{1}{2}} \tag{5}$$

where c is the phase velocity in the fluid, J_o and J_1 are zero and first-order Bessel functions of the <u>first</u> kind and

$$\xi^2 = -s/\nu \tag{6}$$

The characteristic impedance is related to the propagation operator by

$$Z_c = \rho_o c_o^2\ \gamma/s \tag{7}$$

The magnitude of the additional attenuation due to turbulence is a function of the Reynold's number and the frequency range of interest; this aspect is discussed in Section II. 3. The relationship between mean flow velocity and the adiabatic speed of sound dictates the phase velocity to be used in Equation (5). Section II. 2 discusses the effect of mean flow convection.

II. 2   Possible Convective Influences

As indicated previously, the terms $v_o \, \partial \overline{v} / \partial x$ and $v_o \, \partial \rho / \partial x$ in Equations (1) and (2), respectively, represent the convective effect of the mean flow v_o. The question to be answered at this point is: Are these terms of enough significance to be retained in the final model? Ideally we would like to retain the convective terms at all times, but, from a practical standpoint, they increase considerably the complexity of the final solution.

To judge the importance of the convective terms, it is convenient to consider a nondissipative, one-dimensional form of Equations (1) and (2) or

$$\frac{\partial v_x}{\partial t} + v_o \frac{\partial v_x}{\partial x} = -\frac{1}{\rho_o} \frac{\partial p}{\partial x} \tag{8}$$

and

$$\frac{\partial \rho}{\partial t} + \rho_o \frac{\partial v_x}{\partial x} + v_o \frac{\partial \rho}{\partial x} = 0 \tag{9}$$

Transformation of Equations (3), (8), and (9) into the Laplace domain, and the subsequent elimination of ρ and P, yields one equation in V_x (V_x is the transform of v_x), or

$$(c_o^2 - v_o^2) \frac{d^2 V_x}{dx^2} - 2s \, v_o \frac{dV_x}{dx} - s^2 V_x = 0 \tag{10}$$

where

$$s \qquad\qquad = \text{Laplace variable}$$
$$c_o = (\varkappa / \rho_o)^{\frac{1}{2}} \quad = \text{isentropic speed of sound}$$
$$v_o \qquad\qquad = \text{axial mean flow velocity}$$

Assuming a solution for Equation (10) of the form

$$V_x = Ce^{\gamma x} \tag{11}$$

we find the characteristic equation to be

$$(c_o^2 - v_o^2) \, \gamma^2 - 2s \, v_o \gamma - s^2 = 0 \tag{12}$$

whose roots or values for γ are

$$\gamma = \left(\frac{sv_0}{c^{*2}}\right) \pm \left\{\frac{s^2 v_0^2}{c^{*4}} + \frac{s^2}{c^{*2}}\right\}^{\frac{1}{2}}$$

$$\gamma = \left(\frac{sv_0}{c^{*2}}\right) \left\{1 \pm \left[1 + \frac{c^{*2}}{v_0^2}\right]^{\frac{1}{2}}\right\} \qquad (13)$$

where $c^{*2} = c_0^2 - v_0^2$. The plus sign applies to waves traveling in the retrograde direction, and the negative sign to waves traveling in the mean flow direction.

From these results, it is found that for propagation in the +x direction, with the mean flow, the phase velocity is greater than c_0. To demonstrate this result, recall that the propagation operator is functionally equivalent to the Laplace variable divided by a velocity quantity. Substituting the equivalent expression for c^* into Equation (13), the following result is obtained:

$$\gamma = \frac{s(v_0 \pm c_0)}{(v_0 + c_0)(v_0 - c_0)} \qquad (14)$$

For propagation in the mean flow direction,

$$\gamma_{+x} = \frac{s}{c_0 + v_0} \qquad (15)$$

Therefore, the phase velocity for downstream propagation is greater than the adiabatic speed of sound. Similar reasoning verifies that the phase velocity for retrograde propagation is less than the adiabatic speed of sound.

It is important to point out that for normal conditions of liquid propellants flowing in a feedline at velocities up to, say, 50 fps, the phase velocity with mean flow is so minutely changed that this convective effect may be neglected. The reason for this is that the mean velocity is much smaller than the liquid sonic velocity, c_0. The only condition under which this might change would be where sufficient entrained gas is present in the fluid to cause the new effective c_0 value to be, say, an order of magnitude lower than for the pure liquid. Then the convective effect should be included. For example (see Section III. 1), if the level of entrained gas were to approach 0.1 percent by weight of the total liquid mass, then the equivalent speed of sound of the mixture would be approximately 100 fps. In this case, the speed of sound is only twice as large as the maximum mean flow velocity, and the phase velocity would be

8

100 ± 50 fps, depending on the propagation direction. This example, however, is unrealistic because the gas concentration rarely approaches a level where the mean flow velocity is but a small fraction of the mixture speed of sound. Therefore, for all practical purposes, the phase velocity can be taken to be the adiabatic speed of sound.

II. 3   Effect of Turbulence on Damping and Phase Velocity

It is known that the four terminal Laplace domain representation for pressure and flow in a line is extremely accurate when the flow is laminar and the propagation operator is of the following form:

$$\Gamma_L = \left(\frac{sL}{c_o}\right) \left[1 - \frac{2 J_1(\xi r_o)}{\xi r_o J_o(\xi r_o)}\right]^{-\frac{1}{2}} = \gamma_{lam} \, L \qquad (16)$$

In reality, a turbulent flow condition exists for many propellant feed-line operating points, as indicated by Reynold's numbers of the order of 10^5 to 5×10^7. Therefore, the effect of turbulence must be reflected in the propagation operator. As shown in Figures 3 and 4 (from Reference 7), the predominant effect of turbulence is to increase the spatial attenuation at low frequencies. At high frequencies, the laminar and turbulent attenuations coincide. There is some tendency for turbulence to reduce the phase velocity at very low frequencies and high Reynold's numbers. However, after a thorough investigation into existing feedline geometries, propellant properties, mean flow velocities and frequency range for structural-hydraulic coupling, it was concluded that the effect of turbulence on the phase velocity could be neglected.

For the exact distributed parameter line model, the effect of turbulent attenuation was modeled by adding to the existing laminar propagation operator, Γ_L, an additional attenuation contribution, Γ_c, due to turbulence.

$$\Gamma_t = \Gamma_L + \Gamma_c = (\Gamma_{Lr} + \Gamma_c) + i\Gamma_{Li} \qquad (17)$$

The form of turbulence induced increment in attenuation was derived from the form of the attenuation factor of a constant I-R-C, lumped parameter, representation of a line. That is,

$$\Gamma_c = s\sqrt{CI}\,(R/Is + 1)^{\frac{1}{2}} L \qquad (18)$$

9
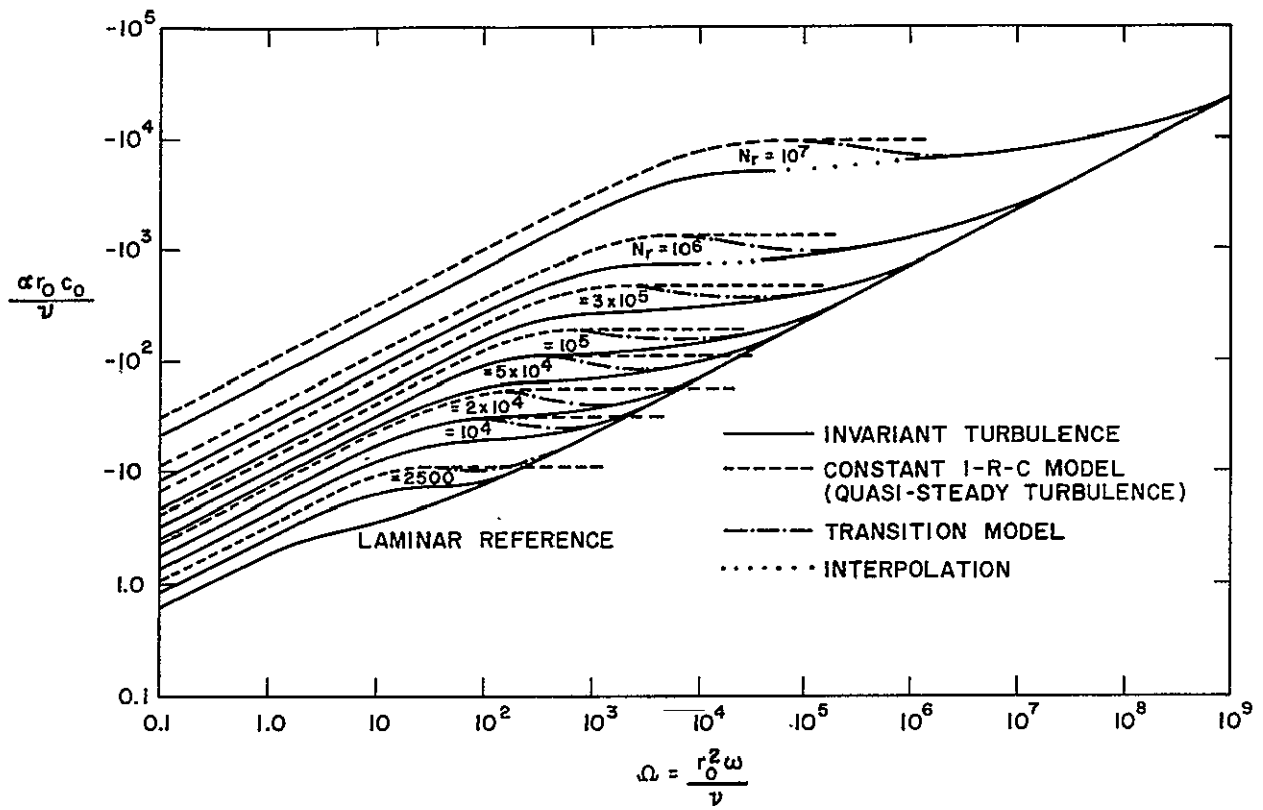
Figure 3. Predictions of Attenuation Factor for Turbulent Flow (Reference 7)
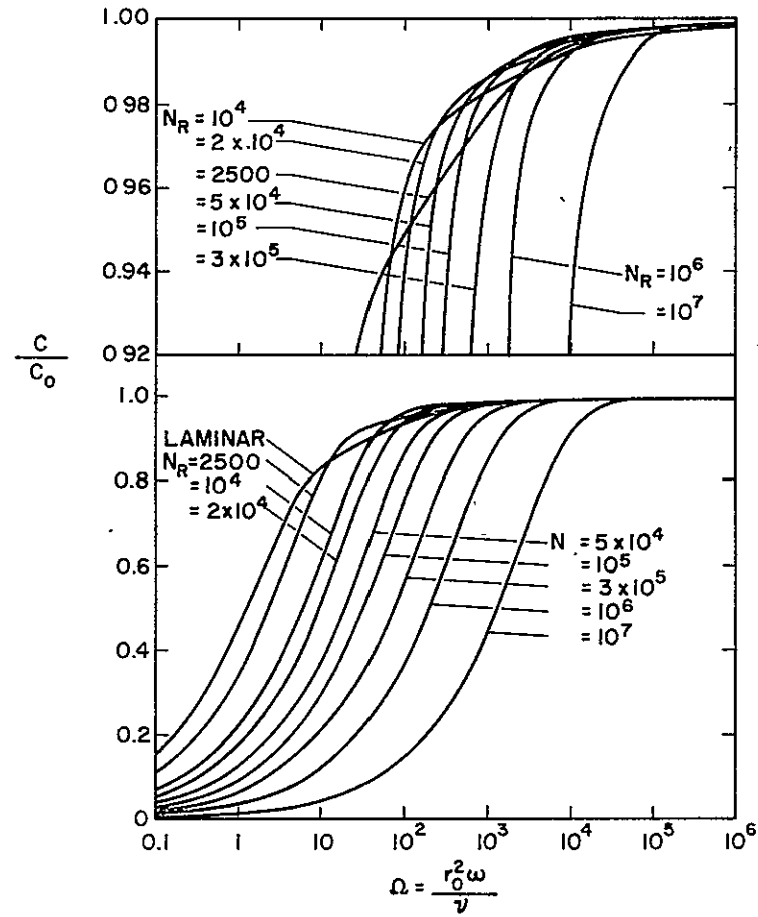
Figure 4. Predicted Phase Velocity with Turbulent
Flow (Reference 7)

By analogy,

$$\Gamma_c = \text{Re} \left[\frac{sL}{c_0} \left(\frac{R_t}{s} + 1 \right)^{\frac{1}{2}} \right] \tag{19}$$

where

$$R_t = \frac{2 \nu K \, N_R{}^n}{r_0{}^2} \tag{20}$$

The constants, K and n, were determined by surface fitting the turbulent attenuation increment in Figure 3 as a function of Reynold's number and frequency. The derived values of these constants are:

$$K = 0.0055$$
$$n = 0.85$$

III. DISTRIBUTED COMPLIANCES

III. 1 Distributed Bubbles

In most practical applications, the liquid rocket propellant in the feedline will contain quantities of either dissolved ullage gas or propellant vapor, or possibly both. It is assumed that the gases or vapor are in the form of small bubbles, homogeneously distributed throughout the liquid. The net effect of distributed bubbles in the liquid is to modify (reduce) the effective fluid sonic velocity and possibly to introduce added damping because of irreversible compression and expansion of the bubbles caused by a periodic disturbance.

Two types of entrained gases have been considered in the model for the acoustic velocity in a two-phase flow:

(1) The flow of a single-component, two-phase mixture, such as LOX and oxygen vapor, and

(2) The flow of a two-component, two-phase mixture, such as LOX with entrained helium ullage gas.

For a single-component, two-phase mixture, the actual flow process is theoretically bounded by the equilibrium process and the constant quality process. In the case of an equilibrium process, the vaporization and condensation rates are large enough to ensure that the vapor temperature and liquid temperature are always equal; both phases are saturated, and the quality (vapor fraction by weight) varies only with pressure. Based on the assumption of thermodynamic equilibrium, Gouse and Brown[8] have shown that the speed of sound in a single-component, two-phase flow can be expressed as

$$c_0 = \left(\frac{v_f}{v_g - v_f} + \chi \right) (S_g - S_f) \left[g_0 \left(\frac{\Delta T}{\Delta S} \right)_v \right]^{\frac{1}{2}} \tag{21}$$

where χ is the mixture quality and $(S_g - S_f)$ is the change in entropy between the saturated vapor and the saturated liquid state. Evaluation of Equation (21) requires the extensive use of a temperature-entropy chart or a tabular representation of the thermodynamic properties of the fluid being considered.

On the other hand, the condensation and vaporization rates in a constant quality process are assumed to be so low that no significant

13

phase change occurs. In a two-component mixture, a constant quality exists at all times if there is no liquid vapor present. Rearranging the derivation by Hsieh and Plesset[9], the speed of sound in a two-component mixture is

$$\frac{1}{c_o^2} = \rho \left\{ \left(\frac{\rho_g}{\rho_g + \Phi \rho_\ell} \right) \frac{1}{\rho_\ell} \frac{1}{c_\ell^2} + \left(\frac{\Phi \rho_\ell}{\rho_g + \Phi \rho_\ell} \right) \frac{1}{\rho_g} \frac{1}{c_g^2} \right\} \tag{22}$$

where

ρ = mixture density

ρ_g = gas density

ρ_ℓ = liquid density

c_ℓ = speed of sound in the liquid

c_g = speed of sound in the gas

and Φ = mass gas/mass liquid.

As the mass ratio, Φ, approaches zero, the speed of sound approaches that for the pure liquid. Plesset and Hsieh[10] have also shown that, for very small gas bubbles dissolved in a liquid, the adiabatic speed of sound in the gas should be replaced by the isothermal speed of sound. The reason is that the gas bubbles have a non-uniform temperature distribution in their interior due to the finite value of the heat conduction rate. Figure 5 presents the isothermal versus the adiabatic model for dissolved helium ullage gas in LOX. For comparison, the equilibrium model for LOX with O_2 vapor is also shown. Reliable experimental data are not available to determine which flow process actually occurs for the flow of a single-component, two-phase mixture. As can be seen by Figure 5, there is a great difference in the acoustic velocity between the equilibrium and the constant quality flow processes. These differences could lead to a large error in the predicted feedline system response, and more work should be devoted to a study of the actual flow process. In the present study, the constant quality model is applied to both single-component and two-component flows. A more detailed discussion of the acoustic velocity in two-phase flow is presented in Appendix B.

The wave propagation characteristics of the mixture depend not only on the gas-to-liquid mass ratio but also on the bubble size and disturbance frequency. Bubbles of a given size resonate when excited at their natural frequency; this natural or resonant frequency

14

$$\Phi = \frac{\text{Mass Of Gas}}{\text{Mass Of Liquid}}$$

Isentropic LOX & He

Isothermal LOX & He

P = 16 psia,
T = 163.4°R

Single Component
Equilibrum Mixture Of
LOX & O_2 Vapor

Speed Of Sound , C_o, ft./sec.

Mass Ratio , Φ

3439
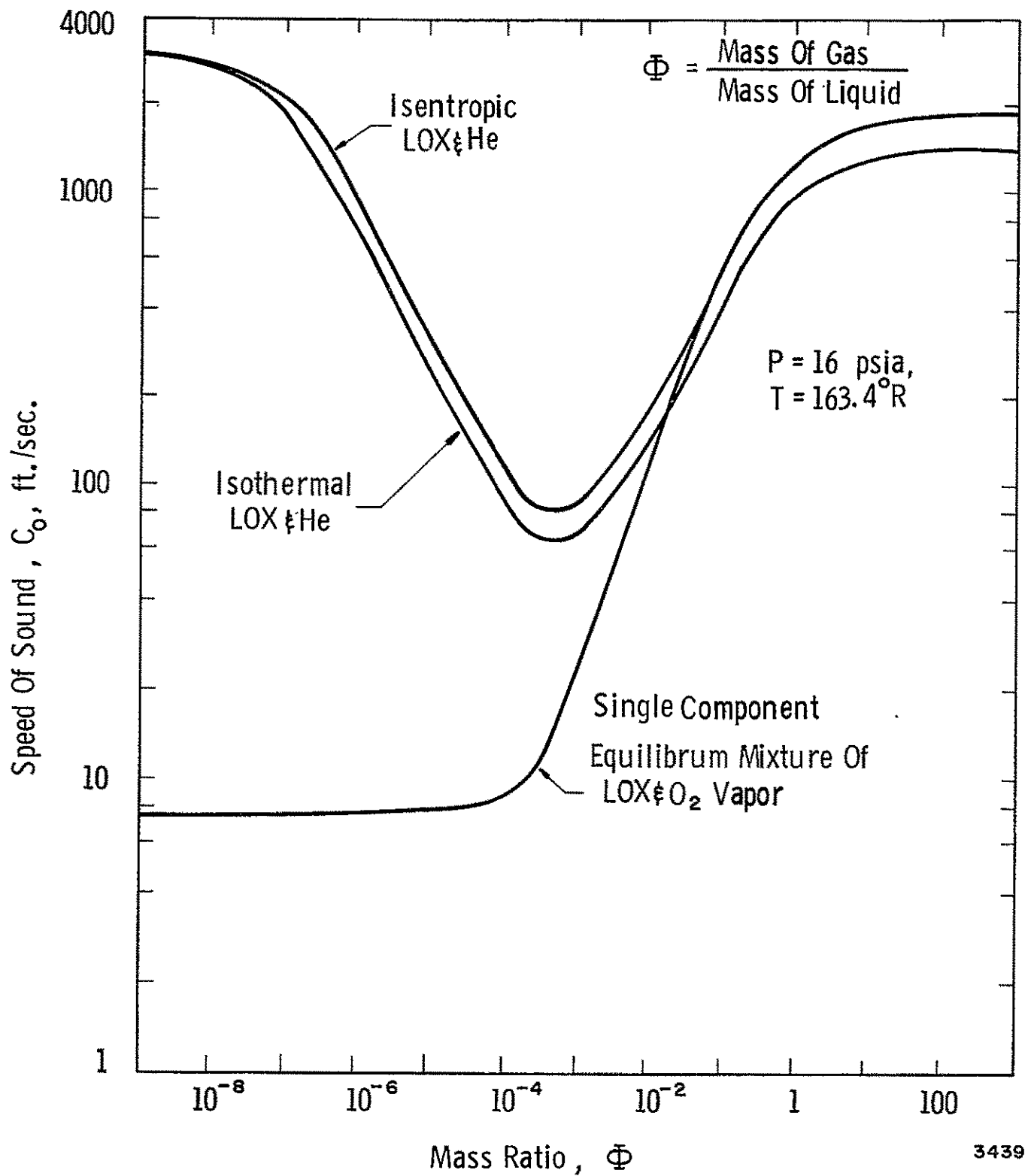
Figure 5.   Variation Of Speed Of Sound With Mass Ratio

15

increases in inverse proportion to the bubble radius[11]. An investigation has been made to determine the variation in effective sonic velocity in a liquid with uniformly distributed gas bubbles as the excitation frequency approaches the bubble resonant frequency.

At frequencies approaching resonance, Equation (22) is no longer useful, even as an approximation. Spitzer[12] derived an expression for the phase velocity at all frequencies by assuming that the gas concentration is small. If surface tension is neglected and if the bubble diameter is assumed to be larger than 0.001 ft, the bubble resonant frequency can be approximated by[13, 14]

$$f_o = \frac{1}{2\pi R_o} \left(\frac{3\eta P_o}{\rho_\ell} - \frac{4\mu_\ell^2}{\rho_\ell^2 R_o^2} \right)^{\frac{1}{2}} \tag{23}$$

where η, the polytropic exponent, is dependent primarily on the bubble size and gas thermal conductivity. For very small bubbles, such as those assumed to be distributed in the propellant feedline, the polytropic exponent is equal to unity.

The theoretical effect of frequency and bubble size on the phase velocity in a mixture of air bubbles in water has been programmed and is presented in Figure 6. The mass ratio, Φ, was assumed to be 3.0×10^{-5}. Note that the speed of sound is only affected at or near the bubble resonant frequency, which increases with decreasing bubble size. For the homogeneous distribution of very small bubbles entrained in the liquid propellant, the net effect over the frequency range of interest is only to lower the phase velocity of the pure liquid, to the value predicted by Equation (22). The effect of larger bubbles, which are assumed to exist only locally (cavitation zones), is discussed in Section IV.

III.2   Distributed Wall Compliance

In general, the flexibility of the feedline wall will produce two possible effects which may be of concern. First, the wall compliance will reduce the phase velocity and increase the spatial attenuation for the longitudinal fluid wave propagation mode (called the zeroth mode in Reference 5), and second, the axial wall stiffness effect, will permit real wave propagation of the higher order modes at low frequency by virtue of a coupling between the fluid and axial wall modes. For typical feedline problems, we have concluded that the amount of energy which is fed into the higher order modes at the line terminations is so small that it can be neglected. Therefore, for all practical purposes, the effect of the axial wall stiffness on

16
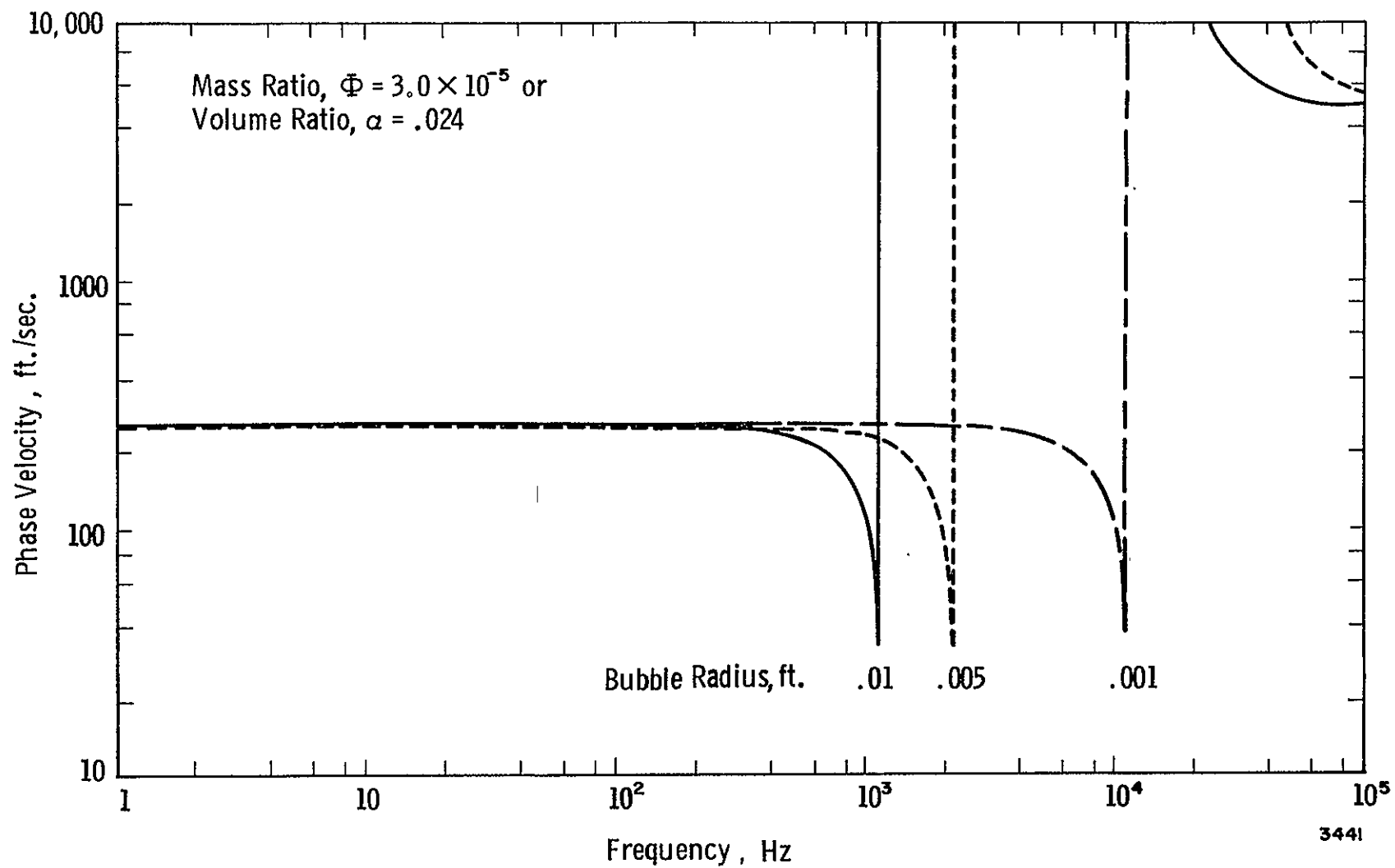
Figure 6. Effect Of Frequency And Bubble Size On Phase Velocity Of Air And
Water Mixture

the wave propagation can be neglected. This topic is thoroughly discussed in Section III. 3.

The influence of the wall compliance (and mass) on the propagation of the zeroth mode cannot be neglected. Gerlach[5] investigated the case of a viscous fluid flowing through a line having elastic flexible walls, i. e. , a line whose walls have finite radial compliance and impedance but do not propagate disturbances axially. By equating the radial impedance of the wall to the radial impedance of the fluid, the latter being subject to the no-slip condition on axial fluid velocity at the wall, the following characteristic equation for the eigenvalue problem was obtained:

$$\frac{(\gamma^2 - \beta^2)\ \rho_0 c_0^2}{\left[\beta \dfrac{J_1(\beta r_0)}{J_0(\beta r_0)} - \dfrac{\gamma^2}{k} \dfrac{J_1(k r_0)}{J_0(k r_0)}\right]} = \rho_t h s^2 + h E_t / r_0^2 \qquad (24)$$

The parameters, β and k, are separation constants of the solution of the Navier-Stokes equations and are related by

$$\gamma^2 = k^2 + s/\nu = \beta^2 + s^2/c_0 \qquad (25)$$

where

h	=	tube wall thickness
r_0	=	tube radius
E_t	=	Young's modulus for tube material
ρ_t	=	density of tube wall
s	=	Laplace variable
c_0	=	isentropic speed of sound in the fluid
ν	=	fluid kinematic viscosity
ρ_0	=	fluid density
J_0, J_1	=	zero and first-order Bessel functions of the first kind.

Equations (24) and (25) were solved numerically on the computer. Figures 7 and 8 illustrate the effect of an "elastic, flexible wall" (a wall with radial compliance and mass) on the spatial attenuation and phase velocity for the zeroth mode. The area of interest in these figures corresponds to dimensionless frequency numbers, $\omega r_0/c_0$, less than 1.0, since it is known that coupled structural-
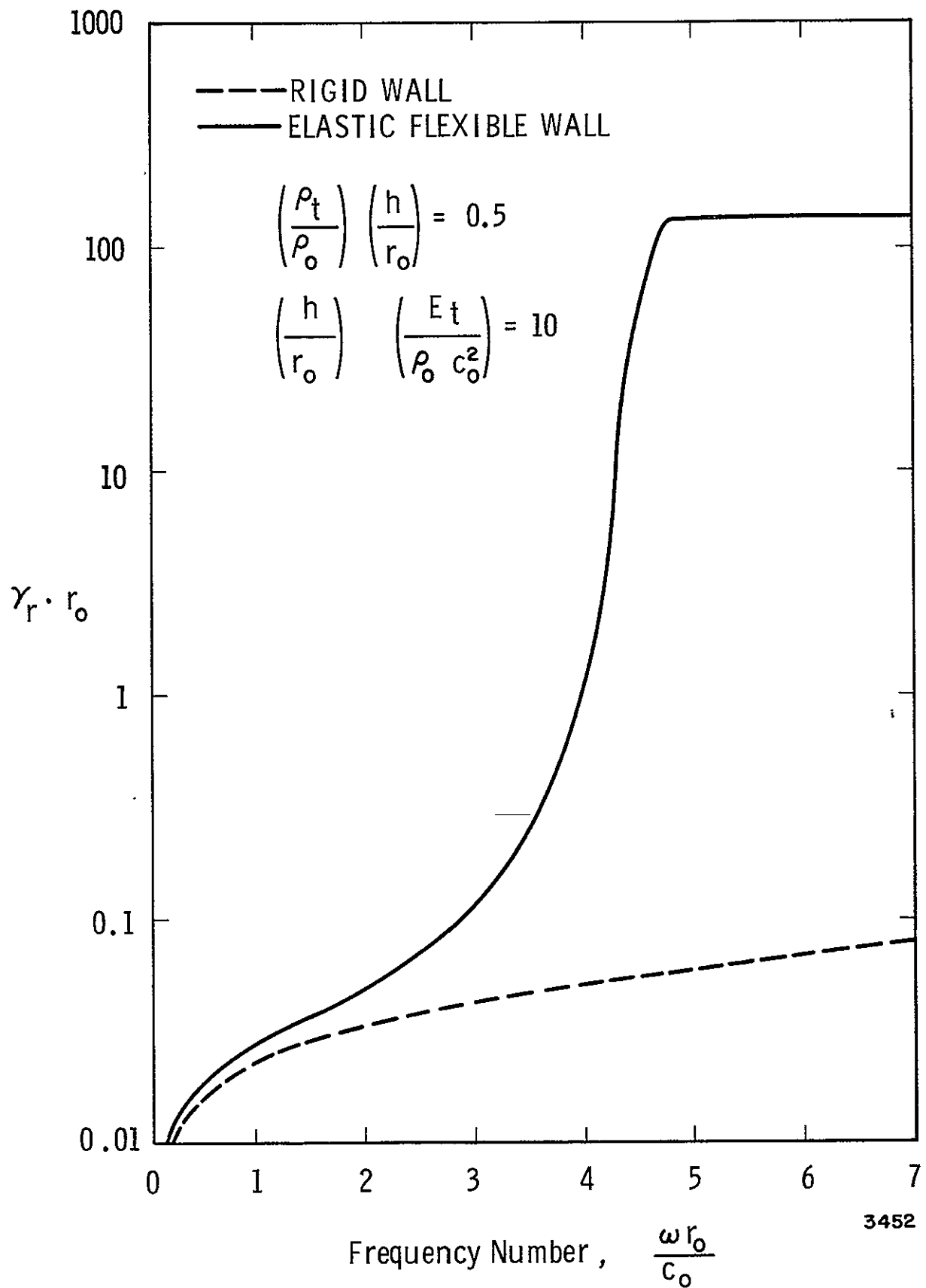
Figure 7.   Zeroth Mode Spatial Attenuation Versus Frequency
Number For A Rigid And An Elastic Flexible Wall

19
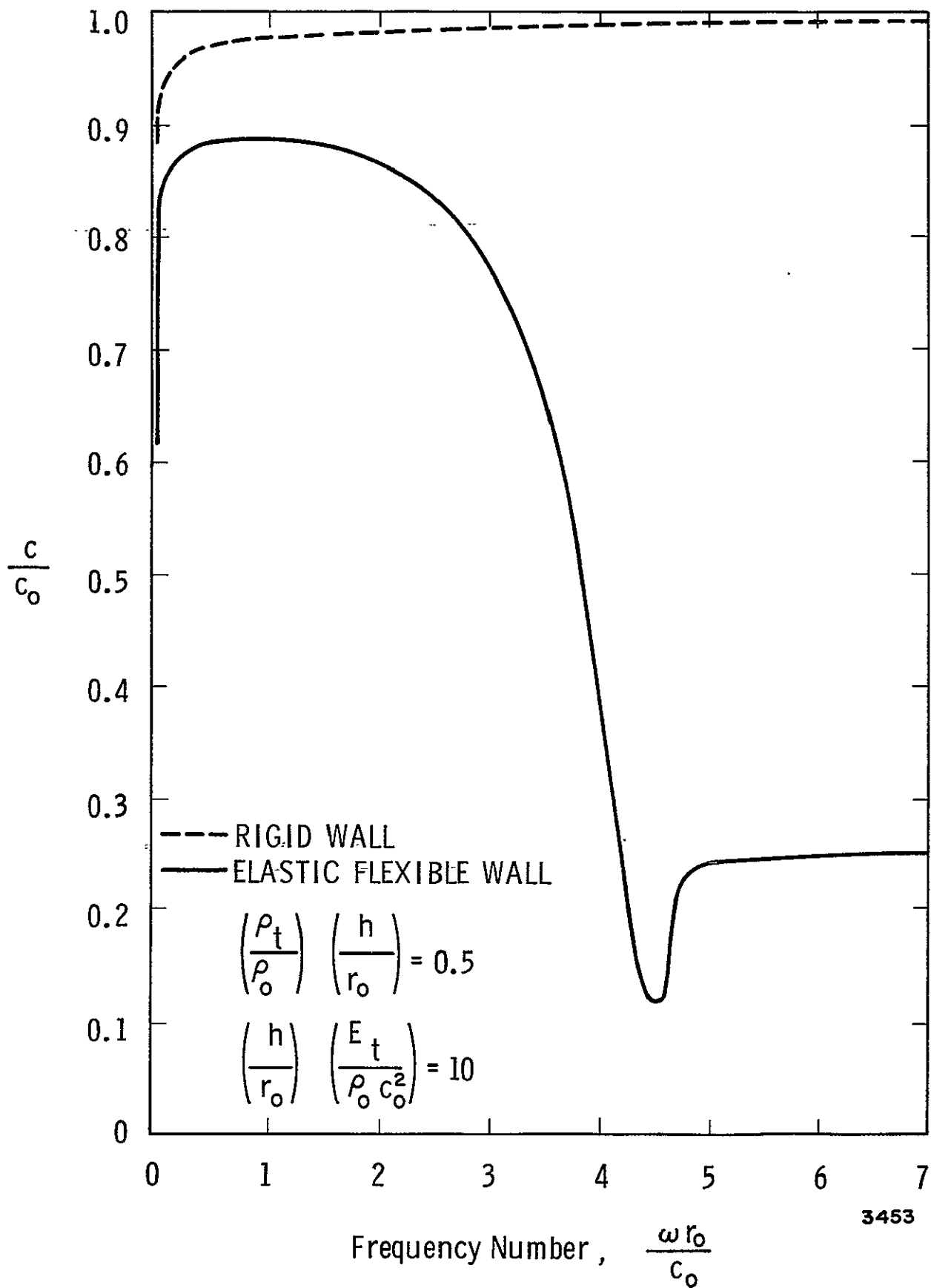
Figure 8. Zeroth Mode Dimensionless Phase Velocity, c/c_o, Versus Frequency Number For A Rigid And An Elastic Flexible Wall

20

feedsystem instabilities occur in this frequency range. In this range, the wall behaves in a spring-like manner and inertia effects are negligible; radial attenuation for the elastic wall is virtually indistinguishable from the attenuation of the rigid wall. It has been established that for any practical feedline problem, this is the case; hence, only the wall radial compliance need be considered. Wall mass effects are negligible. Therefore, the classic Korteweg correction to the phase velocity is valid. That is,

$$c = \frac{c_0}{\left(1 + \frac{2\rho_0 c_0^2 r_0}{E_t h}\right)^{\frac{1}{2}}} \tag{26}$$

It must be remembered, however, that this correction is the result of applying a boundary condition to the fluid dynamic formulation.

III. 3   Axial Wall Stiffness

In the preceding section, it was stated that the effect of axial wall stiffness on higher mode wave propagation could be neglected. That statement can be justified by proving the following points:

(1)   Due to observable flow processes in feedlines, there is a minimal amount of energy available in the higher modes of the fluid for coupling with the wall.

(2)   The energy that is available in each higher fluid mode has an attenuation rate, below the cut-off frequency, of approximately two orders of magnitude larger than that for the zeroth mode. Therefore, the energy level and attenuation rate do not permit sustained coupling of the fluid and the wall in the higher modes.

The physical effect of higher modes must be considered, because the proposed distributed parameter line model is based on only the zeroth mode of propagation, and the existence of substantially higher modes would invalidate its functional form.

Recall that the magnitude of Reynold's numbers in a typical feedline indicates a turbulent flow condition. Hence, the velocity profile should be relatively flat. Gerlach[5] has calculated the perturbation velocity profiles of the first four modes for the laminar, viscous pipe-flow problem. Characteristic results are shown in Figures 9 and 10 where $F_{xn}(r)$ is the velocity distribution function. Observe closely that, for the wide range of frequencies and damping

21
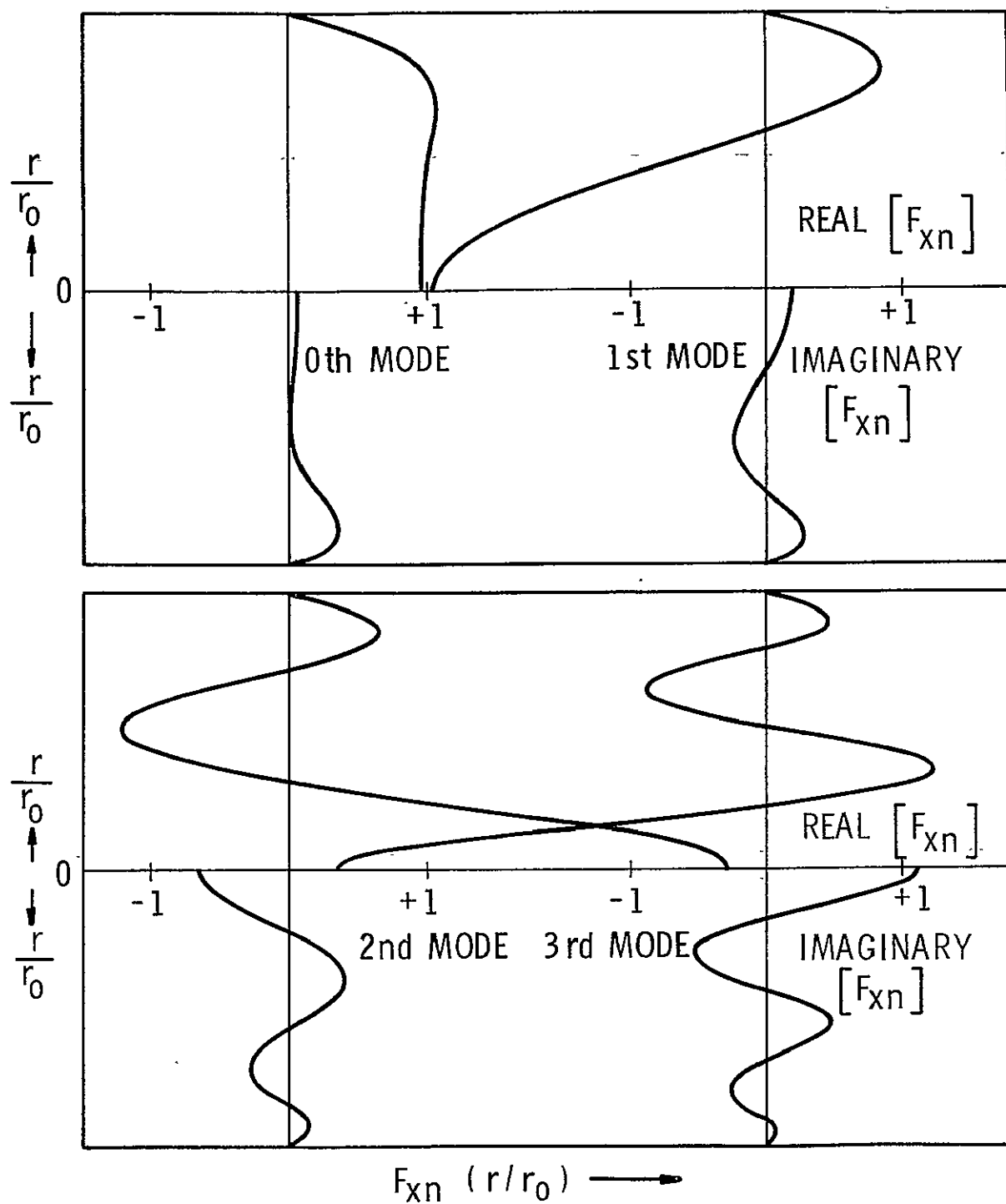
Figure 9. Axial Velocity Profile Function, $F_{xn}(r)$, for Four Modes ($\omega r_0 / c_0 = 1.0$, $\nu / r_0 c_0 = 0.01$)

3657

22
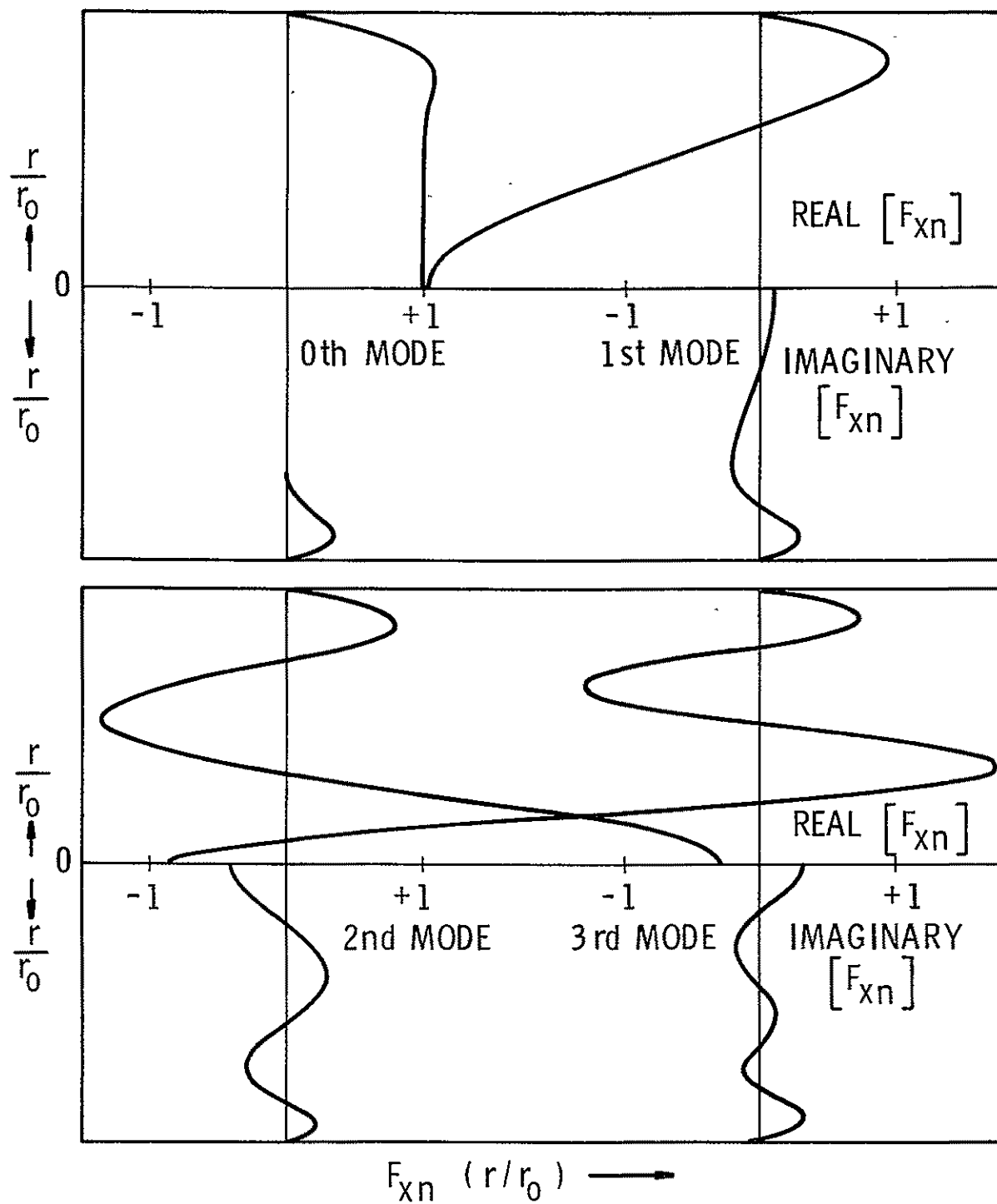
Figure 10. Axial Velocity Profile Function, $F_{xn}(r)$, for Four Modes ($\omega r_0 / c_0 = 0.2$, $\nu / r_0 c_0 = 0.001$)

23

numbers considered, the zeroth mode velocity distribution is near-
ly constant across the cross-section. The obvious conclusion is
that the zeroth mode perturbation profile approximates a turbulent
profile, and, hence, a minimal contribution from the higher modes
is required to fill out the turbulent profile. Therefore, it follows
that the energy level in the higher modes is negligible.

Based on the foregoing discussion, there is admittedly a
small contribution of the higher modes to the velocity profile. How-
ever, Gerlach[5] has also shown that the spatial attenuation (the real
part of the propagation operator) for these higher modes is substan-
tially larger than for the zeroth mode. The net effect is that the
higher modes are rapidly damped out over a broad frequency range,
and therefore have neither the time nor the energy levels required
to excite (couple) corresponding modes of transmission in the con-
duit wall. Figure 11 illustrates the elevated damping level of higher
modes, while the zeroth mode attenuation is roughly insensitive to
the frequency range.

The above discussion substantiates the validity of the zeroth
mode transfer equations for the line. In addition, the foregoing con-
clusions which were derived on a qualitative basis, have also been
verified quantitatively by Lin and Morgan[15].
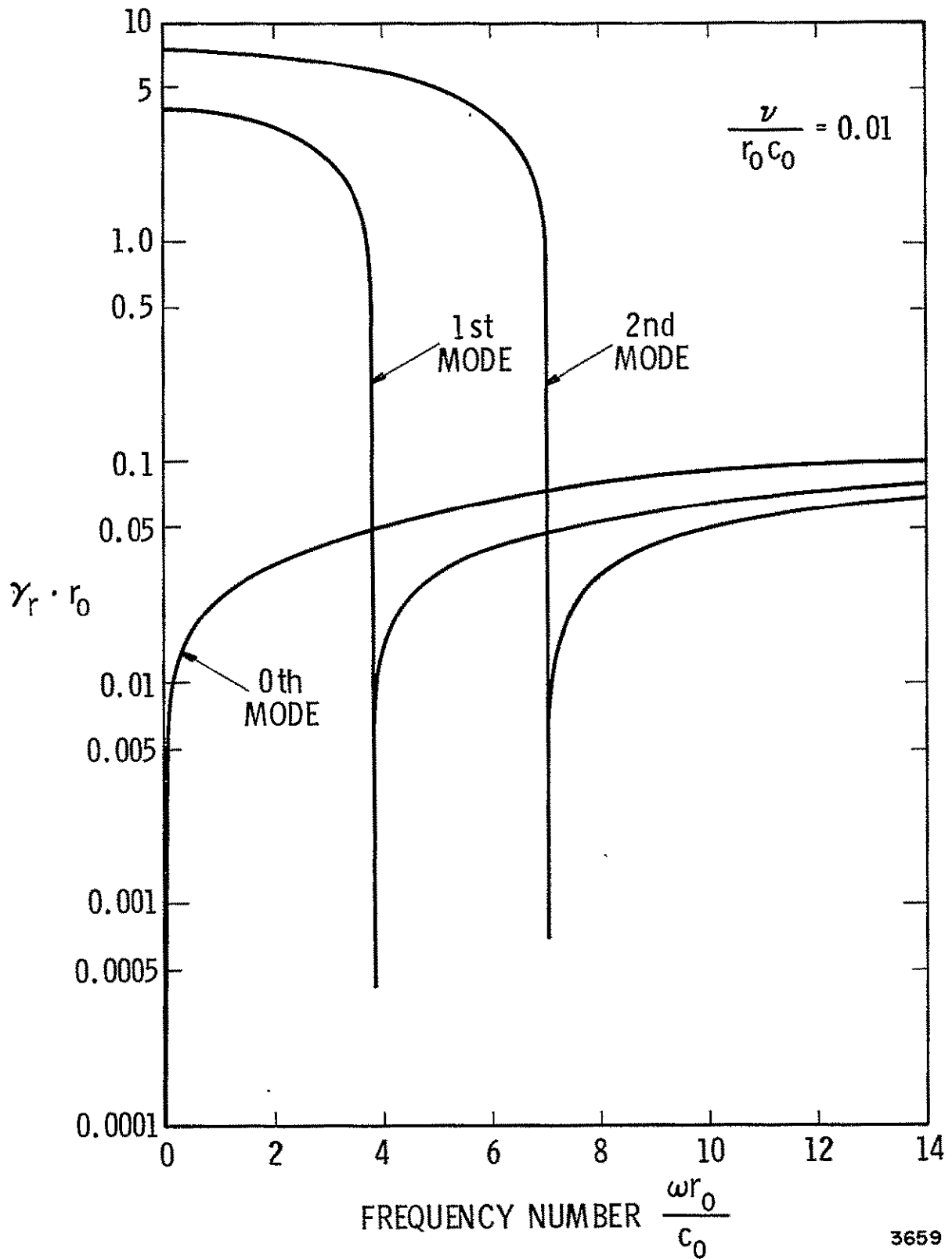
Figure 11. Plot of the Spatial Attenuation Factor Versus
Radial Frequency Number for Three Modes

IV. LOCAL COMPLIANCES

IV. 1   Cavitation Zones or Large Gas Bubbles

At elbows or bends in the feedline, or at the pump inlet, local pressure drops are likely to create regions of cavitation. In most cases, these regions are composed of localized bubbles of vapor. These larger cavitation bubbles in the line are modeled by considering the bubbles to be local compliances. As the excitation frequency approaches the bubble resonant frequency, which can be quite low for large bubbles, the volume pulsations may be described by the following linear, second-order differential equation:

$$\frac{\rho_\ell}{4\pi R_o} \ddot{v} + b\dot{v} + \frac{\eta P_o}{V_o} v = -p(t) \tag{27}$$

or

$$m_2 \ddot{v} + b\dot{v} + kv = -p(t) \tag{28}$$

where

ρ_ℓ = liquid density

P_o = steady state line pressure

V_o = steady state bubble volume

R_o = steady state bubble radius

b = coefficient accounting for viscous, thermal and radiation damping.

The continuity equation relating the flow upstream and downstream of the bubble is

$$q_2 - q_1 = dv/dt \tag{29}$$

where q_1 and q_2 represent the upstream and downstream volumetric flow rate, and dv/dt is the change in bubble volume with time. Equations (28) and (29) can be combined conveniently in the Laplace transform domain to yield an expression for the change in flow rate due to the presence of the bubble.

$$Q_2(s) - Q_1(s) = \frac{-s P(s)}{(m_2 s^2 + bs + k)} \tag{30}$$

26

where the term $1/(m_2 s^2 + bs + k)$ can be visualized as a "complex" compliance. The damping term, b, has been estimated by Devin[16], and is represented by a combination of the losses originating from three processes:

(1) Thermal damping resulting from the thermal conduction between the gas in the bubble and the surrounding liquid;

(2) Sound radiation damping caused by energy dispersed by radiating spherical sound waves when the bubble is excited into volume pulsations;

(3) Viscous damping from viscous forces at the liquid-gas interface.

In the literature, there is considerable disagreement as to the theoretical expressions that should be used to evaluate the damping constant, δ, which is related to the coefficient of damping, b, by

$$\delta = \frac{b}{\omega m_2} \tag{31}$$

The reason for this disagreement is that, while the theory is applicable to all frequencies, experimental verification has been obtained only at the resonant condition. However, it is hypothesized that the theory which is summarized here and has been incorporated into the computer code is valid over a broad range of frequencies.

The total damping constant is given by

$$\delta = \delta_{th} + \delta_{rad} + \delta_{vis} \tag{32}$$

or, $\quad b = b_{th} + b_{rad} + b_{vis}$

where

$$b_{th} = \left\{ \frac{\dfrac{\sinh(2\phi_1 R_0) + \sin(2\phi_1 R_0)}{\cosh(2\phi_1 R_0) - \cos(2\phi_1 R_0)} - \dfrac{1}{\phi_1 R_0}}{\dfrac{2\phi_1 R_0}{3(\gamma-1)} + \dfrac{\sinh(2\phi_1 R_0) - \sin(2\phi_1 R_0)}{\cosh(2\phi_1 R_0) - \cos(2\phi_1 R_0)}} \right\} \times \frac{\eta P_0}{V_0 \omega} \tag{33}$$

$$b_{rad} = \frac{\rho_\ell \omega^2}{4\pi c_\ell} \tag{34}$$

$$b_{vis} = \frac{\mu}{\pi R_0^3} \tag{35}$$

27

In these expressions,

μ = liquid viscosity

ρ_ℓ = liquid density

c_ℓ = liquid speed of sound

γ = ratio of specific heats irrespective of the thermo-dynamic process indicated by the polytropic exponent, η.

Also, the argument

$$\phi_1 R_o = \left(\frac{\omega}{2 D_1}\right)^{\frac{1}{2}} R_o \tag{36}$$

is a measure of the rate at which heat is conducted over a distance, R_o, from the bubble center to the liquid-gas interface. The thermal diffusivity of the entrained gas is denoted by D_1.

For zero damping of the oscillations,

$$\dot{Q}_1(s) - Q_2(s) = \frac{s\,P(s)}{k\left(1 + \frac{m_2}{k}\,s^2\right)} \tag{37}$$

At frequencies considerably below the bubble natural frequency, ω_o,

$$Q_1(s) - Q_2(s) = \frac{s\,P(s)}{k} \tag{38}$$

where ω_o is defined as

$$\omega_o = \sqrt{k/m_2} \tag{39}$$

For these low frequency cases, the compliance becomes simply

$$C = \frac{V_o}{\eta P_o} \tag{40}$$

The correct value of the polytropic exponent η in the stiffness term $k = \eta P_o/V_o$ depends on the bubble size and frequency,

28

as well as the thermal properties of the gas and liquid. This varia-
tion with bubble size and frequency of excitation is shown in Figure
12. For a given bubble undergoing successive compressions, the
gas near the center behaves adiabatically, while the gas near the
liquid-gas interface undergoes no change in temperature since the
liquid behaves as a large heat sink. The value of the polytropic
exponent has been found to be

$$\eta = \frac{\gamma \left[1 + \delta_{th}^2 \right]^{-1}}{\left[1 + \frac{3(\gamma-1)}{2\phi_1 R_o} \left(\frac{\sinh(2\phi_1 R_o) - \sin(2\phi_1 R_o)}{\cosh(2\phi_1 R_o) - \cos(2\phi_1 R_o)} \right) \right]} \tag{41}$$

where δ_{th} is equal to the term in brackets in Equation (33).

IV.2 Complex Side Branch

The types of side elements typical of a rocket feed system
(accumulators and gas-filled pressure sensing lines) behave as local
compliance-like elements.

In general, any type of complicated side element may be
modeled; these side elements can be visualized as local or lumped
"compliances," even though they may not be compliance-like ele-
ments. The model used for an arbitrary complex side element,
such as a gauge and line connected onto a feedline, may be put in the
form of a local compliance, as shown in Figure 13. This element
is assumed to consist of a side branch line having an inertance, I,
and resistance, R, and with a capacitance termination, C. The
line inertance, I, and the line resistance, R, have been pro-
grammed respectively as:

$$I = \rho_o L/A_b \tag{42}$$

and

$$R = 128 \frac{\mu L}{\pi d_b^4} \tag{43}$$

Here, ρ_o = fluid density, L = side branch length, and A_b
is the branch cross sectional area; μ is the fluid viscosity, and d_b
is the side branch diameter. To consider the effects of compressi-
bility in the side branch, the inertia and resistance effects are neg-
lected, and

29
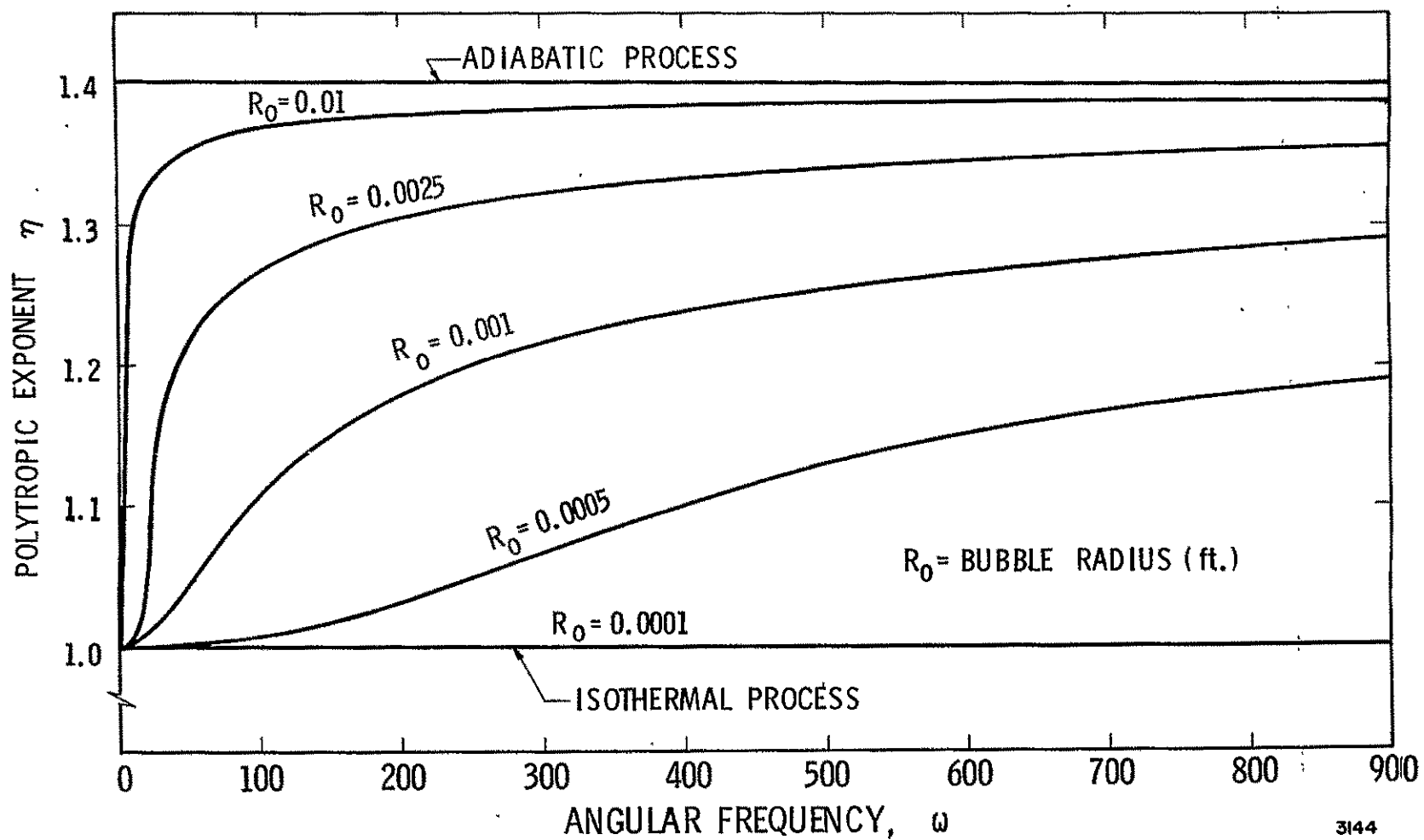
Figure 12. Polytropic Exponent for O_2 Bubble in LOX vs Angular Frequency and Bubble Size

(a) PHYSICAL SITUATION

$p_1(t), q_1(t)$

$q_3(t)$

$p_4(t)$

$q_4(t)$

$p_2(t), q_2(t)$

$p_1(t) = p_2(t)$

(b) MODEL

Resistance, R
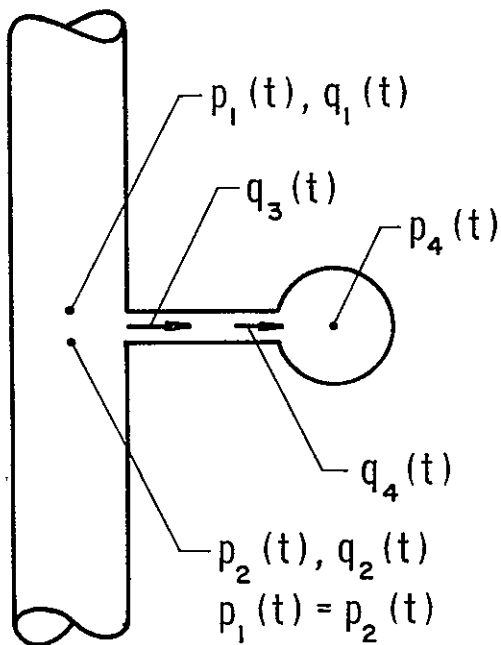
Capacitance, C
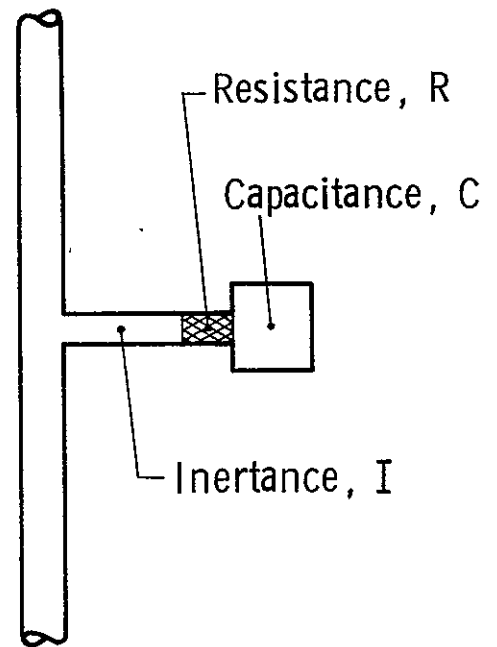
Inertance, I

(c) MODEL EQUATIONS IN LA PLACE DOMAIN

CONTINUITY IN LINE

$$Q_1(s) - Q_2(s) = Q_3(s)$$

GAUGE LINE (Assumed simple inertance plus resistance only)

$$Q_3(s) = Q_4(s)$$

$$P_2(s) - P_4(s) = Is Q_3 + RQ_3$$

CAPACITANCE

$$Q_4(s) = C_S P_4$$

"COMPLIANCE MODEL"

$$Q_1(s) - Q_2(s) = \left\{ \frac{C}{IC_S{}^2 + RC_S + 1} \right\} s P_1(s)$$

2751

Figure 13. Example Treatment Of More General
"Local Compliance" in Feed Line

31

$$q_4 = \frac{V}{\gamma P}\left(\frac{dp}{dt}\right) \quad \text{for gases}$$

$$q_4 = \frac{V}{\varkappa}\left(\frac{dp}{dt}\right) \quad \text{for liquids} \tag{44}$$

where q_4 is the flow into the branch, V is the volume of the compressible fluid contained within the side branch, γ is the ratio of specific heats for the fluid (if a gas), and $\varkappa$ is the liquid bulk modulus.

For the case of a gauge connected to a feedline containing a liquid by a branch line partially filled with air, the lumped model is obtained by summing the effects of the branch inertance, resistance, and capacitance.

The resultant expressions in the Laplace domain relating the pressure and flow upstream and downstream of the side branch become

$$P_2(s) = P_1(s) \tag{45}$$

$$Q_2(s) = Q_1(s) - \left[\frac{C}{ICs^2 + RCs + 1}\right] sP_1(s) \tag{46}$$

The quantity in the brackets can be visualized as a complex "compliance" for this case, and represents a local compliance so far as the feedline is concerned.

32

V. COUPLED RESPONSES

Four possible modes of structural-hydraulic coupling are shown in Figure 14. In cases a, c, and d, an externally imposed, rigid-body acceleration acts on a length of feedline. Because of viscous shearing forces at the propellant-conduit interface and/or body forces applied through the end impedances, the imposed line motion will couple with the fluid motion to produce modifications to the pressure-flow equations for the stationary line (Section II. 1). The functional forms of these modifications are derived herein.

V. 1   Accelerated Line   (Cases c and d)

The fluid may be characterized by the familiar axisymmetric, linearized, perturbation equations of motion, continuity and state.

$$\frac{\partial v}{\partial t} = -\frac{1}{\rho_o} \frac{\partial p}{\partial x} + \nu \left[\frac{\partial^2 v}{\partial r^2} + \frac{1}{r} \frac{\partial v}{\partial r} \right] + \frac{F_x}{\rho_o} \qquad (47)$$

$$\frac{\partial \rho}{\partial t} + \rho_o \frac{\partial v}{\partial x} = 0 \qquad (48)$$

$$\frac{\partial \rho}{\rho_o} = \frac{\partial p}{\varkappa} \quad , \qquad \varkappa = \rho_o c_o^2 \qquad (49)$$

Implicit in this formulation is the assumption that the radial perturbation velocity is negligible compared to the axial perturbation velocity, v. Note that the pressure <u>has not</u> been assumed to be independent of the radial coordinate. The body force F_x, can be replaced by the equivalent D'Alembert force, $-\rho_o a_x$, due to the imposed acceleration. Utilizing this substitution, combining the continuity and state equations and applying the Laplace transformation with zero initial conditions, yields the following pair of coupled differential equations:

$$sV = -\frac{1}{\rho_o} \frac{\partial P}{\partial x} + \nu \left[\frac{\partial^2 V}{\partial r^2} + \frac{1}{r} \frac{\partial V}{\partial r} \right] - A_x \qquad (50)$$

$$P = -\frac{\rho_o c_o^2}{s} \frac{\partial V}{\partial x} \qquad (51)$$

where P and V represent the transformed fluid pressure and velocity. These equations can be combined into a single equation in the dependent variable V.
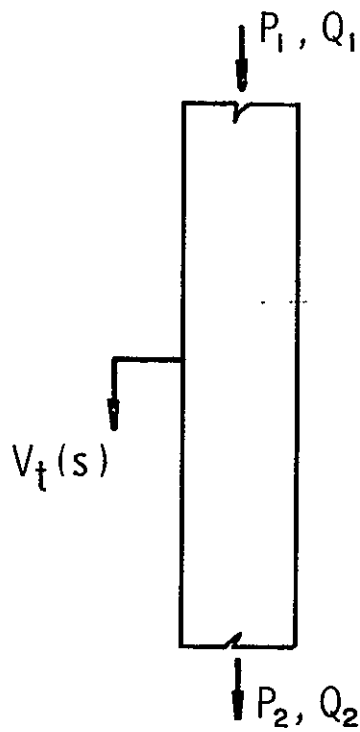
(a) COUPLING THROUGH VISCOUS WALL SHEAR
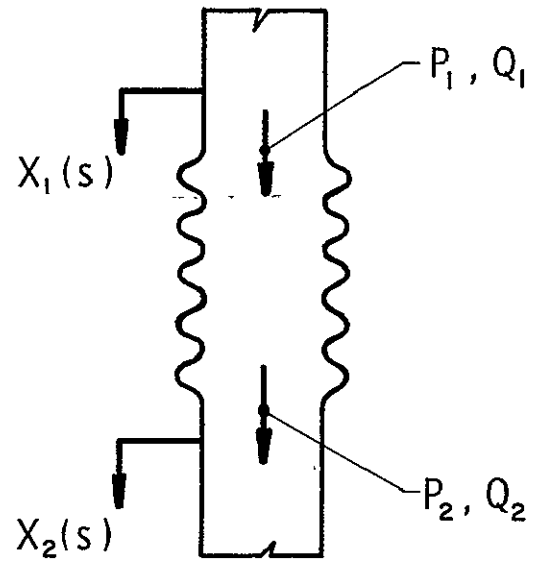
(b) COUPLING THROUGH RELATIVE AXIAL MOTION OF BELLOWS
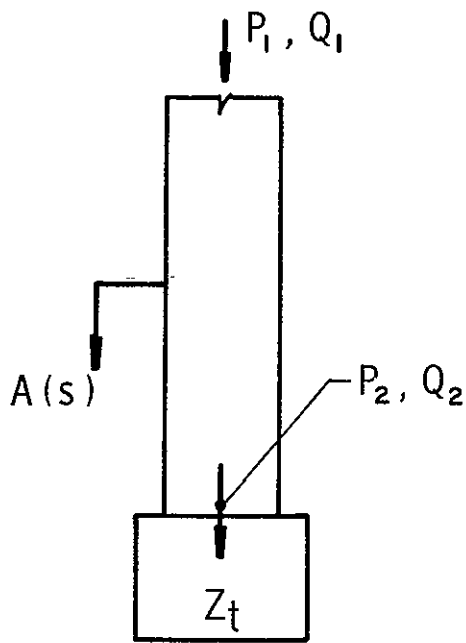
(c) COUPLING THROUGH END IMPEDANCE MOTION
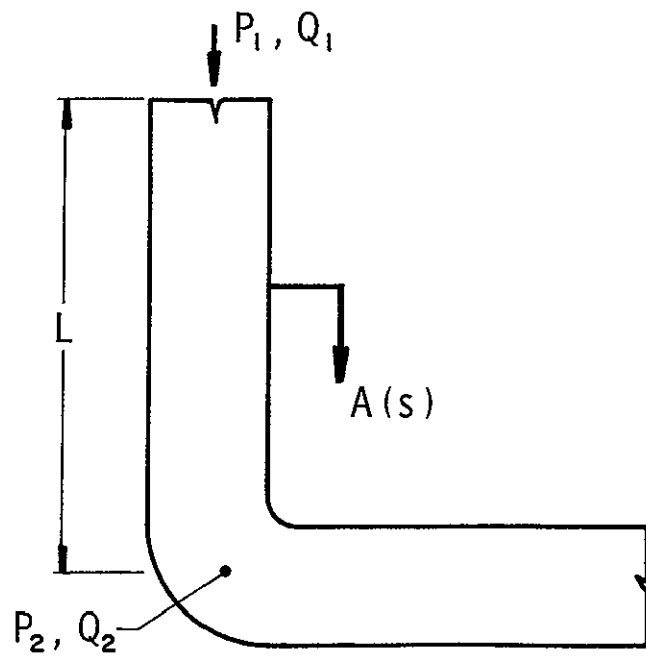
(d) COUPLING THROUGH LINE MOTION

2752

Figure 14. Elementary Structural-Fluid Coupling Cases

34

$$sV = \frac{c_o^2}{s} \frac{\partial^2 V}{\partial x^2} + \nu \left[\frac{\partial^2 V}{\partial r^2} + \frac{1}{r} \frac{\partial V}{\partial r} \right] - A_x \qquad (52)$$

Making use of the fact that A_x is a function only of the Laplace variable, s, and redefining the dependent variable to be

$$U(r, x, s) = V + A_x/s \qquad (53)$$

results in the following easily solved, ordinary differential equation:

$$\frac{\nu}{s} \left[\frac{\partial^2 U}{\partial r^2} + \frac{1}{r} \frac{\partial U}{\partial r} - \frac{s}{\nu} U \right] + \frac{c_o^2}{s^2} \frac{\partial^2 U}{\partial x^2} = 0 \qquad (54)$$

This equation is amenable to solution by the standard separation of variables technique which yields

$$U = (A \cosh \lambda x + B \sinh \lambda x) J_o(\alpha r) \qquad (55)$$

where

$$\alpha^2 = \frac{s}{\nu} \left(\lambda^2 \frac{c_o^2}{s^2} - 1 \right)$$

λ^2 = separation constant

A, B = integration constants.

By definition, λ is the propagation operator, $Y(s)$ which governs the spatial attenuation of axially propagated waves in the fluid. This operator may be stated a priori:

$$Y(s) = \frac{s}{c_o} \frac{1}{\left(1 - \frac{2 J_1(\xi r_o)}{\xi r_o J_o(\xi r_o)} \right)^{\frac{1}{2}}} \qquad (56)$$

where

$$\xi^2 = -s/\nu , \qquad r_o = \text{conduit radius}$$

In addition, the characteristic impedance of the line, Z_c, is defined to be

$$Z_c = \frac{\rho_o c_o^2}{s} Y(s) \qquad (57)$$

35

Utilizing these definitions, the fluid pressure and velocity become

$$V(r, x, s) = [A \cosh \gamma x + B \sinh \gamma x] J_o(\alpha r) - A_x/s \qquad (58)$$

$$P(r, x, s) = -Z_c[A \sinh \gamma x + B \cosh \gamma x] J_o(\alpha r) \qquad (59)$$

The dependence on the radial coordinate may be eliminated by averaging these expressions across the cross section.

$$\overline{V} = [A \cosh \gamma x + B \sinh \gamma x] \frac{2}{\alpha r_o} J_1(\alpha r_o) - A_x/s \qquad (60)$$

$$\overline{P} = -Z_c[A \sinh \gamma x + B \cosh \gamma x] \frac{2}{\alpha r_o} J_1(\alpha r_o) \qquad (61)$$

Constants, A and B, can be evaluated at the origin of the line (z=0) by applying the boundary conditions.

$$\overline{V}(o, s) = \overline{V}_1 ; \qquad \overline{P}(o, s) = \overline{P}_1 \qquad (62)$$

which results in the following expressions:

$$\overline{V} = \overline{V}_1 \cosh \gamma x - \frac{\overline{P}_1}{Z_c} \sinh \gamma x - A_x/s (1 - \cosh \gamma x) \qquad (63)$$

$$\overline{P} = \overline{P}_1 \cosh \gamma x - Z_c \overline{V}_1 \sinh \gamma x - \frac{Z_c A_x}{s} \sinh \gamma x \qquad (64)$$

The desired four-terminal representation for the mean exit pressure and flow velocity are obtained by evaluating the above expressions at x = L.

$$\overline{V}_2 = \overline{V}_1 \cosh \gamma L - \overline{P}_1/Z_c \sinh \gamma L - V_x (1 - \cosh \gamma L) \qquad (65)$$

$$\overline{P}_2 = \overline{P}_1 \cosh \gamma L - Z_c \overline{V}_1 \sinh \gamma L - V_x Z_c \sinh \gamma L \qquad (66)$$

where the acceleration has been replaced by its Laplace equivalent $s V_x$. These equations can be referred to local volumetric flow rate by introducing the line cross-sectional area, A.

V. 2   Relative Motion of Bellows and PVC Joints

Bellows

Bellows are commonly used elements in propulsion feed systems, and in their most important application, they serve as a "fix"

for the POGO instability. Bellows vary in their structural complexity from the simple array of axisymmetric convolutes shown in Figure 15a to the configuration in Figure 15b which incorporates a gas trap liner. The following discussion is directed toward the latter configuration which includes the simple bellows as a special or degenerate case.

When the ends of a bellows execute relative motion, the change in volume flow rate between the inlet and exit can be considered to be the sum of two separate effects:

(1) A flow rate change due to the compliance of the gas trapped under the liner, and

(2) An apparent local volume production.

It should be noted that the first item exists even in the absence of relative motion.

First, the pressure drop across a bellows in the flow direction is expressed in the Laplace domain by

$$P_2(s) = F(\rho V_x^2, G) \ P_1(s) \ , \tag{67}$$

where $F(\rho V_x^2, G)$ is a loss factor, dependent on the dynamic pressure and bellows geometry. Now, the change in flow rate due to trapped gas can be written in terms of the bellows inlet pressure.

$$q_2' - q_1' = -C \frac{dp_1}{dt} \tag{68}$$

or in the transform domain

$$Q_2'(s) - Q_1'(s) = -Cs \ P_1(s) \tag{69}$$

where C is the lumped compliance of the gas and is defined by the ratio of the gas volume to the gas bulk modulus of elasticity.

The apparent volume production can be derived from the continuity equation

$$q_2'' - q_1'' = dv/dt \tag{70}$$

or in the Laplace domain

$$Q_2''(s) - Q_1''(s) = -s \, Vol(s) \tag{71}$$

37

a. Simple Bellows

Trapped Gas

$$q_1 = q_1^I + q_1^{II}$$

$$q_2 = q_2^I + q_2^{II}$$
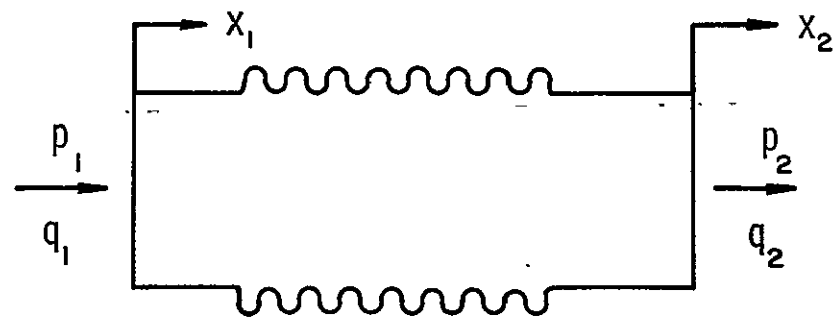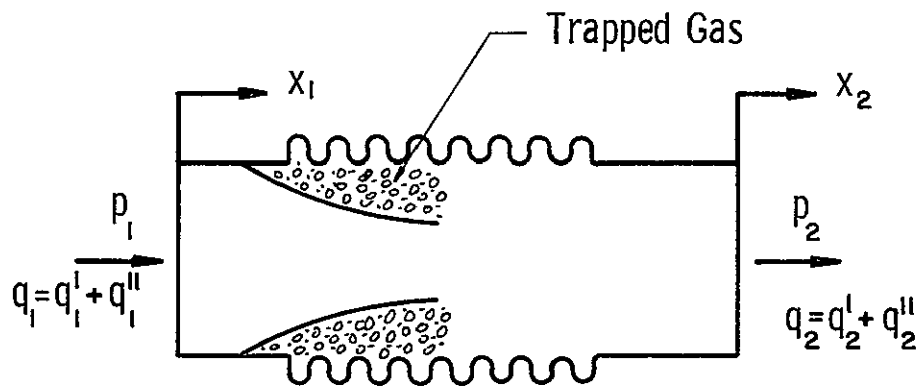
( )^I - quantities associated with compliance
of trapped gas

( )^{II} - quantities associated with volume
production

b. Bellows With Gas Trap Liner

3442

Figure 15. Nomenclature For Relative Motion Of Bellows

38

The volumetric production is related to the axial displacement of the bellows ends by

$$\text{Vol}(s) = K_b [X_1(s) - X_2(s)] \tag{72}$$

where K_b is a "volume change" constant, also dependent on the bellows geometry. The resulting flow equation is

$$Q_2''(s) - Q_1''(s) = sK_b [X_1(s) - X_2(s)] \tag{73}$$

or in terms of relative velocities

$$Q_2''(s) - Q_1''(s) = K_b [V_1(s) - V_2(s)]. \tag{74}$$

The combined effect, expressed as the sum of Equations (67) and (74) produces the following result for the change in flow rate:

$$Q_2(s) = Q_1(s) - CsP_1(s) + K_b [V_1(s) - V_2(s)] \tag{75}$$

Equations (67) and (75) describe completely the four terminal pressure-flow relationship for a bellows.

PVC Joints

In many applications, the PVC (pressure-volume compensator) joint is often used in place of an elementary bellows where the local volumetric change effect described above is judged undesirable. A typical PVC joint, shown in Figure 16, generally consists of a bellows to allow line flexibility (either axially, or to allow angulation, or both) and a compensation chamber to "absorb" the excess volume of fluid created in the line when the bellows is displaced axially. In theory, the PVC joint is designed to permit axial length changes without introducing a corresponding fluid volume disturbance in the line. In practice, however, the PVC joint is not a perfect compensation device.

The "volume flow production" of the bellows Q_4, may be written as

$$Q_4(s) = Q_2(s) - Q_3(s) = K_b [V_1(s) - V_2(s)] \tag{76}$$

where $V_i(s)$, $i = 1$ or 2, is the transformed velocity associated with coordinate X_i. Similarly, the ideal volume compensation of the PVC may be written as

39
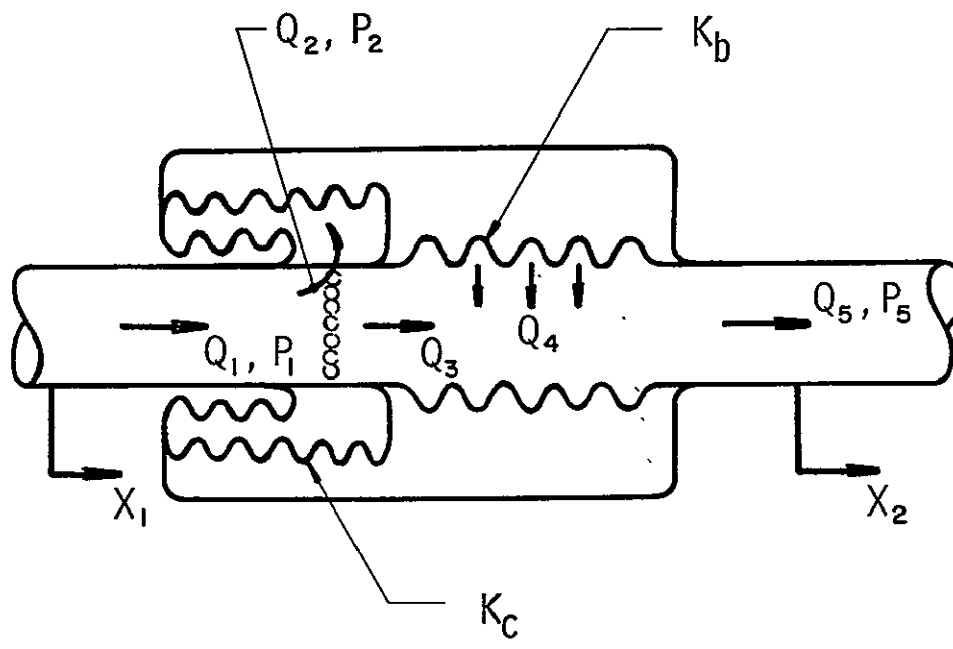
Figure 16.   Illustration Of Typical PVC Joint

2756

40

$$Q_2(s) = Q_1(s) - Q_3(s) = K_c [V_1(s) - V_2(s)]. \tag{77}$$

Continuity requires that

$$Q_5(s) = Q_1(s) + Q_4(s) - Q_2(s). \tag{78}$$

Combining Equations (76), (77), and (78), the resultant flow becomes

$$Q_5(s) = Q_1(s) + (K_b - K_c) [V_1(s) - V_2(s)]. \tag{79}$$

It is normally intended that $K_b = K_c$ so that perfect compensation is obtained. However, there is a dynamic effect associated with the action of the compensation unit, so a more general form of Equation (77) is

$$Q_2(s) = \frac{K_c}{G(s)} [V_1(s) - V_2(s)] \tag{80}$$

where $G(s)$ might be a simple lag, e.g., $(1+\tau s)$, caused by a combination of the PVC structure elasticity and fluid compressibility. Equation (79) was selected as the PVC flow rate expression in the feedline computer code. The pressure drop across the joint was assumed to have the same functional form as Equation (67).

V. 3. Forced Changes in Line Length

The POGO phenomenon is a coupled dynamic instability involving the vehicle structure, propulsion system, and propellant feed system. Propellant feedlines are normally supported by the vehicle structure at discrete points on the line as opposed to a continuous support. A forced change in the length of the line between consecutive supports occurs when vehicle structural inputs to these supports differ in phase and/or magnitude. In this section, the effects of changes in line length are analyzed and the transfer matrices that describe the pressure flow response to this type of excitation are derived.

The effect that length changes produce on the pressure-flow relationships for the liquid in the line can be analyzed from two different viewpoints. The first approach requires the solution of the fluid dynamic equations of motion subject to an inhomogeneous boundary condition on the spatial variation of the axial wall velocity as dictated by the structural inputs, V_1 and V_2. An alternate approach assumes that the dynamic length change can be modeled as the linear superposition of (1) the axial vibration of the rigid line, and (2) a volume production region that reflects the relative motion between the ends of the line as indicated in Figure 17.

41

$$Q_2^{\text{II}} = A \left[V_2 - V_1 \right]$$
$$Q_2 = Q_2^{\text{I}} + Q_2^{\text{II}}$$

ASSUMED VOLUME
PRODUCTION REGION
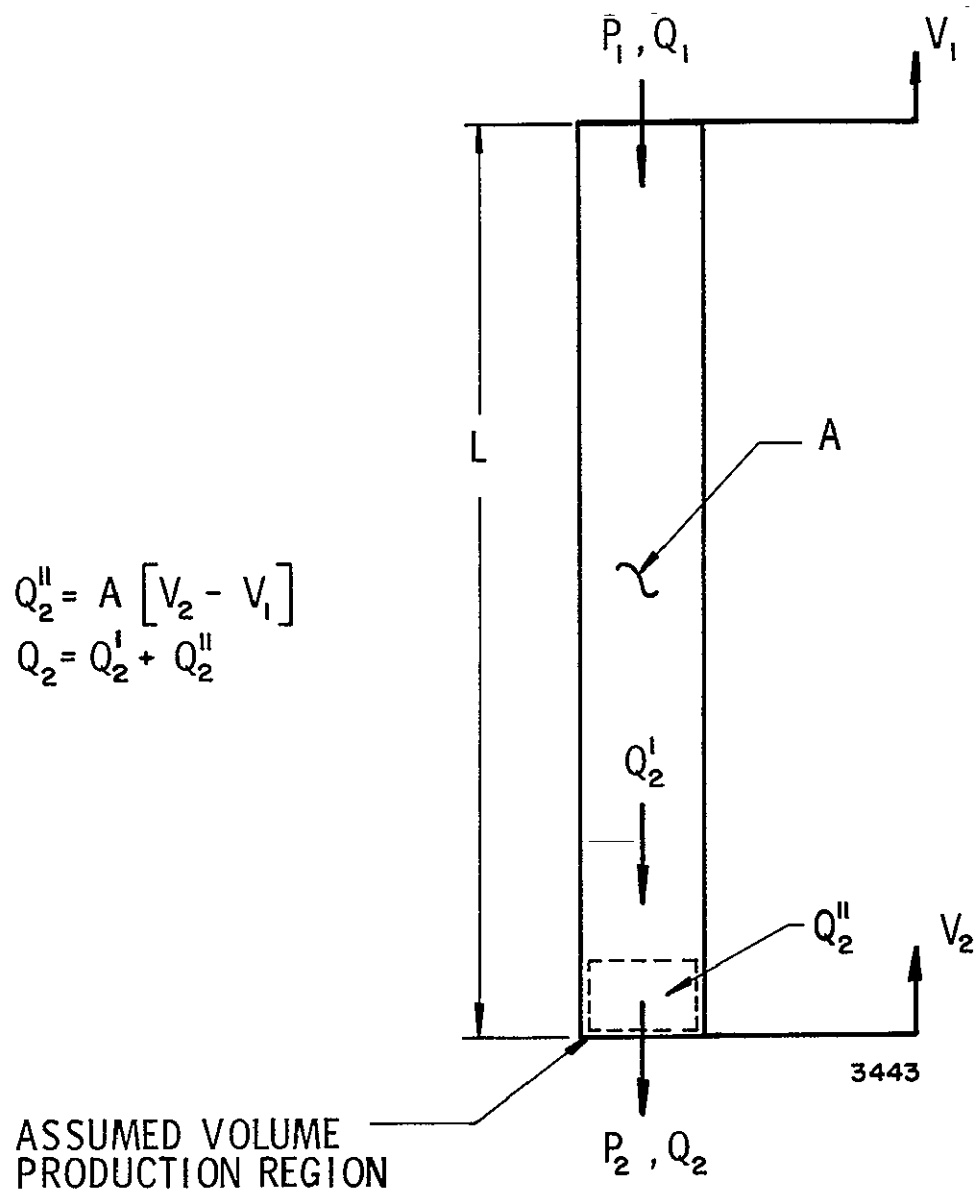
Figure 17. Illustration Of Approximate Modeling Procedure For
Forced Changes In Line Length

42

The first method of analysis begins with the Laplace transform version of the linearized (1) radial and axial equations of motion for the fluid, (2) continuity equation, and (3) the equation of state. These equations are reduced to one-dimensional form by averaging across the feedline cross section. The solution of the resulting differential equations for the transformed axial velocity is matched to the transformed, inhomogeneous compatibility condition on wall velocity. This boundary condition is obtained by solving the undamped wave equation for the wall.

The physical problem is shown in Figure 18. Liquid propellant is flowing through a constant area duct of length L, internal radius r_o, and wall thickness t. The terminal ends of the line are acted upon by structural velocities having arbitrary relative phase and magnitude. The relative motion due to this excitation is assumed to be small in the linearized sense.

X = 0
p = p$_1$(t)
q = q$_1$(t)

X = L
p = p$_2$(t)
q = q$_2$(t)
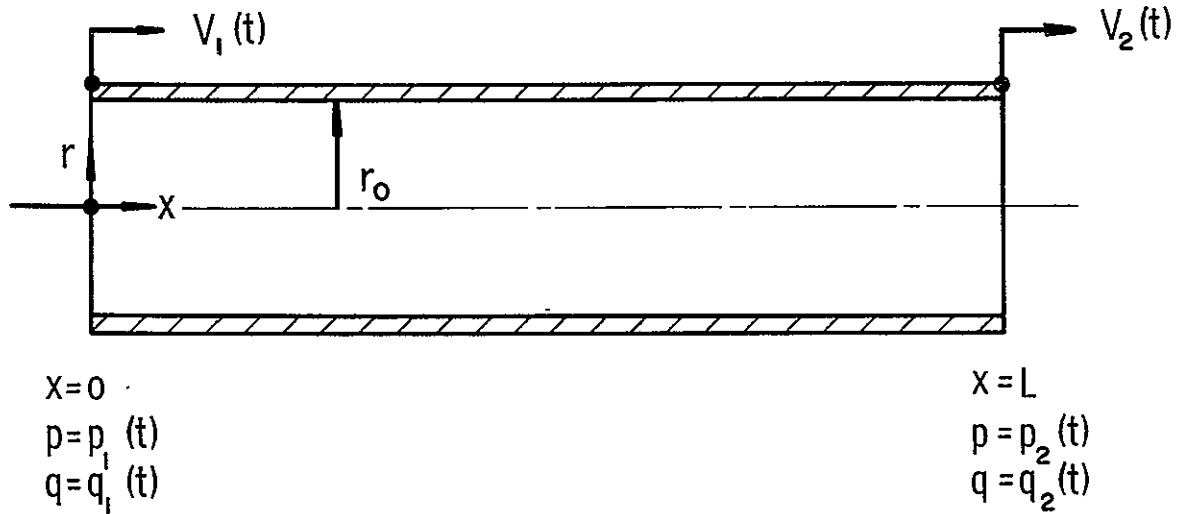
Figure 18. Geometry For Forced Changes In Line Length

The following assumptions and assertions are made with regard to the fluid flow:

(1) The flow is viscous, incompressible and axisymmetric;

(2) Viscosity remains constant;

(3) The flow is laminar; this assumption is not a severe constraint because the added attenuation due to turbulence can be adequately taken into account through the use of the modified propagation operator described in Section II;

(4) The pressure and the axial and radial components of flow consist of a steady-state level plus a perturbation value;

(5) The axial velocity perturbation, v, is much larger than the radial perturbation, v_r;

(6) Velocity gradients in the axial direction contribute a negligible amount to the viscous dissipation forces;

(7) Spatial derivatives of the density can be neglected since the compressibility of the liquid propellant is extremely low.

D'Souza and Oldenberger[17] have shown that when these assumptions are applied to the Navier-Stokes equations in cylindrical coordinates, the continuity equation and the equation of state, the following linearized differential equations describe the flow field:

$$\rho_o \frac{\partial v}{\partial t} = -\frac{\partial p}{\partial x} + \mu_o \left[\frac{\partial^2 v}{\partial r^2} + \frac{1}{r} \frac{\partial v}{\partial r} \right] \tag{81}$$

$$\frac{1}{\varkappa} \frac{\partial p}{\partial t} + \frac{\partial v_r}{\partial r} + \frac{v_r}{r} + \frac{\partial v}{\partial x} = 0 \tag{82}$$

These expressions are easily recognizable as the equation of motion in the axial direction and the combined continuity and state equations, where $\varkappa$ is the fluid bulk modulus of elasticity. In addition, absence of an equation of motion in the radial direction implies that the pressure is constant across the cross section, i.e., $p = p(x, t)$.

The relative motion in the line wall is governed by the wave equation

$$\frac{\partial^2 y}{\partial t^2} = c_w^2 \frac{\partial^2 y}{\partial x^2} , \qquad c_w^2 = \frac{E_t}{\rho_t} \tag{83}$$

where y is the axial displacement of a point in the wall and c_w is the longitudinal wave speed in the wall. Equation (83) is subject to the imposed boundary conditions

$$\frac{\partial y(o, t)}{\partial t} = V_1(t) \qquad \text{and} \qquad \frac{\partial y(L, t)}{\partial t} = V_2(t) \tag{84}$$

The no-slip compatibility condition at the wall-fluid interface is

$$\frac{\partial y(x,t)}{\partial t} = v(x, r_o, t) \tag{85}$$

The solution for the flow field proceeds in the Laplace transform domain noting that the average pressure perturbation at an arbitrary cross section, $\bar{p}(x,t)$, is equal to the actual perturbation, $p(x,t)$. The transform of the equation of motion with zero initial conditions yields ·

$$\frac{\partial^2 V}{\partial r^2} + \frac{1}{r} \frac{\partial V}{\partial r} - \frac{s}{\nu} \left(V + \frac{1}{\rho_o s} \frac{\partial \bar{P}}{\partial x} \right) = 0 \tag{86}$$

where the upper case letters indicate transformed variables. Since $\bar{P}$ is independent of the radial coordinate, Equation (86) can be reduced to an expression involving only one dependent variable by the transformation of variables

$$U = V + \frac{1}{\rho_o s} \frac{\partial \bar{P}}{\partial x} \tag{87}$$

Combining Equations (86) and (87) yields a Bessel type differential equation with one finite solution at $r = 0$.

$$U = f(x, s) J_o (\xi r) \tag{88}$$

where $\xi = \sqrt{-s/\nu}$ and $f(x, s)$ is an undefined function which must be determined. Therefore, the transformed velocity, V, becomes

$$V = f(x, s) J_o(\xi r) - \frac{1}{\rho_o s} \frac{\partial \bar{P}}{\partial x} \tag{89}$$

Solution of the wave equation in the wall subject to the prescribed boundary conditions yields

$$Y(x, s) = B_1 \cosh \frac{sx}{c_w} + B_2 \sinh \frac{sx}{c_w} \tag{90}$$

where $B_1 = \dfrac{V_1(s)}{s}$ and $B_2 = \dfrac{V_2(s) - V_1(s) \cosh sL/c_w}{s \sinh sL/c_w}$.

Combining the transformed compatibility condition, Equation (85), with (89) and (90), produces

$$\frac{1}{\rho_o s} \frac{\partial \bar{P}}{\partial x} = f(x, s) J_o(\xi r_o) - s\left[B_1 \cosh \frac{sx}{c_w} + B_2 \sinh \frac{sx}{c_w} \right] \tag{91}$$

45

Substituting this result into Equation (89) and averaging over the cross section yields

$$\bar{V} = f(x, s)\left[\frac{2J_1(\xi r_0)}{\xi r_0} - J_0(\xi r_0)\right] + s\left[B_1 \cosh\frac{sx}{c_w} + B_2 \sinh\frac{sx}{c_w}\right] \quad (92)$$

As before, barred quantities indicate average values. If the continuity equation is transformed and then averaged across the cross section, the result is

$$\bar{P} = -\frac{\kappa}{s}\frac{\partial \bar{V}}{\partial x} \quad (93)$$

Note that the dependence on radial velocity vanishes since there is no net radial flow. Differentiating this result with respect to x and incorporating Equations (92) and (91) yields a second-order, inhomogeneous, ordinary differential equation for the arbitrary function f(x, s). After considerable algebraic manipulation, the equation takes the following form:

$$\frac{d^2f}{dx^2} - \gamma^2 f = -\left(1 - \frac{c_0^2}{c_w^2}\right)\frac{s\gamma^2}{J_0(\xi r_0)}\, g(x, s) \quad (94)$$

where

$$\gamma^2 = \frac{s^2}{c_0^2\left[1 - \frac{2J_1(\xi r_0)}{\xi r_0 J_0(\xi r_0)}\right]}$$

and

$$g(x, s) = B_1 \cosh\frac{sx}{c_w} + B_2 \sinh\frac{sx}{c_w}$$

A particular integral of Equation (94) is easily obtained by the method of undetermined coefficients because of the cyclic nature of the inhomogeneous function g(x, s). The general solution of Equation (94) is

$$f(x, s) = (A_1 \cosh\gamma x + A_2 \sinh\gamma x) + \left(C_1 \cosh\frac{sx}{c_w} + C_2 \sinh\frac{sx}{c_w}\right) \quad (95)$$

where A_1 and A_2 are undetermined functions of the Laplace variable s and C_1 and C_2 are related to B_1 and B_2 by

$$C_i = \frac{-\left(1 - \frac{c_0^2}{c_w^2}\right)s\gamma^2 B_i}{\left(\frac{s^2}{c_w^2} - \gamma^2\right)J_0(\xi r_0)} \qquad i = 1, 2 \quad (96)$$

46

After simplification, the transformed velocity field, Equation (92) becomes

$$\overline{V} = (A_1 \cosh \gamma x + A_2 \sinh \gamma x) \left(\frac{2 J_1(\xi r_0)}{\xi r_0} - J_0(\xi r_0) \right) +$$

$$\frac{s \left(\dfrac{s^2}{c_0^2} - \gamma^2 \right)}{\left(\dfrac{s^2}{c_\mathrm{W}^2} - \gamma^2 \right)} \left(B_1 \cosh \frac{sx}{c_\mathrm{W}} + B_2 \sinh \frac{sx}{c_\mathrm{W}} \right) \qquad (97)$$

Noting that $\varkappa = \rho_0 c_0^2$, the pressure field is obtained from Equation (93).

$$\overline{P} = \frac{-\rho_0 c_0^2}{s} \left[(A_1 \gamma \sinh \gamma x + A_2 \gamma \cosh \gamma x) \left(\frac{2 J_1(\xi r_0)}{\xi r_0} - J_0(\xi r_0) \right) + \right.$$

$$\left. \frac{s \left(\dfrac{s^2}{c_0^2} - \gamma^2 \right)}{\left(\dfrac{s^2}{c_\mathrm{W}^2} - \gamma^2 \right)} \left(B_1 \frac{s}{c_\mathrm{W}} \sinh \frac{sx}{c_\mathrm{W}} + B_2 \frac{s}{c_\mathrm{W}} \cosh \frac{sx}{c_\mathrm{W}} \right) \right] \qquad (98)$$

Coefficients A_1 and A_2 can be eliminated by evaluating the pressure and velocity at the extremities of the line, i.e.,

$$\overline{P}(o, s,) = \overline{P}_1 \qquad\qquad \overline{P}(L, s) = \overline{P}_2$$

$$\overline{V}(o, s,) = \overline{V}_1 \qquad\qquad \overline{V}(L, s) = \overline{V}_2 \qquad (99)$$

In the process of making these evaluations, the characteristic impedance, Z_c, can be defined in terms of the propagation operator, γ,

$$Z_c = \frac{\rho_0 c_0^2 \gamma}{s}$$

Applying boundary conditions (99) to Equations (98) and (97) incorporating the expressions for B_1 and B_2, and imposing the condition that $V_2(s) = G(s) V_1(s)$ and $Q(s) = AV(s)$

$$\begin{bmatrix} \overline{P}_2 \\[2ex] \overline{U}_2 \end{bmatrix} = \begin{bmatrix} \cosh \gamma L & - Z_c \sinh \gamma L \\[2ex] - Z_c^{-1} \sinh \gamma L & \cosh \gamma L \end{bmatrix} \begin{bmatrix} \overline{P}_1 \\[2ex] \overline{U}_1 \end{bmatrix} - \frac{\left(\dfrac{s^2}{c_0^2} - \gamma^2 \right)}{\left(\dfrac{s^2}{c_\mathrm{W}^2} - \gamma^2 \right)} V_1(s) \begin{bmatrix} \alpha_1 \\[2ex] \alpha_2 \end{bmatrix} \qquad (101)$$

where

47

$$\alpha_1 = \frac{\rho_0 c_0^2}{s}\left[\left(\frac{s}{c_H}\sinh\frac{sL}{c_H} - \gamma\sinh\gamma L\right) + \frac{\left(G - \cosh\frac{sL}{c_H}\right)}{\sinh\frac{sL}{c_H}}\frac{s}{c_H} \times \left(\cosh\frac{sL}{c_H} - \cosh\gamma L\right)\right] \quad (102)$$

$$\alpha_2 = -\left[\left(\cosh\frac{sL}{c_H} - \cosh\gamma L\right) + \frac{\left(G - \cosh\frac{sL}{c_H}\right)}{\sinh\frac{sL}{c_H}}\left(\sinh\frac{sL}{c_H} - \frac{s}{c_H\gamma}\sinh\gamma L\right)\right] \quad (103)$$

The assumed dependence of $V_2(s)$ on $V_1(s)$ is entirely realistic since the vehicle structural velocities, which are the forcing functions, are generally describable by transfer functions.

Equation (101) represents the desired result for forced changes in line length. The column matrix in Equation (101) represents a pressure-flow modification to the square matrix that describes pressure and flow in the absence of external excitation. It can be shown that when $V_1 = V_2$ the above expressions degenerate to

$$\begin{bmatrix} P_2 \\ Q_2 \end{bmatrix} = \begin{bmatrix} \cosh\gamma L & -Z_c A^{-1}\sinh\gamma L \\ -A Z_c^{-1}\sinh\gamma L & \cosh\gamma L \end{bmatrix}\begin{bmatrix} P_1 \\ Q_1 \end{bmatrix} + Vf\begin{bmatrix} Z_c\sinh\gamma L \\ A(1-\cosh\gamma L) \end{bmatrix} \quad (104)$$

where

$$f = \frac{2 J_1(\xi r_0)}{\xi r_0 J_0(\xi r_0)}$$

This latter result was predicted by Gerlach[18] for rigid body, axial vibration of a line, where coupling occurs through viscous shear.

In the second modeling approach, the pressure-flow equations for the rigid body motion of a line are modified with a volume production element that reflects the relative motion of the ends of the line. For a rigid line oscillating with velocity, V_1,

$$\begin{bmatrix} P_2 \\ Q_2' \end{bmatrix} = \begin{bmatrix} \cosh\gamma L & -A^{-1} Z_c\sinh\gamma L \\ -Z_c^{-1} A\sinh\gamma L & \cosh\gamma L \end{bmatrix}\begin{bmatrix} P_1 \\ Q_1 \end{bmatrix} - V_1\begin{bmatrix} Z_c\sinh\gamma L \\ A(1-\cosh\gamma L) \end{bmatrix} \quad (105)$$

The rate of volume generation due to relative motion is

$$Q_2'' = A(V_2 - V_1) \quad (106)$$

Total volumetric flow rate is then the sum of Q_2' and Q_2''. Combining Equations (105) and (106) yields

$$\begin{bmatrix} P_2 \\ Q_2 \end{bmatrix} = \begin{bmatrix} \cosh \gamma L & -A^{-1} Z_c \sinh \gamma L \\ -Z_c^{-1} A \sinh \gamma L & \cosh \gamma L \end{bmatrix} \begin{bmatrix} P_1 \\ Q_1 \end{bmatrix} - V_1 \begin{bmatrix} Z_c \sinh \gamma L \\ A(2 - \cosh \gamma L - G(s)) \end{bmatrix} \quad (107)$$

As before, $G(s)$ describes the relationship between the externally imposed velocities, V_1 and V_2.

Equations (101) and (107) cannot be compared directly since, in the first case, the excitation is coupled to the fluid by a boundary condition and, in the latter case, the coupling takes the form of a body force applied to the fluid.

We believe that the result obtained by treating the problem as an inhomogeneous boundary valued problem is the most accurate, and it is this expression, Equation (101), that has been incorporated into the computer code.

V. 4.   Mounting Stiffness

Propellant feedlines are anchored to the primary vehicle structure by mounting brackets that exhibit varying degrees of elasticity and damping. These brackets act as filters which modify the structural excitation that is transmitted to the feedline. There are two techniques that can be utilized in modeling the effect of mounting stiffness: (1) discrete parameter-acceleration, and (2) impedance. Both of these methods are summarized in this section. The transfer equations for the discrete parameter-acceleration technique have been programmed as Subroutine Eight in the computer program while the impedance approach is programmed in Subroutine Ten.

Discrete Parameter-Acceleration Technique

Consider the idealized configuration shown in Figure 19. The entire line, which has two bends, is assumed to be infinitely rigid and elastically restrained. A single linear spring in parallel with a viscous damper represents the combined effect of all the discrete mounting stiffnesses whose line of action coincides with that of the equivalent mounting stiffness. In Section V. 1, an expression was derived for the pressure and flow rate in a vertical line that is excited by a velocity, V_ℓ, applied directly to the line. That expression forms the starting point for the analysis of the present configuration. Initially, the velocity, $V_\ell(s)$, is replaced by its Laplace equivalent, $a_\ell(s)/s$. It was shown in Section V. 1 that the four-terminal representation of a vertically accelerated line is

49

Figure 19. Model For A Line With Mounting Stiffness

$$\begin{bmatrix} P_3 \\ \\ Q_3 \end{bmatrix} = \begin{bmatrix} \cosh\gamma L & -Z_c A^{-1}\sinh\gamma L \\ \\ -AZ_c^{-1}\sinh\gamma L & \cosh\gamma L \end{bmatrix} \begin{bmatrix} P_2 \\ \\ Q_2 \end{bmatrix} - \frac{a_\ell(s)}{s} \begin{bmatrix} Z_c\sinh\gamma L \\ \\ A(1-\cosh\gamma L) \end{bmatrix} \qquad (108)$$

The problem is to express the resultant line acceleration, $a_\ell(s)$, in terms of the applied structural acceleration, $a_i(s)$, the viscoelastic support parameters, and the fluid mass contained in the horizontal limbs of the feedline. By neglecting the elbow at the exit to the fuel tank, this aspect of the problem is easily overcome by viewing the entire system as a damped, harmonic oscillator whose mass is equivalent to the combined liquid mass in the horizontal limbs. The support is excited by $a_i(s)$, and the inertial effects in the vertical line segment are taken into account by applying the dynamic fluid pressure forces on the projected areas of the elbows on the system mass.

During oscillatory motion, the mass of fluid contained in the transverse limbs of the feedline contributes an added mass, $(m_1 + m_3)$, effect. The inertial loading, due to the fluid mass in the vertical segment of the line, is replaced by the equivalent dynamic pressure forces. For a support of negligible mass, the differential equation of motion for mass M about its equilibrium position is.

$$M\ddot{x} = -k(x-y) - b(\dot{x}-\dot{y}) + A(p_3-p_2) \qquad (109)$$

Transforming this result into the Laplace domain and noting that

$$\mathscr{L}\{x\} = X, \qquad \mathscr{L}\{y\} = Y \qquad (110)$$

and

$$s^2 X = a_\ell(s), \qquad s^2 Y = a_i(s) \qquad (111)$$

the following result is obtained.

$$a_\ell(s) = a_i(s)\left[\frac{sb+k}{Ms^2+sb+k}\right] + A[P_3(s)-P_2(s)]\left[\frac{s^2}{Ms^2+sb+k}\right] \qquad (112)$$

The first term in Equation (112) reflects the externally imposed acceleration, and the second term reflects a passive inertial loading.

51

A straightforward combination of Equations (112) and (108) produces, after some manipulation,

$$
\begin{bmatrix} P_3 \\ \\ Q_3 \end{bmatrix} = \begin{bmatrix} \dfrac{L_{11}+\beta'}{1+\beta'} & \dfrac{L_{12}}{1+\beta'} \\ \\ \dfrac{L_{21}+\beta''(1-L_{11})}{1+\beta'} & \dfrac{L_{22}-\beta''L_{12}}{1+\beta'} \end{bmatrix} \begin{bmatrix} P_2 \\ \\ Q_2 \end{bmatrix} - \dfrac{a_i(s)}{1+\beta'} \begin{bmatrix} \alpha' \\ \\ \alpha'' \end{bmatrix}
\tag{113}
$$

where the L_{ij} $(i, j = 1, 2)$ are the elements of the original square matrix in Equation (108) and

$$
\alpha' = \frac{sb+k}{s(Ms^2+sb+k)} \, Z_c \sinh \gamma L
$$

$$
\beta' = \frac{As}{(Ms^2+sb+k)} \, Z_c \sinh \gamma L
$$

$$
\tag{114}
$$

$$
\alpha'' = \frac{sb+k}{s(Ms^2+sb+k)} \, A(1-\cosh \gamma L)
$$

$$
\beta'' = \frac{A^2 s(1-\cosh \gamma L)}{Ms^2+sb+k}
$$

All other terms have been defined previously. The input acceleration, $a_i(s)$, could be replaced by the equivalent velocity representation, $s V_i(s)$. However, this replacement would require a minor computer code modification since the program currently determines the response to acceleration, $a_i(s)$. As the support becomes progressively stiffer, Equation (113) degenerates into the expression for a simple accelerated line.

Equations (113) and (114) represent the complete transfer functions for the discrete parameter-acceleration technique for a feedline segment with external accelerations applied through a mounting structure with arbitrary stiffness. This technique has been programmed into the computer code as Subroutine Eight.

A second method of analysis of problems involving structural mounting stiffness will now be presented, where the line accelerations (or velocities) are expressed in terms of the structural driving point impedance.

52

Impedance Technique

The impedance technique will now be applied to the same line configuration that was used in the previous case with the exception that the mounting stiffness which consisted of a grounded acceleration, a_1, and a viscoelastic support is replaced by a driving point impedance, Z_s. As before, the starting point for the analysis is the four-terminal representation of line that is subject to velocity excitation, $V_\ell(s)$. It is required that the line velocity be expressed in terms of the imposed forces and ultimately in terms of the driving point impedance. The support exerts a force, F, on the feedline, and the equation of motion for this system that corresponds to Equation (109) is

$$M\ddot{x}_\ell = -F + A_{-}(p_3 - p_2) \tag{115}$$

Applying the Laplace transformation to this expression yields

$$Ms\, V_\ell(s) = -F(s) + A\,[p_3(s) - p_2(s)] \tag{116}$$

The driving point impedance is, by definition,

$$Z_s(s) = \frac{F(s)}{V_\ell(s)} \tag{117}$$

Eliminating $F(s)$ between Equations (116) and (117) produces

$$V_\ell(s) = \frac{A(P_3 - P_2)}{Z_s + Ms} \tag{118}$$

Equation (118) may be introduced into Equation (108) and the following result is obtained after rearrangement:

$$
\begin{bmatrix} P_3 \\ \\ Q_3 \end{bmatrix} =
\begin{bmatrix} \dfrac{L_{11}+\alpha}{1+\alpha} & \dfrac{L_{12}}{1+\alpha} \\ \\ L_{21}+\dfrac{\beta(1-L_{11})}{1+\alpha} & L_{22}-\dfrac{\beta L_{12}}{1+\alpha} \end{bmatrix}
\begin{bmatrix} P_2 \\ \\ Q_2 \end{bmatrix} \tag{119}
$$

where

$$\alpha = \frac{AZ_{c2}\sinh\Gamma_2}{Z_s + Ms}$$

$$\beta = \frac{A^2(1-\cosh\Gamma_2)^2}{Z_s + Ms}$$

$$L_{ij} = \text{elements of original square matrix in Equation (108).}$$

53

The obvious difference between Equations (113) and (119) is that the latter does not contain the trailing column vector that reflects the enforced excitation. In the latter formulation the effect of the mounting support (structural impedance) is absorbed into the square matrix. Both formulations degenerate into the simple stationary line representation for an infinitely stiff support.

VI. GENERALIZED FEEDLINE COMPUTER CODE

A versatile computer code has been generated to calculate the frequency response of propellant feedlines. Program philosophy and logic are discussed in this section, and the mechanics of setting-up and execution including specific example problems are presented in Appendix D.

The construction of a computer code to generate the frequency response of a propellant feedline is a relatively straightforward task when the sequence of feedline components (lines, bellows, PVC joints, etc.) is fixed by a specific design configuration. However, for preliminary design analyses, it is advantageous to determine the effect that a reordering of line components would produce on the overall feedline response. For example, various sequences of components could materially affect the structural-hydraulic coupling that is known to influence the instabilities that were delineated in Section I. It can readily be visualized that reprogramming the feedline response equations for numerous changes in the component sequence is an extremely expensive, time-consuming task. To alleviate this situation, a master computer code was written in FORTRAN IV for the CDC 6400 to provide the systems engineer with a design tool for obtaining the frequency response of a feedline in which the type, number and sequence of basic line components between the propellant tank and the turbopump inlet can be specified in a completely arbitrary fashion. The dominant criterion employed in generating this code was that the "user" be required to perform a minimal amount of manual conditioning of a given problem prior to machine execution.

Formulation of the code is based on the fact that the four-terminal pressure-flow relationship across <u>any line component</u> can be represented in matrix form when the perturbation equations are transformed into the Laplace domain. That is, with no loss in generality,

$$\begin{bmatrix} P_{i+1} \\ Q_{i+1} \end{bmatrix} = \underline{D}_i \begin{bmatrix} P_i \\ Q_i \end{bmatrix} \pm K \underline{C}_i; \qquad i = 1, 2, \ldots . n \qquad (120)$$

where n represents the number of components in the line. In this expression, the transformed output pressure and flow for a given component are related to the corresponding input quantities through a 2×2 square matrix, $\underline{D}_i$, plus a column matrix, $\underline{C}_i$, that is present only if that particular component is being excited by an

55

external forcing function, K. The parameter, K, may be the Laplace transform of an externally imposed acceleration or velocity, or the volume perturbation due to a side branch pulser. In general, it is desired to determine the perturbation pressure at some point in the line in response to any one of the class of forcing functions that K represents. With regard to propellant feedline analyses, the important pressure point is located at the entrance to the turbopump because dynamic variations in the inducer inlet suction head are instrumental in the growth of structural-fluid dynamic instabilities. Having established the desired output variable, the functional form of the transfer function for the overall line is obtained by applying Equation (120) to each line component followed by sequential matrix substitution to arrive at the following generalized transfer equation:

$$\underline{P} = \underline{D}\,\underline{Q} \pm K\,\underline{B} \tag{121}$$

Through experience we have found that matrix $\underline{D}$ can be stated a priori for any feedline composed of n ordered components.

$$\underline{D} = \underline{D}_n\,\underline{D}_{n-1}\,\underline{D}_{n-2}\,\ldots\,\underline{D}_1 \tag{122}$$

Matrix $\underline{B}$, however, does not possess such a well-defined property. In general,

$$\underline{B} = \underline{B}_1 + \underline{B}_2 + \ldots + \underline{B}_m \tag{123}$$

The value of "m" is strongly dependent on the line configuration as is the matrix structure of each $\underline{B}_j$. The distinguishing feature of each $\underline{B}_j$ is that it consists of a column matrix of one of the $\underline{C}_i$'s pre-multiplied by one or more $\underline{D}_i$'s. Matrix $\underline{P}$ in Equation (121) contains the desired pressure response to the perturbation, K, and matrix $\underline{Q}$ contains the pressure-flow perturbations at the exit to the fuel tank. By assuming that the impedance at the tank exit, Z_1, is known and that the turbopump-injector-engine combination can be lumped into an equivalent impedance, Z_t, Equation (121) can be expanded into its constituent equations to obtain the explicit form of the transfer function

$$\frac{P_n}{K} = \pm \frac{[\,(d_{21}Z_1 + d_{22})\,b_{11} - (d_{11}Z_1 + d_{12})\,b_{21}\,]}{(d_{21}Z_1 + d_{22}) - (d_{11}Z_1 + d_{12})/Z_t} \tag{124}$$

where the b_{ij} and d_{ij} are the elements of matrix $\underline{B}$ and $\underline{D}$, respectively.

56

To illustrate the concepts that have been presented, consider the feedline shown in Figure 20. It is desired to determine the transfer function relating the pressure at the turbopump inlet, P_6, to the line excitation velocity, V_ℓ. Adjacent to each line component is a matrix expression of the type presented in Equation (120). Performing the previously indicated matrix substitution yields

$$\begin{bmatrix} P_6 \\ P_6/Z_t \end{bmatrix} = \underline{D}_5\,\underline{D}_4\,\underline{D}_3\,\underline{D}_2\,\underline{D}_1 \begin{bmatrix} Z_1\,Q_1 \\ Q_1 \end{bmatrix} + V_\ell(\underline{D}_5\,\underline{C}_4 - \underline{D}_5\,\underline{D}_4\,\underline{C}_3 - \underline{D}_5\,\underline{D}_4\,\underline{D}_3\,\underline{C}_2) \quad (125)$$

The subscripts on pressure and flow rate pertain to specific points in the line while the subscripts on matrices $\underline{D}_i$ and $\underline{C}_i$ refer to the component location in the line. Equation (125) completely defines the generalized matrices in Equation (121). An expression similar to Equation (124) follows directly from Equation (125).

The foregoing discussion forms the basis for constructing a computer code to determine the frequency response of a feedline containing an arbitrary number and sequence of components. The computer code contains a controller program and a separate subroutine for each component in which the elements of each $\underline{D}_i$ and $\underline{C}_i$ are calculated. The program has the capability of synthesizing a feedline with as many as fifteen different types of components. However, the program listing that is presented in the Appendix contains eleven component subroutines; the four vacancies are available for the addition of components during future programs. In addition, the source deck contains two subroutines for constructing matrices $\underline{B}$ and $\underline{D}$ and one subroutine for calculating the Bessel functions J_1 and J_0 and their ratio for complex arguments.

Another subroutine calculates the speed of sound in a liquid that may or may not contain a homogeneous distribution of bubbles. In either case, the radial elasticity effects of the line may be taken into account through the Korteweg equation.

Since substitution of $i\omega$ for the Laplace variable "s" implies calculations in the complex plane, liberal use has been made of the complex variable operations afforded by FORTRAN IV. Complex quantities have been subscripted with as many as three indices to facilitate bookkeeping within the program.

In summary, the user merely defines the feedline structure as was done in Figure 20 and indexes the components sequentially beginning with the component that is attached directly to the propellant

	Station No.	Component No.	Matrix Pressure Flow Expressions
	1		$\begin{bmatrix} P_2 \\ Q_2 \end{bmatrix} = \underline{D}_1 \begin{bmatrix} P_1 \\ Q_1 \end{bmatrix}, \quad P_1 = z_i Q_1$
Stationary Line		①	
Bellows	2	②	$\begin{bmatrix} P_3 \\ Q_3 \end{bmatrix} = \underline{D}_2 \begin{bmatrix} P_2 \\ Q_2 \end{bmatrix} - V_\ell \, \underline{C}_2$
	3		
Line with Velocity Excitation		③	$\begin{bmatrix} P_4 \\ Q_4 \end{bmatrix} = \underline{D}_3 \begin{bmatrix} P_3 \\ Q_3 \end{bmatrix} - V_\ell \, \underline{C}_3$
Bellows	4	④	$\begin{bmatrix} P_5 \\ Q_5 \end{bmatrix} = \underline{D}_4 \begin{bmatrix} P_4 \\ Q_4 \end{bmatrix} + V_\ell \, \underline{C}_4$
	5		
Stationary Line		⑤	$\begin{bmatrix} P_6 \\ Q_6 \end{bmatrix} = \underline{D}_5 \begin{bmatrix} P_5 \\ Q_5 \end{bmatrix}, \quad Q_6 = P_6 / z_t$
	6		3444

V_ℓ

Combined Turbopump-Injector-Engine Impedance, z_t

Figure 20. Matrix Representation Of A Feedline In The Laplace Domain

tank. An expression of the type presented in Equation (121) is then assigned to each component. From this point, a minimal amount of matrix manipulation is then required to arrive at an expression similar to Equation (125), but which reflects the particular configuration under consideration. The flow of subsequent calculations in the program is governed by the following inputs:

(1) A coded set of integers describing the type of elements in the order in which they appear in the line,

(2) The number of $\underline{B}_i$'s that are to be summed to arrive at matrix $\underline{B}$ and

(3) The number and type of matrices that are contained in each $\underline{B}_i$.

Using the codes in Item (1), additional data, relevant to each component type, are read in and associated with a specific component location in the line. Categorically, this data can include component lengths, line radii, friction factors, bubble radii, spring constants, damping constants, liquid-vapor mass ratios, etc. The complete input package also includes information that pertains to the line in general, e.g., input and terminal impedances, thermodynamic and fluid dynamic properties of the propellant, mean flow velocity, the elastic and geometric properties of the conduit wall, and the frequency band over which the response is to be determined.

VII. EXPERIMENTAL VERIFICATION OF
THE FEEDLINE MODEL

An experimental test program has been conducted to determine the validity of the analytical model and corresponding computer program for a liquid rocket propellant feedline. A basic test apparatus, which simulated in an elementary way a typical liquid rocket feed system, was constructed and assembled; this facility was sized so that the test parameters spanned the ranges of interest. From initial baseline tests, the system complexity was expanded by introducing various effects, and experimental responses were obtained for comparison with the computer analysis.

VII.1 Experimental Feedline Test Facility

The basic objectives in the design of the experimental feedline test facility were to approximately simulate the pressure response (amplitude and frequency) generated by a typical feedline excited by various means, while using water as the internal fluid rather than an actual rocket propellant or LOX. One feedline perturbation technique is illustrated in Figure 21 in which the feedline is externally excited by introducing a dynamic volume flow perturbation superposed on the steady mean flow. This technique has been used by other researchers [1, 19, 20] to obtain the dynamic response of specific feedline configurations, and it was chosen as the excitation scheme for the initial tests conducted in this experimental program due to its relative controlability.

Dimensional analysis of a problem involving a typical LOX feedline with a finite terminal resistance and excited by a flow pulsar revealed that the following similarity parameters should be observed for exact simulation by the experimental facility:

$$\frac{P_{1_m}}{Z_{t_m} Q_m} = \frac{P_1}{Z_t Q} \tag{126}$$

$$\frac{Q_{1_m}}{Q_m} = \frac{Q_1}{Q} \tag{127}$$

$$\frac{Q_{4_m}}{Q_{1_m}} = \frac{Q_4}{Q_1} \tag{128}$$

$$\frac{\rho_m Q_m}{\mu_m d_m^2} = \frac{\rho Q}{\mu d^2} \tag{129}$$

$$\frac{c_{o_m}^2 \rho_m}{Z_{t_m} Q_m} = \frac{c_o^2 \rho}{Z_t Q} \tag{130}$$

$$\frac{L_m^4 Z_{t_m}}{Q_m \rho_m} = \frac{L^4 Z_t}{Q \rho} \tag{131}$$

$$\frac{L_m}{d_m} = \frac{L}{d} \tag{132}$$

$$\frac{Q_{d_m}}{Q_m} = \frac{Q_d}{Q} \tag{133}$$

60

$$\frac{P_4}{\rho_0 C_0 A^{-1} Q_d} = \frac{\sinh \gamma L}{\rho_0 C_0 Z_t^{-1} A^{-1} \sinh \gamma L + \cosh \gamma L}$$

LIQUID (ρ_0, C_0)

Z_t = TERMINAL IMPEDANCE

γ = PROPAGATION OPERATOR
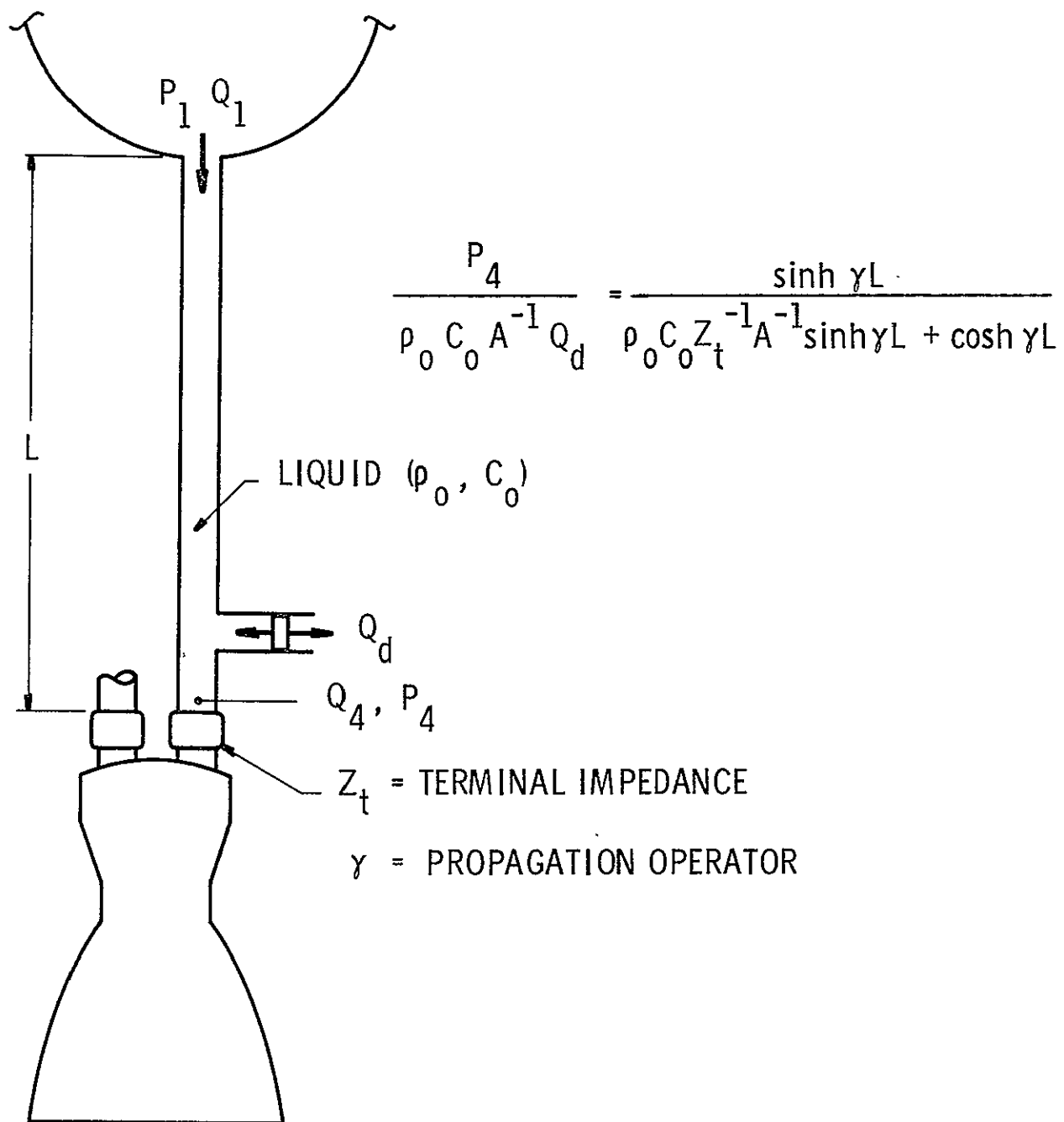
Figure 21. Illustration of Feedline Excited by a Pulsar

$$\frac{\omega_m L_m}{c_{o_m}} = \frac{\omega L}{c_o} \qquad (134)$$

$$\gamma_m L_m = \gamma L \qquad (135)$$

$$\frac{P_{4_m}}{Z_{t_m} Q_m} = \frac{P_4}{Z_t Q} \qquad (136)$$

where m = model.

Ideally, it was initially desired to simulate a typical LOX feedline approximately 30 ft long and 8 in. in diameter with water as the fluid medium in a line 3 in. in diameter. The 3-in. diameter line was chosen based on available pumping equipment and power requirements. This allowed for the generation of a turbulent mean flow at the test conditions, which was necessary for verification of the turbulent flow propagation operator model developed for the computer program. The actual length of the line was 27 ft, and this dimension was chosen to obtain a first longitudinal mode resonant frequency with water in a rigid line of approximately 45 Hz. This provided a low enough resonant frequency such that the hydraulic actuator which drove the side branch pulsar piston operated with a suitable amplitude so as to produce a reasonable (measurable) pressure response slightly past the first anti-resonance.

From the scaling laws presented above, the response of a LOX-filled line of the same relative geometry as that of the model can be easily obtained. The primary frequency responses obtained during the test were the terminal impedance amplitudes, defined as the dynamic pressure perturbation amplitude, P_4, at the line terminus divided by the input dynamic volume flow perturbation amplitude, Q_d.

Dividing the similarity parameter in Equation (136) by Equation (133), the corresponding LOX line pulsar impedance amplitude can be obtained from the experimental model amplitude as

$$\frac{P_4}{Q_d} = \left(\frac{P_4}{Q_d}\right)_m \frac{Z_t}{Z_{t_m}} \qquad (137)$$

Combining Equations (129) and (130), the ratio of the terminal resistances required for the simultaneous simulation of viscous effects (Reynolds number) and compressibility (acoustic effects) becomes

$$\frac{Z_t}{Z_{t_m}} = \frac{\rho^2 c_o^2}{\rho_m^2 c_{o_m}^2} \frac{\mu_m d_m^2}{\mu d^2} \qquad (138)$$

while the corresponding frequencies are determined from

$$\omega = \omega_{\text{m}} \frac{L_{\text{m}}}{c_{o_{\text{m}}}} \left(\frac{c_o}{L} \right) \tag{139}$$

From the remaining similarity or scaling laws, all the parameters that would exist in the simulated LOX feedline can be computed; each variable in the model has a corresponding value in the simulated LOX feedline case.

A schematic of the feedline flow facility used for the basic tests is presented in Figure 22. Shown are the relative locations of the lower reservoir, pump, hydraulic motor, upper reservoir, supply line and feedline, the pulsar piston, hydraulic actuator and terminal impedance or resistance. The photograph in Figure 23 reveals the actual relative sizes of each of the lower components, including the tower and support structure. The flow was produced by a five-stage, deep-well type turbine pump, capable of producing 600 gallons/minute with a total dynamic head of 460 ft at 3500 rpm. The pump was powered by a Vickers fixed-displacement, piston-type hydraulic motor rated at 100 HP at 3600 rpm. The side branch pulsar piston was driven by a MOOG hydraulic servo valve and actuator assembly with a static force capability of 10,000 lb force decreasing to 6,000 lb at 100 Hz. The maximum stroke of this unit was 2.84 inches. The piston area was designed large enough to produce a dynamic pressure amplitude equal to 50 psi (100 psi peak-to-peak) with the use of a relatively low terminal resistance, $Z_t = 1.9 \times 10^5$ lb-sec/ft^5.

The transfer function relating the pressure response at the line terminal to the input dynamic flow perturbation, Q_d, for the line configuration used in the base line tests is given by

$$\frac{P_4}{Q_d} = \frac{Z_c A^{-1} \sinh (\gamma L) \cdot}{(Z_c/AZ_t) \sinh (\gamma L) + \cosh (\gamma L)} \tag{140}$$

For an inviscid model, the terminal impedance amplitude at resonance is simply equal to the value of the terminal resistance,

$$\frac{P_4}{Q_d} = Z_t \tag{141}$$

and from this expression, the required volume flow perturbation amplitude was found to be $Q_d = 0.076$ ft^3/sec. It was desired to conduct a given test with constant input perturbation amplitude over the frequency range; therefore, the piston stroke required was given by

63
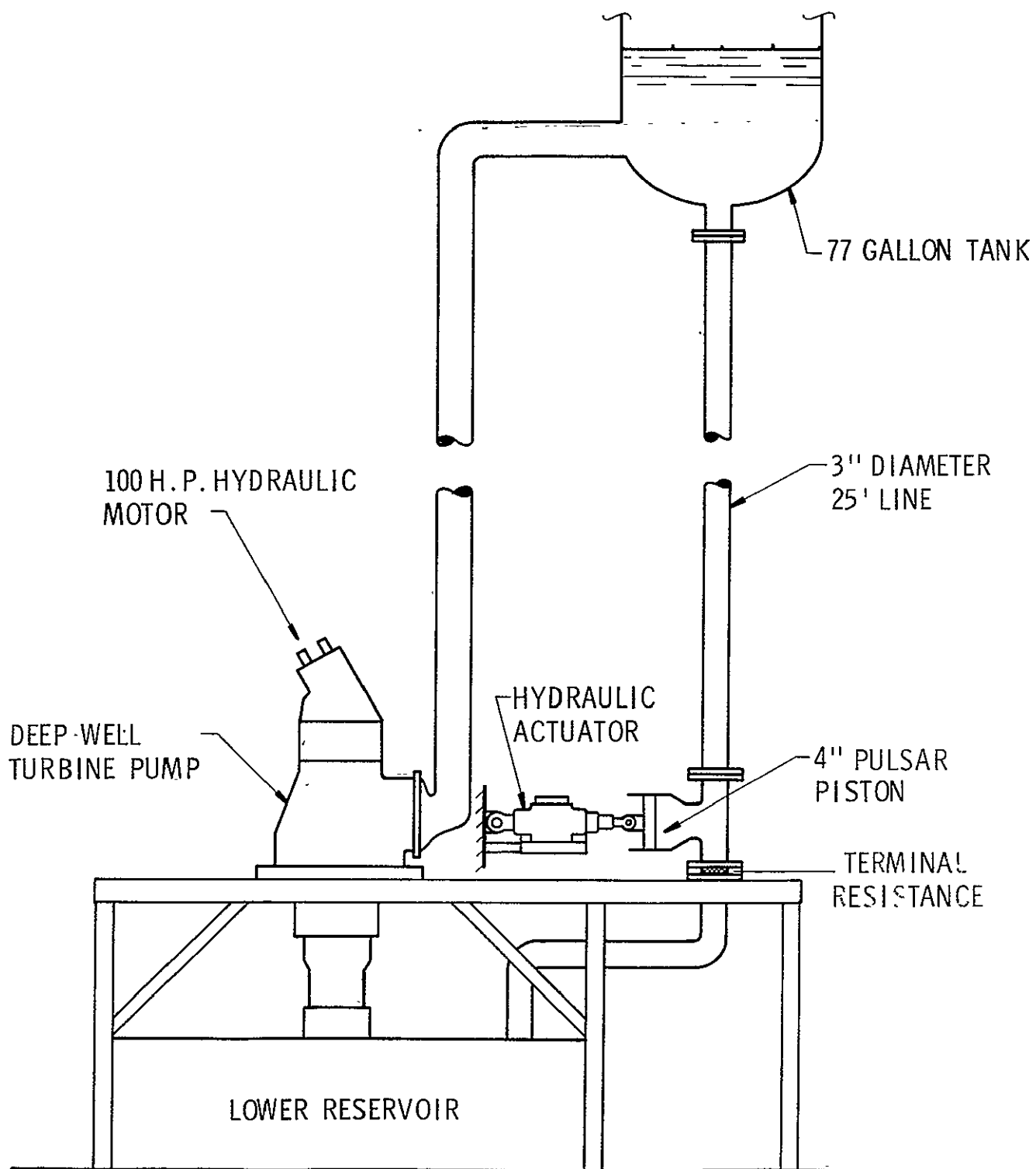
Figure 22. Flow Facility for Current Experimental Program

77 GALLON TANK

3" DIAMETER 25' LINE

100 H.P. HYDRAULIC MOTOR

HYDRAULIC ACTUATOR

DEEP-WELL TURBINE PUMP

4" PULSAR PISTON

TERMINAL RESISTANCE

LOWER RESERVOIR
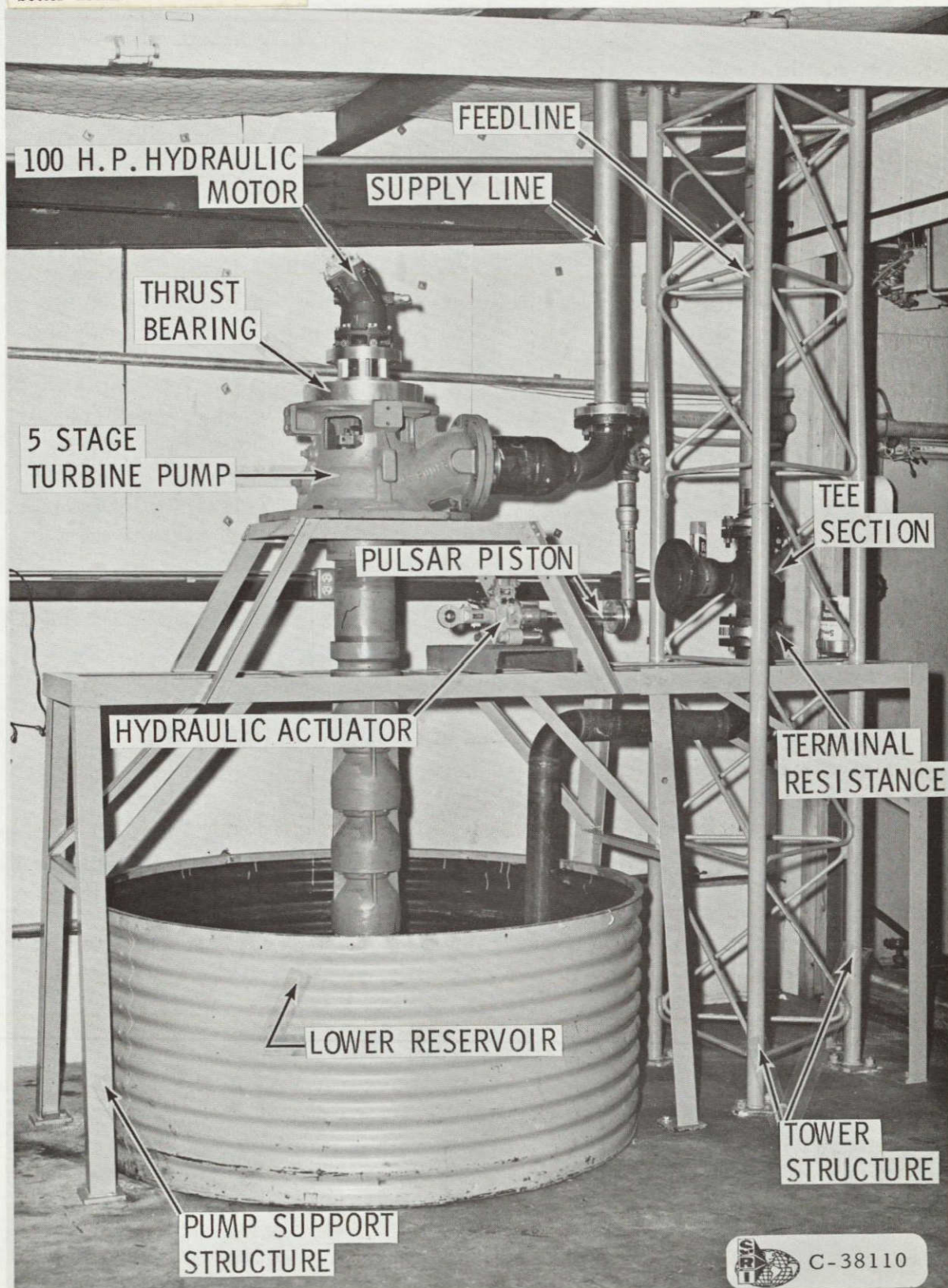
Figure 23. Lower Portion of Feedline Facility

65

$$X_o = \frac{Q_d}{2\pi f A_p}$$

(142)

where f is the input or excitation frequency and A_p is the piston frontal area. Figure 24 presents the hydraulic actuator stroke limit, which is based on a maximum servo valve flow amplitude of 44.8 cubic inches per second (peak-to-peak) at 100 Hz and an internal actuator piston area equal to 3.3 inches^2. Also shown is the stroke required versus frequency for the pulsar piston with diameter equal to 4 inches.

The upper reservoir was fabricated from a 77-gallon stainless steel tank, rated at 400 psi. For all tests conducted, an inlet impedance approximately equal to zero was provided by trapping air in the top of the tank so as to provide a liquid-gas interface. The base of the reservoir support structure was 30 ft above ground level, and was supported by a triangular tower composed of three sections, each 10 ft long. The actual length of each line was 25 ft, the remaining 2 ft being 1 ft for the pulsar "tee" section and the other length connected to the tank outlet. Figure 25 presents a photograph showing a close-up view of the pulsar "tee" section, the hydraulic actuator, and the pulsar piston cylinder. The piston was sealed with an "O" ring, and lubrication was provided from the rear by filling the remainder of the cylinder bore with hydraulic oil, which was displaced periodically into the attached accumulator.

Instrumentation

A simplified schematic of the basic instrumentation required for the experimental testing is shown in Figure 26. The flow of hydraulic pressure into the actuator was controlled by the servo controller. The servo control system consisted basically of a DC "set point" input which set the hydraulic actuator at the mid-range of its stroke, plus a sinusoidal input to generate the flow perturbations. The feedback from the piston was obtained by means of a velocity transducer. The servo controller electronic circuit is shown in Figure 27. The servo controller/valve was driven by an electronic oscillator, from which the input frequency and amplitude could be manually controlled. The input flow perturbation amplitude was measured with a Sanborn linear velocity transducer, which had a sensitivity of 94 millivolts/inch/second and a maximum stroke of 1.0 inch. From the known piston area, the flow perturbation amplitude, Q_d was calculated in cubic ft/second. The flow perturbation amplitude was displayed on the oscilloscope and controlled manually at each frequency setting since the control loop was open. The velocity transducer can be seen in Figure 25.

The dynamic pressure response was measured through the employment of Kistler 603A piezoelectric quartz dynamic pressure

66
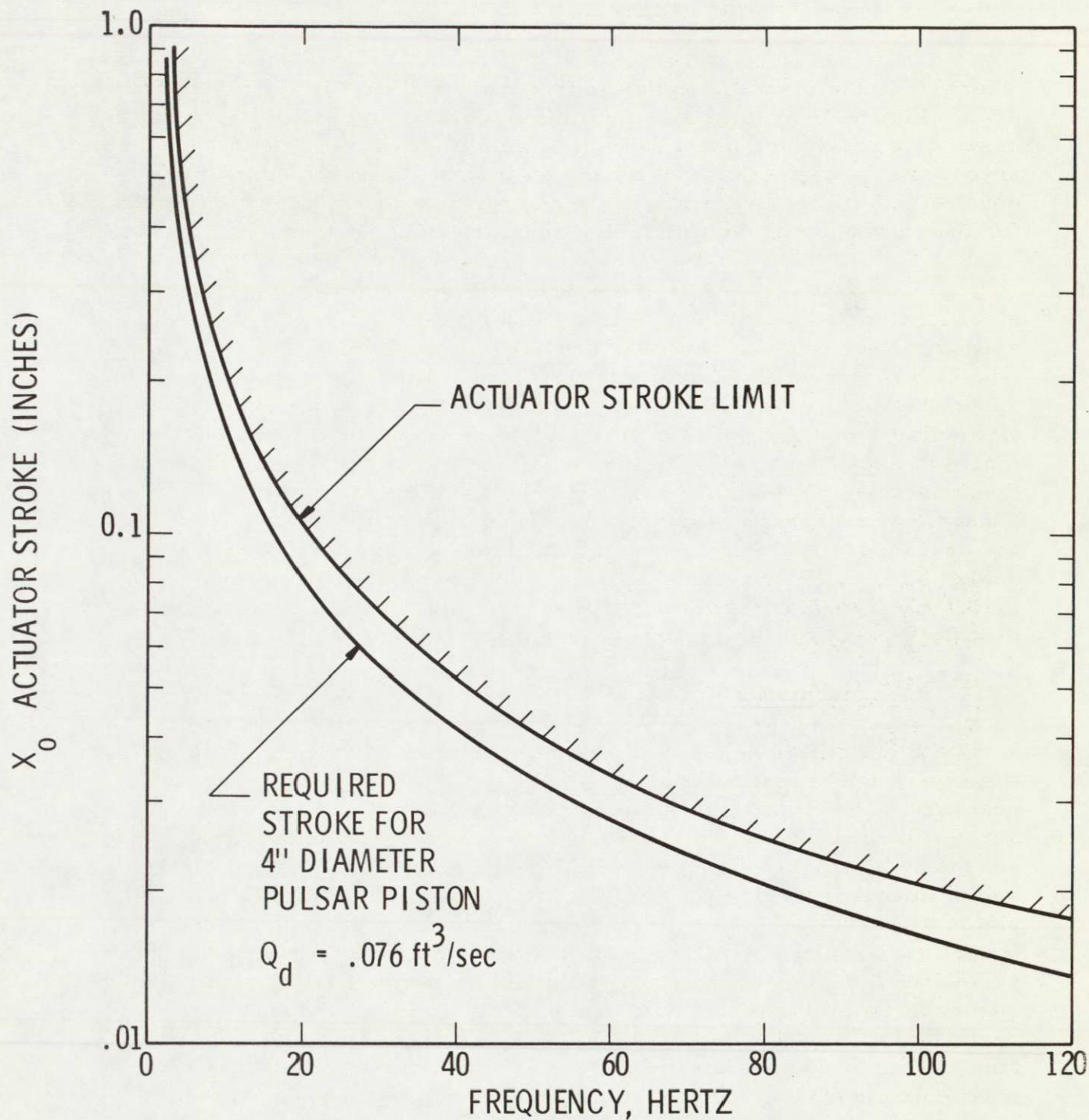
Figure 24. Stroke Required to Produce a Flow Perturbation Amplitude of .076 ft^3/sec

ACCUMULATOR & OIL RESERVOIR

PULSAR PISTON CYLINDER

SHAFT

BLEED VALVE

SERVO VALVE

HYDRAULIC ACTUATOR

VELOCITY TRANSDUCER

TEE SECTION

C-40464
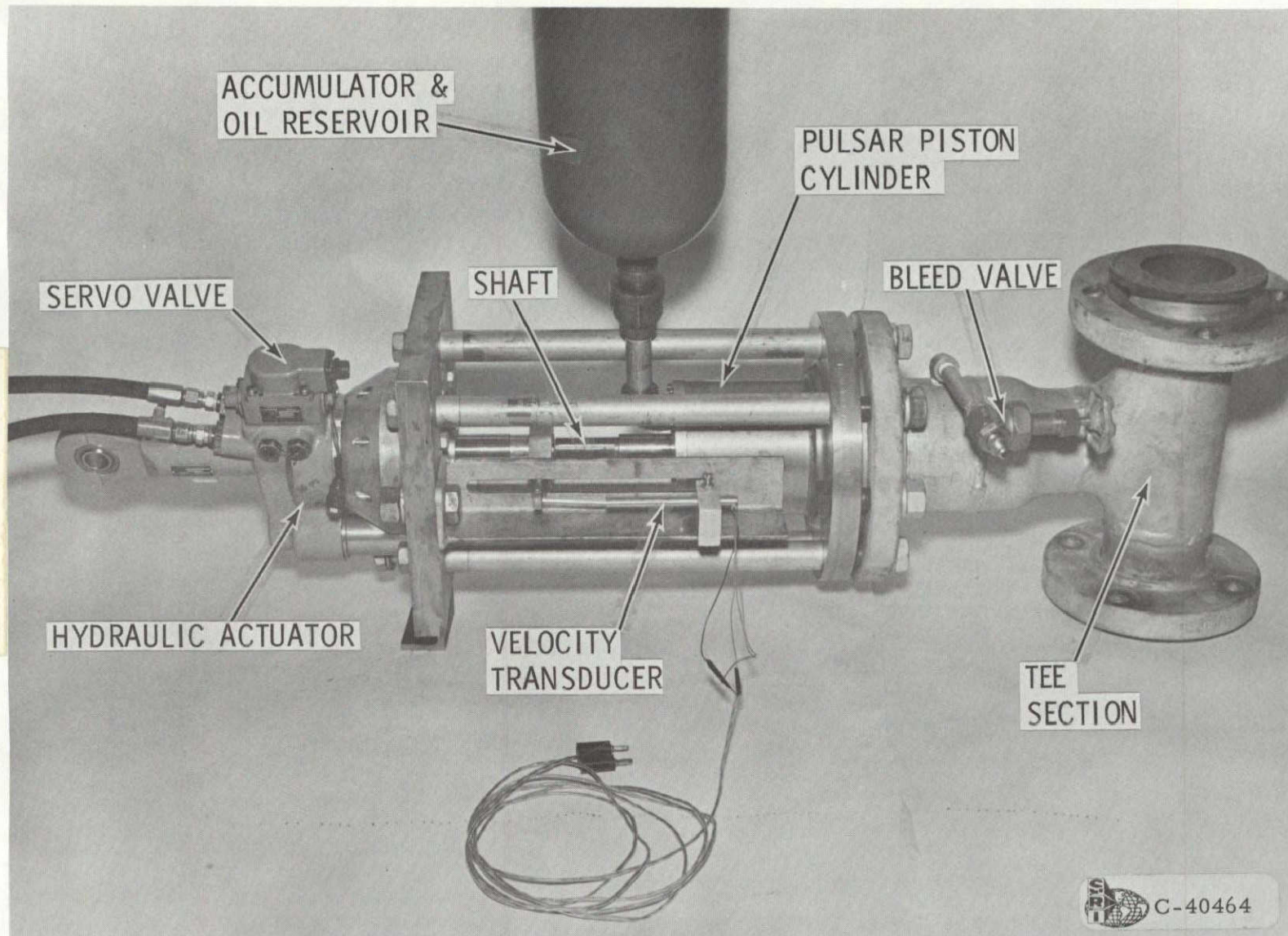
Figure 25. Hydraulic Actuator and Pulsar Assembly

Figure 27. Servo Controller System

transducers; the charge signals were converted to voltage readings with Kistler Model 504D electrostatic charge amplifiers. Special ultra-low noise cables were used to interconnect the transducers and amplifiers. These transducers were small with .22 mm diameter faces, and were mounted flush with the internal feedline wall. These transducers had a resolution of 0.01 psi and were acceleration-compensated to null out spurious vibrations. Each transducer was calibrated with the charge amplifier to determine its actual sensitivity in psi/volt.

It was discovered during early testing that the dynamic flow perturbation inputs were somewhat distorted from pure sinusoidal waveforms; this distortion was produced by mechanical friction along the hydraulic actuator shaft and pulsar piston. These input distortions not only made reading the correct flow perturbation amplitude difficult, but also produced distortions in the pressure signals and made measurements of its phase lag doubtful. A two-channel SKL 308A variable electronic filter was used to clarify both the input and pressure response signals. The low-pass cutoff frequency for each channel was set at 1.5 times the excitation or input frequency. In this manner, the phase lags created by the filters were equal, keeping the phase lag between the input signal and the pressure response equal to its unfiltered value.

The dynamic pressure and flow perturbation signals were then recorded on a CEC Type 5-116-P4-14 oscillograph recorder, which was operated at various paper speeds ranging from 8 to 64 inches/second, depending upon the input frequency. Each channel was calibrated so as to obtain the inches deflection/volt input, and from the known pressure and velocity transducer sensitivities, the pressure and velocity sensitivities were obtained as psi/inch and cubic ft per second/inch, respectively. Figure 28 presents typical raw oscillograph data obtained, with and without the electronic filters in the system. Also shown is the method used to determine the phase angle, ϕ, from the raw data records.

VII.2 Base Line Test Results

The feedline configuration used for the base line tests is presented in Figure 22. The initial tests were conducted with the termination of the line blocked. Also, the initial feedline employed was fabricated from thick-walled (Schedule 40S) type 304W stainless steel pipe, 3 in. nominal pipe size. With this material and geometry, the effects of the radial wall compliance were negligible or slight. By blocking the line terminal, possible effects of a mean steady flow component were eliminated from consideration, and the problem reduced to that of a closed hydraulic conduit connected to a large reservoir at one end and excited by a flow perturbation at the closed end. This simplified problem allowed for an evaluation of the instrumentation and testing techniques applied since

71
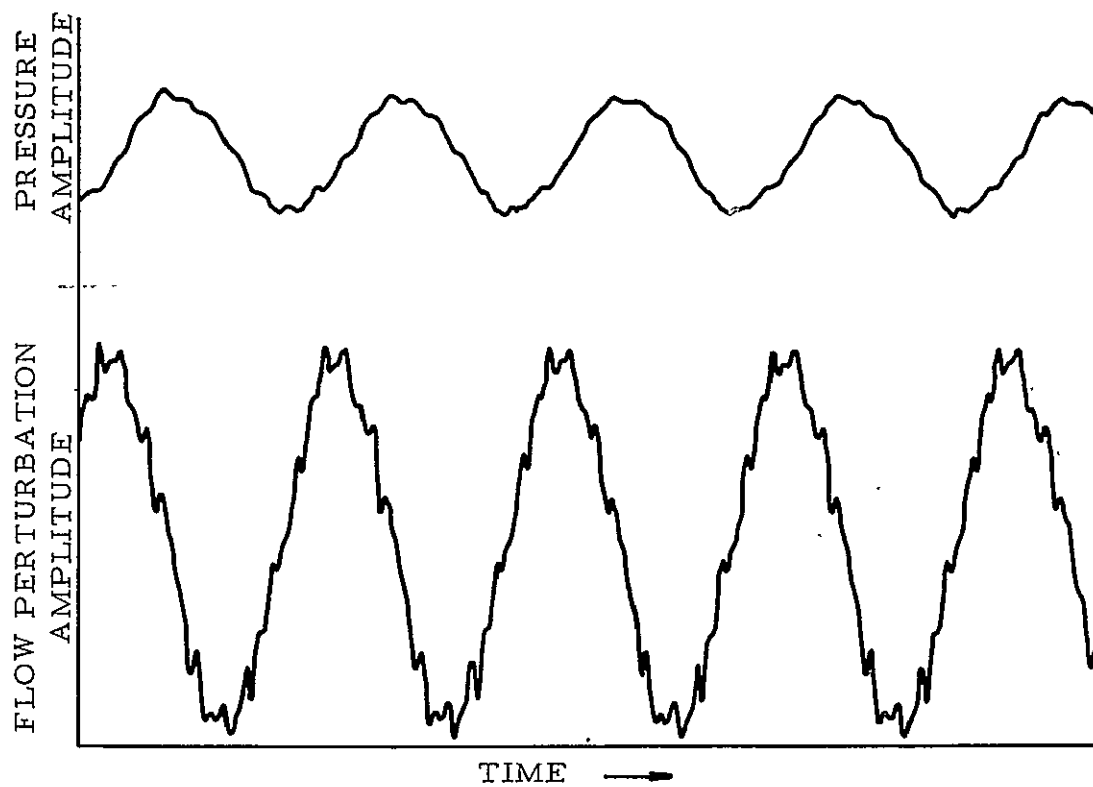
(a) UNFILTERED SIGNALS

$$\phi = -360 \left(\dfrac{B}{A} \right)$$
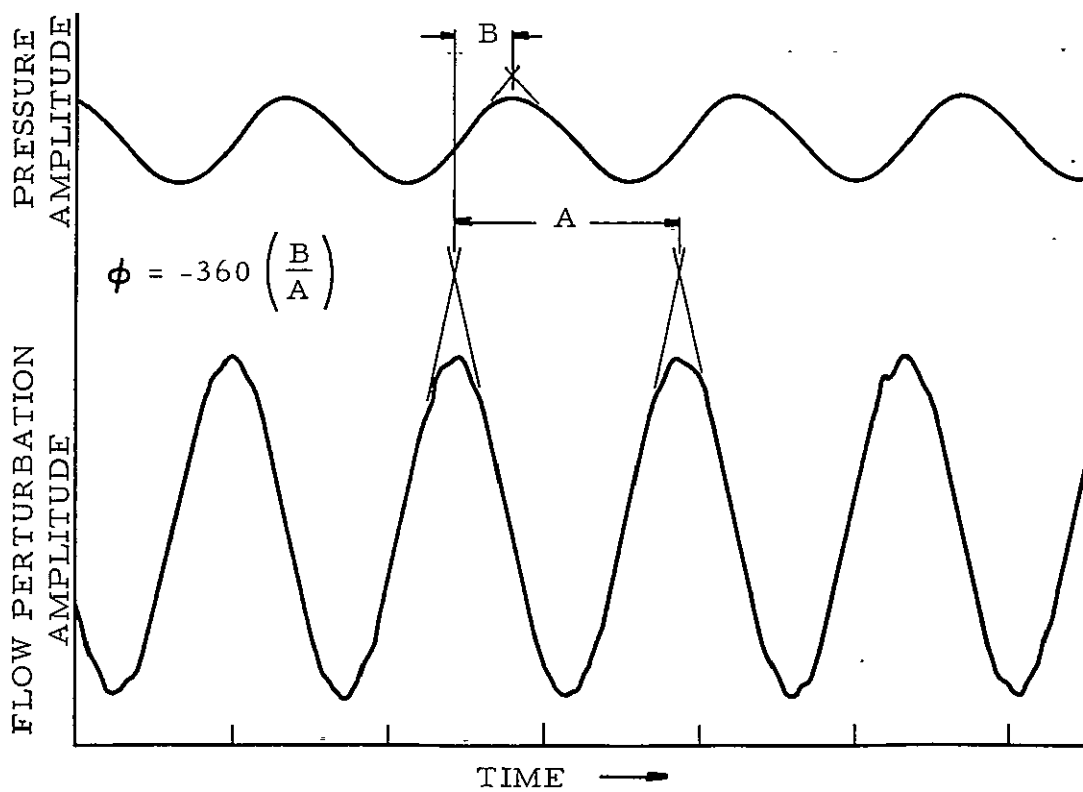
(b) FILTERED SIGNALS

Figure 28. Typical Signals from Oscillograph Recorder

72

for this case, excellent agreement between theory and experiment should exist, as was the result obtained by Gerlach in Reference 18. This was the most elementary configuration tested. For this test, the pressure amplitude and its phase angle with the dynamic flow perturbation input was recorded at the line terminal and also in the reservoir. The pressure amplitudes generated in the upper reservoir, even at line resonance, were insignificant, indicating that the assumption of zero impedance at the line inlet was reasonably correct.

Figure 29 presents the frequency response obtained for a stainless steel line 27 ft long and 3.068 in. in diameter, with a wall thickness equal to 0.216 in., and excited by the side branch flow pulsar. The pulsar flow perturbation double amplitude was set at $Q_d = 0.007 \text{ ft}^3/\text{sec}$, while the excitation frequency was increased from 5 to 100 Hz. Since the flow perturbation amplitude proved difficult to control at this exact amplitude for all frequencies, the resultant pressure amplitude was divided by the input flow perturbation amplitude to produce a dynamic terminal impedance amplitude, P_T/Q_d. The linearity of the system thus allows the pressure response at any frequency and input amplitude to be obtained from Figure 29. The terminal pressure response phase lag was also obtained and is plotted as a function of input frequency in Figure 30. The data were obtained by pressurizing the liquid to 100 psig by pumping the water into a "dead" head; 100 psig was chosen to eliminate any possible cavitation problems which might have been developed by the large amplitude dynamic pressures at resonance. Figure 29 indicates excellent agreement between theory and experiment, except there appears to be more damping at resonance than predicted by the analytical model with an infinite terminal resistance. The apparent disagreement in phase angle near resonance can be attributed to the poor measurements of the phase relationships from the data traces, as these data were recorded before it was realized that electronic filtering of the signals was required as discussed earlier in Section VII.1.

Effect of the Terminal Resistance

To determine the effect of the terminal resistance, several tests were conducted with various values of the terminal impedance, $\Delta P/Q$. Tests were accomplished with both linear and nonlinear resistance elements; the resistance for small perturbations from the steady mean value was assumed linear in the analytical model, and the validity of this assumption was to be verified. This is important for a liquid propellant feed system since the pump and injectors being simulated by the resistance element actually have nonlinear steady flow characteristics which are generally linearized for modeling purposes.

73
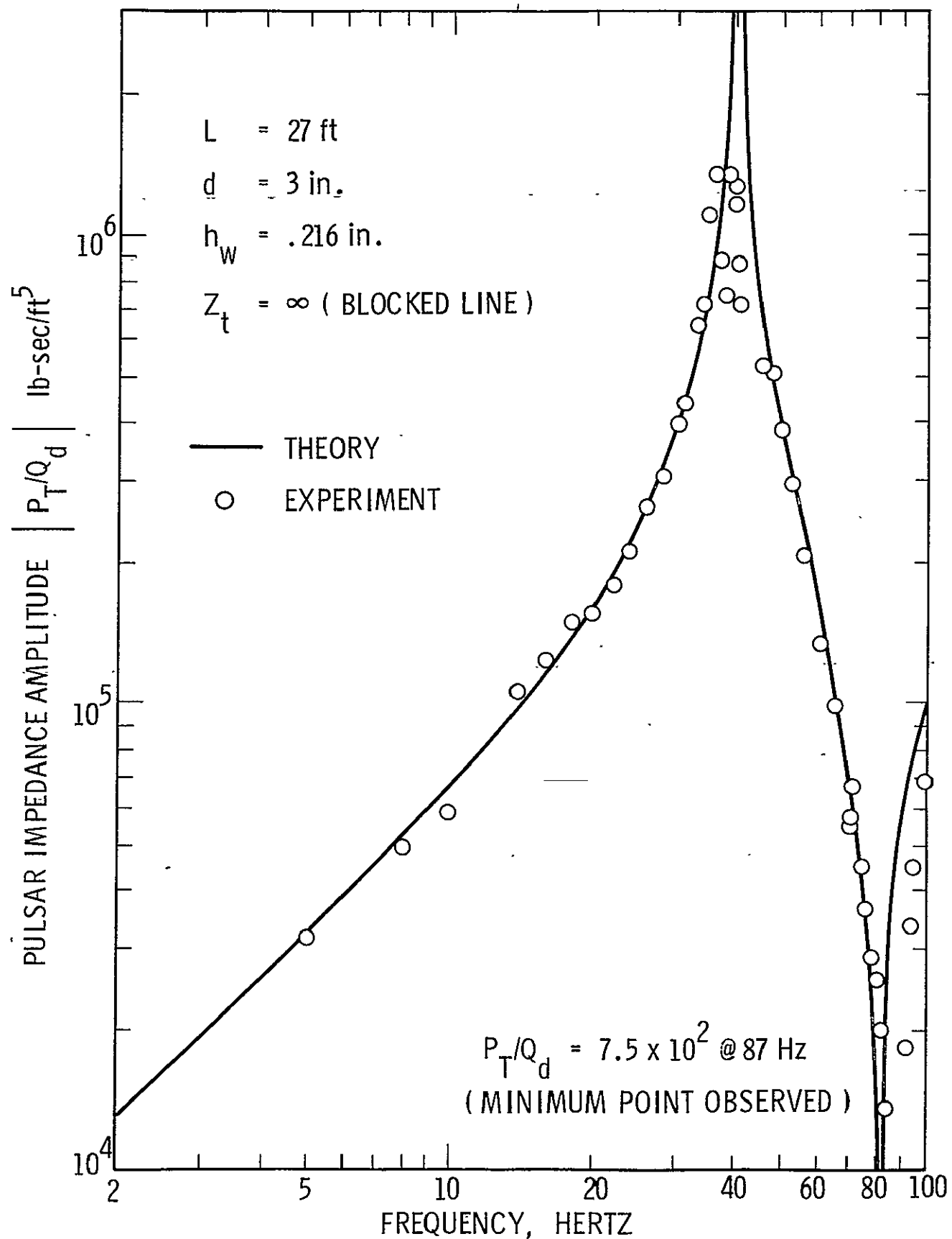
Figure 29. Frequency Response of a Blocked Stainless Steel Line
Excited by a Side Branch Pulsar

74
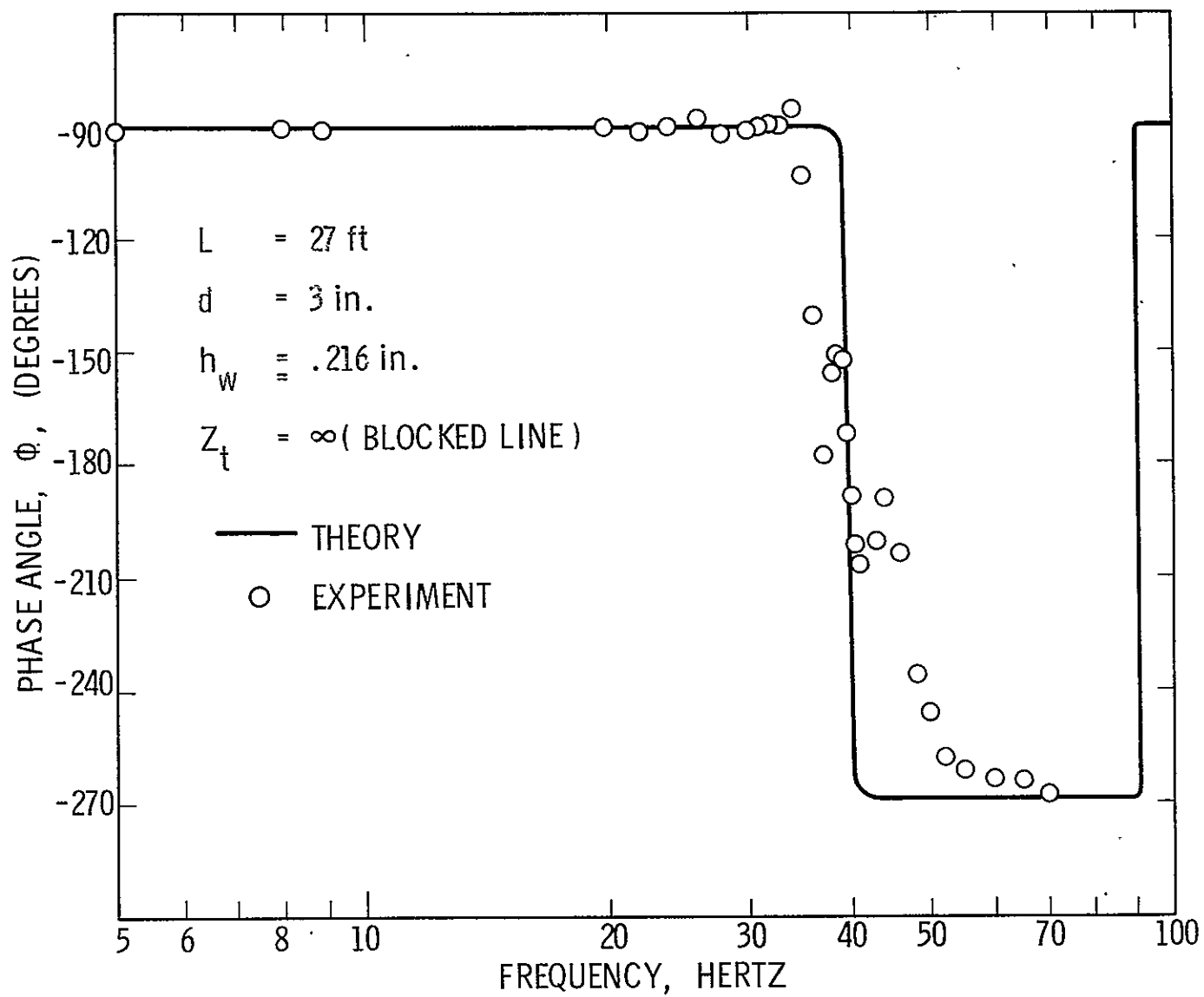
Figure 30 . Phase Lag for a Blocked Stainless Steel Line Excited by a Side Branch Pulsar

By using various degrees of resistance in the experimental tests, various mean flow velocities were also established. In most cases these flow velocities were large enough that turbulent flow was established in the system, which was required to determine the success of the modified propagation operator for a turbulent mean flow discussed in Section II. 3.

Tests with Linear Flow Resistance

A considerable effort was directed toward the development of a suitable linear flow resistance element for the line terminus. The basic requirement for a linear relationship between pressure drop and flow rate through a hydraulic element was that the flow be laminar in the local passages of that particular component. Laminar flow required a local Reynolds number less than approximately 2000 for internal flows. From the definition of Reynolds number,

$$N_R = \frac{\rho V d}{\mu} \tag{143}$$

a low Reynolds number was obtained for a given fluid and velocity by decreasing the passage diameter, d.

Initial attempts at constructing a linear resistance was through the use of fine mesh wire screen (325 mesh). This proved successful for low values of resistance, $\Delta P/Q$. However, as the flow velocity and pressure drop increased, the relation between pressure and flow approached that of an ordinary orifice, $\Delta P = kQ^2$. A suitable linear resistance was finally obtained by packing assorted diameter glass beads between two 325 mesh wire screens and into a cylinder 3 inches in diameter and 4 inches long. This length was selected based on the experimental data collected in Figure 31 for several attempts at developing a true linear pressure-flow relationship. Figure 32 presents the actual pressure drop versus volume flow measured for this configuration, in which the bead diameters ranged from 0.0117 in. to 0.0029 in., providing very small diameter flow passages. The 4-in. thickness provided a much more linear flow-pressure behavior than any of the other configurations shown, with the pressure drop and flow being related by $\Delta P = kQ^{1.19}$. The trend in the summary calibration of the various "linear" resistance elements tested indicates a true linear resistor might be approached or obtained but would require a considerably long or thick resistor. Increasing the length also increased the magnitude of the resistance, requiring an extremely high pressure drop for a given flow rate. For these reasons, the 4-in. thick resistance element was selected.

The tests conducted with this linear resistance element were quite similar to those described for the base line test with an infinite terminal resistance. Figure 33 presents the frequency response obtained for an

The chart shows EXPONENT, n, in $\Delta P = KQ^n$ (y-axis, ranging from 1.0 to 2.0) versus RESISTANCE ELEMENT LENGTH, INCHES (x-axis, ranging from .2 to 10 on a logarithmic scale).

RANDOM MIXTURE OF GLASS BEADS
$.0029'' < DIAM < .0117''$
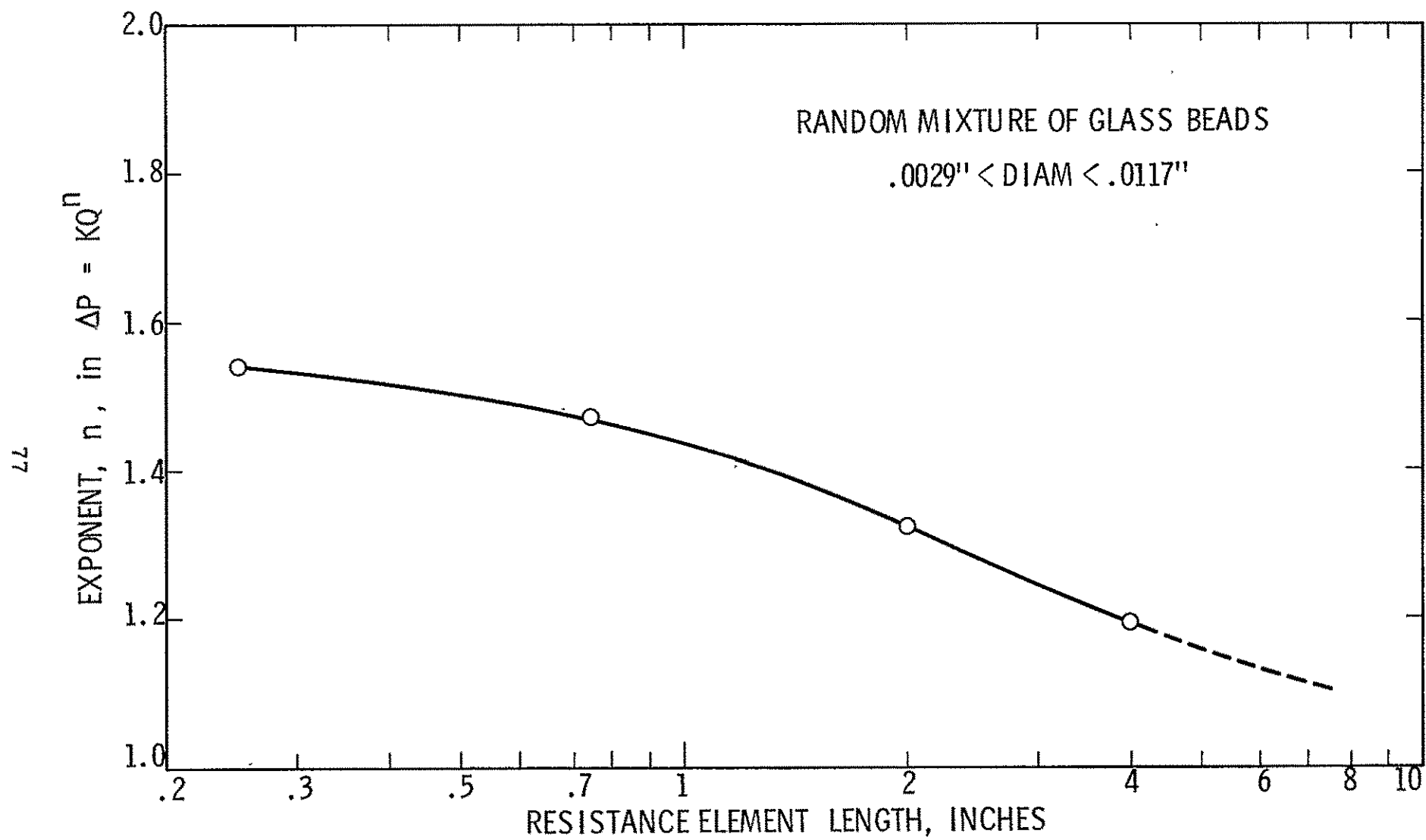
Figure 31. Comparative Linearity of Four Resistance Elements Tested

$$\Delta P = KQ^n$$

$$\Delta P = 1.77 \times 10^6 Q^{1.195}$$

$$Z_t = 1.195 KQ^{.195}$$

RANDOM MIXTURE OF
GLASS BEADS

$.0029'' < DIAM < .0117''$

LENGTH = 4.0''
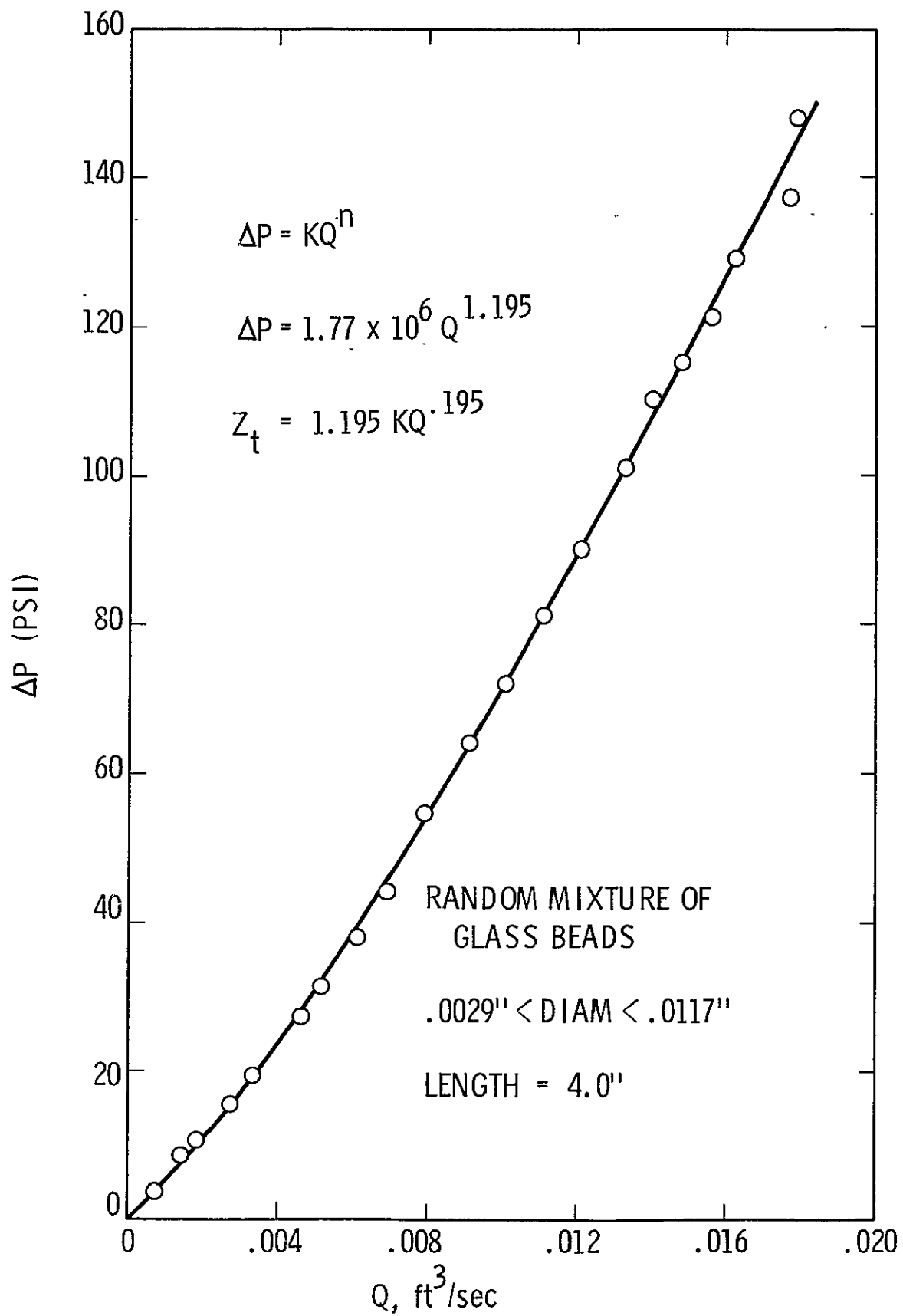
Figure 32. Calibration of "Linear" Resistor

78
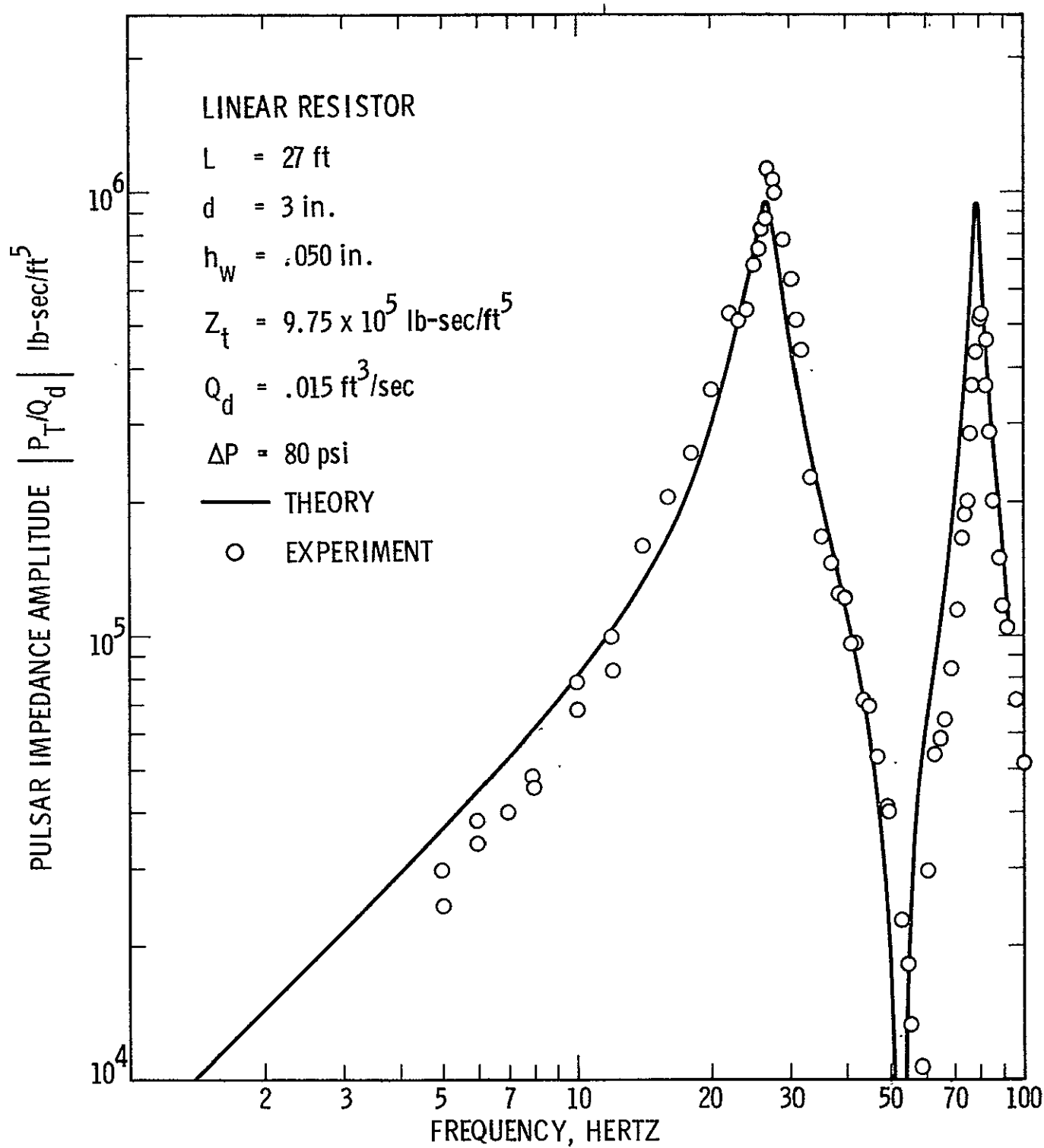
Figure 33. Frequency Response of an Aluminum Line with a Linear
Terminal Impedance, Excited By a Side Branch Pulsar

aluminum line 27 ft long and with a diameter of 3 in., excited by the side branch pulsar located just above the line terminal. The wall thickness was 0.050 in. and the terminal impedance, Z_t, was 9.75 X 10^5 lb-sec/ft^5 producing a mean flow rate $Q = 0.0108$ ft^3/sec at 80 psid pressure drop through the resistor. The corresponding phase lag versus frequency is shown in Figure 34. The predicted amplitude, phase, and resonant frequencies agree quite well with the experimental data for the first and second longitudinal modes.

Tests with Flow - Nonlinear Resistance

Tests were conducted with the feedline configuration described above for nonlinear type resistors at the line terminal. These resistors were simple orifice plates; one designed to produce a terminal impedance value, Z_t, near that of the already described linear resistor and another had a nominal impedance much lower. The resultant terminal pressure responses versus excitation frequency were obtained with 7/16-in. and 1/4-in. diameter orifices installed in the 3-in. internal diameter feedline. The discharge coefficient, k_d, for the resultant diameter ratio, β, and Reynolds number was obtained from standard tables[21] and checked by a direct calibration while installed at its position in the flow facility. With a knowledge of the discharge coefficient, the pressure drop versus mean flow rate was calculated from

$$Q = k_d A_o \sqrt{\frac{2\Delta P}{\rho}} \qquad (144)$$

where A_o was the cross-sectional area of the orifice. From the definition of the terminal impedance, $\Delta P/Q$, the value of the resistance at the operating point was obtained by writing Equation (144) as $\Delta P = f(Q^2)$ and differentiating to obtain the slope of the pressure drop versus flow curve. Since the orifice had a nonlinear pressure-flow characteristic, the magnitude of the resistance varied with the mean flow rate. The nominal value of the resistance or terminal impedance was therefore computed from

$$Z_t = \frac{d(\Delta P)}{dQ} = \frac{\rho Q}{(k_d A_o)^2} \qquad (145)$$

where Q was the mean flow rate at the operating or test conditions.

The frequency response of the 27-ft long aluminum feedline described earlier was obtained for two nonlinear resistance elements (orifices). The 7/16-in. orifice provided a nominal terminal impedance of $Z_T = 3.91$ X 10^5 lb-sec/ft^5 at a pressure drop of 100 psid; the terminal pressure response is presented in Figure 35 and the phase lag between the pressure and input flow perturbations is shown in Figure 36.
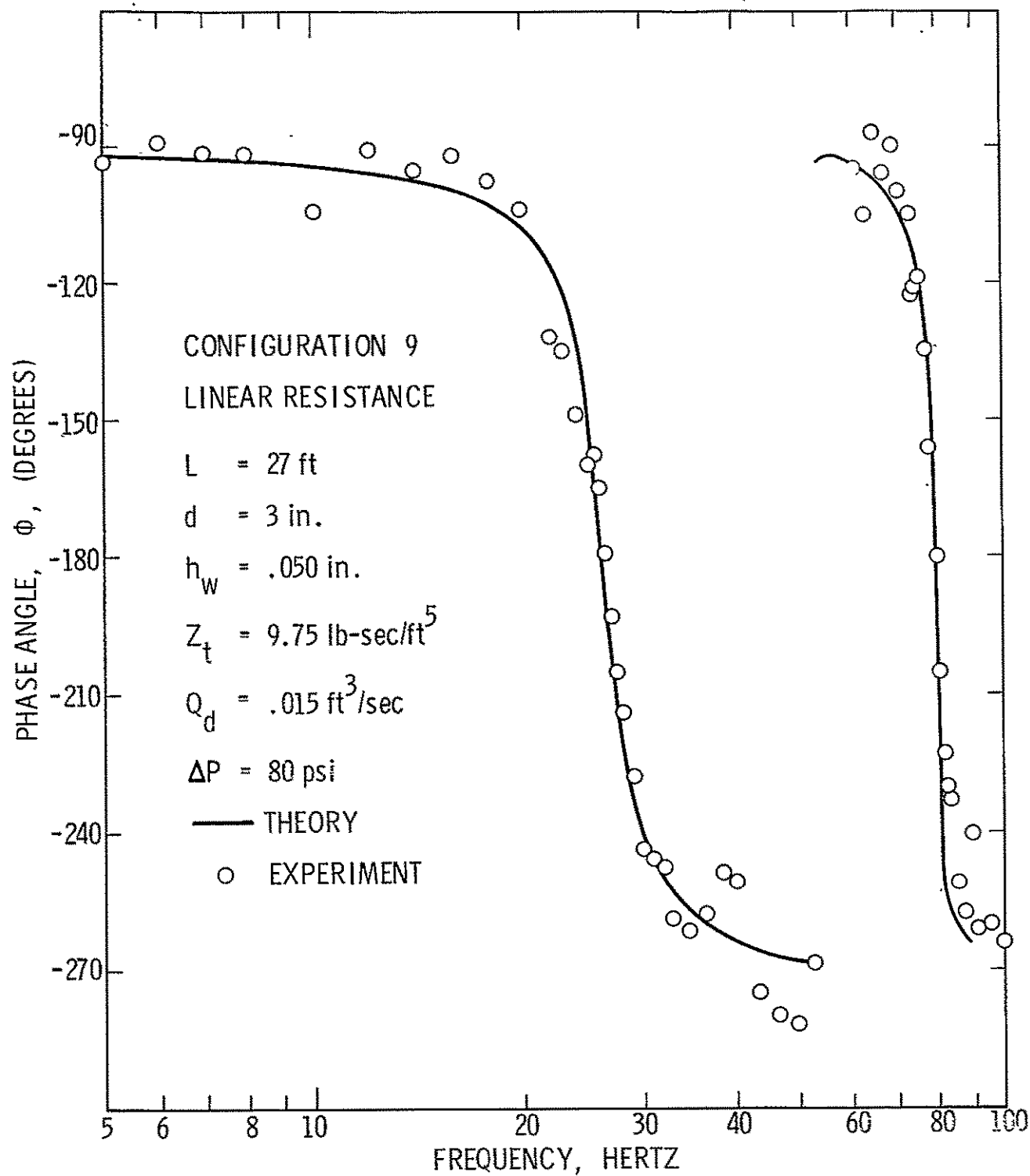
Figure 34. Pressure Phase Lag of an Aluminum Line with a Linear Terminal Impedance

81

Figure 35. Frequency Response Of A Thin Walled Aluminum Feedline
Terminated By An Orifice

82
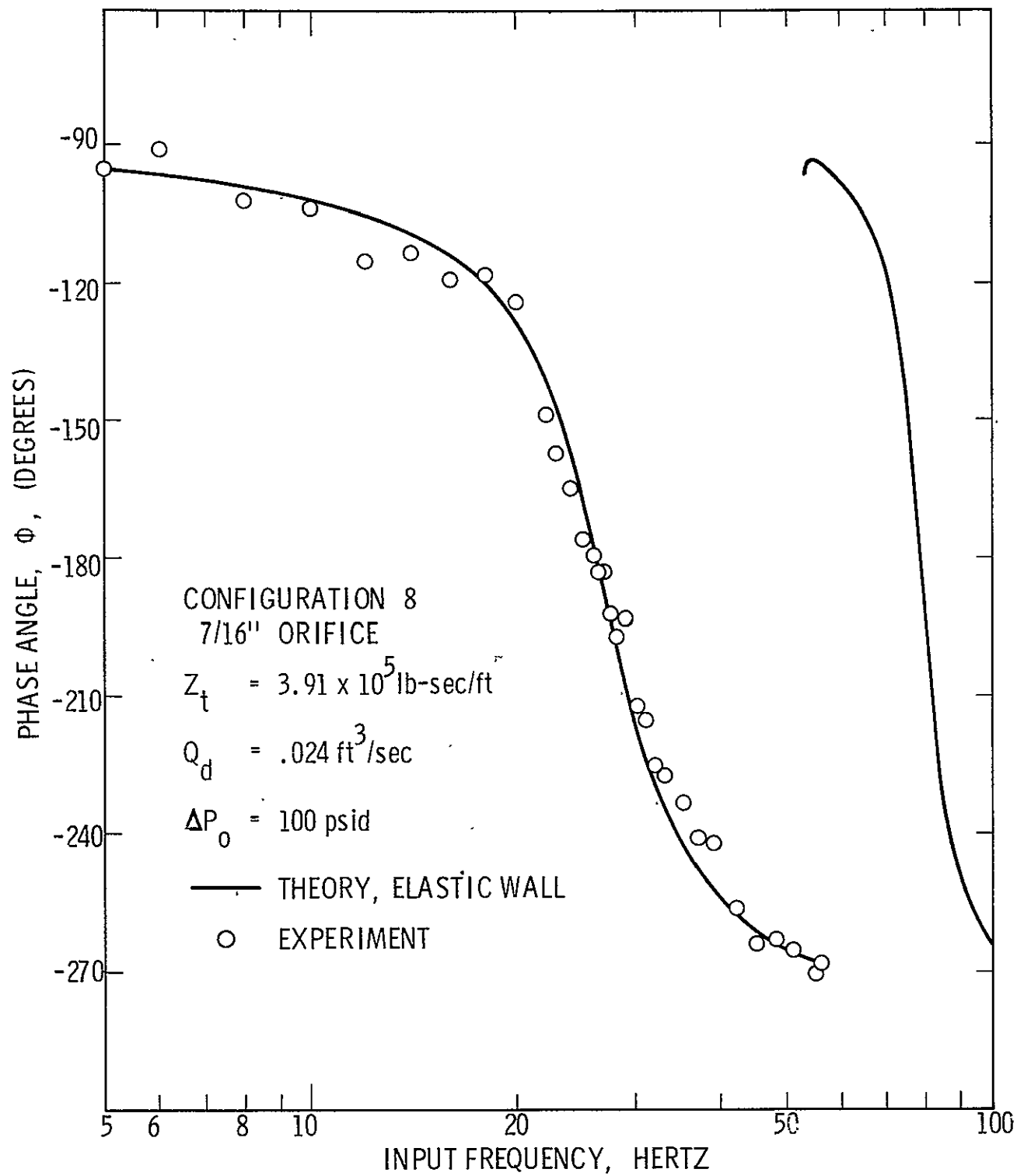
Figure 36. Phase Angle vs Frequency for a Thin Walled Aluminum Feed-line Terminated by an Orifice

For all data points, the amplitude of the dynamic flow perturbations created by the side branch pulsar was maintained at approximately $Q_d = 0.024$ ft^3/sec. The second orifice had a diameter of 1/4-in., producing a much higher terminal resistance at any given mean pressure drop measured across the orifice. Tests were conducted on the same feedline as used for the 7/16-in. orifice plate with a steady state operating pressure drop of 80 psid with the 1/4-in. diameter orifice.

Figures 35 through 38 indicate fairly good agreement with the analytical computer model response, plotted as the solid curve in all figures. At the line longitudinal resonant frequencies there appears to be greater damping in the experimental tests than predicted by the computer simulation of the same problems. Later tests conducted with an aluminum line with a smaller wall thickness indicate that this discrepancy cannot be necessarily attributed to the nonlinearity of the terminal resistance.

An aluminum line with a 3-in. internal diameter, 27 ft long, and a wall thickness, $h = 0.022$ in., was tested with the 7/16-in. diameter orifice employed as the terminal impedance element. The steady flow pressure drop at the line terminus was 80 psid, producing an operating or nominal terminal impedance, $Z_t = 3.47 \times 10^5$ lb-sec/ft^5. The measured frequency response of the terminal pressure/input flow perturbation is plotted in Figure 39 along with the analytical model prediction. The experimentally measured phase lag is also given in Figure 40 along with the corresponding theoretical response. It should be emphasized that here the nonlinear resistance was again linearized for the computer computation and excellent agreement with theory resulted. The lower amplitudes of the response at resonance in Figures 35 and 37 are probably the results of experimental inaccuracies, as it was noted during several tests that the pressure response amplitudes near resonance were difficult to repeat consecutively. Later tests with nonlinear resistance elements also produced very good agreement with theory for all cases where the dynamic flow perturbation amplitudes were considerably less than the mean flow rate.

VII.3 Distributed Compliances

Two types of distributed compliances were discussed in Section III, and analytical models were developed for their influence on the response of liquid propellant feedlines. Both effects have been examined experimentally. First, distributed wall compliance effects were examined by using three different feedlines of the same length and internal diameter but with a different wall thickness, h, and in one case constructed of a different material. Second, the effects of entrained gases were experimentally examined by keeping the geometric and elastic parameters of the feedline constant and varying the gas mass ratio, Φ.

84
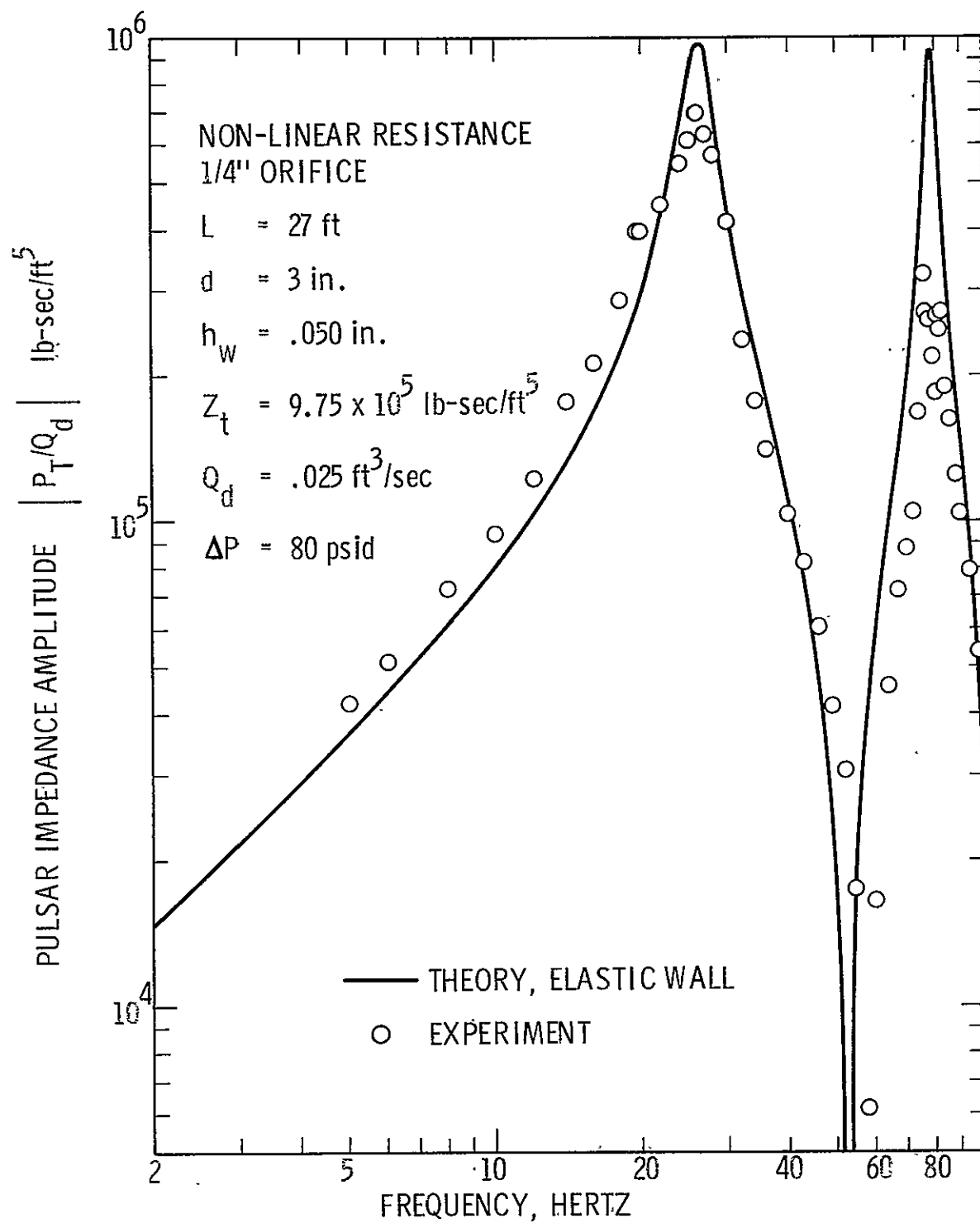
Figure 37. Frequency Response of a Thin Walled Aluminum
Feedline Terminated by an Orifice

85

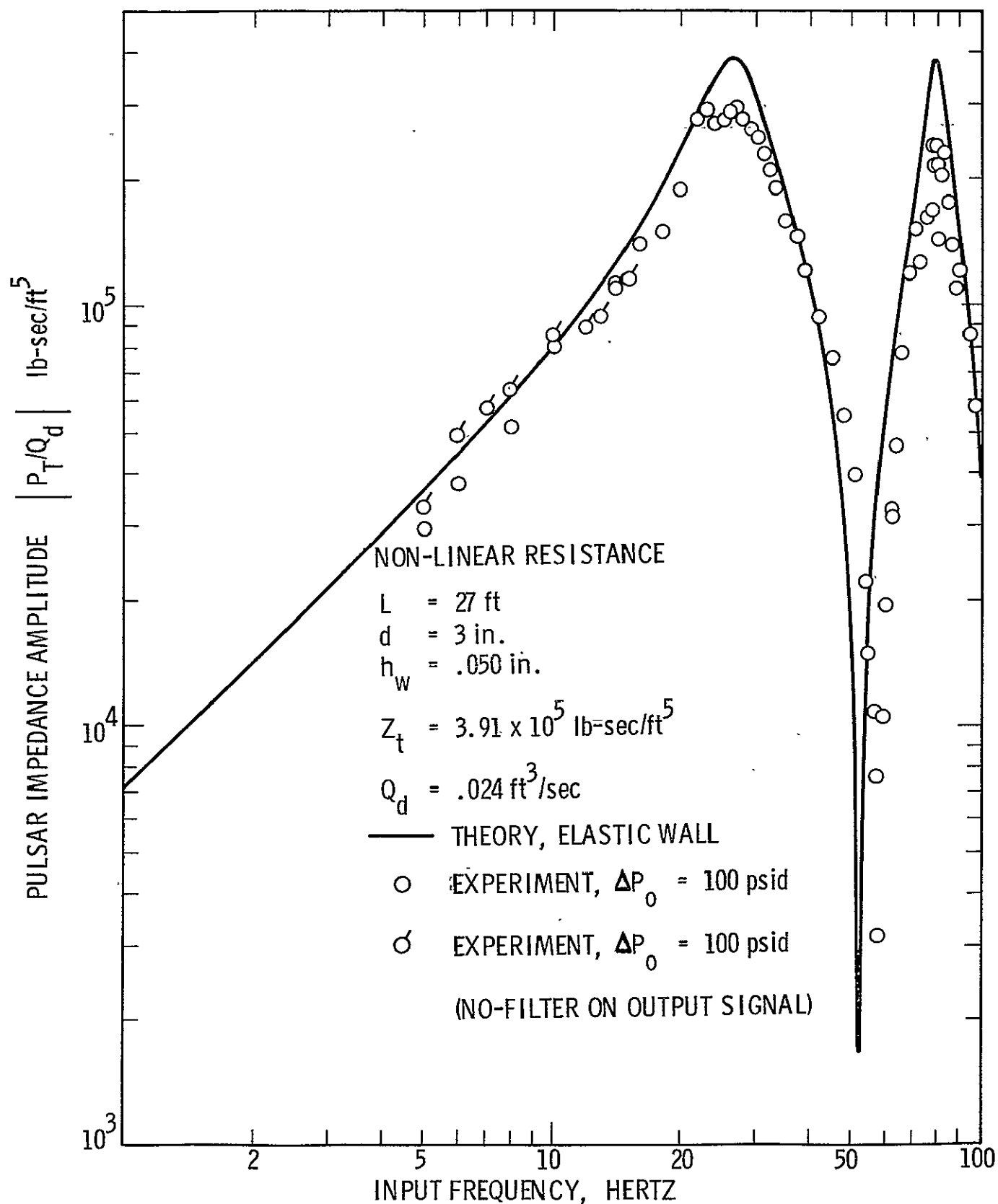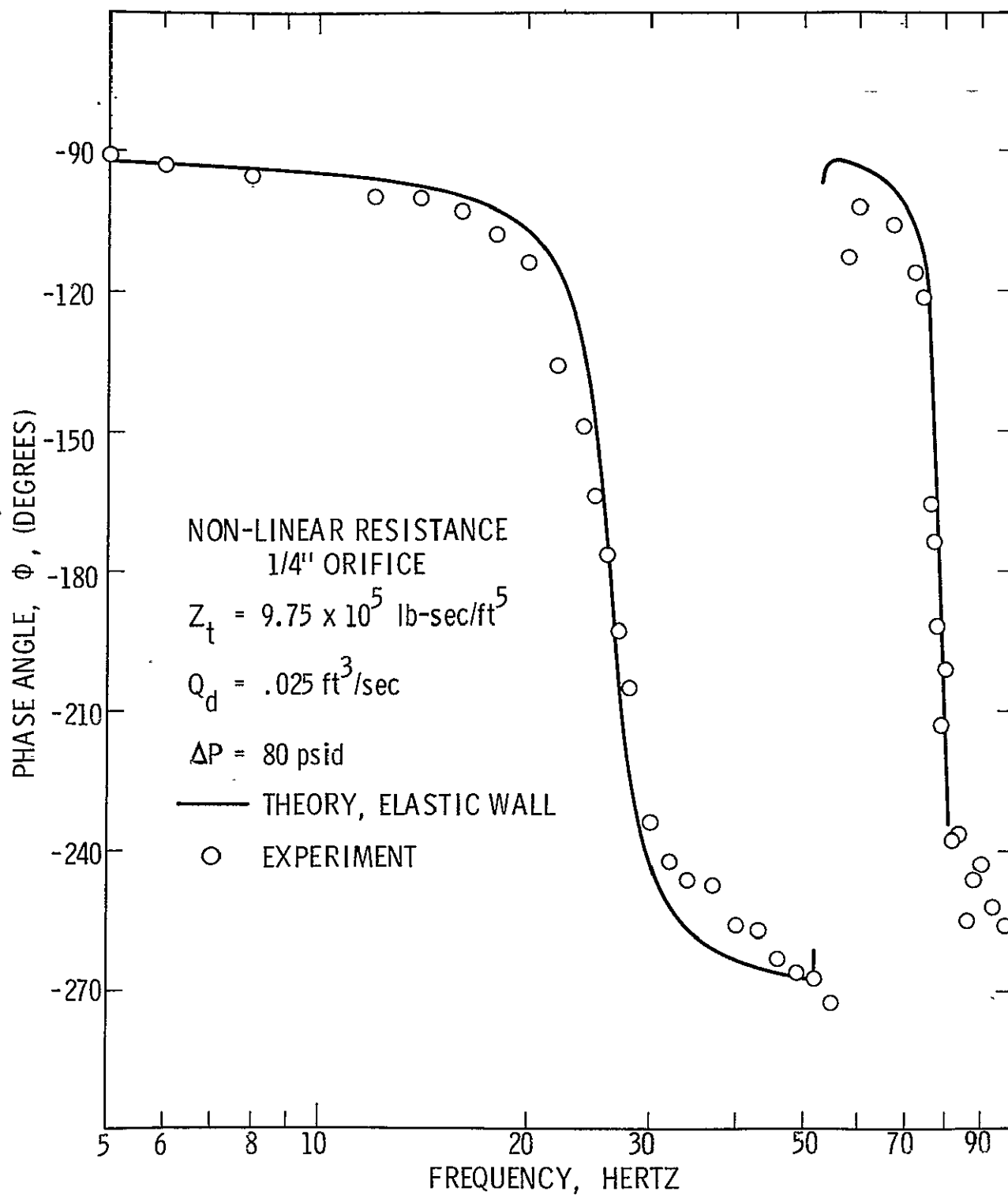Figure 38. Phase Angle for a Thin Walled Aluminum Feedline Terminated by an Orifice
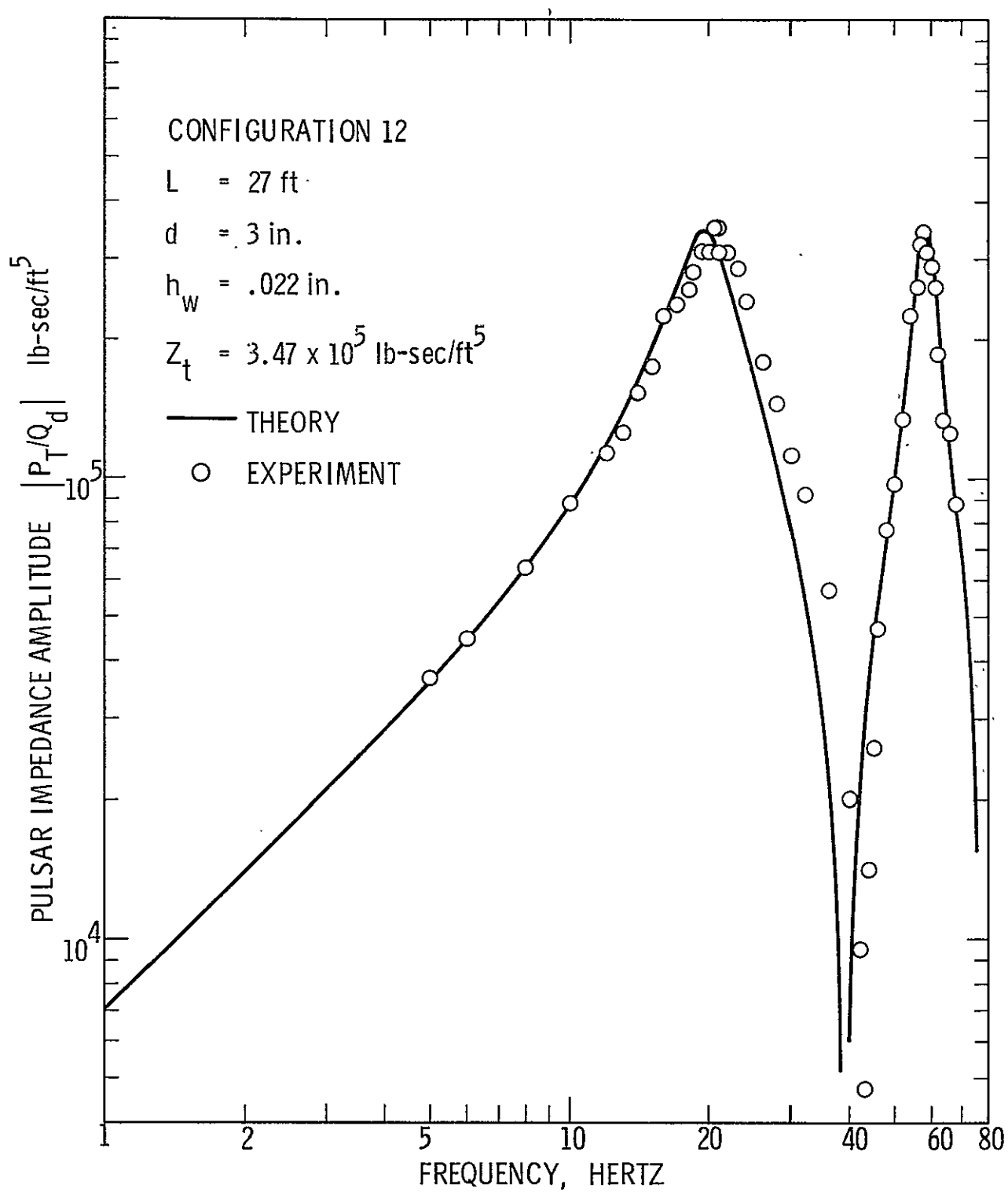
Figure 39 . Frequency Response of a Thin Walled Aluminum Line
Terminated by an Orifice
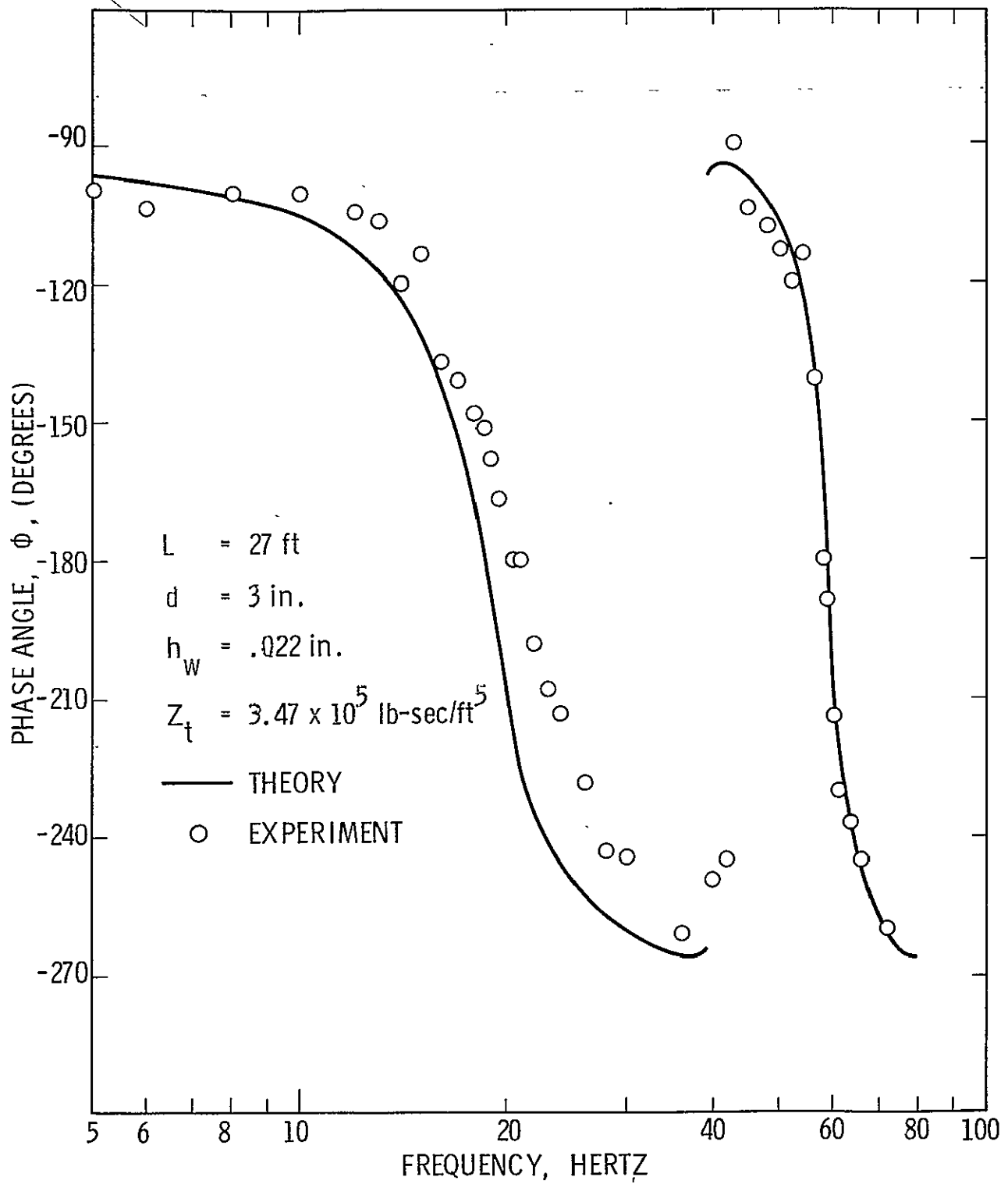
Figure 40 . Phase Angle for a Thin Walled Aluminum Feedline Terminated by an Orifice

Distributed Wall Compliances

In general, the flexibility of the feedline wall will produce two possible effects which may be of concern. First, the axial wall stiffness effect would permit real wave propagation of higher order modes at low frequency by virtue of a coupling between the fluid and axial wall modes. However, it was found in Section III. 3 that for all practical feedline applications this effect of the axial wall stiffness on the wave propagation can be neglected, since the amount of energy which is fed into the higher order modes at the line termination is small. Second, the wall compliance reduces the phase velocity, and increases the spatial attenuation for the longitudinal fluid wave propagation mode. The classic Korteweg correction to the phase velocity was incorporated into the analytical model to account for the wall compliance; the correction being

$$c = c_o \left(1 + \frac{\rho_o c_o^2 d}{E_t h} \right)^{-\frac{1}{2}} \tag{146}$$

The validity of this correction has been determined from its effect on the resonant frequency of the feedline, since the first longitudinal mode frequency is

$$f_o = \frac{1}{2\pi} \left(\frac{c_o}{4L} \right) \tag{147}$$

and a shift in resonant frequency is a good measure of the phase velocity change, providing the lengths are equal.

For feedlines of equal lengths, L, and diameters, d, and with the same internal fluid, the phase velocity and resonant frequency become a function of the elastic parameter, $E_t h$.

The responses of three feedlines terminated by an infinite resistance (blocked line) were obtained for the 304 stainless steel line with a wall thickness, h = 0.216 in. and two aluminum lines of the same length and internal diamter, but with wall thicknesses, h = 0.050 and 0.022 inch. The response of the relatively stiff stainless line was presented in Figure 29, while the results for the two aluminum lines are plotted in Figures 41 through 44. In all cases, the excitation was provided by the side branch pulsar piston. A summary plot, Figure 45, reveals the accuracy and validity of the model for distributed wall compliances. Shown on this plot are the measured and calculated values of the first mode resonant frequencies for the three feedlines tested. The resonant frequencies are plotted as a function of the elastic parameter, $E_t h$. The results indicate that the Korteweg correction to the phase velocity is a valid means for modeling the effects of the wall radial compliance for thin-walled feedlines.

89
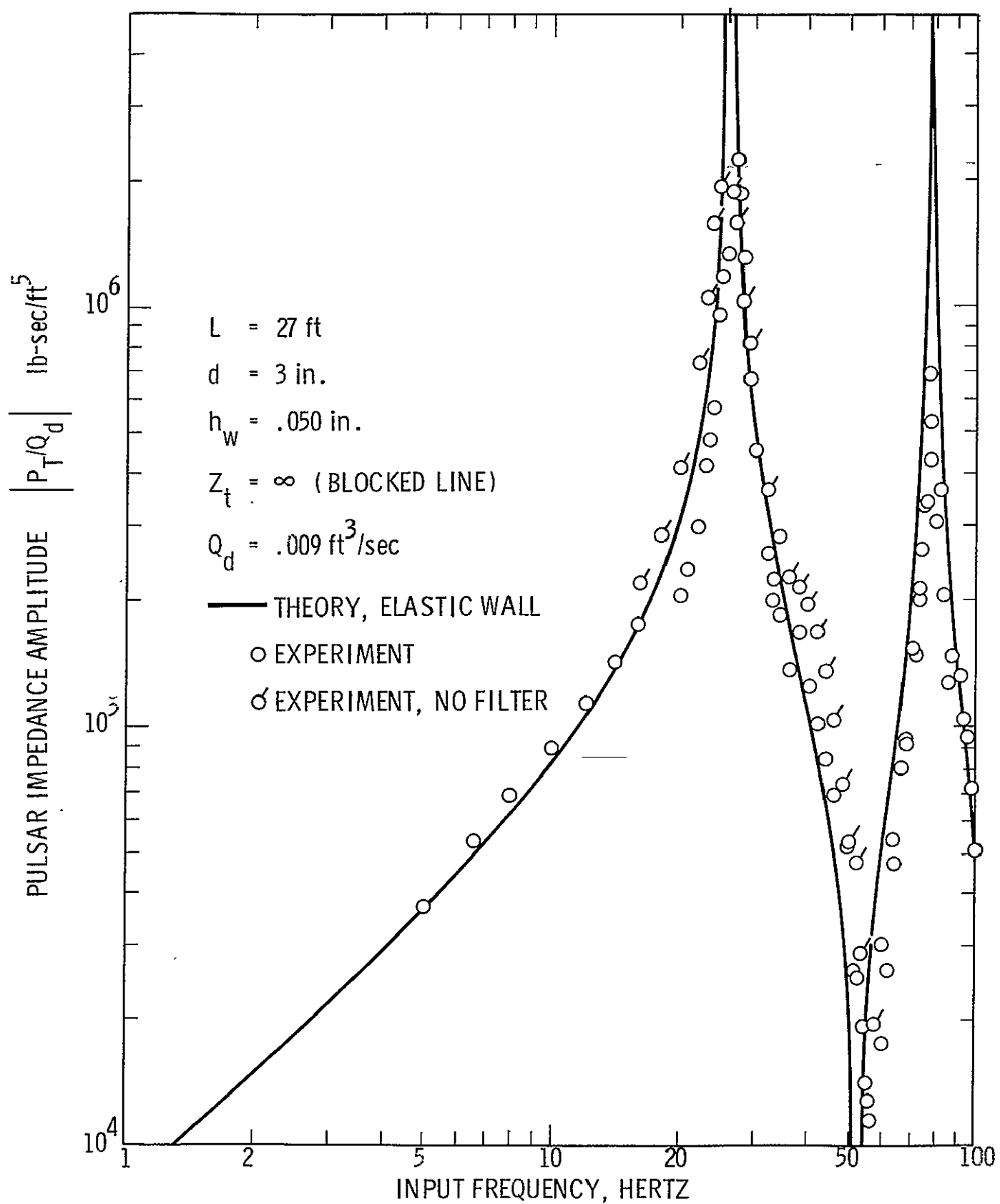
Figure 41. Frequency Response of Thin-Walled Aluminum Feedline
With a Blocked Line
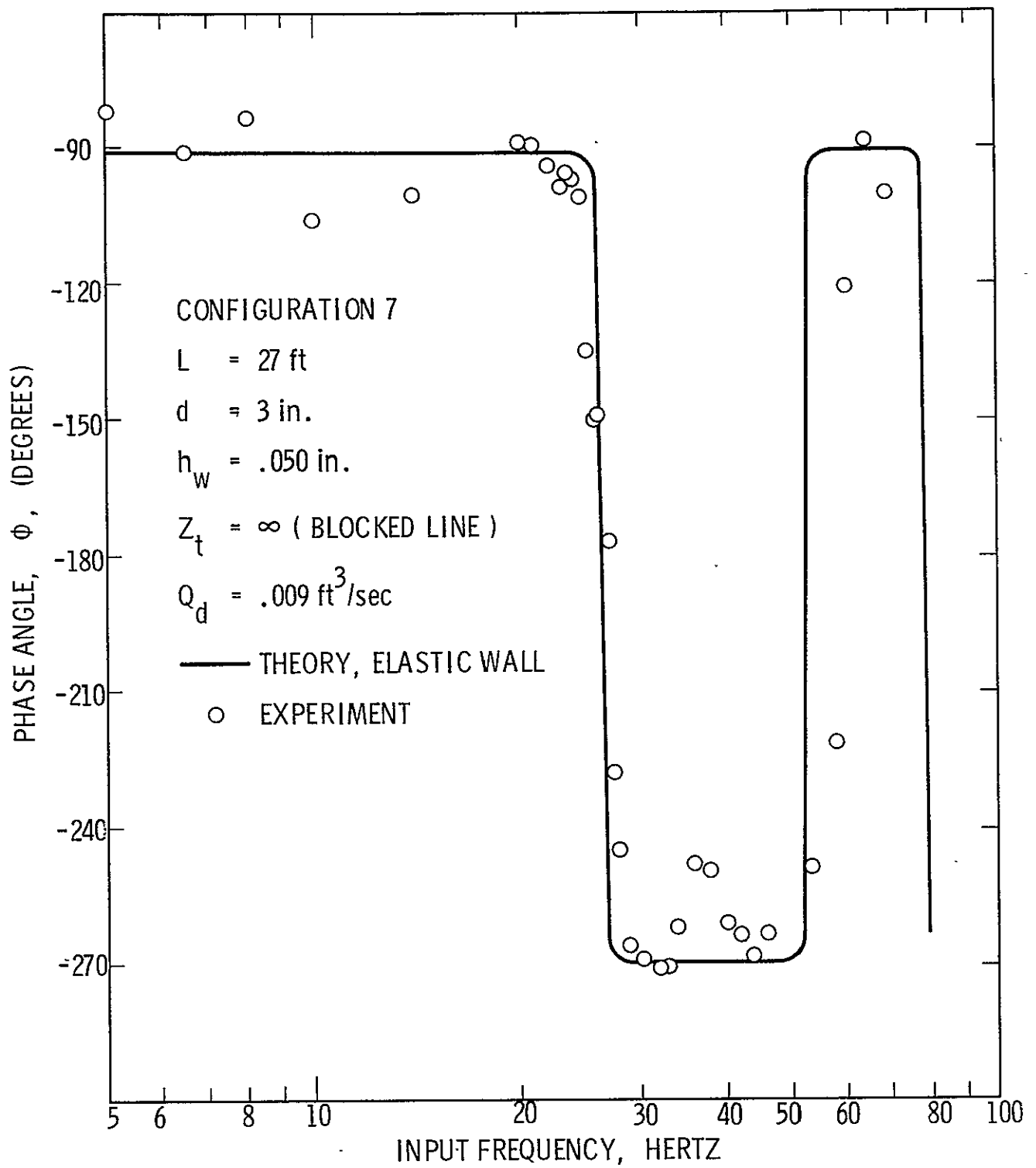
Figure 42. Phase Angle vs Frequency for a Blocked, Thin-Walled, Aluminum Feedline
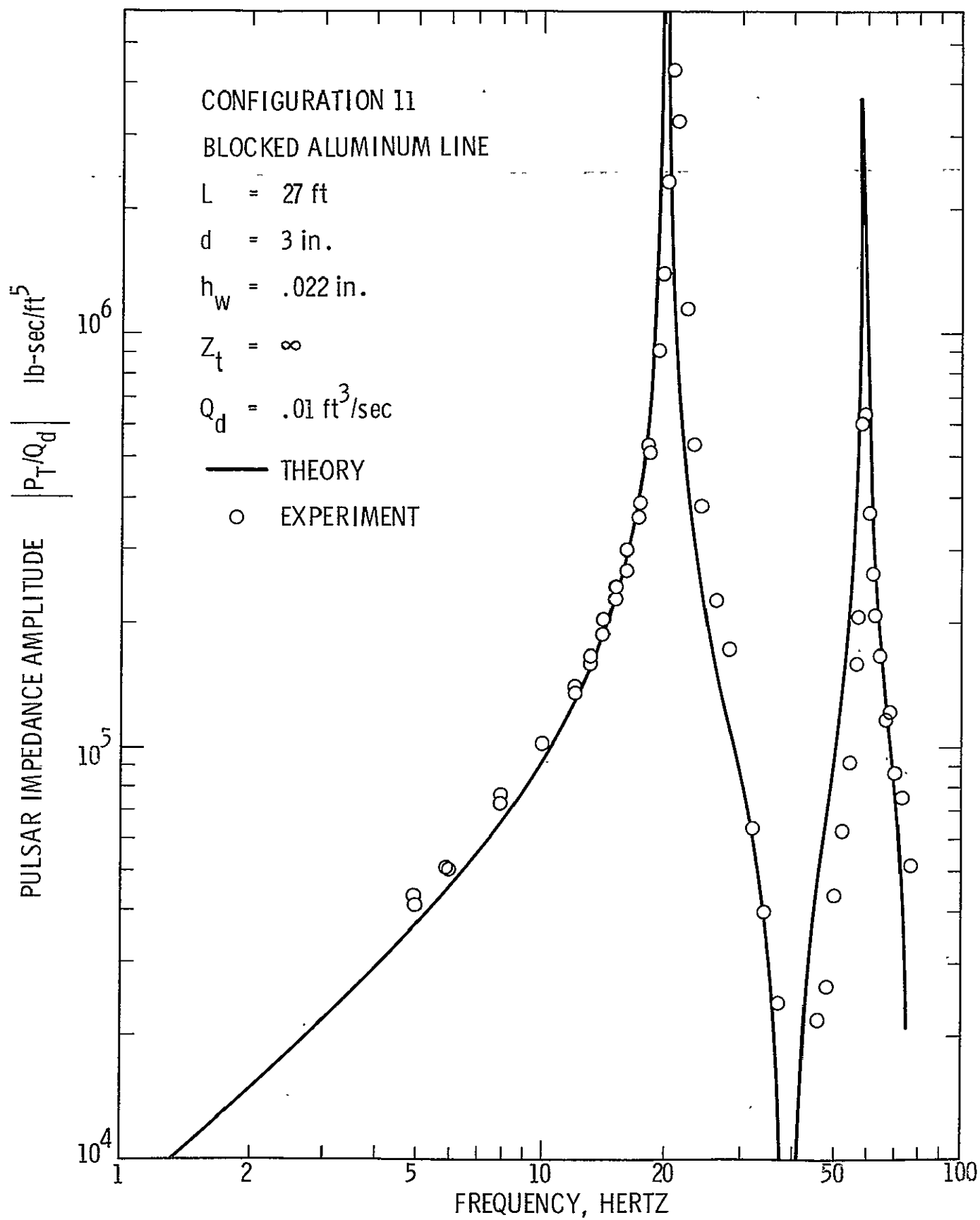
Figure 43. Frequency Response of a Thin-Walled Blocked Aluminum Line
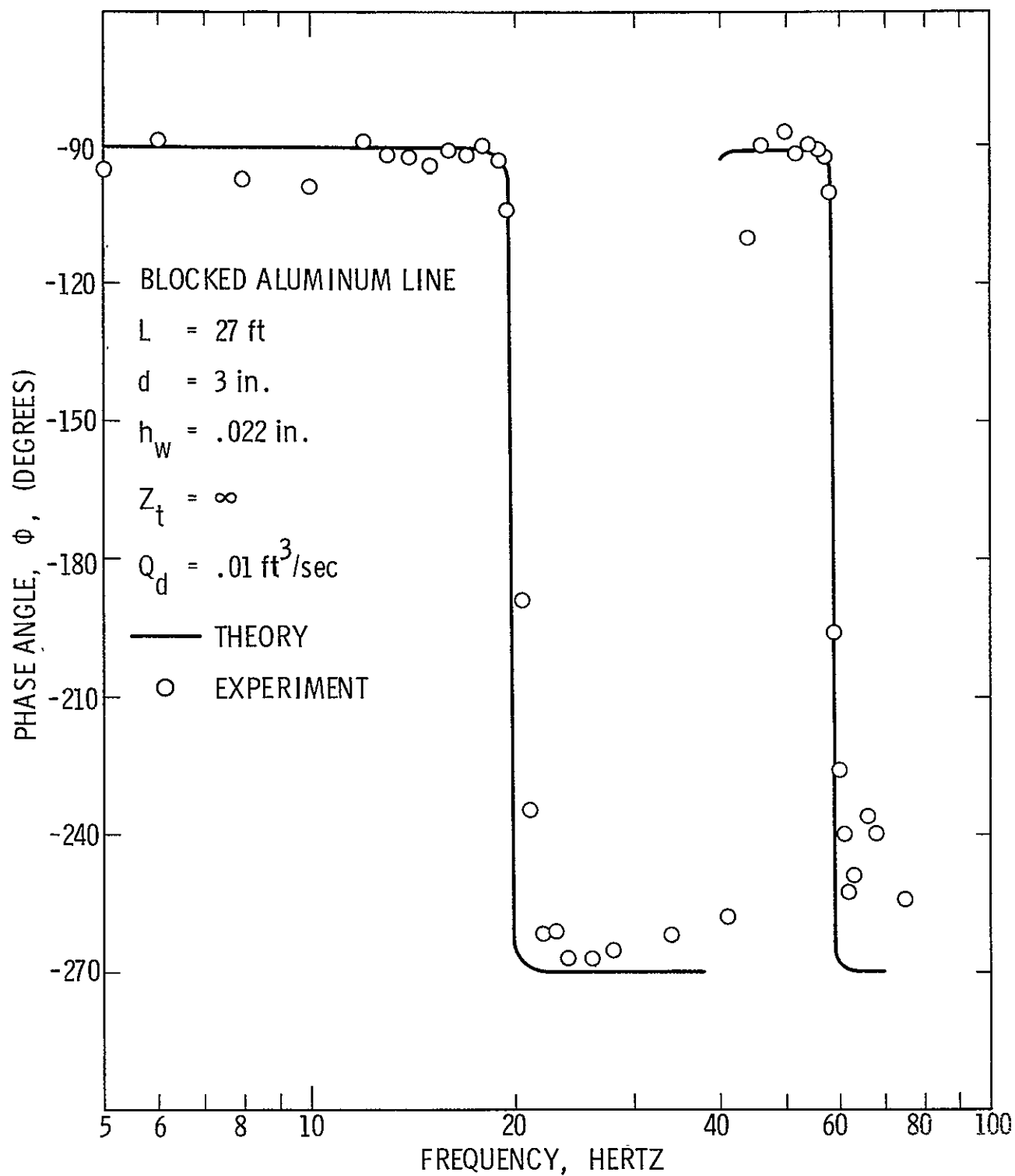
Figure 44. Phase Angle for a Thin-Walled Blocked Aluminum Line
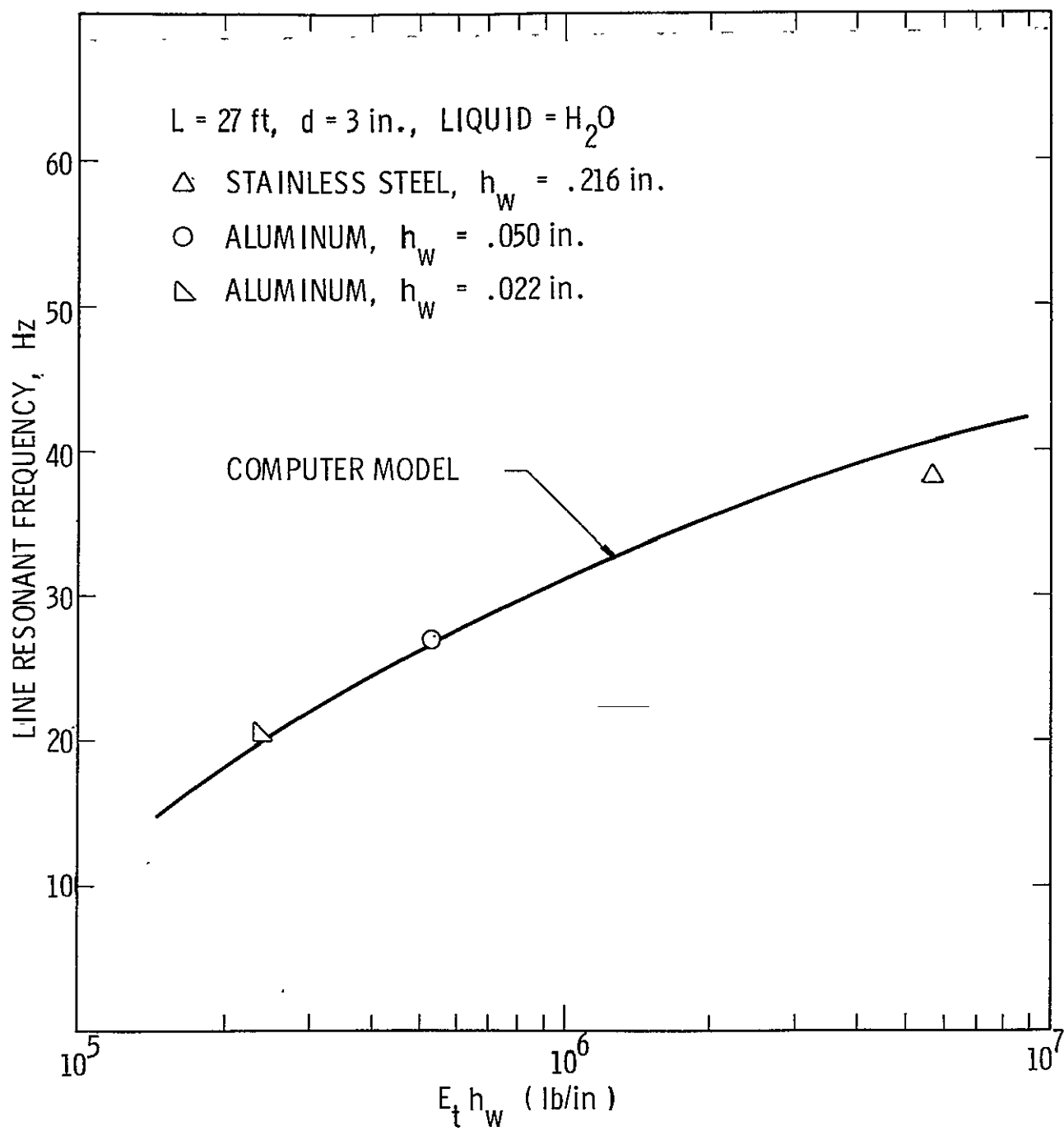
Figure 45 . Effect of Radial Wall Compliance on the Feedline Resonant
Frequency

Tests were also conducted to verify the use of the Korteweg correction to the phase velocity for practical applications, where the terminal resistance or impedance has a finite value and where any increased damping due to wall elasticity (which has been neglected in the analytical model) might show up. The response of an aluminum feedline with a wall thickness, $h = 0.050$ in., and terminated with a nonlinear terminal impedance element operating such that the nominal terminal impedance value, $Z_t = 3.91 \times 10^5$ lb-sec/ft^5, is presented in Figure 46. The corresponding phase relation between the terminal pressure perturbations and the input dynamic flow perturbations is plotted in Figure 47. Also shown in Figure 46 is the computed theoretical response of the same configuration except that the feedline was assumed to be infinitely rigid; it is obvious that a correction is indeed required to properly model wall elastic effects. The results of Figure 46, where the terminal impedance was a finite value, justify the conclusion that the increased spatial attenuation for a line with an elastic wall is negligible over the frequency range of most practical feedline applications.

Entrained Gases

The net effect of entrained gases in the propellant or simulation fluid has been found to decrease the phase velocity and also increase the spatial attenuation by introducing added damping. In determining the effect of a uniform distribution of gas bubbles on the frequency response of feedlines, it was found that a very accurate means of measuring the mass of gas present in the system at the time of testing was necessary. Nitrogen gas was chosen for these tests, and its theoretical effect on the reduction of the speed of sound in the water-gas mixture was computed for several mixture pressures and is shown in Figure 48. From these computations it was evident that only a small mass of entrained gas would drastically vary the frequency response of a given feedline requiring a sensitive method for the measurement of the mass ratio. An injector was also designed and fabricated to generate a uniform distribution of small nitrogen gas bubbles assumed by the analytical model.

The mass ratio, Φ, of the liquid-gas mixture was determined from measurements made of nitrogen gas mass flow rate into the feedline system. The gas bubbles were injected at the upper end of the feedline, just below the tank or upper reservoir. The mixture of nitrogen gas bubbles and water were then swept downstream with the mean flow at the rate

$$v_B = v_O - v_{BR} \tag{148}$$

where v_O was the velocity of the water in the line and v_{BR} was the bubble

95
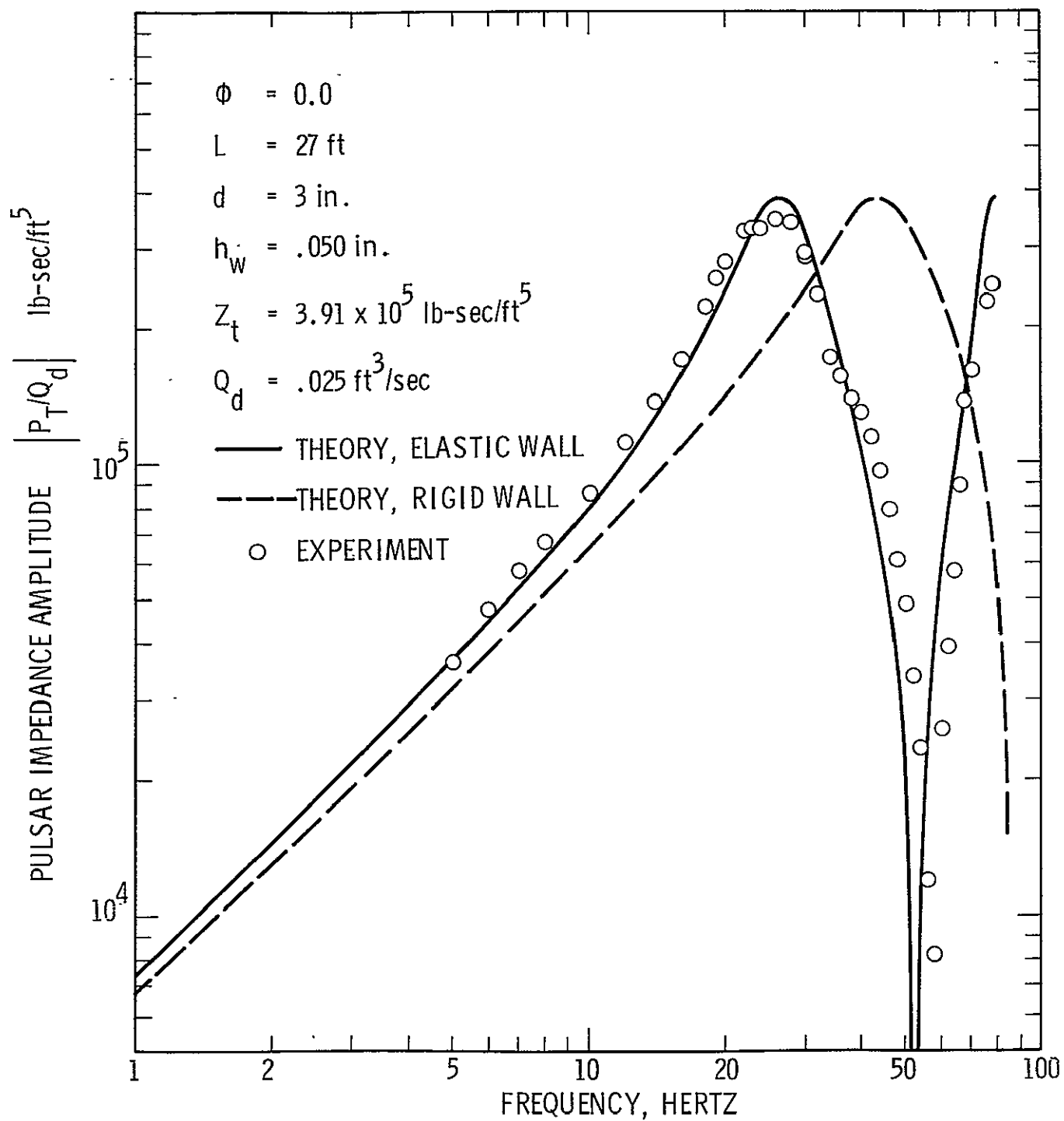
Figure 46. Frequency Response of an Aluminum Line Excited by a Side Branch Pulsar
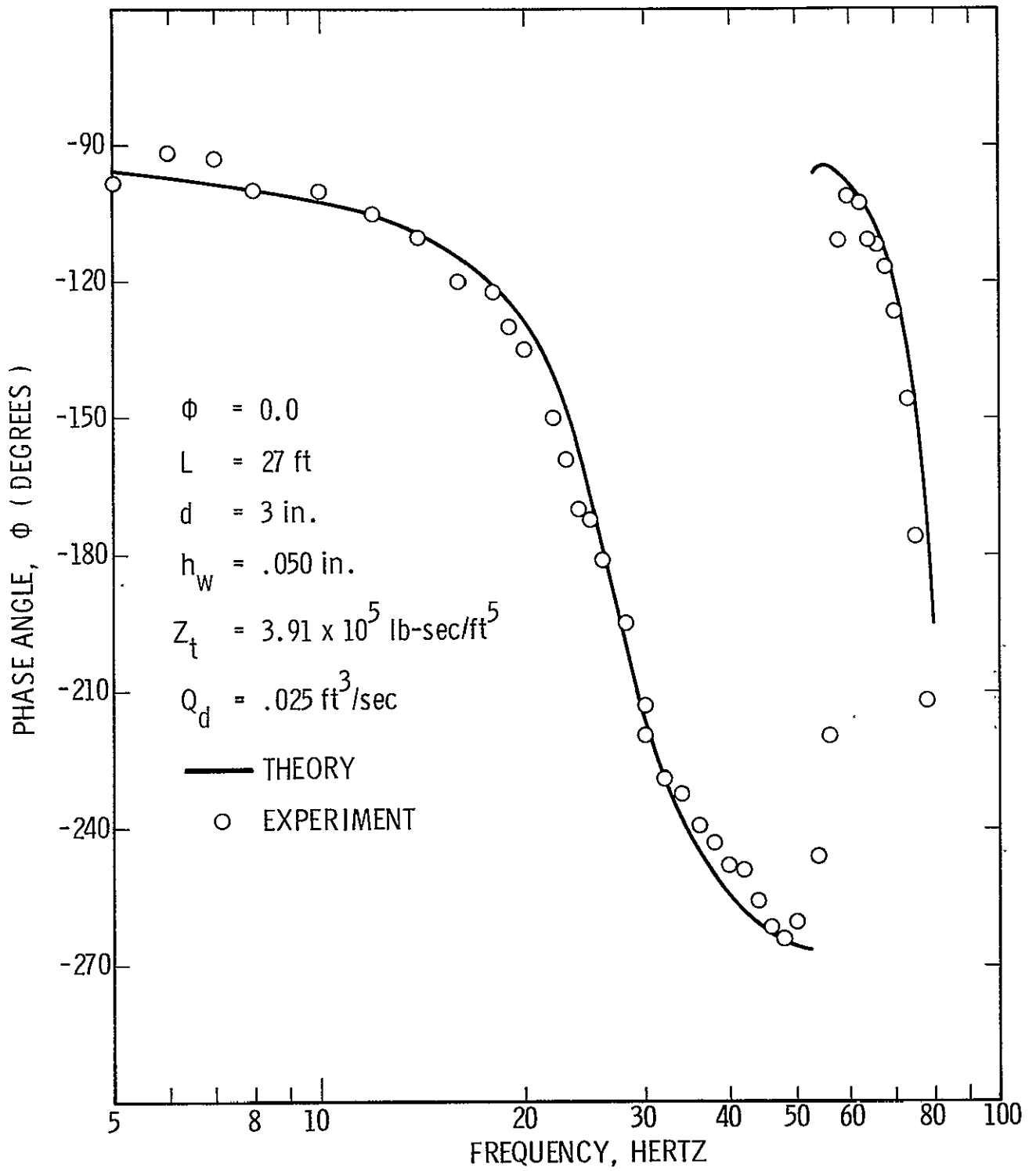
Figure 47. Phase Angle vs Frequency for a Line Excited by a Side Branch Pulsar
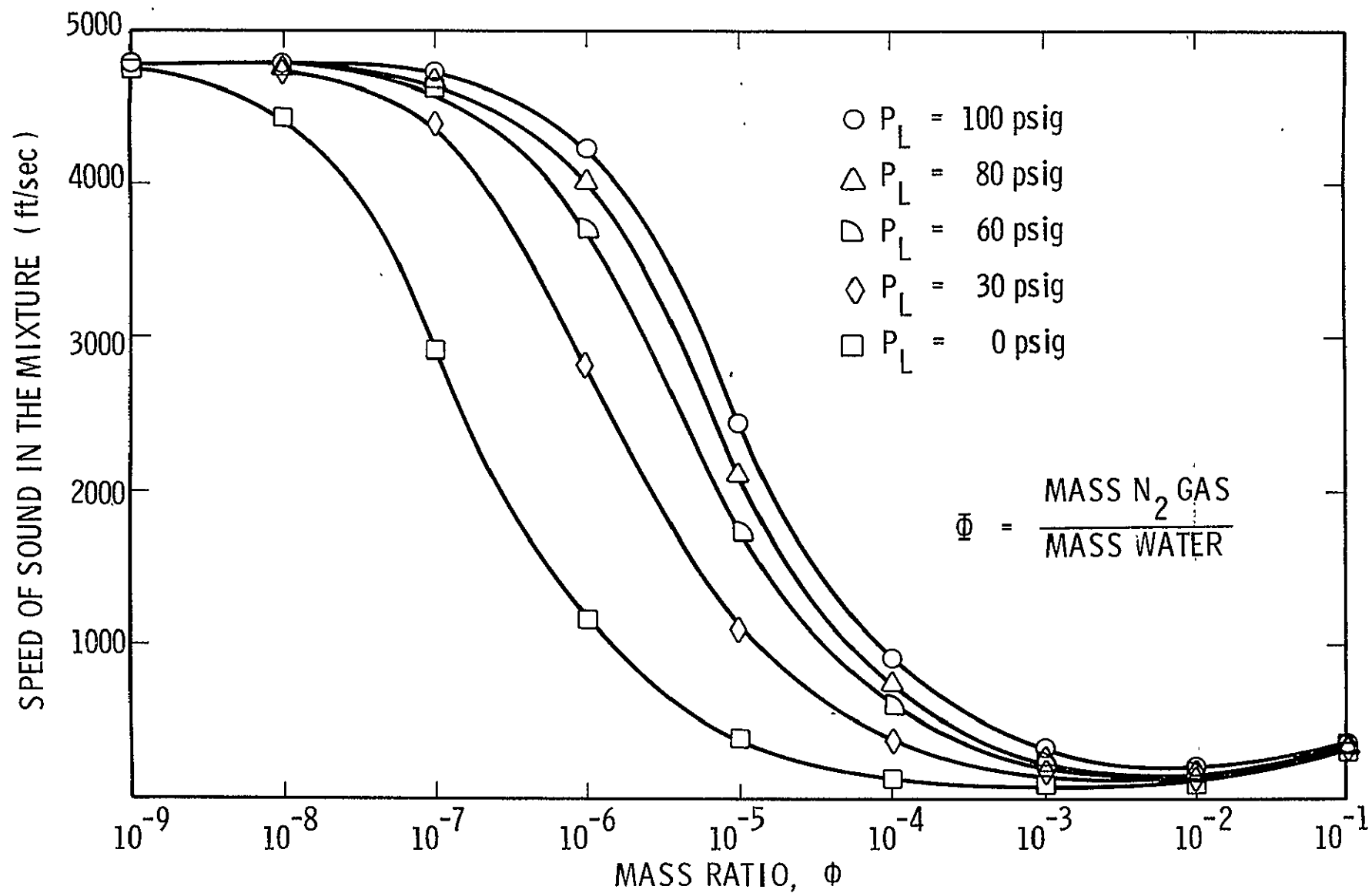
Figure 48. Speed of Sound in Water with Nitrogen Gas Bubbles

rise velocity. In all cases, the bubble rate of rise had to be less than the mean water velocity; the gas flow rate measurements would have been meaningless if an unknown loss into the upper reservoir occurred. By making the bubbles small, their rates of rise were well below that of the water velocity at the test conditions. A Cole-Parmer low volume flow meter which had a range of 10 to 1900 cubic centimeters per minute was used to measure the volume flow rate; the pressure at the meter was recorded and used to calculate the gas density at the meter, from which the nitrogen gas mass flow rate into the feedline system was obtained.

With the feedline facility being operated "open loop", the total mass of flow into the system at the injector was assumed to pass downward through the feedline; i.e., none was assumed to escape upward into the reservoir. To verify the assumption regarding the bubble rise velocities, a special bubble calibration chamber was designed to measure both the bubble sizes being generated by the injection device and their rates of rise. The photograph (Figure 49) shows the calibration tube, constructed of acrylic tubing (plexiglass) and partially filled with water. The chamber was pressurized to value approximating those at the feedline entrance (tank exit) which would occur during tests. For calibration purposes, the gas injector was installed at the bottom of the tube; and the nitrogen gas was injected at approximately the rates required for the test mass ratios, Φ. The pressure was maintained constant by allowing the gas to bleed from the upper volume at the same rate as it was being injected. Figure 50 shows a photograph taken close-up, with a scale mounted on the chamber wall from which measurements were made of the bubble sizes. From these visual observations, it was determined that the bubble distribution was nearly homogeneous. The bubble rates of rise were obtained by dividing a known distance marked on the calibration chamber wall by the time required for a selected group of bubbles to traverse that distance. The bubble rise velocities varied from 0.2 to 0.4 ft/sec, depending on the bubble size.

A close-up photograph of the bubble injector is presented in Figure 51. This injector was designed to bolt between the flange at the tank exit and the upper feedline flange. The nitrogen gas entered the injector at two ports located 180° apart, and passed around a channel cut circumferentially around the injector flange. The bubbles were finally created by passing the gas through small diameter tubes, fabricated from hypodermic tubing and drawn down by heating and stretching one end until the diameter was of the order of 0.001 inch. Other researchers, Carstensen and Foldy[22], and Fox, Curley, and Larson[23], performed tests requiring a uniform distribution of gas bubbles in a liquid; it was from their experience that ideas were drawn for the development of this gas injector.

99
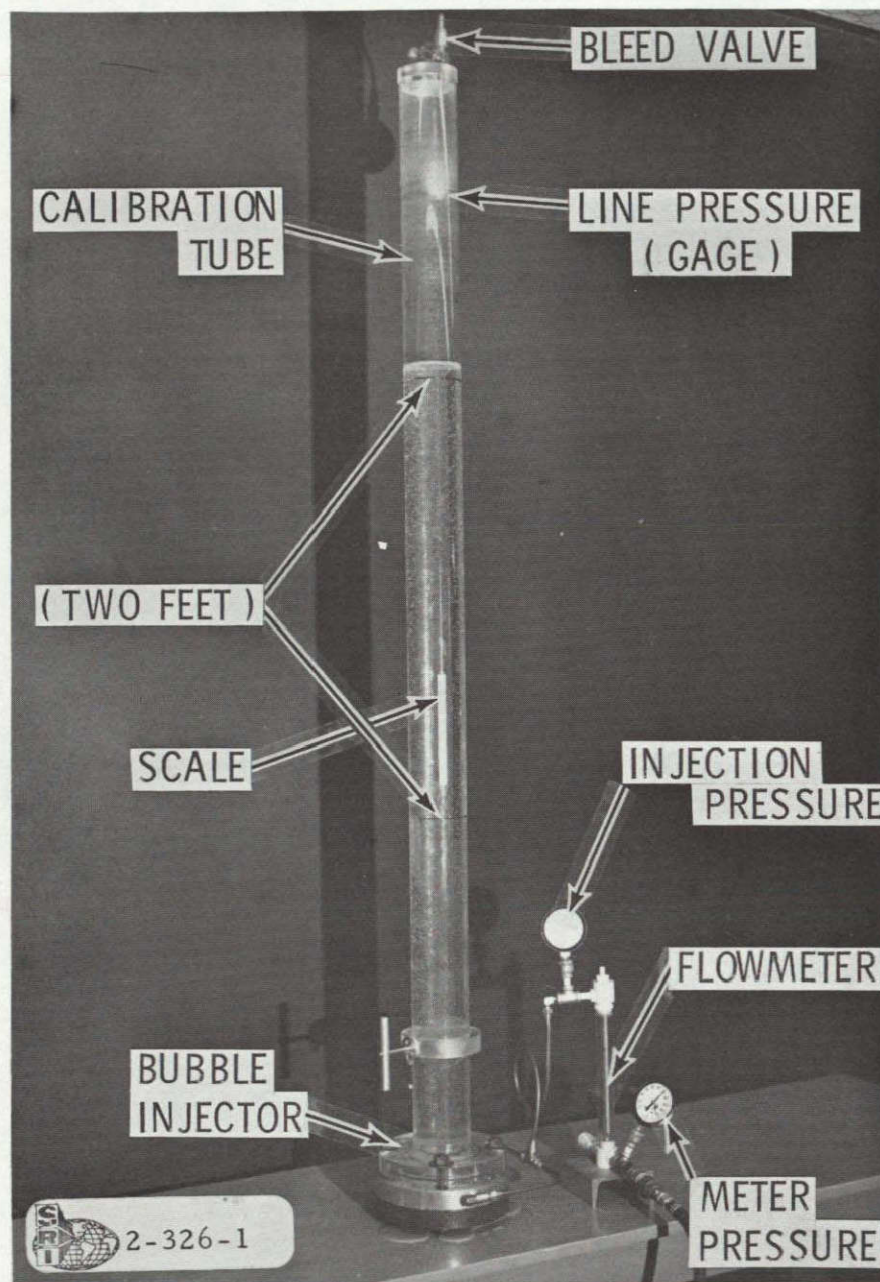
Figure 49. Calibration Tube for Bubble Measurements
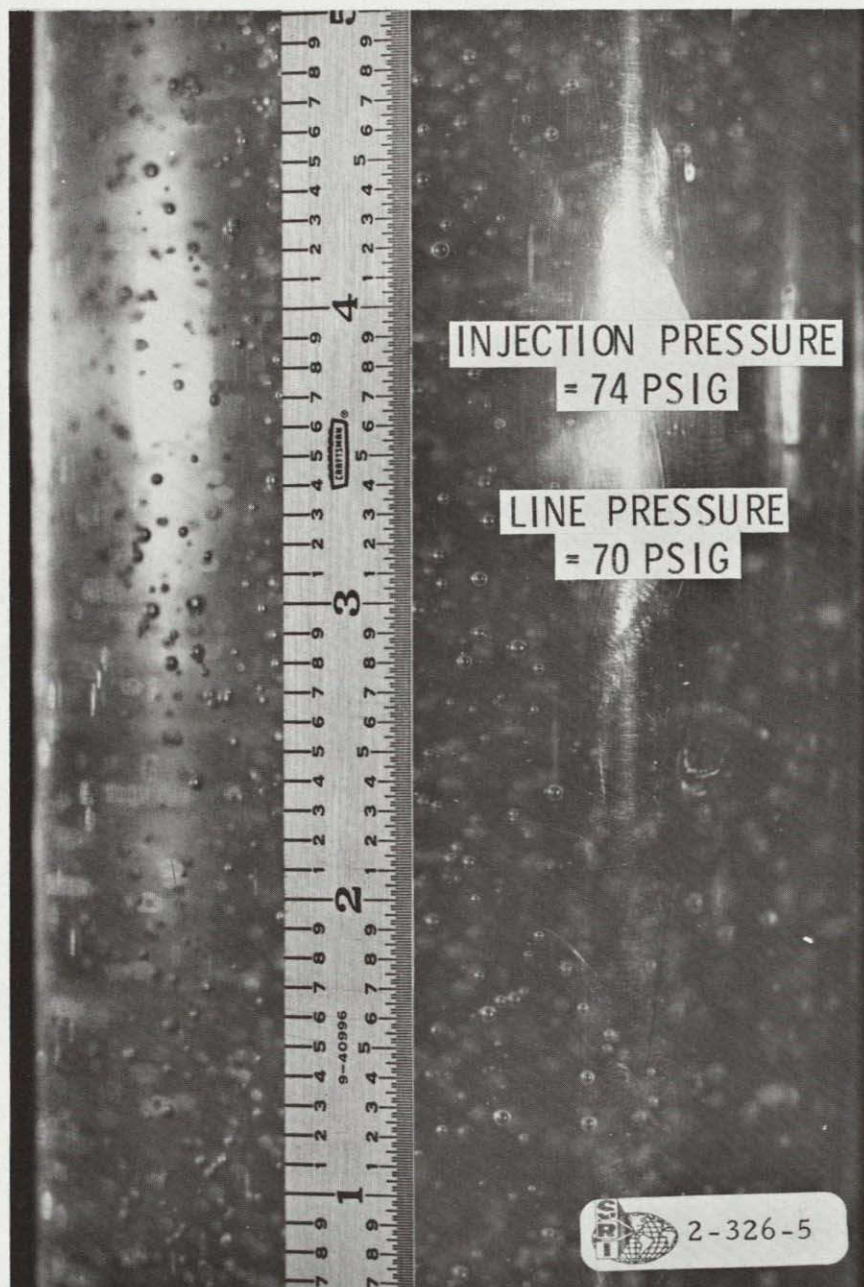
Figure 50. Close-Up of Bubble Sizes and Distribution

ANNULAR DISTRIBUTION CHANNEL

TO FLOW METER AND GAS SUPPLY

3"

INJECTION NOZZLES DIAM. ≈ 0.001"

C-40465
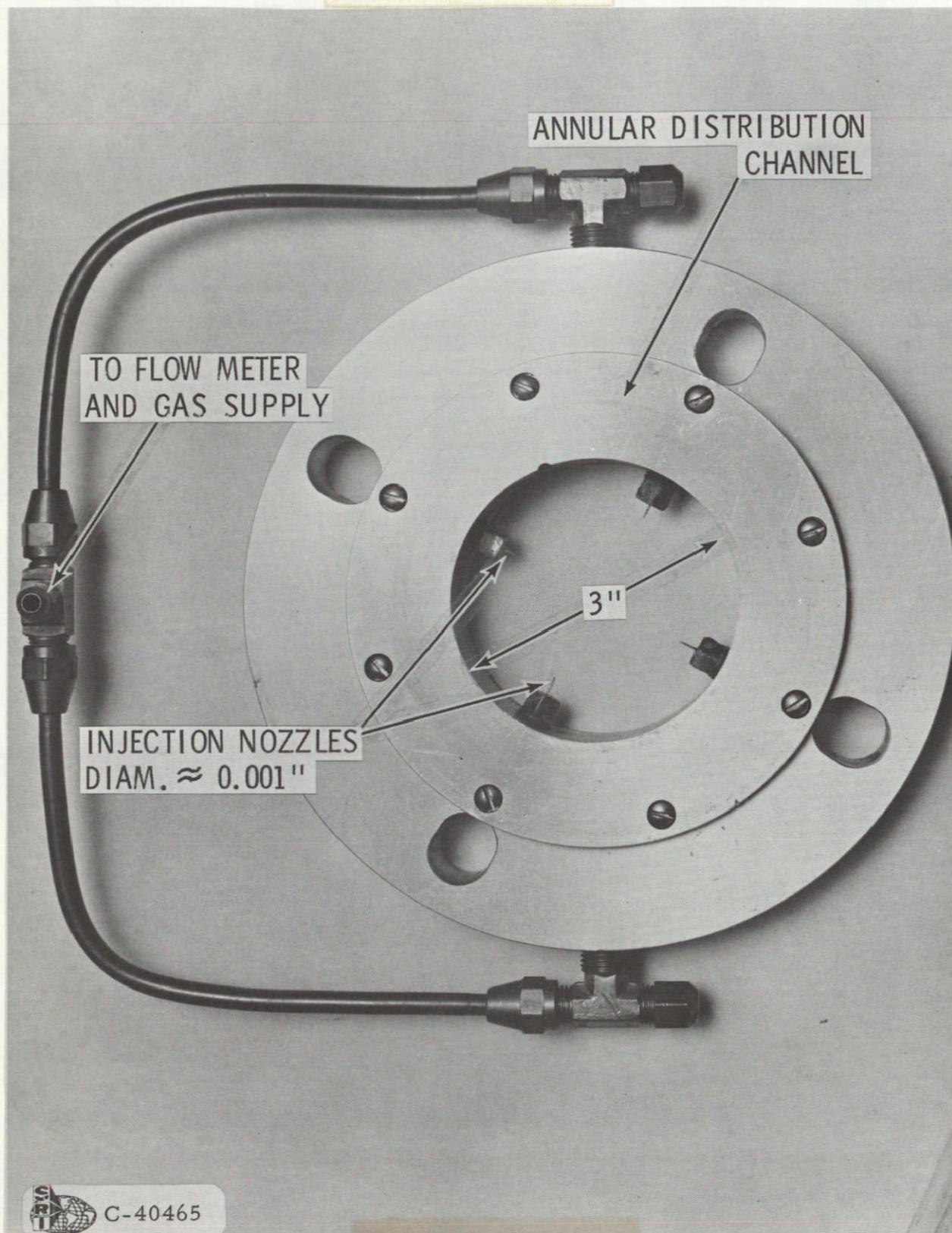
Figure 51. Nitrogen Gas Bubble Injector

102
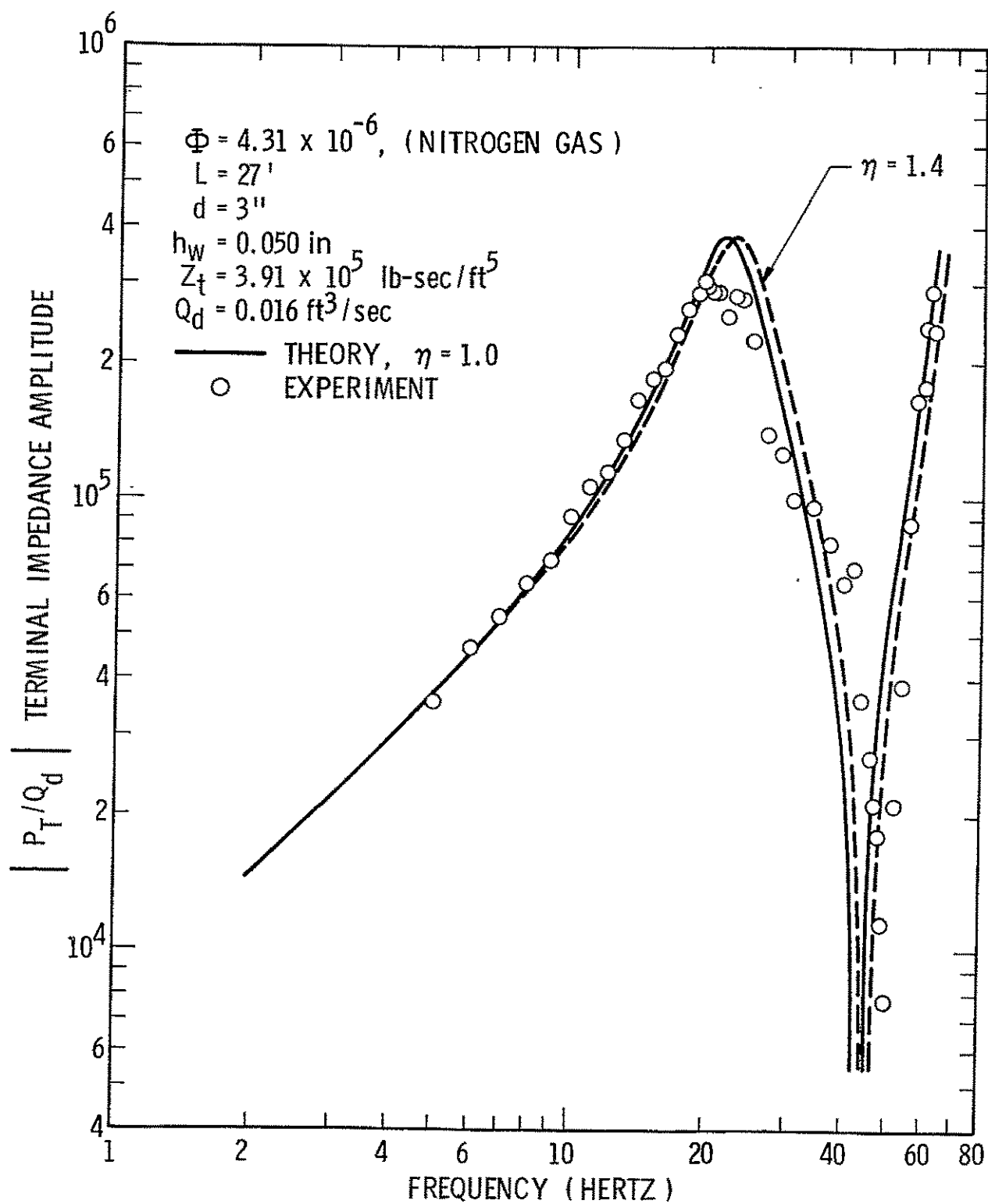
Figure 52. Frequency Response of An Aluminum Feedline
with A Water – N_2 Mixture
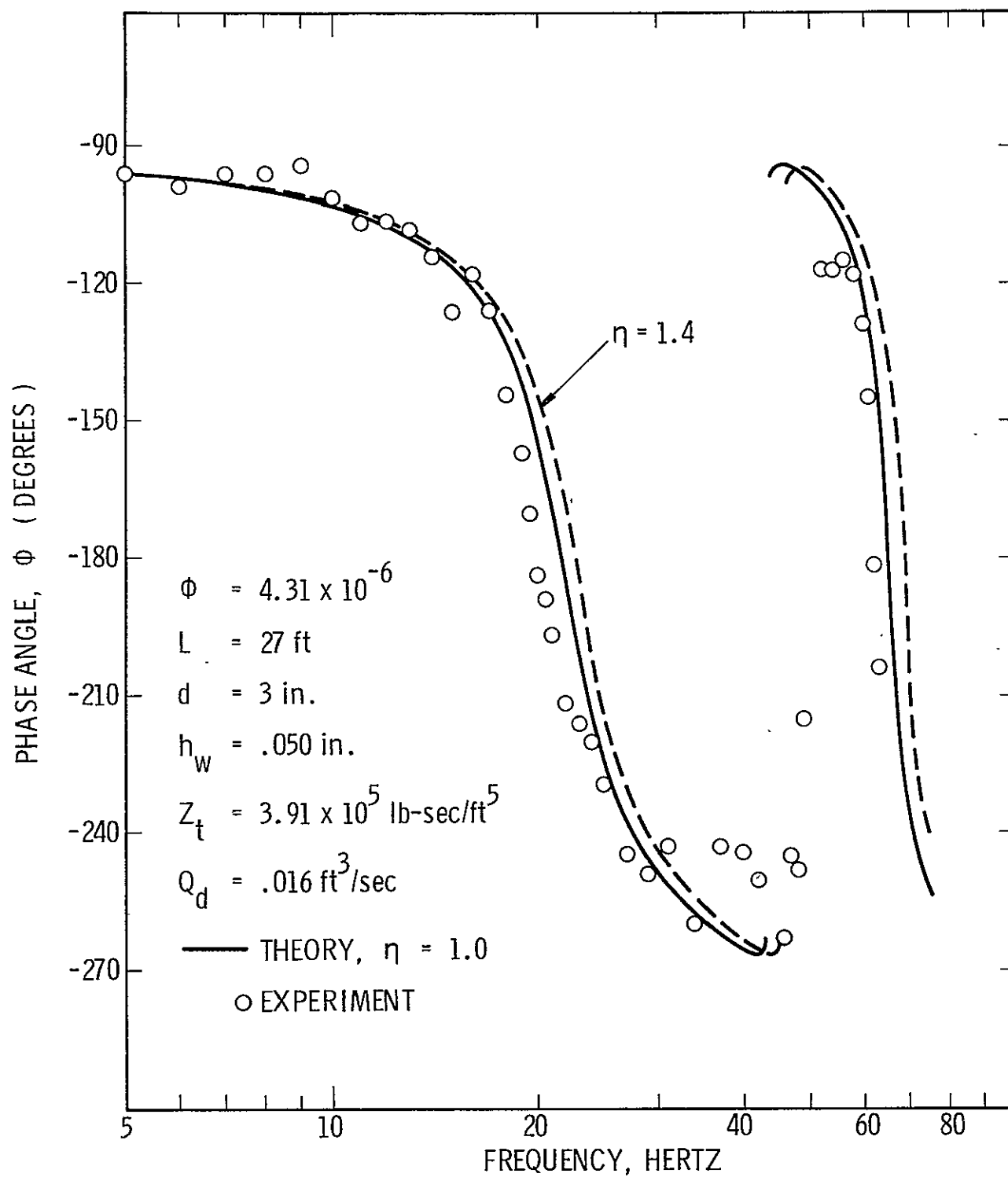
Figure 53. Phase Angle vs Frequency for an Aluminum Line with a Water-Nitrogen Gas Mixture

105
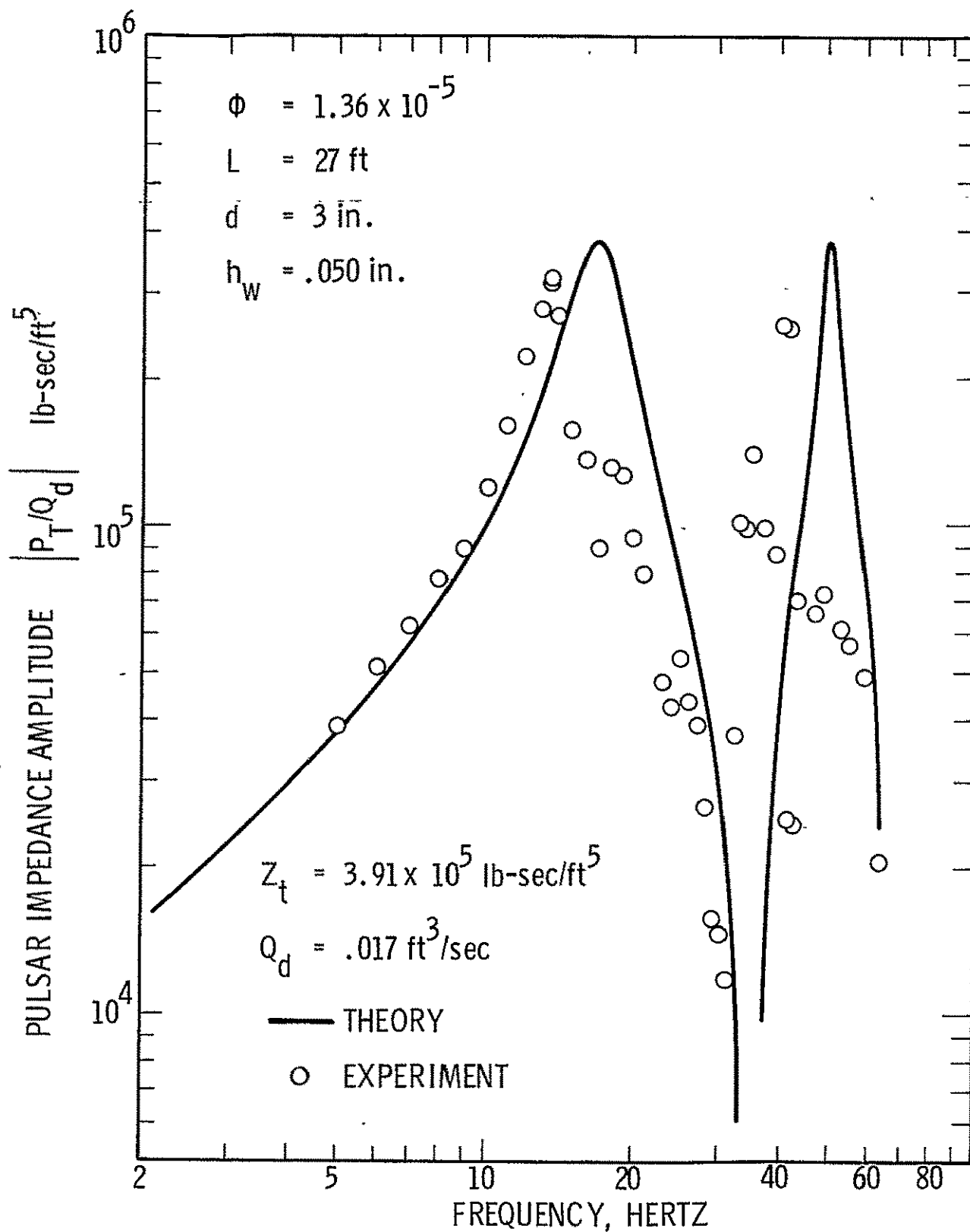
Figure 54. Frequency Response of an Aluminum Feedline with a Water-Nitrogen Gas Mixture
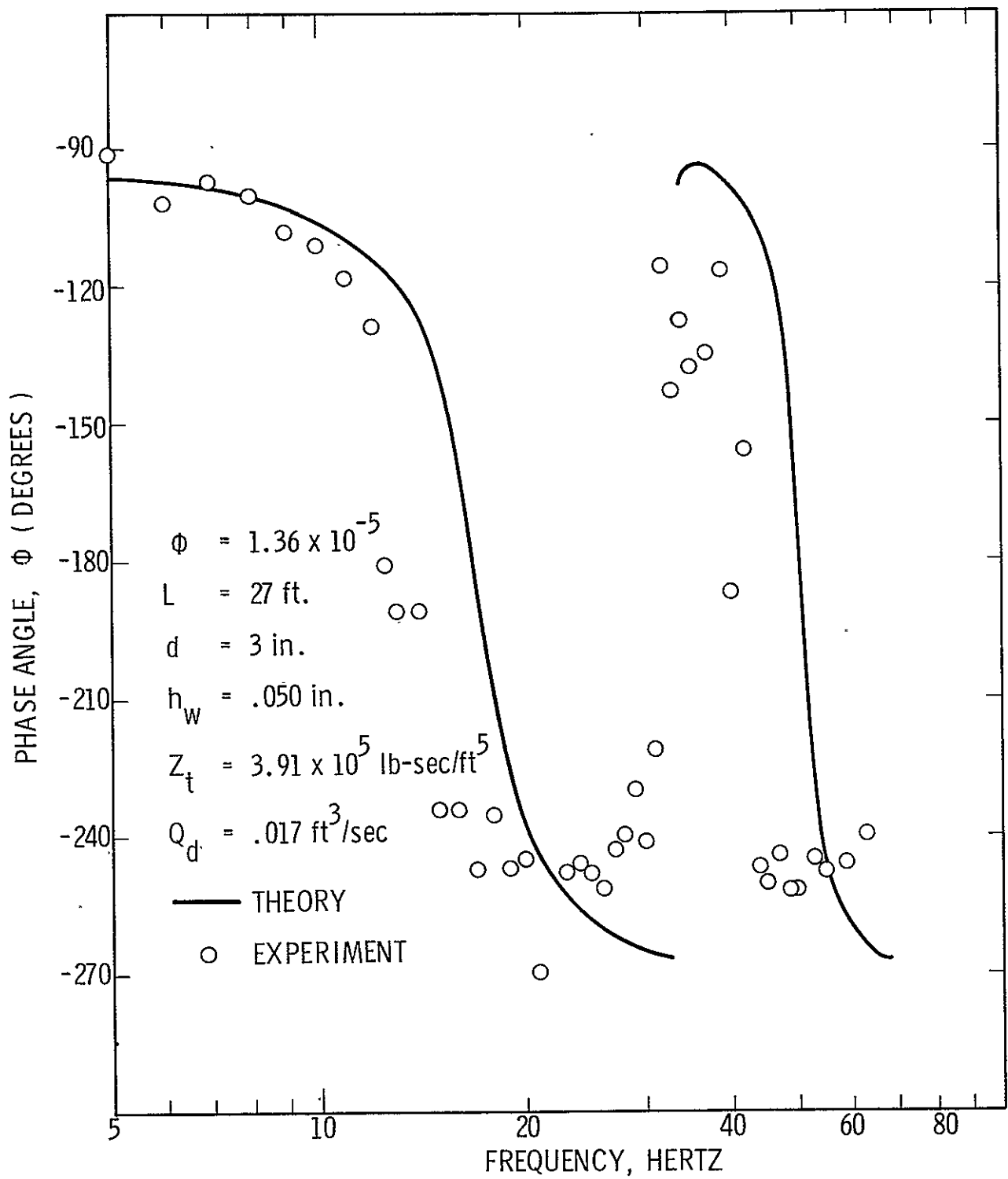
Figure 55. Phase Angle vs Frequency for an Aluminum Line with a Water-Nitrogen Gas Mixture

than for the $\bar{\Phi} = 4.31 \times 10^{-6}$ and $\bar{\Phi} = 0$ cases, indicating a possible increased damping with mass ratio, $\bar{\Phi}$. It should be noted, however, that the difference in amplitude between theory and experiment at resonance is really no greater than that observed without bubbles, as evidenced by Figures 35 and 37. The difference could be only a result of experimental inaccuracies in measuring the correct amplitude at resonance.

From Figure 48 it can be observed that near $\bar{\Phi} = 10^{-5}$, the rate of change of the mixture speed of sound with mass ratio is near its maximum; hence, a small error in the measurement of mass ratio, $\bar{\Phi}$, could have produced the apparent discrepancy between the theoretical and experimental resonant frequencies for this configuration and shown in Figure 54. The experimental data indicate that the mass ratio was larger than that measured and thought present. Data were also recorded for a measured mass ratio, $\bar{\Phi} = 5.61 \times 10^{-6}$, which was the greatest mass ratio produced for any of the experiments conducted. The results are shown in Figures 56 and 57. Again, the data showed a lower resonant frequency for both the first and second longitudinal modes than the theoretical predictions, although in this case the resonant frequency was off by only 1.5 Hz for the first mode and 5 Hz for the second peak. The pressure/flow perturbation amplitudes at resonance were considerably damped with this much greater volume of distributed nitrogen gas in the system. The theoretical response also indicated more dissipation of energy at resonance, but the degree of damping was significantly less than that which was obviously present. It is possible that further refinements should be made to the analysis to reflect this observed increase in attenuation for the larger mass ratios of gas to liquid. This increased attenuation with increasing gas/liquid mass ratio, $\bar{\Phi}$, suggests that injection of inert gases, as suggested in earlier research[24], might be a very suitable method of POGO suppression. Measurements made and reported in Reference 24 indicate that for reasonable volume fractions (volume gas/volume of liquid) the thrust produced is hardly affected.

VII.4   Local Compliances

The next phase of the experimental test program conducted for verification of the analytical model and computer program involved generating local compliances or compliance-type elements and experimentally measuring their effects on the frequency response of feedlines. More specifically, the validity of the model used to simulate "complex" side branches and localized gas or vapor bubbles was established. The term complex side branch refers to any type branch in which there exists a fluid resistance and/or inertance as well as a compliant-type element. The analytical models for both categories of local compliances were discussed in Section IV of this report.
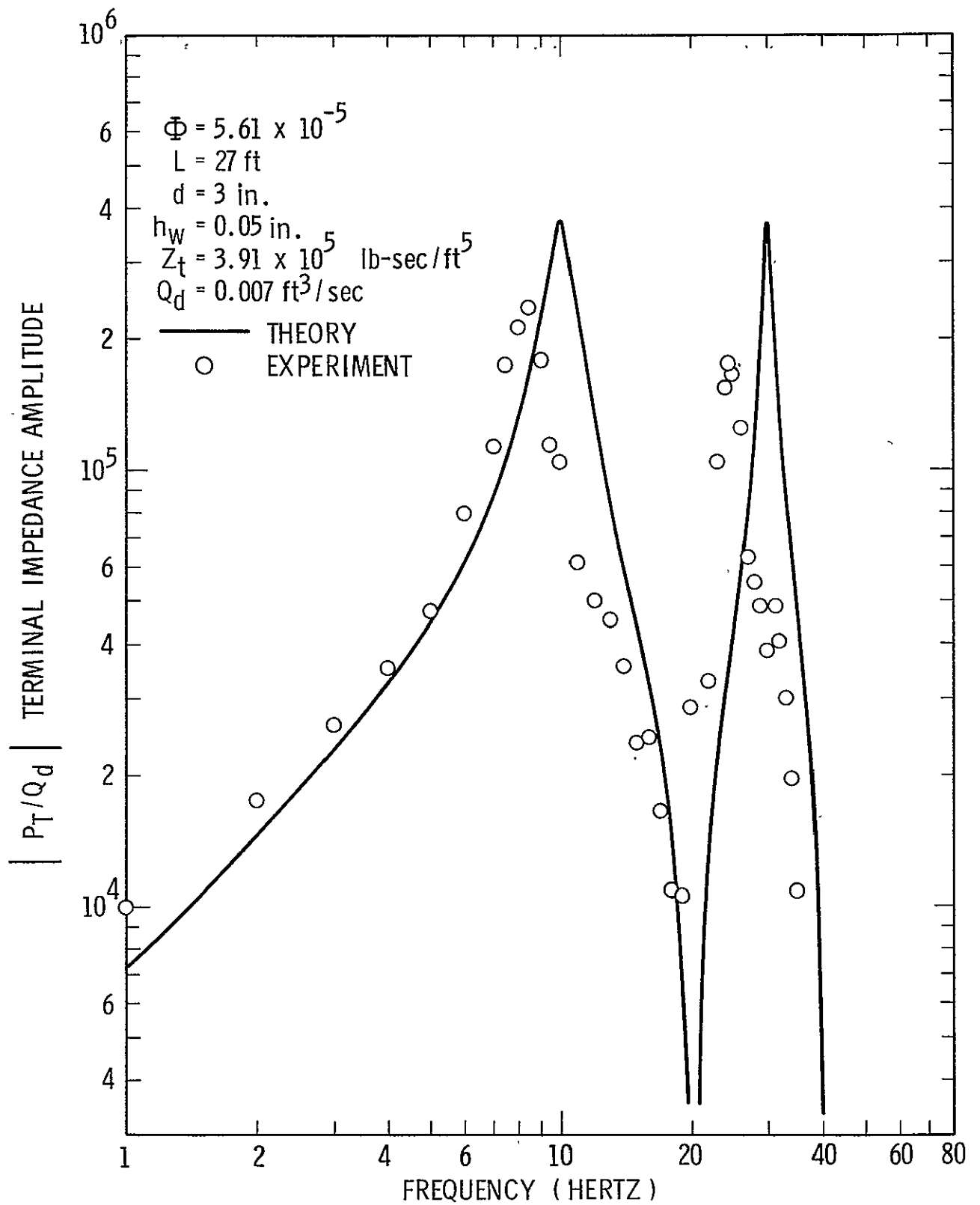
Figure 56. Frequency Response of An Aluminum Feedline
with A Water – N_2 Mixture
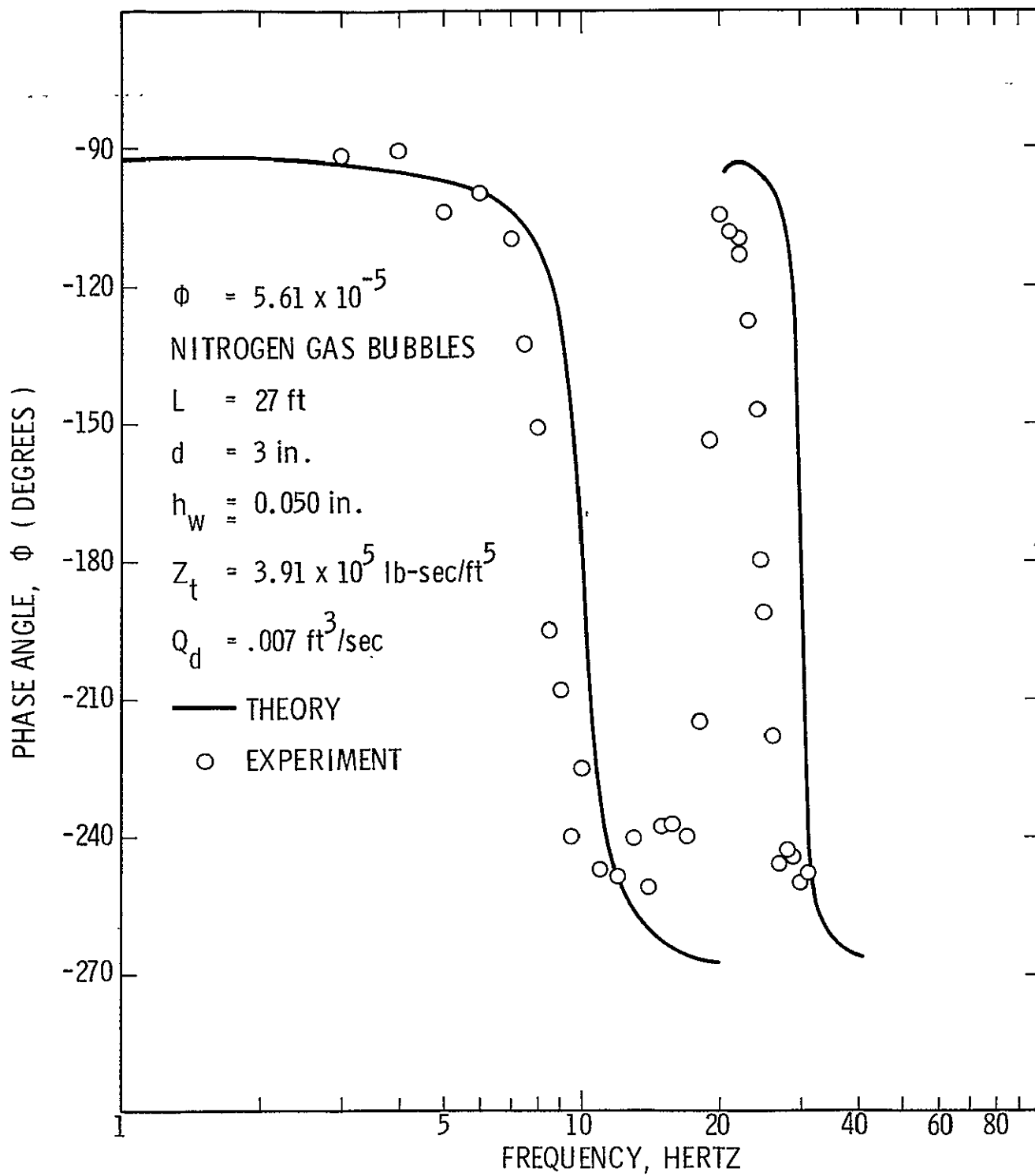
Figure 57. Frequency Response of an Aluminum Feedline with a Water-
Nitrogen Gas Mixture

The figure shows phase angle ϕ (degrees) versus frequency (hertz) with the following parameters:

$\phi = 5.61 \times 10^{-5}$

NITROGEN GAS BUBBLES

$L = 27$ ft

$d = 3$ in.

$h_w = 0.050$ in.

$Z_t = 3.91 \times 10^5$ lb-sec/ft^5

$Q_d = .007$ ft^3/sec

—— THEORY

○ EXPERIMENT

110

Complex Side Branch

The types of side elements typical of rocket feet systems (accumu-lators and partially gas-filled pressure-sensing lines) behave as local compliance-like elements. The experimental arrangement used to verify the computer simulation (analytical model) is shown in Figure 58. The side branch was located 4 feet above the line terminal; the length of the branch was 10.2 feet and the diameter was 1.4 inches, with a wall thickness equal to 0.049 inch. A short (4-inch long) plexiglass tube was attached vertically at the end of the branch; this allowed for visual obser-vation and measurement of the volume of trapped gas at the branch termi-nus. Tests were performed to obtain response curves (amplitude ratio and phase angle) for the main feedline, with the system excited by the side branch pulsar. In addition, dynamic pressures were recorded at the end of the side branch for several of the tests.

The feedline geometry described above was tested with water as the fluid media, and various volumes of gas (air) were trapped at the side branch terminus. Figure 59 presents the frequency response obtained with a terminal impedance, $Z_t = 3.91 \times 10^5$ lb-sec/ft^6, and with a branch terminal volume equal to 0.769 in.^{3}. It appears that the measured reso-nant frequencies have been shifted (lowered) by the amount predicted by theory, but the damping effect created by the side branch is somewhat greater than that predicted by the analytical model. The phase relation between the terminal pressure perturbations and the input flow perturba-tions are plotted in Figure 60.

Figures 61 and 62 present the measured pressure-to-flow pertur-bation ratio amplitudes and their corresponding phase relation for the same line geometry with a larger air bubble volume ($V_0 = 2.67$ in.^{3}) at the side branch terminus. These data also generally agree with the theoretical results, also plotted in the same figures as solid lines, ex-cept the experimentally determined amplitudes at resonance are some-what less than expected. The effects of a further increase in bubble size to a bubble volume equal to 5.25 in.^{3} with the same terminal impedance and feedline geometry are presented in Figures 63 and 64. In general, these data represent the poorest agreement with theory of all the data collected for a feedline with a complex side branch.

Close examination of Figures 59 through 64 reveal that the net effect for an accumulator-type complex side branch element, terminated by a trapped volume of gas, is to shift (lower) the resonant frequency in proportion to the trapped gas volume and to also produce increased damping due to the resistance in the branch line. Perhaps an improved model of side branch elements would be to treat the branch line as a

111

$d_1 = 3.0$ in.

$d_b = 1.4$ in.

$L_1 = 23$ ft

$L_2 = 4$ ft

BL $= 10.2$ ft

P_1 Q_1

d_1

L_1

GAS
VOLUME

Q_2, P_2 ← BL →

$P_2 = P_3$

Q_3, P_3 Q_B, P_B

Q_4, P_4 — FLOW PULSAR

L_2

Q_d

Q_5, P_5

$Z_t = P_5/Q_5$
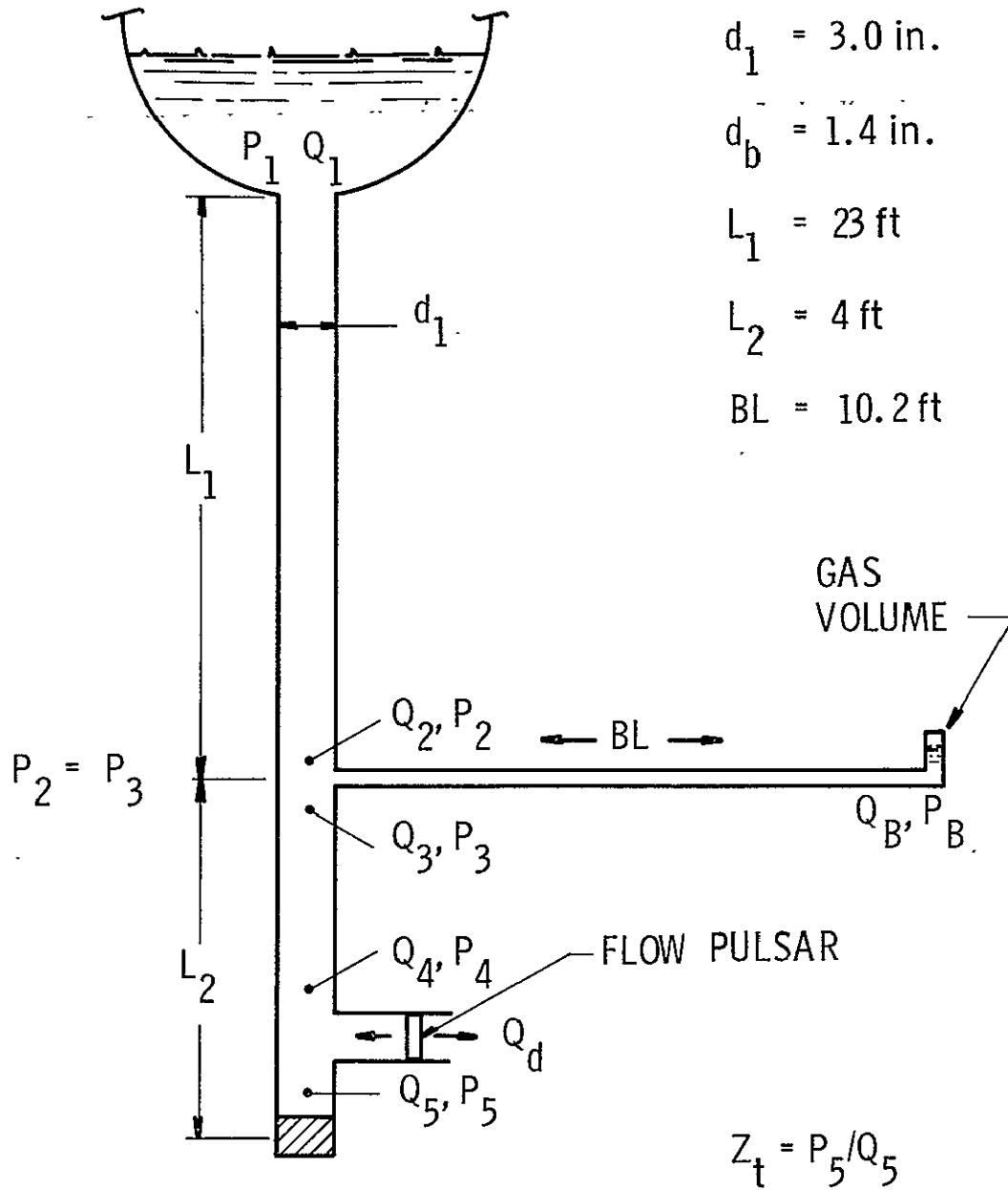
Figure 58. Geometry of Feedline Excited by a Pulsar with a Complex Side Branch
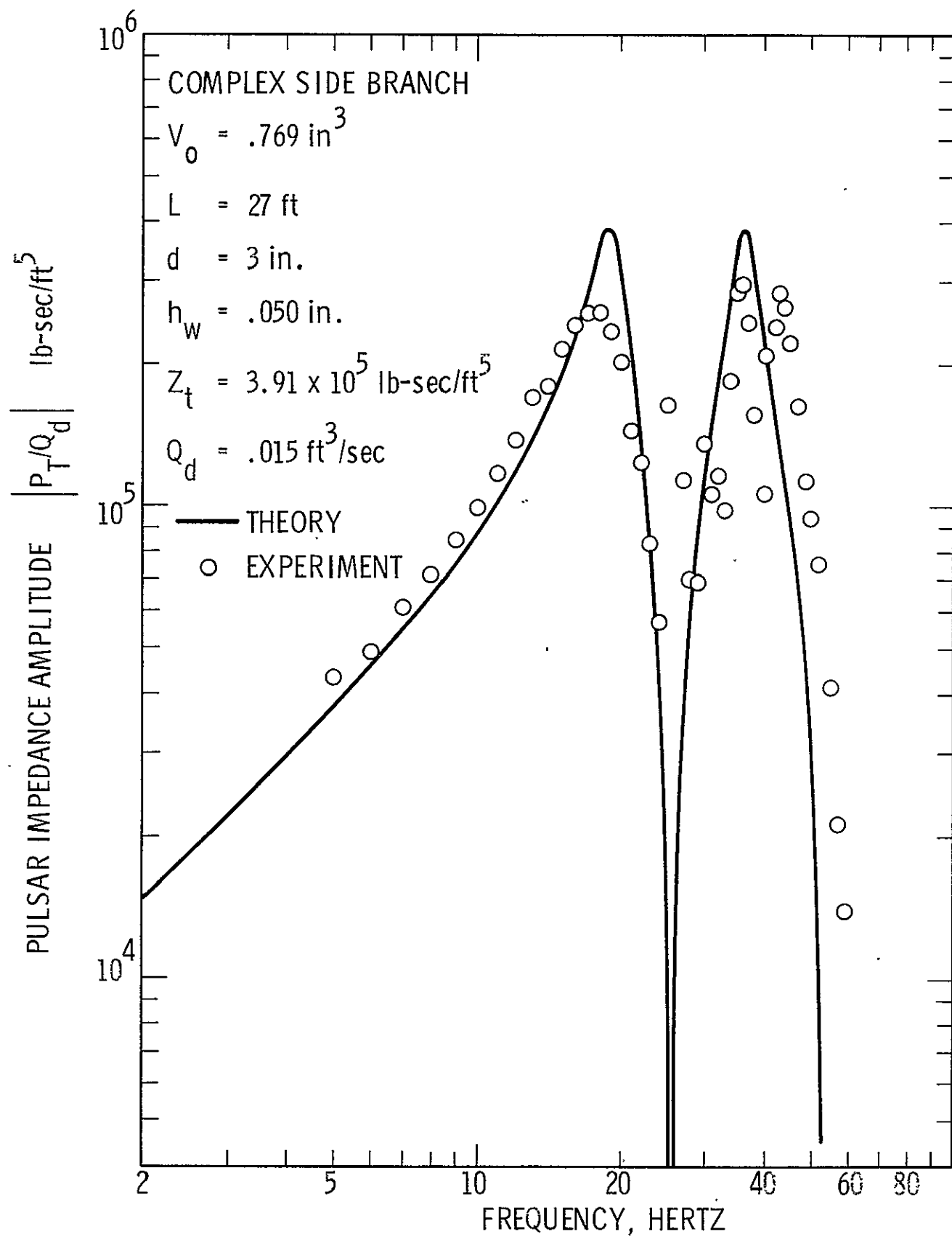
Figure 59. Frequency Response of Line with a Side Branch
Element with Trapped Air

COMPLEX SIDE BRANCH
CONFIGURATION 14D

v_B = .769 in.^{3}

Q_d = .015 ft^3/sec

Z_t = 3.91 x 10^5 lb-sec/ft^5
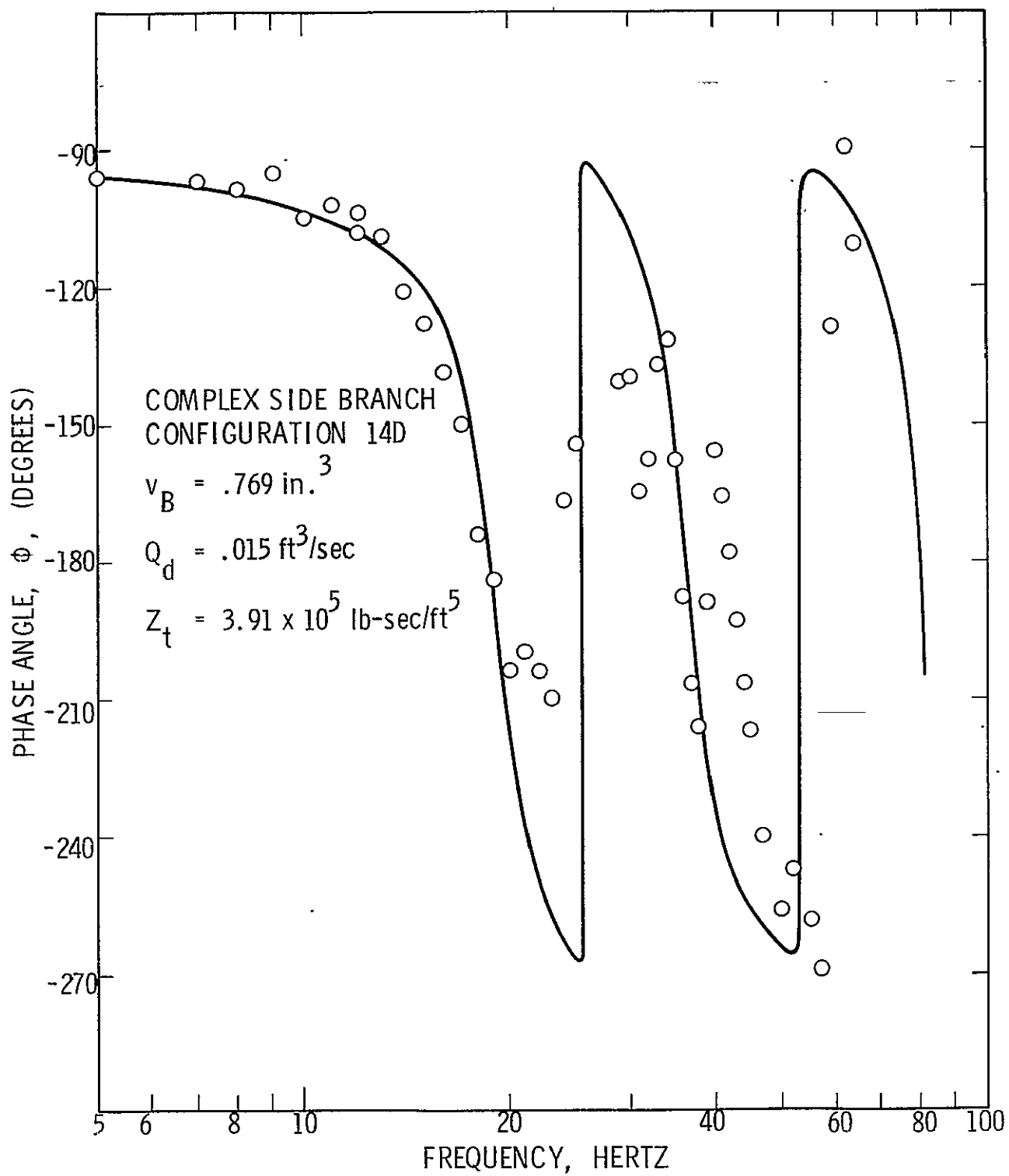
Figure 60. Phase Angle vs Frequency for a Line with a Side Branch
Element with Trapped Air

114
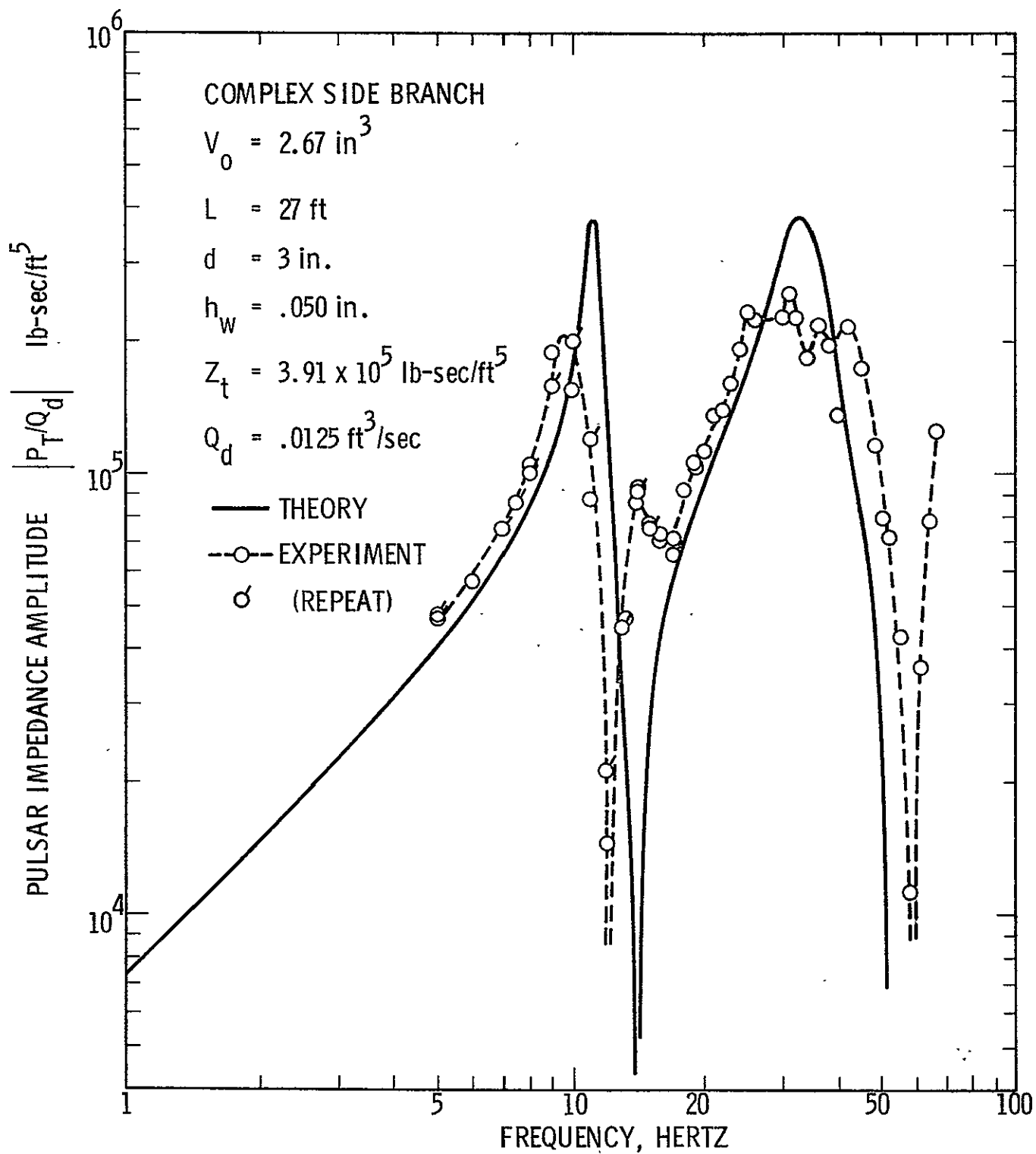
Figure 61. Frequency Response of a Line with a Side Branch Element with Trapped Air

115
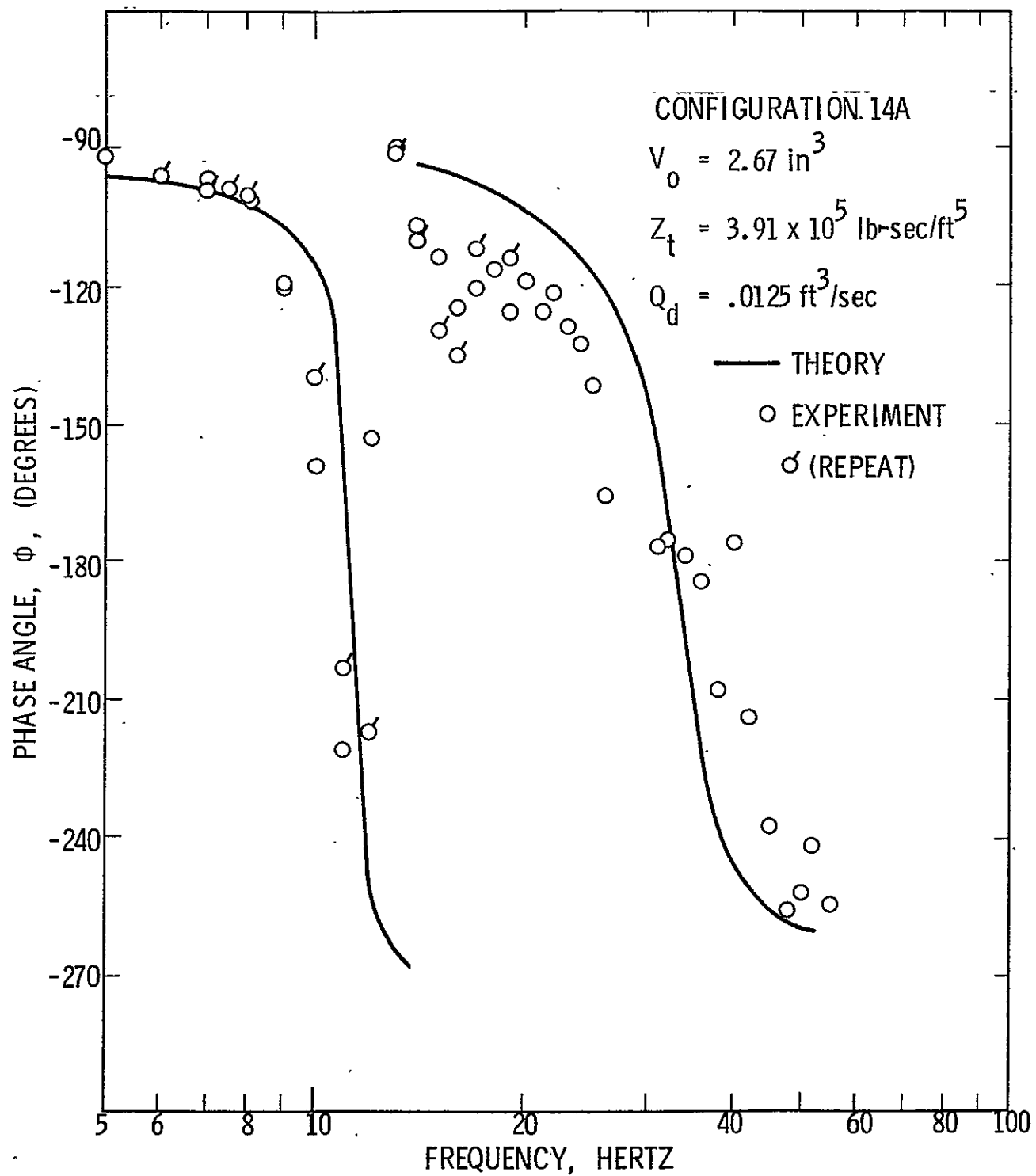
Figure 62. Phase Angle vs Frequency for a Line with a Side Branch with Trapped Air
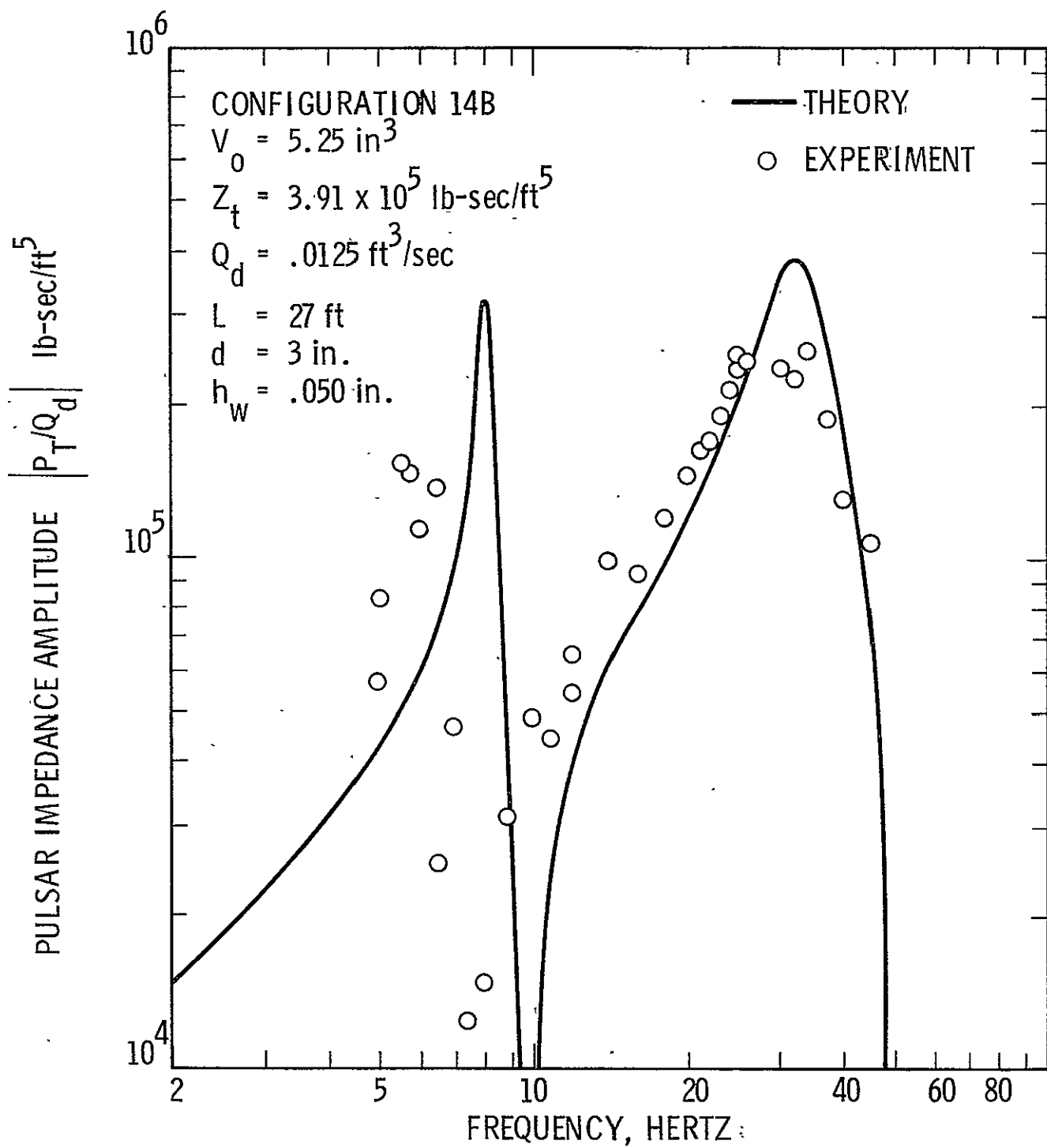
Figure 63. Frequency Response of a Feedline with a Side Branch
with Trapped Air
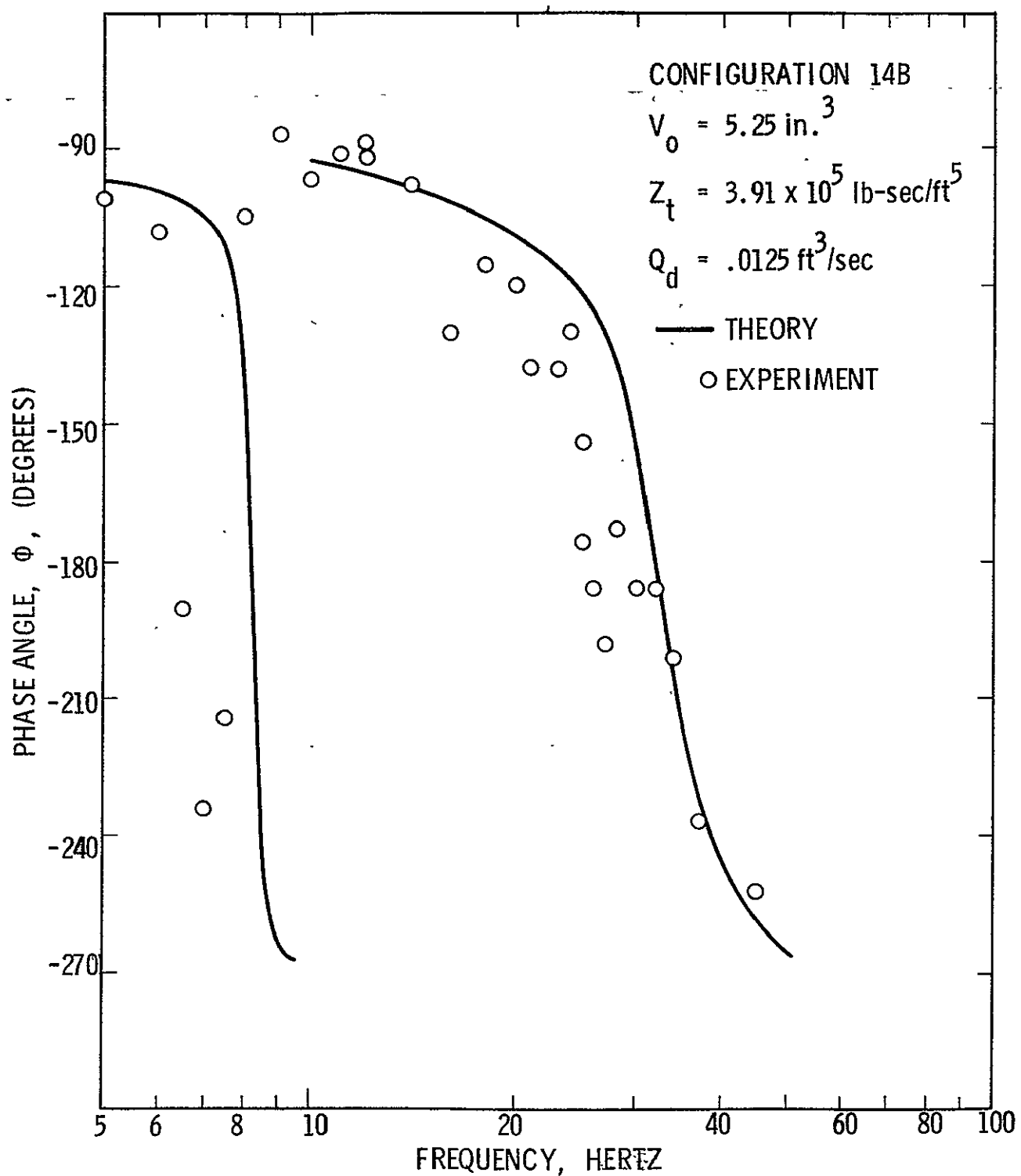
Figure 64. Phase Angle vs Frequency for a Line with a Side Branch
Containing Trapped Air

distributed parameter system rather than as a lumped element as described in Section IV.

The above described tests experimentally measured the effects of an accumulator-type side branch on the frequency response of a simulated feedline. A separate test was also conducted to simulate a pressure-sensing line partially filled with gas. This side branch element was of a much smaller diameter than that used in the previous tests; the diameter was 1/4 inch, and the overall branch length was 89 inches. This branch was connected to the primary feedline at the line terminus, 1 inch above the resistance element and at the same longitudinal station as the pressure transducer used to monitor the terminal pressure perturbation amplitude. The branch line was curved slightly upward and was partially filled with air trapped between the liquid column and the branch terminal. A pressure transducer was also mounted at the end of the branch line to measure the dynamic pressure at the branch terminal in order that it might be compared with the actual pressure in the feedline at the same station. The volume of trapped air was measured to be 1.96 in.^{3}. The perturbation pressure/flow amplitude and phase versus excitation frequency are shown in Figures 65 and 66, respectively, for this configuration. The sharp, low-frequency peak at 4.6 Hz predicted by theory was not detected or measured with the original test conducted[25] since no data were collected below 5 Hz. After the computer simulation of the same problem was obtained, the response at 4.6 Hz was observed on the computer print-out, and the test was set up and re-conducted and data were obtained from 1 Hz to 7 Hz. Excluding the low-frequency response, the measured data shown in Figures 65 and 66 agree extremely well with the analytical model.

The experimentally determined transfer function relating the pressure amplitude measured at the branch terminus to that actually existing in the primary line at the same longitudinal station (terminal) is plotted in Figure 67. This problem simulates a remotely located pressure sensor, connected by a partially gas-filled pressure-sensing transmission line; it is obvious that care should always be taken in determining the transfer function relating the pressure amplitude at the remote sensor to that at the actual feedline in order that the correct pressure amplitudes in the feedline are determined.

Large Localized Gas Volumes (Bubbles)

Section IV.1 presented the analytical model developed for localized compliances, such as a large pocket of trapped gas or cavitation bubbles. For this particular model, it was assumed that a cavitation region could be approximated by a large spherical bubble, and that the condensation and

119

CONFIGURATION 14C

$V_o = 1.96 \text{ in}^3$

$L = 27 \text{ ft}$

$d = 3 \text{ in.}$

$h_w = .050 \text{ in.}$

$Z_t = 3.91 \times 10^5 \text{ lb-sec/ft}^5$

$Q_d = .015 \text{ ft}^3/\text{sec}$

$L_b = 89 \text{ in.}$

$d_b = .250 \text{ in.}$

—— THEORY
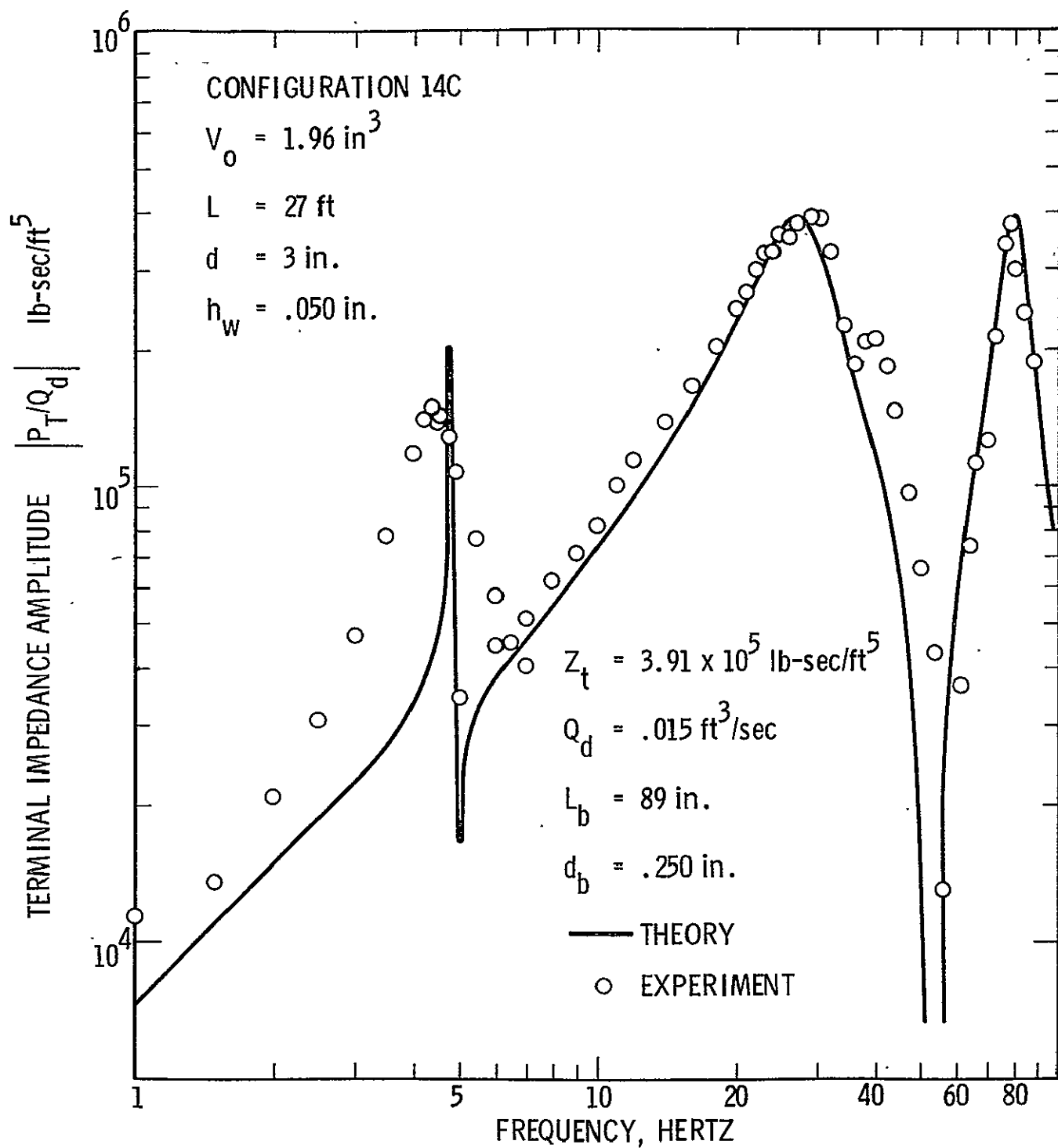
O EXPERIMENT

Figure 65. Frequency Response of a Feedline with a Side Branch Containing Trapped Air and Excited by a Flow Pulsar

120
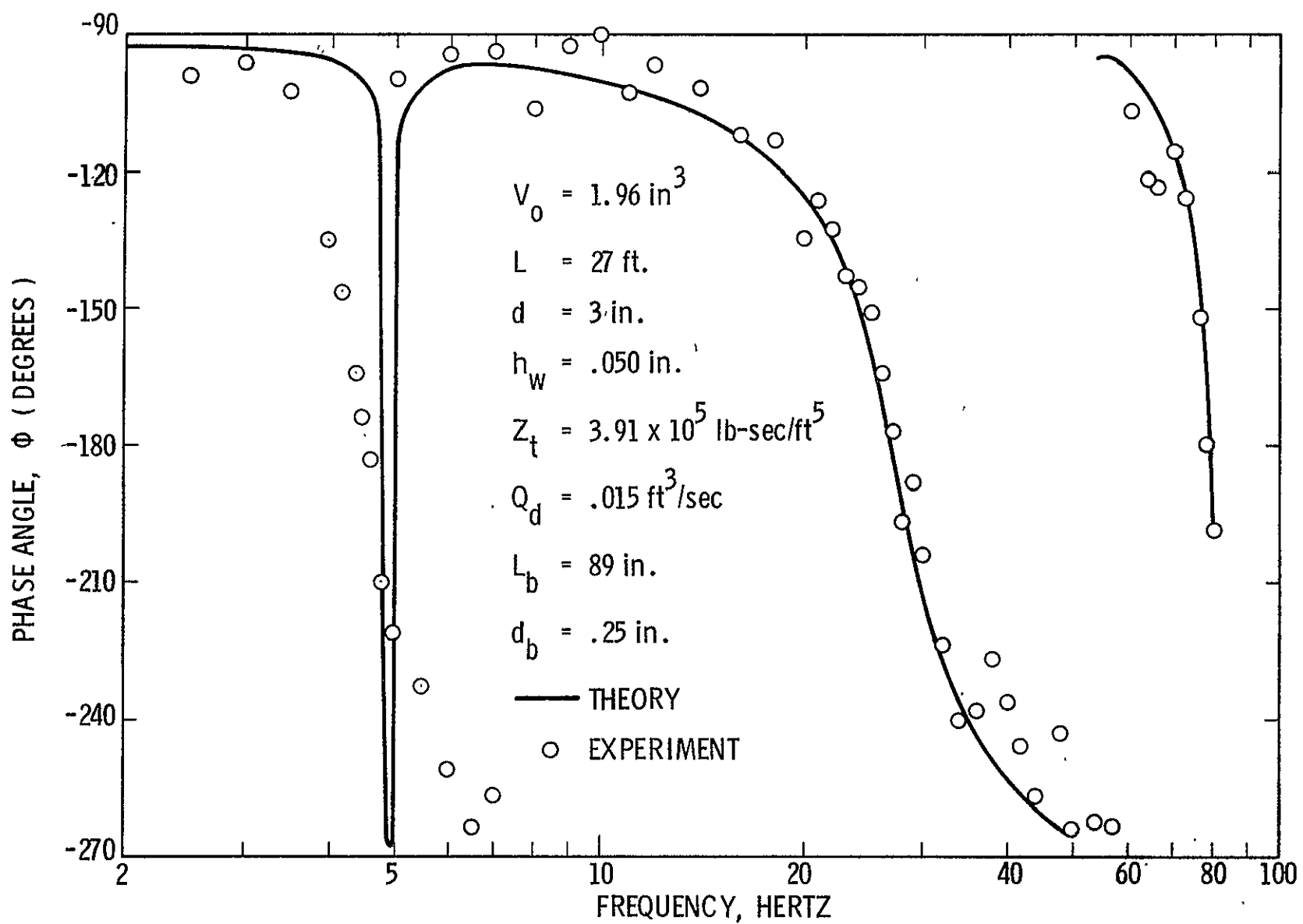
Figure 66. Phase Angle for a Feedline with a Side Branch Containing
Trapped Air and Excited by a Flow Pulsar

V_0 = 1.96 in^3

L = 27 ft

d = 3 in.

h_w = .050 in.

Z_t = 3.91 x 10^5 lb-sec/ft^5

Q_d = .015 ft^3/sec

L_b = 89 in.

d_b = .250 in.
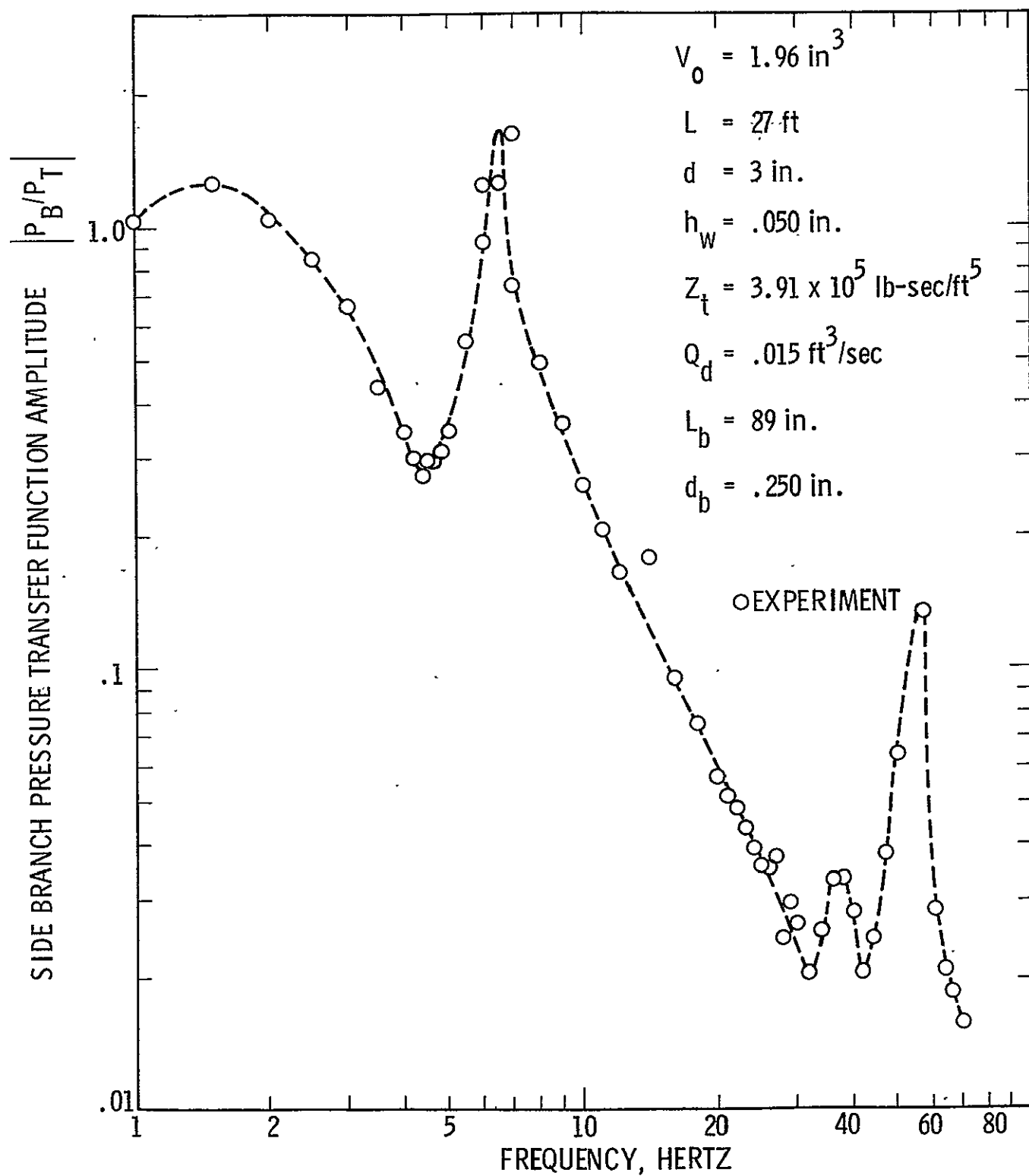
◦EXPERIMENT

Figure 67. Experimental Transfer Function Relating Side Branch Pressure
Amplitude to the Feedline Terminal Pressure

evaporization rates were such that a single-component, two-phase mixture of a liquid and its vapor could be treated as a constant quality process; that is, there is no change of state during successive expansions or contractions of the cavitation region. For a two-component mixture, such as LOX and a large localized region or bubble of captured helium ullage gas, the above assumption is unquestionably valid.

Tests were conducted with the experimental feedline test facility to measure the effect of a local compliance located at an arbitrary position longitudinally along the feedline. Since the model used in the computer simulation assumed a spherical gas bubble of constant mass (no phase changes), it was desired to create a spherical bubble and keep it stationary in the feedline at any designated longitudinal station. This was accomplished by using a nearly spherical rubber balloon; a schematic showing how the balloon was held in place and the apparatus used to measure its compliance or pressure and volume is given by Figure 68. A plexiglass section 4 inches long was inserted into the feedline at a point just above the side branch pulsar, or 1 foot from the line terminal.

In order to calculate the gas volume compliance, accurate measurements of the balloon volume and pressure were required at the test conditions. To accomplish these tasks, the bubble was initially filled to an arbitrary volume by pressurizing it with the feedline operating pressure near 1 atmosphere. The feedline was then pressurized to its desired internal test pressure. Valve B was then slightly opened, and the external pressure on the rubber balloon from the fluid forced the balloon to collapse until its volume was either zero or negligible. Valve B was then closed. The reservoir volume and the volume of the line connecting valves A and B, as well as the volume of the line to the pressure gage, were measured previously and recorded as V_c. Valve A, which connected this apparatus to a high-pressure supply of nitrogen gas, was then opened and the known volume region was pressurized to approximately 10 psi over the pressure existing in the feedline; this pressure, P_1, was then recorded after valve A was closed. Valve B was then again opened and the entire system was allowed to come to equilibrium at pressure P_2. From Boyles' law,

$$P_1 V_c = P_2 V_2 \tag{150}$$

where

$$V_2 = V_c + V_o , \tag{151}$$

and the balloon volume was calculated from

$$V_o = V_c \left(\frac{P_1}{P_2} - 1\right) \tag{152}$$

123
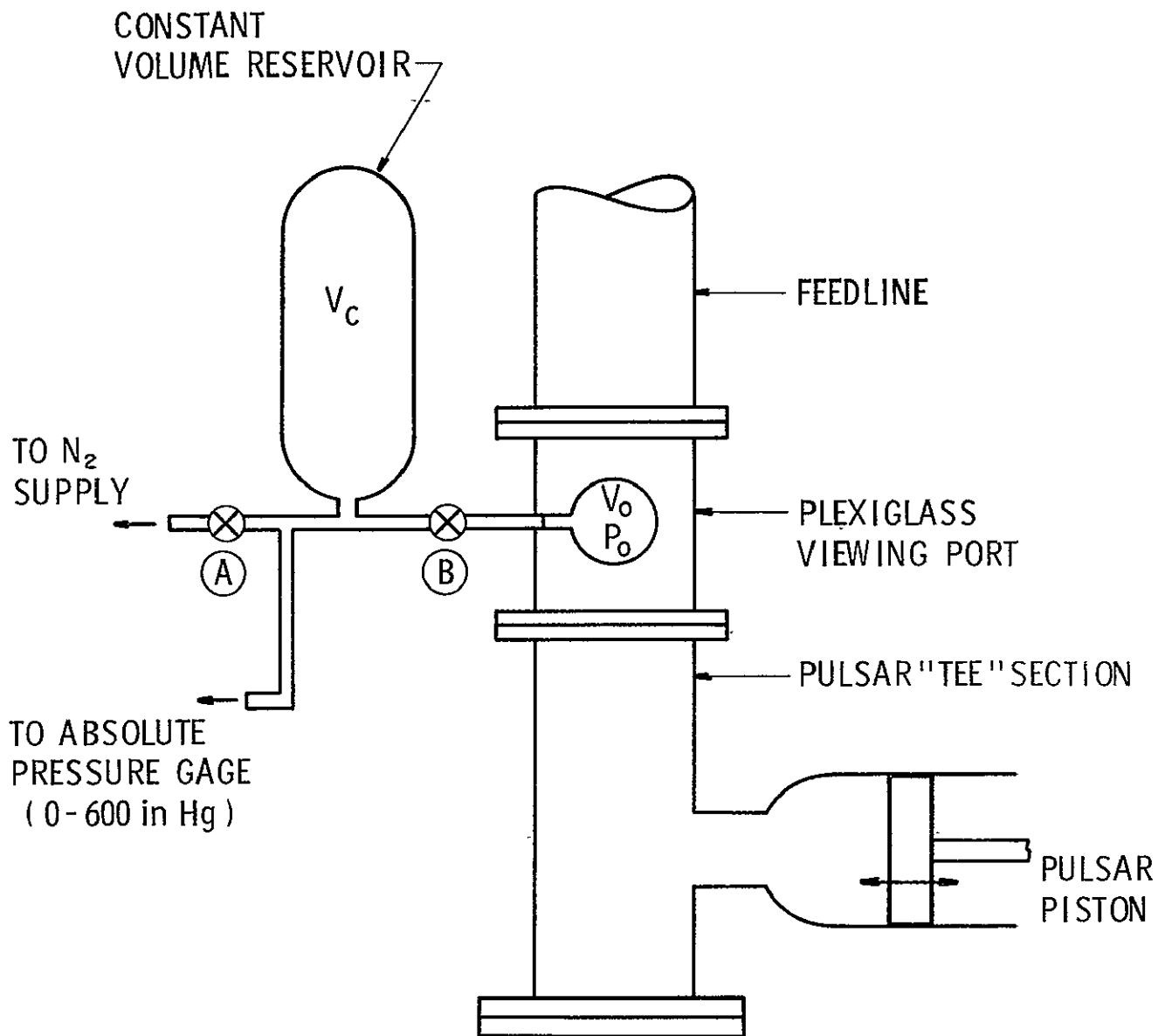
Figure 68. Apparatus for Generation and Measurement
of a Local Compliance

3770

124

This technique allowed for an accurate measurement of the local compliance and also provided a method for keeping the bubble at a stationary longitudinal position along the feedline. Due to the surface tension in the balloon skin, the bubble spring rate (stiffness) could not be given simply by

$$k = \gamma P_o / V_o \tag{153}$$

but needed to be corrected by the addition of a wall tension correction factor, k'. The total balloon or bubble stiffness, k, became

$$k = \gamma P_o / V_o + k' \tag{154}$$

where k was determined experimentally by measuring $-\Delta P / \Delta V$ for the balloon under static conditions. From the measurements obtained previously for P_o and V_o, the added stiffness, k', was then determined. This additional stiffness was determined to be relatively small when compared with the uncorrected value, $k = \gamma P_o / V_o$, at the operating pressures and bubble volumes used in the experimental tests.

Tests were conducted with various values of the local compliance (bubble volume). An aluminum feedline 27 feet long, 3 inches in diameter, and with a wall thickness equal to 0.050 inch was used in the examination of local compliance effects. The frequency response of this same feedline without a localized compliance was presented in Figure 46. Figures 69 and 70 present the pulsar impedance frequency response and phase angle obtained for the first test case in which the bubble volume was 1.645 cubic inches and the local pressure, P_o, was 111.5 psia. Again, the pulsar impedance amplitude refers to the terminal pressure perturbation divided by the input flow perturbation. The terminal resistance, Z_t, was equal to 3.91×10^5 lb-sec/ft^5. The agreement between the analytical model and the experimental data is excellent; the measured amplitudes at resonance are only slightly below that predicted by theory, and the first and second mode resonant frequencies were predicted by the computer simulation within 1 cycle per second or less.

Figures 71 and 72 present data obtained for a bubble whose volume was measured to be 4.88 cubic inches; the pressure was measured to be 109 psia. The bubble was located longitudinally at the same station as that previously tested, 1 foot above the line terminal. The terminal impedance was 3.91×10^5 lb-sec/ft^5; the approximate average flow excitation amplitude was 0.02 ft^3/sec. As predicted by the analytical model, increasing the local compliance value (bubble volume) lowered the first mode resonant frequency and sharpened the second mode peak. Figures 73 and 74 show the measured effect of still further increases in the bubble size. This

125
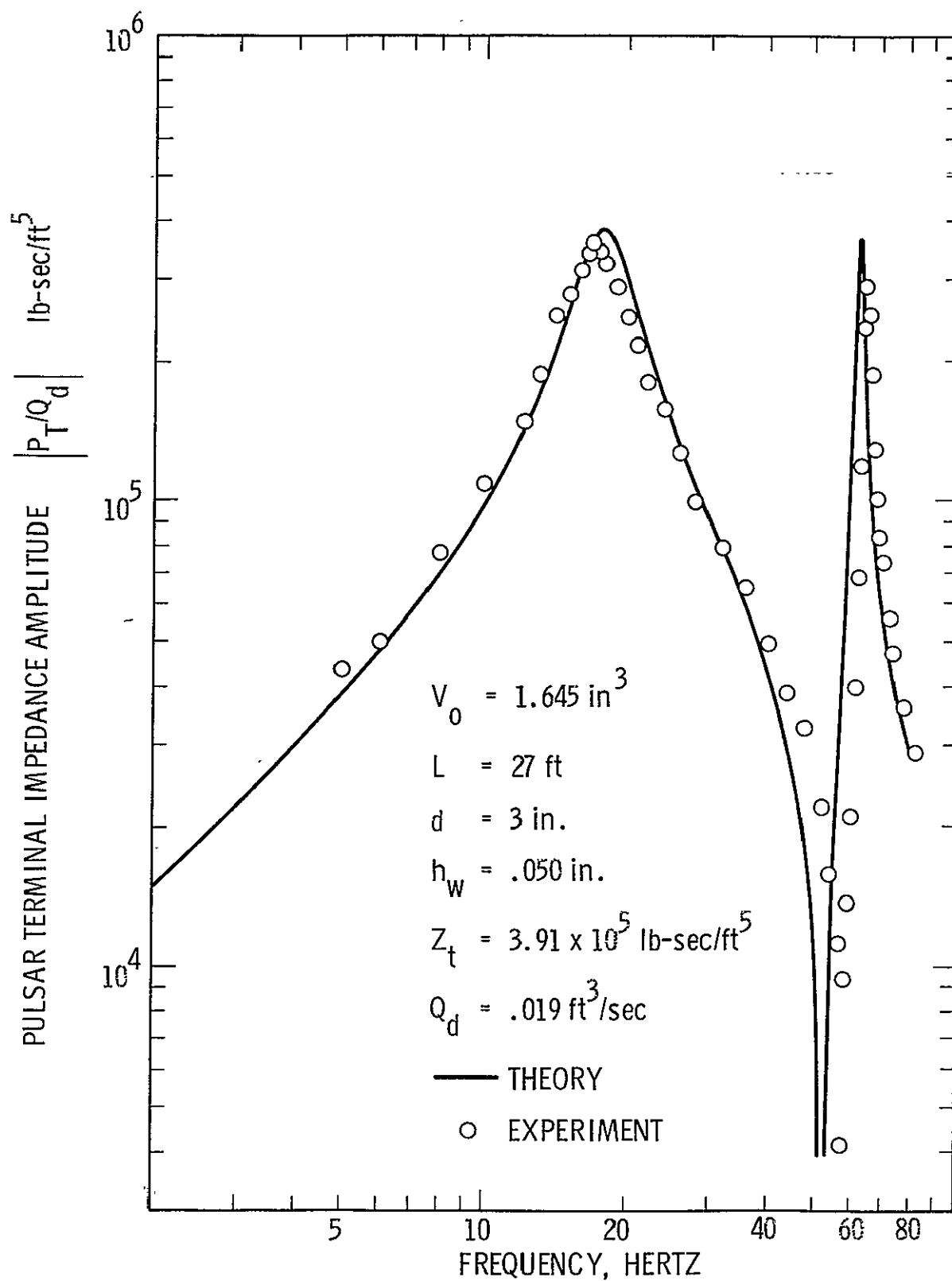
Figure 69. Frequency Response of a Feedline with a Local
Compliance at the Line Terminal and Excited by
a Flow Pulsar. (Bubble Volume = 1.645 in^3)
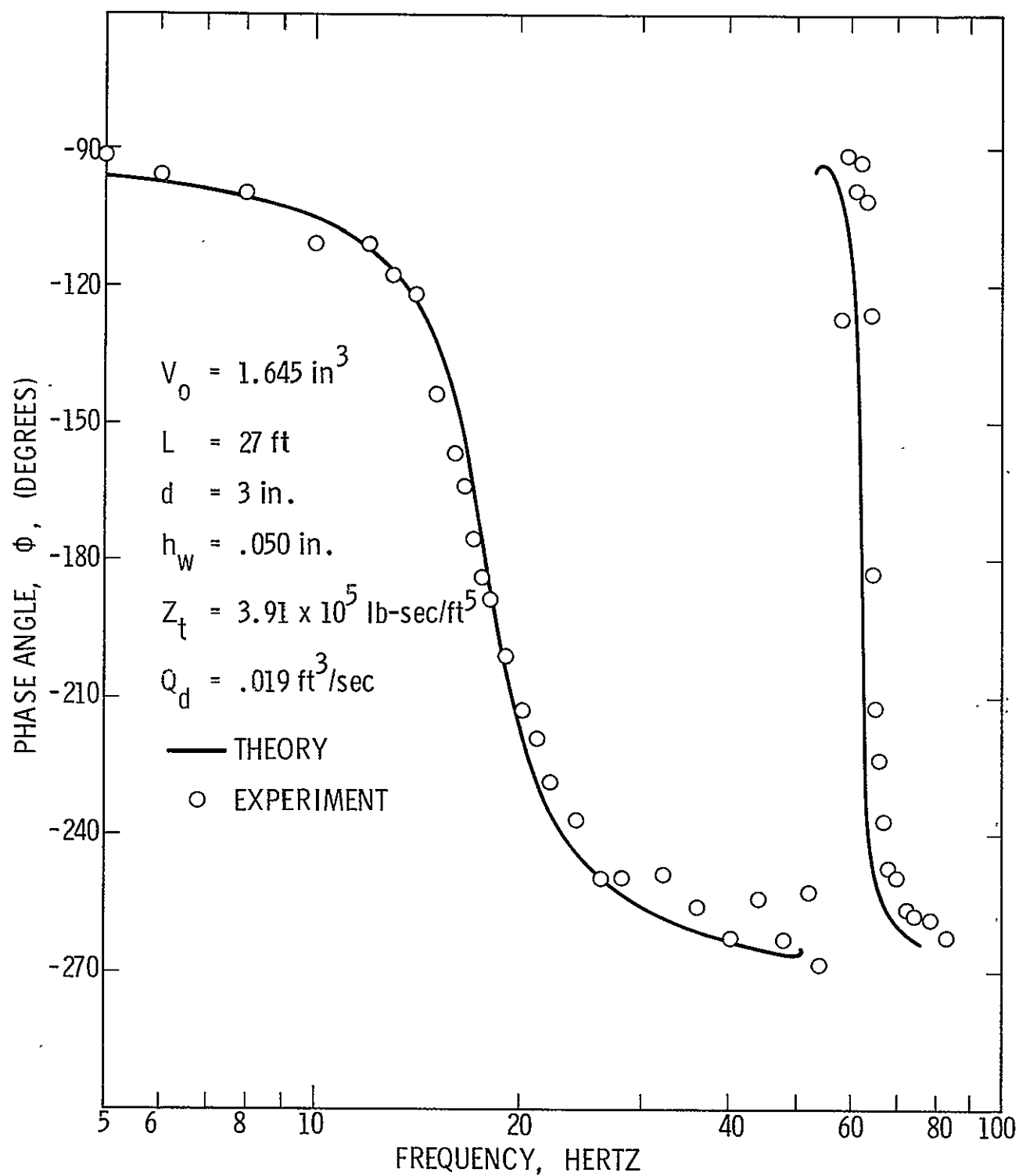
Figure 70. Phase Angle Between the Terminal Pressure and Pulsar Flow
Perturbations for a Line with a Local Compliance
(Bubble Volume = 1.645 in.^{3})
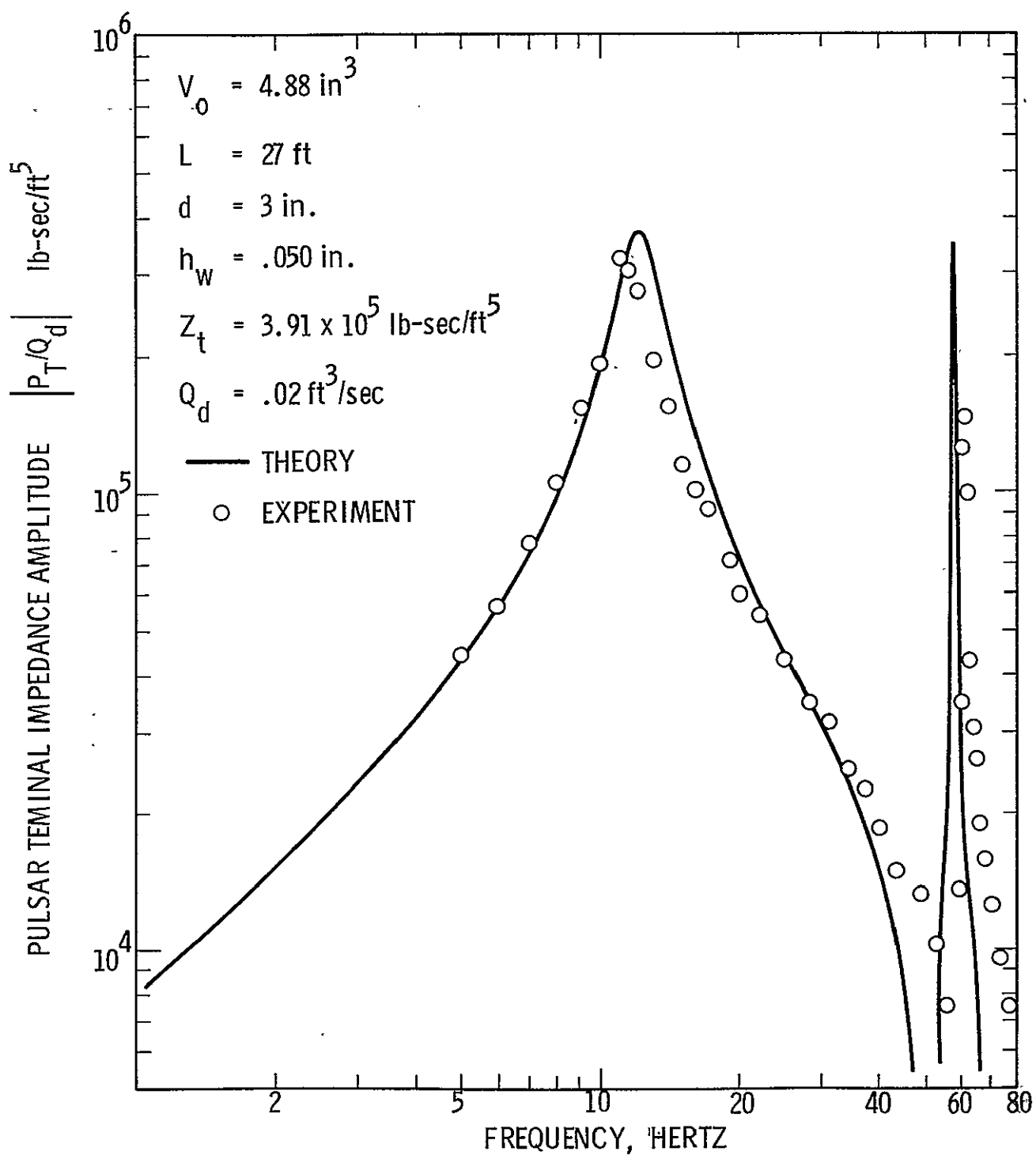
Figure 71. Frequency Response of a Feedline with a Local
Compliance at the Line Terminal and Excited by
a Flow Pulsar. (Bubble Volume = 4.88 in³)
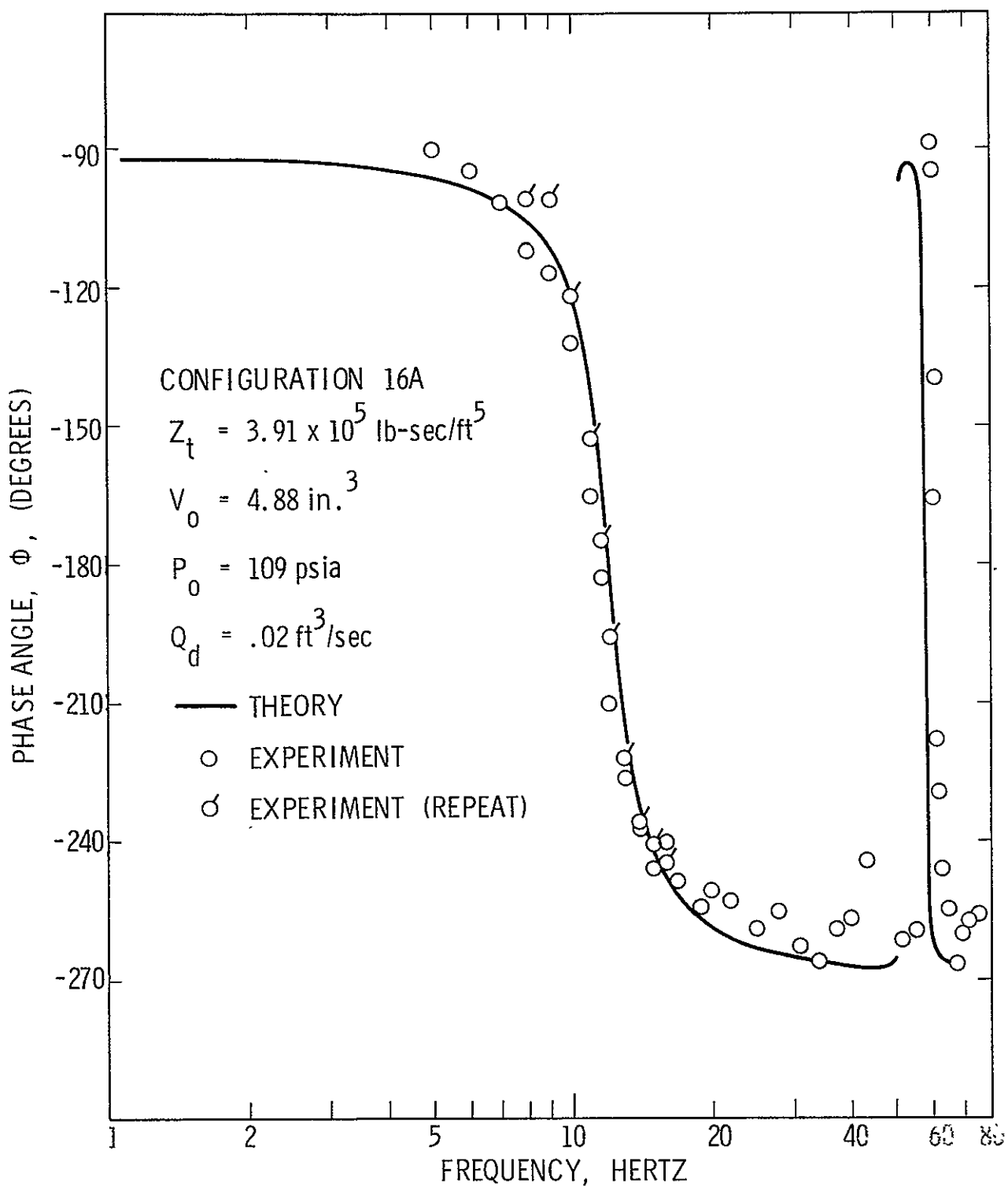
Figure 72. Phase Angle Between the Terminal Pressure and Pulsar Flow Perturbations for a Line with a Local Compliance

129
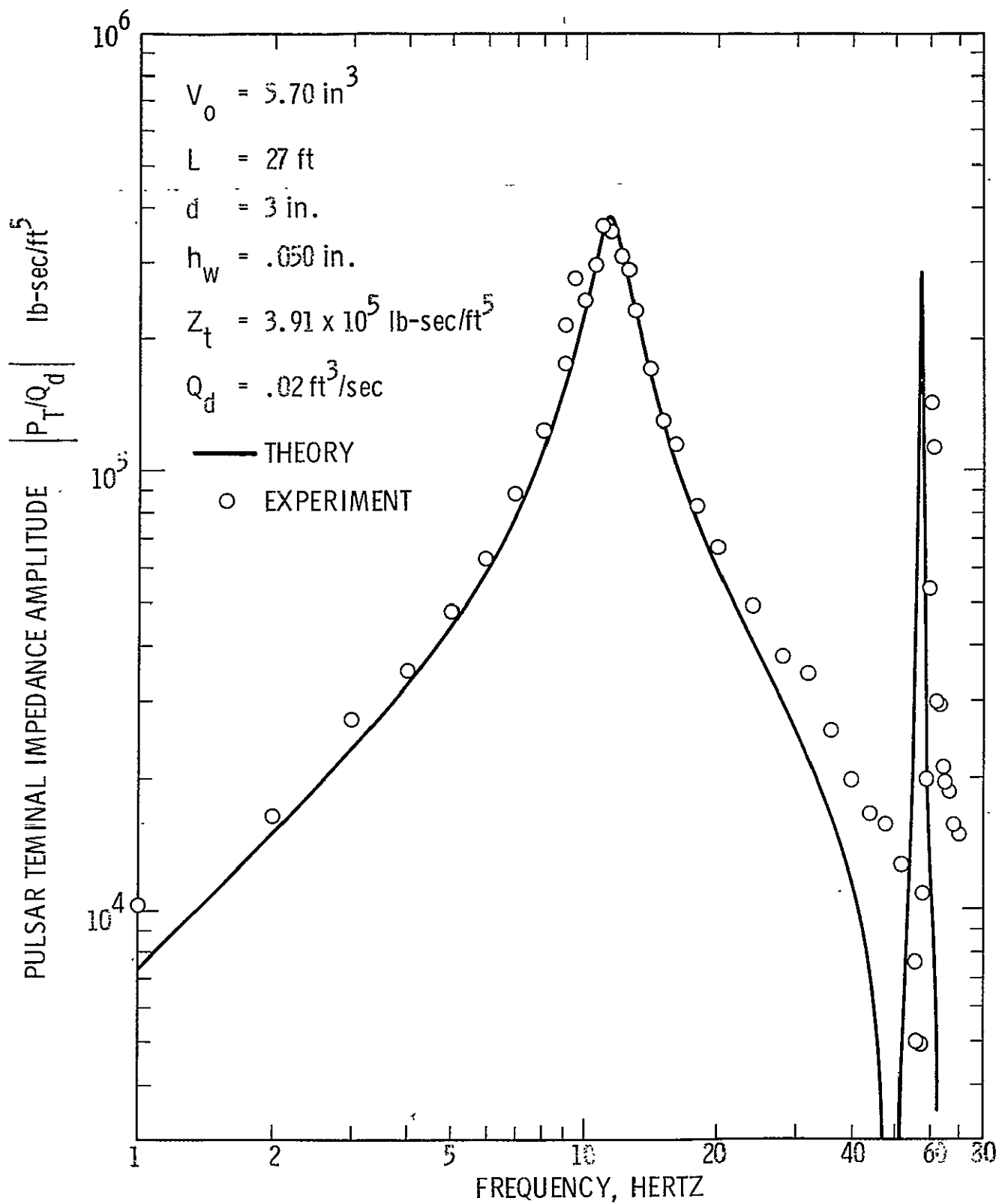
Figure 73. Frequency Response of a Feedline with a Local Compliance at the Line Terminal and Excited by a Flow Pulsar (Bubble Volume = 5.70 in^3)

130
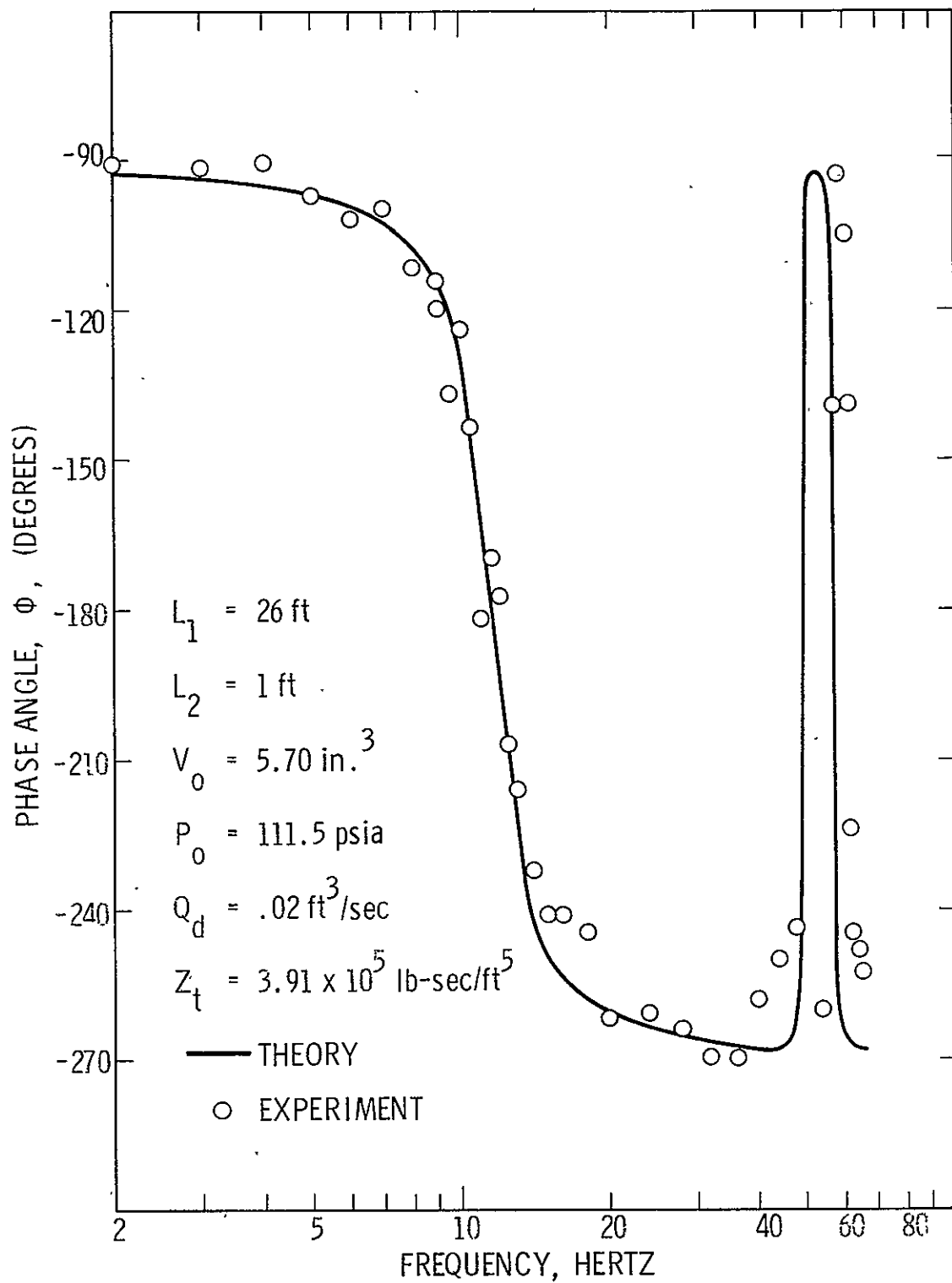
Figure 74. Phase Angle vs Frequency for a Feedline with a Local Compliance

bubble was measured to be 5.70 cubic inches at an internal pressure equal to 111.2 psia. The bubble was also located 1 foot above the terminal resistance element, and the feedline was excited by the side branch flow pulsar. The amplitude at the first longitudinal mode resonant frequency agrees very well with the analytical solution, while the second mode resonant frequency agrees within 3.5%, but appears to be lower than the predicted amplitude.

Figures 75 and 76 present the pulsar impedance frequency response and phase angle obtained for a bubble located at a position other than at the end of the line. For this experiment, the localized volume was 5.75 cubic inches and at an internal pressure equal to 111.5 psia. The nitrogen-gas-filled balloon was located 4.55 feet above the line terminus; the geometry of the feedline was exactly that used for the other three tests. Note that the volume, and hence compliance, of this bubble is almost exactly equal to that described in Figure 73. As evidenced by a close comparison of that data with Figure 75, the major effect of bubble longitudinal location is to increase the first mode resonant frequency and increase the response roll-off after resonance as the bubble is moved up the line toward the tank. The second mode response has a more gradual rate of increase as resonance is approached than did the response for the same bubble volume located nearer the line terminal.

It should also be mentioned that the curves labeled "theory" in all the data collected for localized compliances did not include the previously discussed stiffness correction factor, k'; yet there is good agreement with the experimental data since k' was always small compared with $\gamma P_o / V_o$. The presence of the balloon wall between the gas and liquid also undoubtedly affected the natural damping of this compliant element, but since the bubble resonant frequencies were considerably higher than any of the test frequencies, the bubble dynamics were negligible, indicating that a more simple model can be used for a local compliance when the expected excitation frequencies are far below the bubble resonant frequencies.

VII.5   Structural-Hydraulic Coupling

Experimental tests were conducted to determine the effects of structural-hydraulic coupling produced when the feedline was excited externally. A feedline was fabricated from aluminum pipe; this feedline had two $90°$ bends (short radii elbows), and its geometry was as is shown in Figure 77.

132
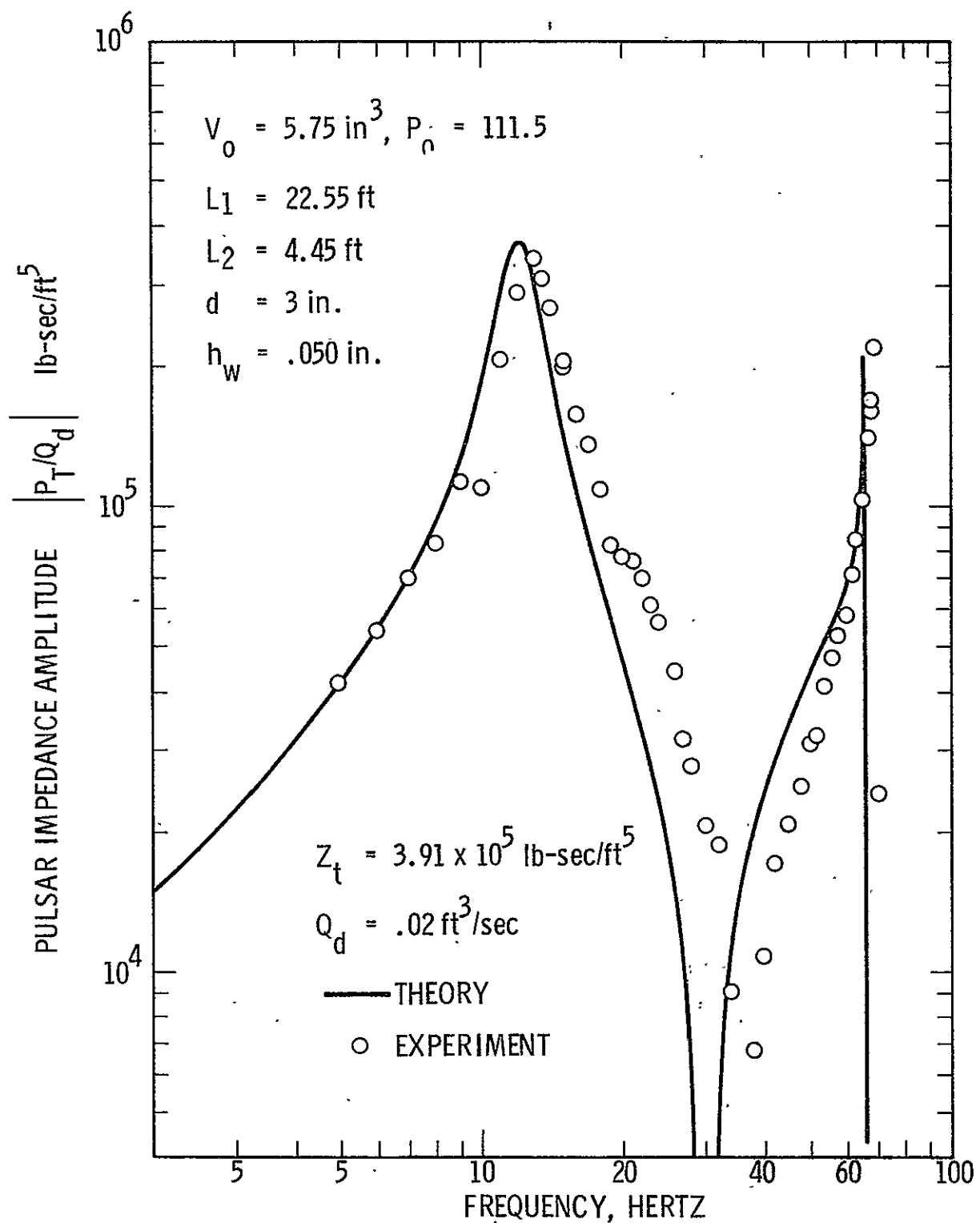
Figure 75. Frequency Response of a Feedline with a Local Compliance Located Above the Line Terminal and Excited by a Flow Pulsar

133
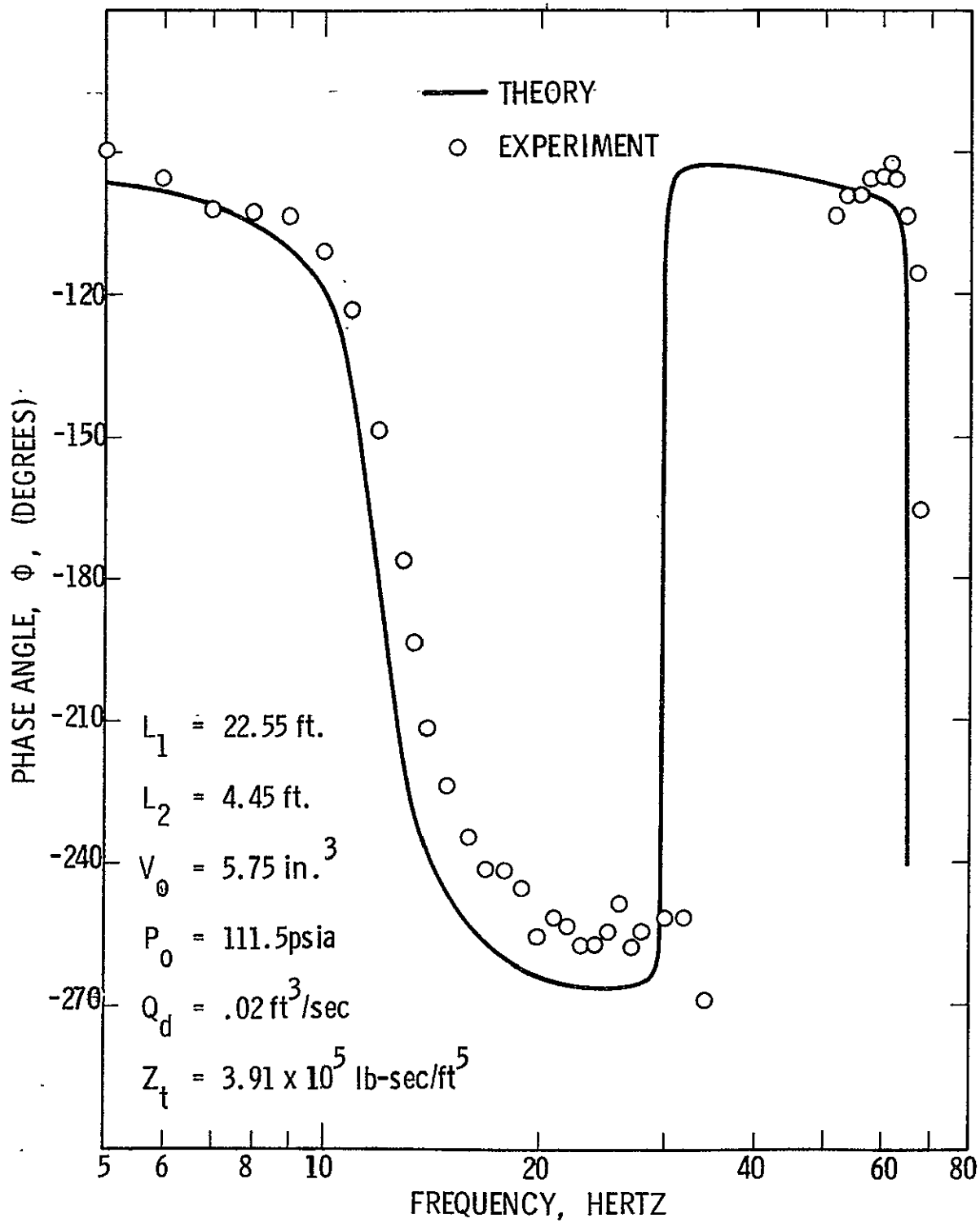
Figure 76 . Phase Angle Between the Terminal Pressure and Pulsar
Flow Perturbations for a Line with a Local Compliance

134

$$L_{1-2} = 21.09'$$
$$L_{2-3} = 5.75'$$
$$L_{3-4} = 6.00'$$
$$DIAM. = 3.35''$$
$$h_w = 0.083''$$

Q_d

TERMINAL RESISTANCE, z_t
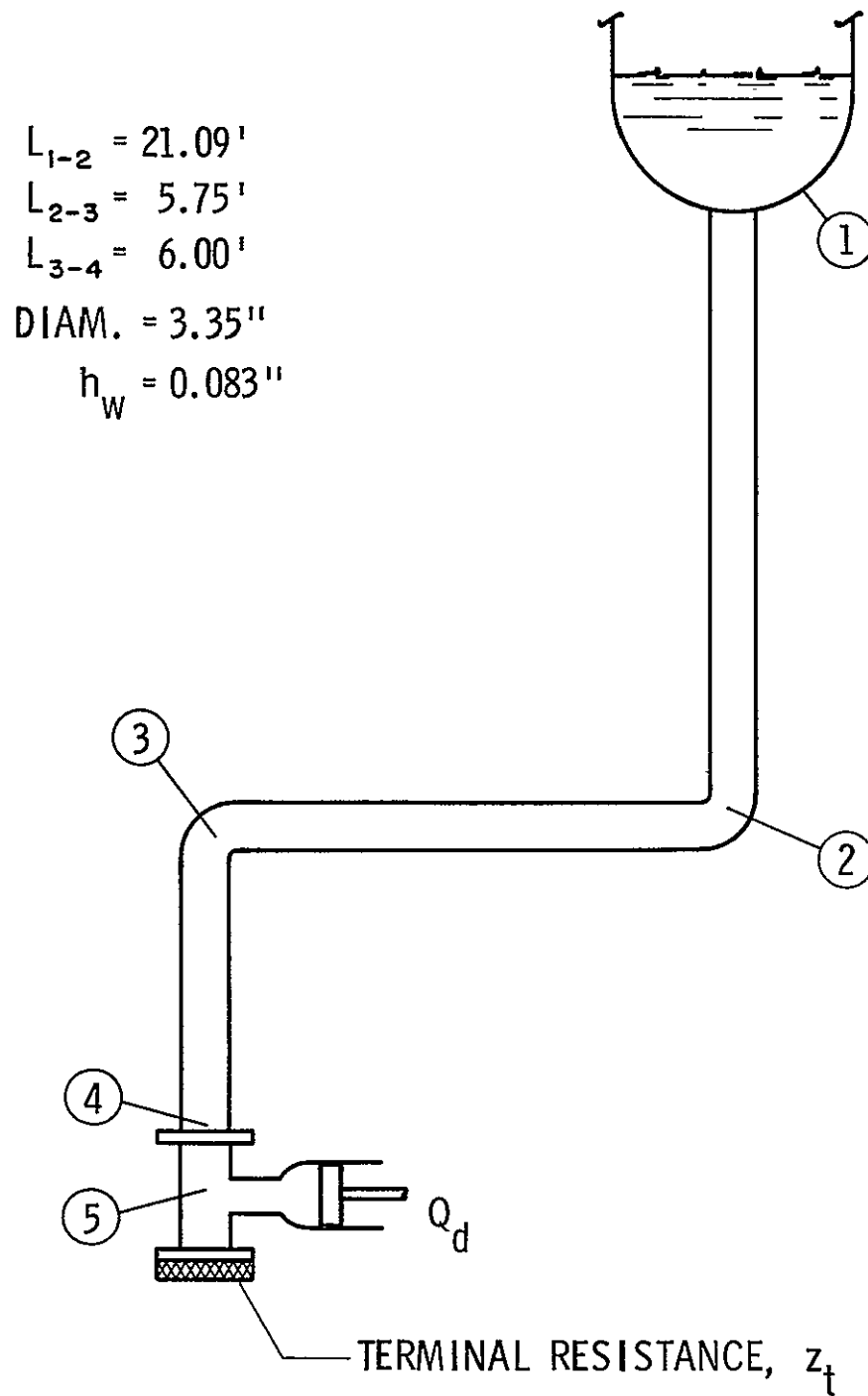
3771

Figure 77. Aluminum Feedline Geometry Used to Measure
the Effect of Elbows

Line with Bends

To determine the effect of bends or elbows on the frequency response, the feedline was installed as shown in Figure 77. For this experiment, it was desired to measure the effect of the bends without external structural acceleration; hence, the excitation was provided by the side branch pulsar, driven by an hydraulic actuator. The resulting frequency response (pulsar impedance amplitude, P_T/Q_d) and the phase relationship between the input flow perturbations and the terminal pressure perturbations are presented in Figures 78 and 79. The terminal resistance was created by a 7/16-inch-diameter orifice which produced, when operated at a steady state flow pressure drop of 100 psia, a terminal impedance, $Z_t = 3.91 \times 10^5 \text{lb-sec/ft}^5$. The results shown in Figures 78 and 79 reveal that for no external structural acceleration inputs, the feedline with the two 90° elbows behaves as a simple, straight feedline of the same total length.

Line with Bends and Structural Excitation

Figure 80 presents the feedline geometry and method of excitation used to experimentally determine the effects of structural-hydraulic coupling. The objective of this test was to verify the analytical model described in Section V.4 for a feedline with external structural acceleration applied at discrete locations. The mounting stiffness of the simulated support structure was quite high; i.e., the mounting structure was almost perfectly rigid. The spring rate, k, of the mounting structure was determined from the elastic properties of the stainless steel shaft of the hydraulic actuator which was attached directly to the feedline 3 inches from the second elbow, as shown in Figure 80. The structural damping of the mounting structure (shaft) was zero for all practical purposes, and was thus programmed into the computer simulation. For the frequency range tested, the stiffness term, k, dominated such that the terms defined by Equation (114) became

$$\alpha' \implies (Z_c/s) \sinh \gamma L$$

$$\beta' \implies \frac{As \ Z_c \sinh \gamma L}{k}$$

$$\alpha'' \implies A/s (1 - \cosh \gamma L)$$

$$\beta'' \implies \frac{A^2 s (1 - \cosh \gamma L)}{k}$$

(155)

and the relation (Equation 112) between the applied structural acceleration to the actual line acceleration, $a_\ell(s)$, simply became
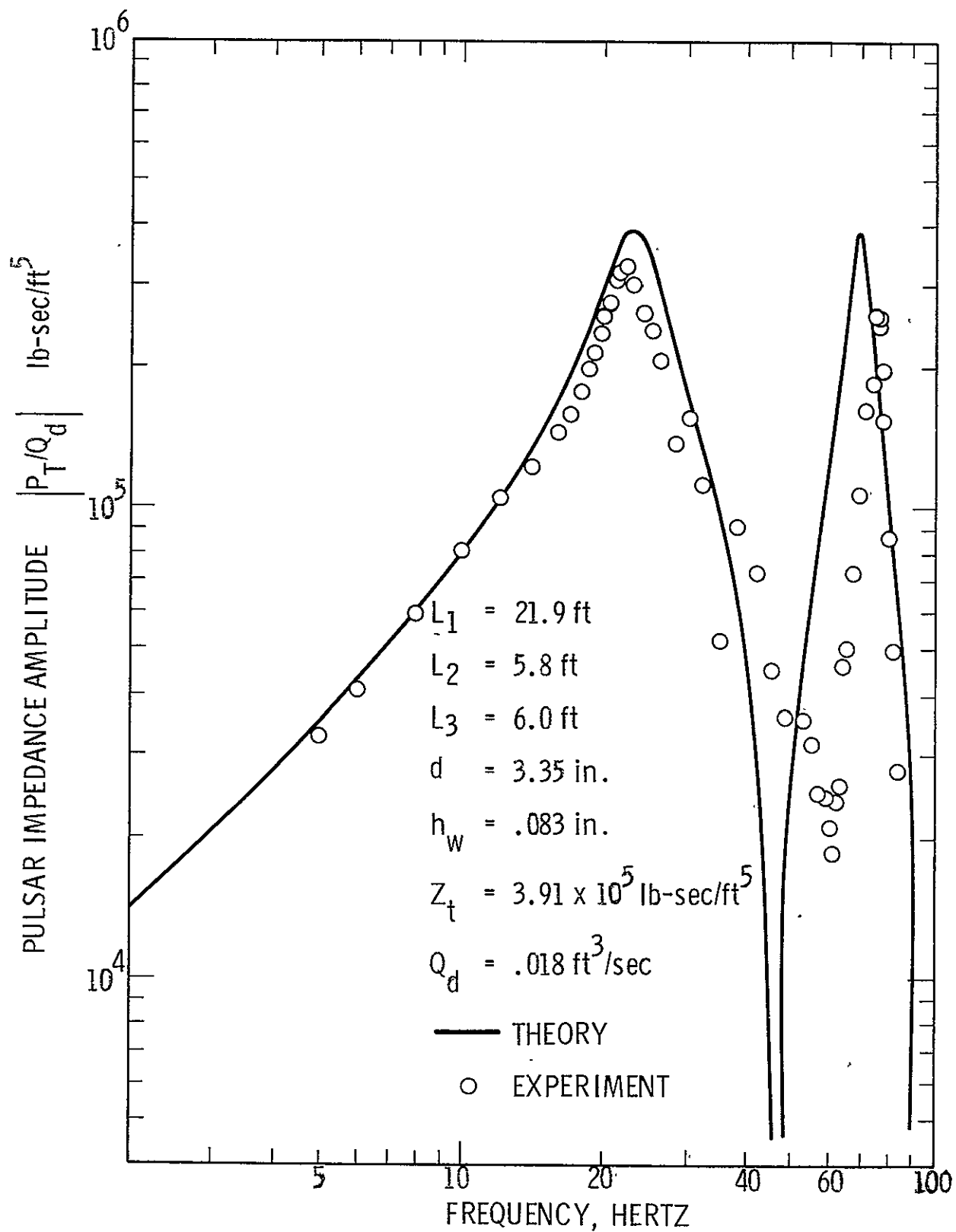
Figure 78. Frequency Response of an Aluminum Line with Two
90⁰ Bends, Excited by a Side Branch Pulsar

137
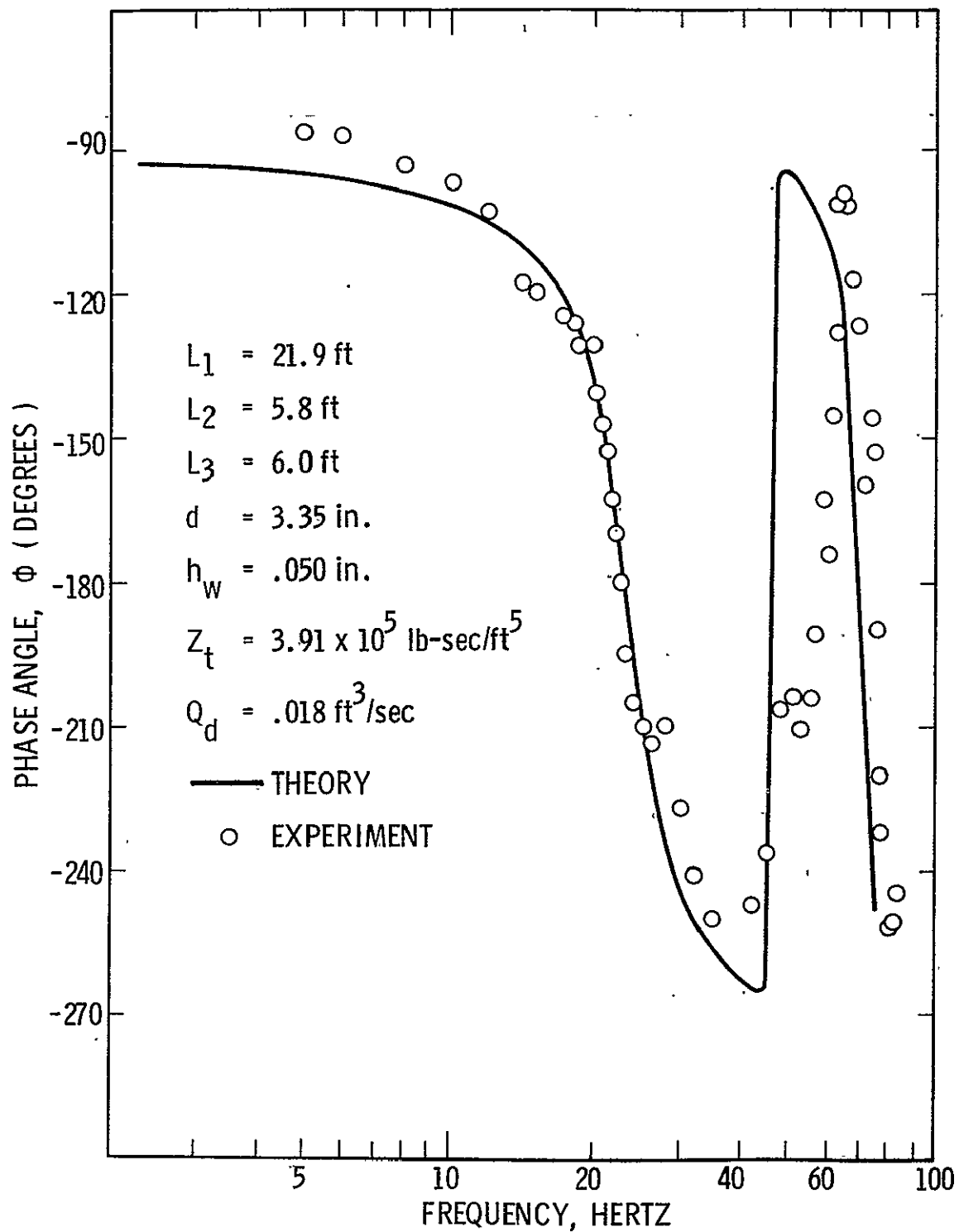
Figure 79. Phase Angle Between the Terminal Pressure and Pulsar Flow Perturbations for an Aluminum Line with Two 90° Bends

$L_1 = 21.09$ ft

$L_2 = 5.75$ ft

$L_3 = 6.0$ ft

$d = 3.35$ in.

$h_w = .050$ in.

$Z_t = 2.95 \times 10^5$ lb-sec/ft^5

$A_\ell(s)$

SECONDARY EXCITATION

L_2

3

L_1

2

HYDRAULIC ACTUATOR

IL_3

PUMP

1

4

BELLOWS

LOWER RESERVOIR
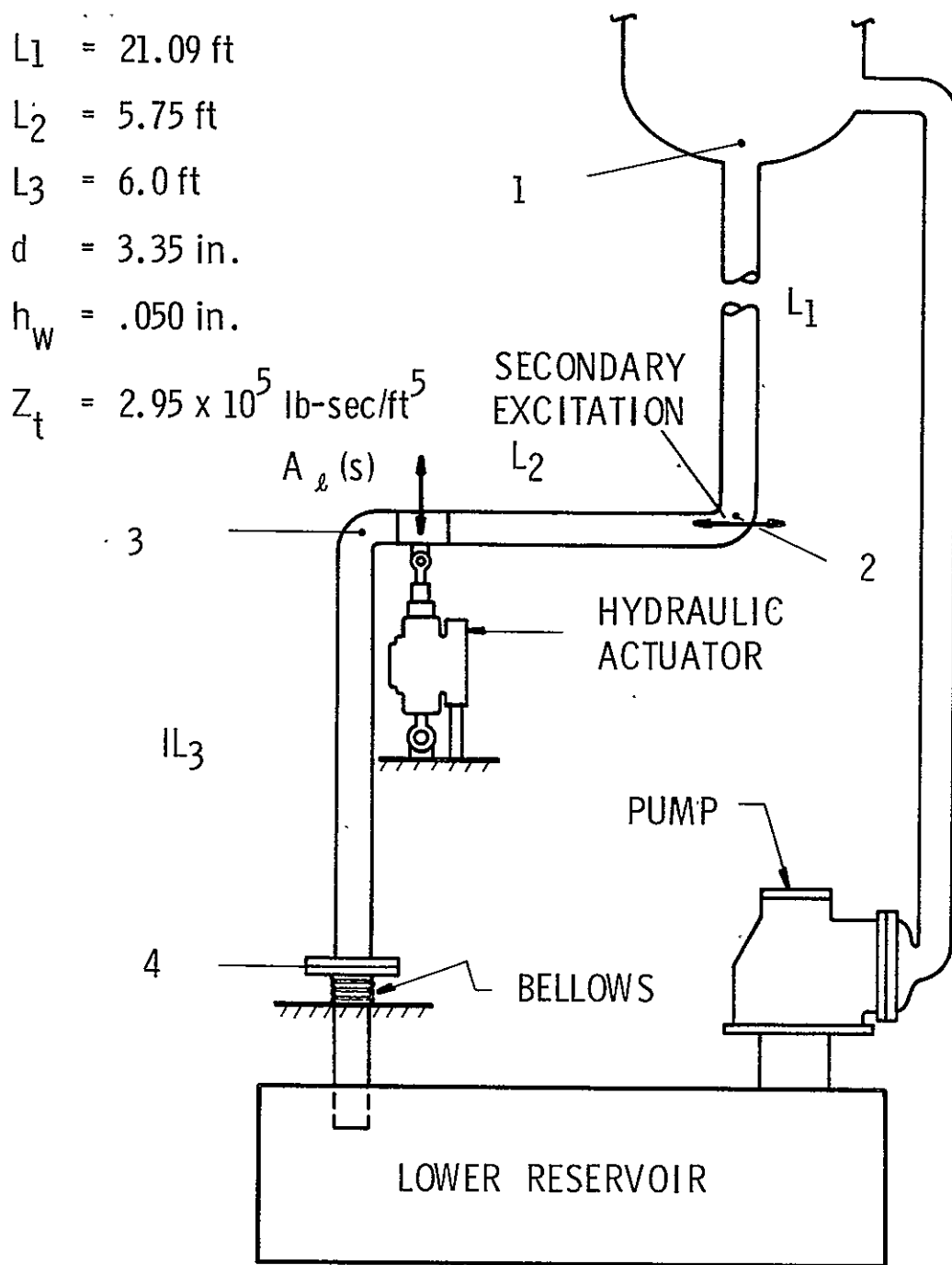
Figure 80. Feedline Configuration for Structural-Hydraulic Coupling Tests

$$a_\ell(s) \Longrightarrow a_1(s) \tag{156}$$

and the problem was essentially reduced to that of an accelerated line, given by Equation (108). Although the stiffness term dominated, the experiment was modeled analytically using the more complex mounting stiffness model, Equation (113). Close examination of subroutine eight (given in Appendix D) reveals that the general computation method requires two horizontal line segments attached to the vertical line segment, one at each end. The problem under consideration, however, had only one horizontal segment. To properly program this problem, an additional horizontal line element was assumed to exist between the end of the vertical segment and the terminal resistance element. This extra horizontal segment was programmed to have a length equal to zero. The addition of this imaginary element was necessary for subroutine eight to properly function.

The <u>initial</u> data collected for this test configuration bore no resemblance to the theoretically predicted response, and considerable time was taken to carefully re-examine the analytical model and the computer code. Re-consideration of the test procedures revealed that the actual input accelerations measured during the test were not the only source of structural-hydraulic excitation. Prior to the experiment it was assumed that the only excitation applied to the system would be that input created by the hydraulic actuator and would essentially invoke a vertical excitation of line segment 3-4 and bending of the horizontal line segment 2-3. Further tests revealed, however, that there was actually a dependent horizontal acceleration of considerable magnitude of the horizontal line segment; this acceleration was actually measured with an accelerometer mounted at the first elbow (point 2) and at certain frequencies was comparable in amplitude to the measured vertical input excitation applied by the actuator. The experimental data were therefore the result of two simultaneous excitations of the feedline. To circumvent this problem, the feedline was attached rigidly to the support tower structure just upstream of the first elbow. This bracing was very rigid, and prevented the secondary horizontal excitation when the second test was performed. The actual structural input was now very near that measured in the vertical plane produced by the hydraulic actuator.

The terminal pressure/input acceleration is presented in Figure 81 for a feedline with two bends and excited through structural-hydraulic coupling. The lengths of the line segments are given in Figure 80; the internal fluid was water at a nominal line pressure of 60 psig at the line terminal. The terminal impedance was produced by the 7/16-inch diameter orifice; the steady-state mean pressure drop was 60 psid producing a linearized terminal resistance, $Z_t = 2.95 \times 10^5$ lb-sec/ft^5. The excitation

140
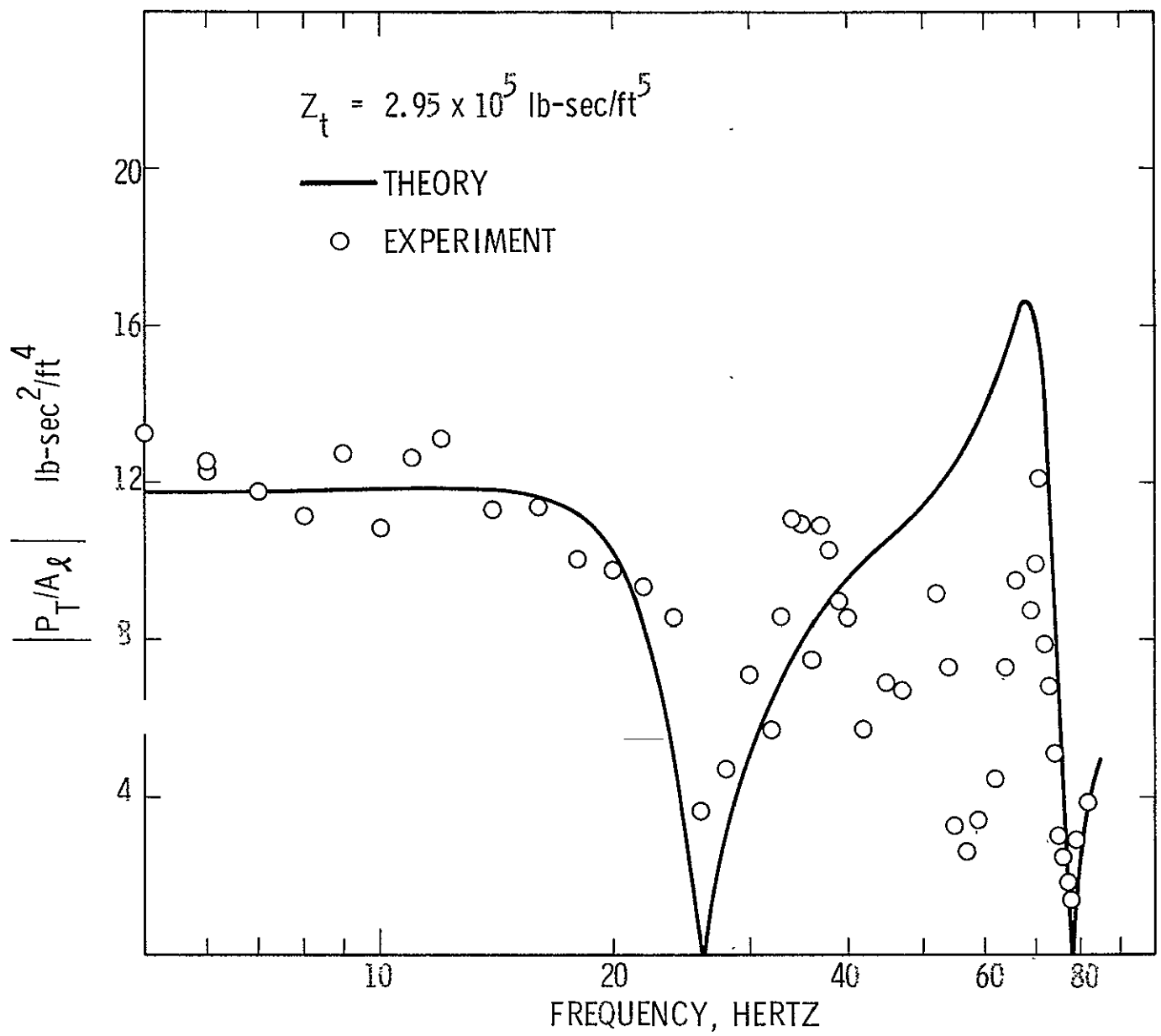
Figure 81. Frequency Response for a Line with Bends and with Structural Excitation

amplitude was measured with the velocity transducer attached to the actuator shaft; the experimental velocity amplitudes were transformed to acceleration amplitudes by

$$\left| a_\ell(\omega) \right| = \omega \left| V_\ell(\omega) \right| \tag{157}$$

Figure 81 indicates that the analytical model does predict the amplitudes reasonably well past the first anti-resonance, as well as predict the frequency at which this anti-resonance occurs. The scatter in amplitude measurements out to approximately 20 Hz is attributed to the low level pressure signals produced on the oscillograph trace, even though the system instrumentation was operated at maximum sensitivity. As yet we have been unable to explain the discrepancy between theory and experiment over the range from 40 Hz to 65 Hz. The analytical model did predict the resonant peak near 68 Hz; the experimental data show this peak to be at 70 Hz. The amplitude at resonance is, however, less than that predicted by theory. Between 70 and 82 Hz the system behaved very similar to the response predicted by the analytical model. The measured phase relations between the terminal pressure and acceleration inputs are presented in Figure 82, and the same general comments expressed above regarding the amplitude versus frequency response can be applied here also.
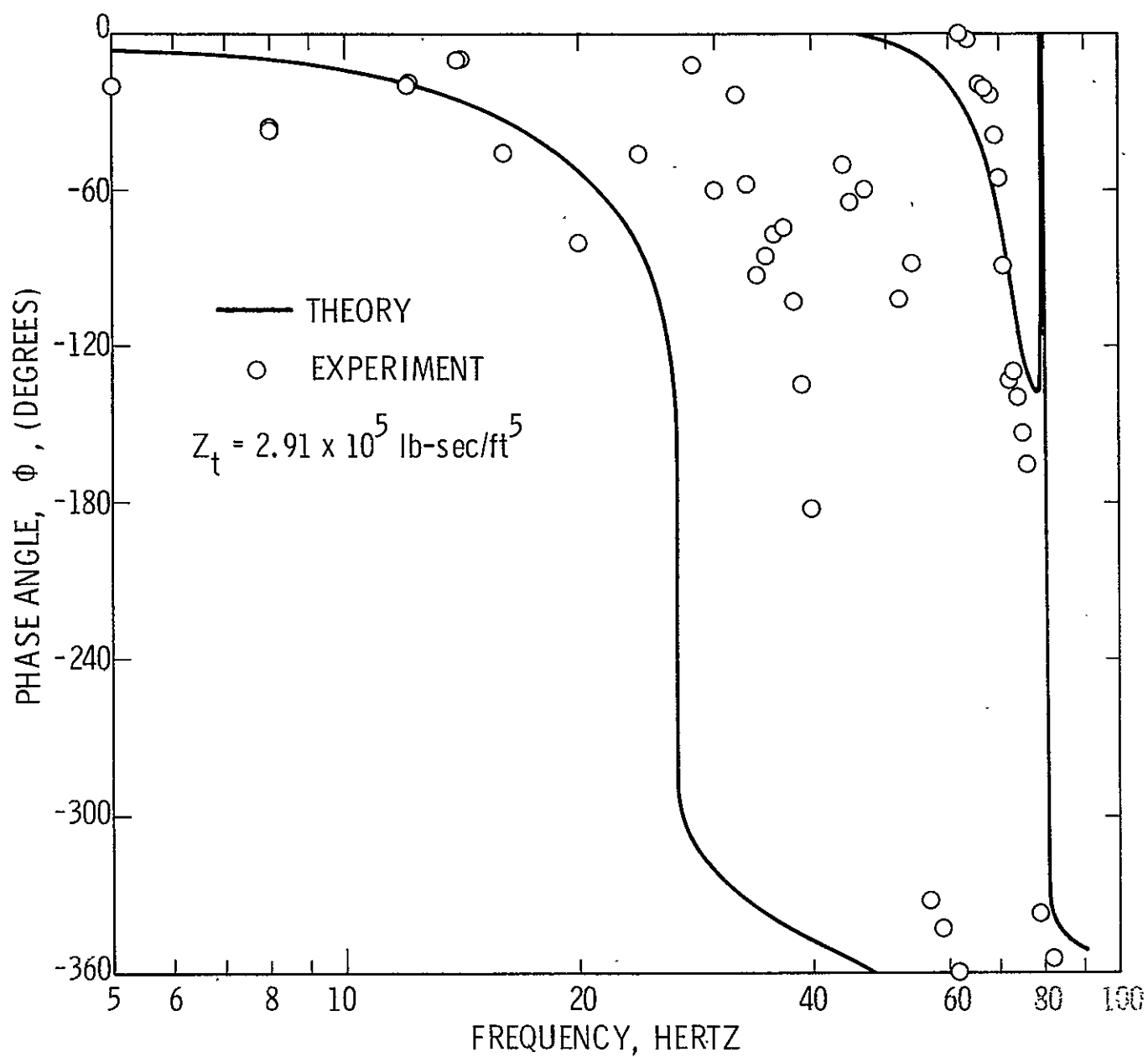
Figure 82. Phase Angle vs Frequency for a Line with Bends and with Structural Excitation

VIII. CONCLUSIONS AND RECOMMENDATIONS

VIII.1 Conclusions.

The objective of this study has been to develop an analytical model and corresponding computer program to allow for the study of disturbances of liquid propellants in typical engine feedline systems. This model has been completed and includes (a) the effect of steady turbulent mean flow, (b) the influence of distributed compliances, such as dissolved ullage gases and flexible walls, (c) the effects of local compliances, such as cavitation regions and complex side branches, and (d) various factors causing structural-hydraulic coupling, such as bends, mounting stiffness, forces changes in line length and bellows or PVC joints. The computer program has been set up such that the amplitude and phase of the terminal pressure/input excitation is calculated over any desired frequency range for an arbitrary assembly of various feedline components. A user's manual has been prepared and is attached as Appendix D of this Final Report.

In addition to the development of the generalized computer code for the analysis of liquid rocket propellant feedline dynamics, an experimental test program has been conducted to verify many of the assumptions and models used in the computer simulation. Specifically, tests have been conducted to determine the validity of the analytical techniques used to model the effects of

      (a)   steady, turbulent mean flow

      (b)   linear and nonlinear resistance elements

      (c)   blocked lines

      (d)   elastic walls

      (e)   dissolved gases

      (f)   complex side branches

      (g)   local compliances

      (h)   bends; and

      (i)   structural-hydraulic coupling with mounting stiffness.

In summary, the following conclusions can be drawn from the experience gained from both the analytical and experimental phases of this program:

(1)   Investigation has shown that the predominant effect of turbulence is to increase the spatial attenuation at low frequencies; at high frequencies the laminar and turbulent attenuations coincide. The effect of turbulence also has a tendency to reduce the phase velocity at low frequencies; however, this effect can be neglected for all feedlines where the parameter $\omega r_o^2/\nu > 10^4$, which includes virtually all cases of interest. An additional factor, Γ_c, has been added to the laminar propagation operator to account for the turbulent attenuation contribution.

(2)   The terminal pressure amplitudes at resonance are affected more by the value of the line terminal impedance (resistance) than any other single factor.

(3)   The use of a linearized model for nonlinear type resistance elements provides satisfactory results for cases where the mean flow rate, Q, is considerably greater than the dynamic flow perturbation amplitude, Q_d.

(4)   It has been concluded that the effect of the wall compliance (or elasticity) can be correctly modeled by the classic Korteweg correction to the phase velocity; the attenuation for the elastic wall is virtually indistinguishable from the attenuation of a rigid wall. We have also concluded that for typical feedline problems, the axial wall stiffness effect will not permit real wave propagation of the higher order modes since the amount of energy which is fed into the higher order modes at the line termination will not permit sustained coupling of the fluid and the wall for these modes.

(5)   For the homogeneous distribution of very small gas bubbles entrained in the liquid propellant, the net effect over the frequency range of interest is to lower the phase velocity of the mixture. Experimental data indicate that there is also greater damping with increasing mass ratio than predicted by theory.

(6)   Small diameter gas bubbles entrained in the liquid reduce the phase velocity in the mixture by the amount predicted by an isothermal model for the gas speed of sound rather than the adiabatic model.

(7)   The model for a complex side branch such as an accumulator, predicts response amplitudes somewhat greater than those obtained experimentally. The experimental resonant frequencies were shifted in accordance with theory, but agreement with theory becomes poorer as the terminal gas volume is increased.

145

(8) The analytical model used for a local compliance (large local gas volume) agrees very well with the data from the experimental tests conducted. The experimental data also indicate that for cases where the gas bubble resonant frequency is far above that encountered through excitation, a more simple model for the compliance would be satisfactory; that is, a model which neglects the bubble dynamics.

(9) A line with bends or elbows behaves exactly like a straight line of equal total length when the method of excitation does not involve structural acceleration of the line.

(10) The model for the structural-hydraulic coupling of a feedline with bends (which provide local impedances) adequately predicts the line resonant frequencies, although the amplitudes measured were considerably different from the theoretical values. However, the specific example tested produced poor agreement with theory over a frequency range of 40 to 65 Hz, and no satisfactory explanation for this behavior has been found.

(11) The initial tests conducted involving structural-hydraulic coupling demonstrated the need for a thorough knowledge of the exact modes of excitation applied to a given feedline geometry. It has been found that certain excitations can produce dependent or secondary modes of excitation which must be properly treated before a correct analytical simulation is possible.

VIII.2 Recommendations

Based on the experience gained from this study of liquid rocket propellant feedline dynamics, recommendations for future work include:

(1) The development of an analytical model and computerized subroutine to compute the speed of sound or phase velocity in two-phase, single-component fluids. The equilibrium model described in Section III.1 of this report would offer an excellent starting point, but would involve programming a vast amount of thermodynamic data for each liquid propellant under consideration.

(2) Improvement of the model used to compute the bubble dynamics of large cavitation bubbles, where the bubble stiffness (or compliance) is also dependent upon the vaporization and condensation rates as the bubble undergoes successive pressure perturbations.

(3) An analytical model should be developed to predict the effects of nonlinear terminal resistances for configurations or operational conditions where $Q \approx Q_d$. The nonlinear distortion created at these conditions

146

could prove significant; this analytical model should also be examined experimentally.

(4) Further experimental tests should be conducted to determine the validity of the model used to simulate structural-hydraulic coupling and the effects of mounting stiffness.

(5) An analytical and experimental study should be conducted to study the apparent added damping due to the presence of entrained gas bubbles. The data obtained in this study indicate that the increased damping is significant and should not be neglected.

(6) General modification of the feedline computer code described herein to allow more versatility in the use of this program. For example, the present program can currently handle only one mode of excitation at a time, whereas, in reality, there can be numerous sources of simultaneous feedline excitation.

REFERENCES

1. Ryan, R. S., Kiefling, L. A., Jarvinen, W. A., and Buchanan, H. J., "Simulation of Saturn V S-II Stage Propellant Feedline Dynamics," Journal of Spacecraft, Vol. 7, No. 12, December, 1970, pp. 1407-1412.

2. Rubin, S., "Prevention of Coupled Structure-Propulsion Instability (POGO) on the Space Shuttle," Space Transportation System Technology Symposium, NASA TM X-52876, Vol. II, July 1970, pp. 249-262.

3. "Investigation of 17-Hz Closed-Loop Instability on S-II Stage of Saturn V," Rocketdyne/NAR, NASA Contract NAS8-19, August 1969.

4. Sack, I. E. and Nottage, H. B., "System Oscillations Associated with Cavitating Inducers," Journal of Basic Engineering, Vol. 87, Series D, No. 4, December 1965, pp. 917-924.

5. Gerlach, C. R., "The Dynamics of Viscous Fluid Transmission Lines with Particular Emphasis on Higher Mode Propagation," Ph. D. Thesis, Oklahoma State University, July 1966.

6. Gerlach, C. R., "Dynamic Models for Hydraulic Conduits," Proc. 1969 Joint Automatic Control Conference, pp. 416-424, AIChE, N.Y., 1969.

7. Brown, F. T., Margolis, D. L., and Shah, R. P., "Small-Amplitude Frequency Behavior of Fluid Lines with Turbulent Flow," Journal of Basic Engineering, Trans. ASME, Vol. 91, No. 4, pp. 678-693, December 1969.

8. Gouse, S. W., and Brown, G. A., "A Survey of the Velocity of Sound in Two-Phase Mixtures," ASME Paper No. 64-WA/F3-35, presented at ASME Winter Annual Meeting, New York, 1964.

9. Hsieh, Din-Yu, and Plesset, M. S., "On the Propagation of Sound in a Liquid Containing Gas Bubbles," The Physics of Fluids, Vol. 4, No. 3, August 1961, pp. 970-975.

10. Plesset, M. S., and Hsieh, Din-Yu, "Theory of Gas Bubble Dynamics in Oscillating Pressure Fields," The Physics of Fluids, Vol. 3, No. 6, 1960, pp. 882-892.

11.   Silberman, E., "Sound Velocity and Attenuation in Bubbly Mixtures Measured in Standing Wave Tubes," the Journal of the Acoustical Society of America, Vol. 29, No. 8, August 1957.

12.   Spitzer, L., Jr., "Acoustic Properties of Gas Bubbles in a Liquid," O.S.R.D. Report No. 6.1-sr 20-918, 1943.

13.   Koger, H. C., and Houghton, G., "Damping and Pulsation of Large Nitrogen Bubbles in Water," Journal of the Acoustical Society of America, Vol. 43, No. 8, 572, 1968.

14.   Chapman, R. B., and Plesset, M. S., "Thermal Effects in the Free Oscillation of Gas Bubbles," ASME Paper No. 70-WA/FE-11, presented at the ASME Winter Annual Meeting, New York, 1970.

15.   Lin, T. C., and Morgan, G. W., "Wave Propagation Through Fluid Contained in a Cylindrical Elastic Shell," Journal of The Acoustical Society of America, Vol. 28, pp. 1165-1176, November 1956

16.   Devin, Charles, Jr., "Survey of Thermal, Radiation, and Viscous Damping of Pulsating Air Bubbles in Water," Journal of the Acoustical Society of America, Vol. 31, No. 72, December 1959, pp. 1654-1667.

17.   D'Souza, A. F., and Oldenberger, R., "Dynamic Response of Fluid Lines," Journal of Basic Engineering, Trans. ASME, Vol. 86, No. 3, September 1964, pp. 589-598.

18.   Gerlach, C. R., et al., "Study of Fluid Transients in Closed Conduits, Annual Report No. 1, " Oklahoma State University, NASA Contract NAS8-11302, July 1965.

19.   Fashbaugh, R. H., and Streeter, V. L., "Resonance in Liquid Rocket Engine Systems," Journal of Basic Engineering, Trans., ASME, Vol. 87, No. 4, December 1965, pp. 1011-1017.

20.   Rocketdyne, Investigation of 17-HZ Closed-Loop Instability on S-II Stage of Saturn V, R-7970, August 1969, Rocketdyne Engineering, Canoga Park, California.

21.   Fluid Meters, Their Theory and Application, ASME, New York, 1959.

22.   Carstensen, E. L., and Foldy, L. L., "Propagation of Sound Through a Liquid Containing Bubbles," Journal of The Acoustical Society of America, Vol. 19, No. 3, May 1947, pp. 481-501.

23.   Fox, F. E., Curley, S. R., and Larson, G. S., "Phase Velocity and Absorption Measurements in Water Containing Air Bubbles," Journal of the Acoustical Society of America, Vol. 27, No. 3, May, 1955, pp. 534-539.

24.   Worlund, A. L., Glasgow, V. L., Norman, D. E., and Hill, R. D., "The Reduction of POGO Effects by Gas Injection," AIAA Paper No. 66-560, 1966.

25.   Holster, J. L., "Analysis of Propellant Feedline Dynamics," Monthly Progress Report No. 18, NASA Contract NAS-25919, September 15, 1972.

26.   Oldenberger, R., and Goodson, R. F., "Simplification of Hydraulic Line Dynamics by Use of Infinite Products," Journal of Basic Engineering, Trans. ASME, Vol. 86, No. 4, pp. 1-10, 1964.

APPENDIX   A

RATIONAL APPROXIMATE MODEL FOR DISTRIBUTED PARAMETER SYSTEMS

The four-terminal representation of a transmission line that has been utilized throughout this report is an exact model for the zeroeth mode transfer function equations. The value of this representation for frequency response analyses has been proven. In many problems, however, the time domain solution is required, and the Laplace transform representation constitutes a convenient technique for obtaining the space-dependent solution independently of the time-dependency. In the final analysis, the Laplace inversion integral must be evaluated. When hyperbolic functions are involved in the inversion, as they are in the distributed parameter line model, an infinite series of time-dependent terms is obtained due to the unbounded number of zeros of the hyperbolic functions. In many cases, closure of this series is extremely difficult, and the desired accuracy does not warrant laborious mathematical operations. The obvious conclusion is that there is a definite need for a simple, accurate, approximate technique for obtaining the time domain solution from the frequency domain representation.

The rudiments of such a technique were first proposed by Oldenberger and Goodson[26], and were later refined and put in a practical form by Gerlach[5, 6]. This technique is based upon expanding the hyperbolic functions into an infinite product of second-order polynomials, i.e.,

$$\cosh \Gamma(s) = \prod_{n=0}^{\infty} \left\{ 1 + \frac{2\zeta_{cn} s}{\omega_{cn}} + \frac{s^2}{\omega_{cn}^2} \right\} \tag{A. 1}$$

$$\sinh \Gamma(s) = \Gamma(s) \prod_{n=1}^{\infty} \left\{ 1 + \frac{2\zeta_{sn} s}{\omega_{sn}} + \frac{s^2}{\omega_{sn}^2} \right\} \tag{A. 2}$$

The coefficients, ζ_{cn}, ω_{cn}, ζ_{sn}, ω_{sn} are evaluated by solving for the value of Laplace operator, s_n at the zeroes of the hyperbolic functions. These quantities are conveniently catalogued in Figures A-1 to A-4. To evaluate any one of these coefficients, it is sufficient to calculate the damping number of the line, D_n. The damping number and the desired term number in the expansion completely define the four coefficients. It may be shown that for approximation purposes the term $\Gamma(s)$, in the expansion for the hyperbolic sine, can be represented adequately by sL/c_0. Characteristic impedance can be approximated by $\rho_0 c_0$.

With these expansions, it is now possible to approximate the hyperbolic functions to any desired degree of accuracy with expressions that can easily be (1) inverted into a time solution using standard transform pairs or (2) integrated in the time domain to
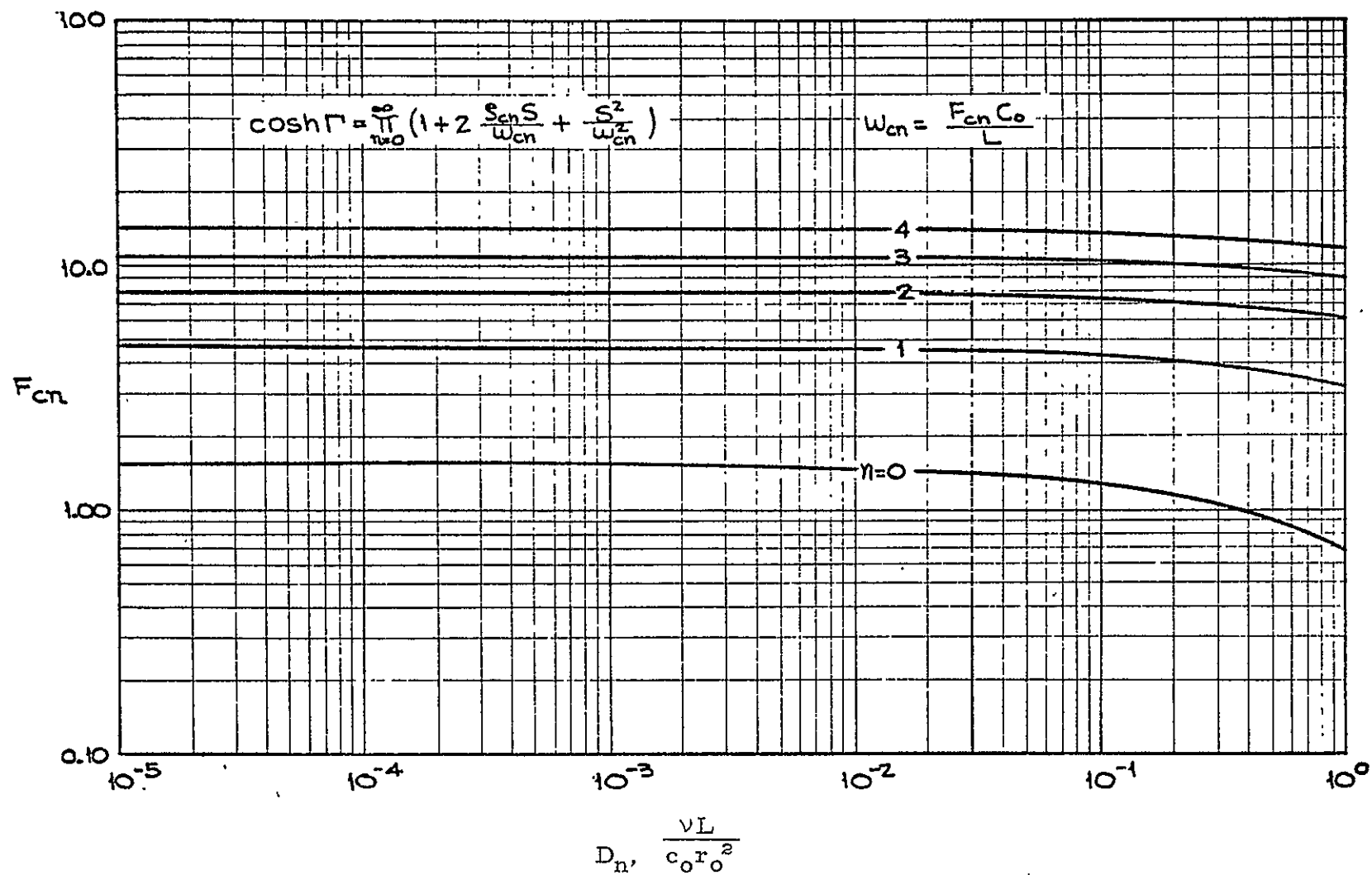
Figure A-1. Variation of the Approximate Model Parameter F_{cn} With Axial Damping Number
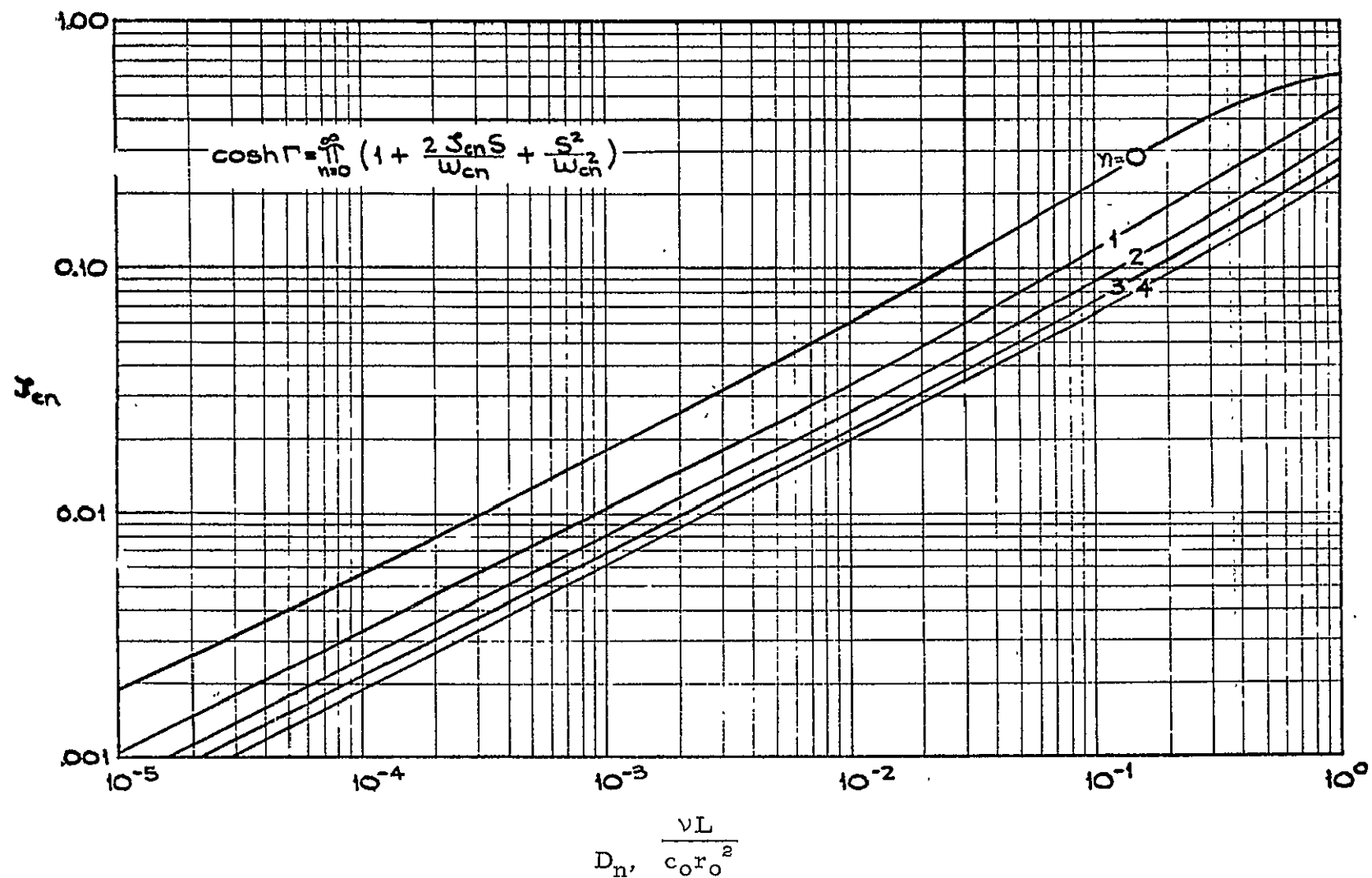
Figure A-2.   Variation of the Approximate Model Parameter
ζ_{cn} With Axial Damping Number

$$\sinh \Gamma = \Gamma \prod_{n=1}^{\infty} \left(1 + \frac{2 \vartheta_{sn} S}{\omega_{sn}} + \frac{S^2}{\omega_{sn}^2}\right)$$

$$\omega_{sn} = \frac{F_{sn} C_0}{L}$$

F_{sn}

$$D_n, \quad \frac{\nu L}{c_0 r_0^2}$$
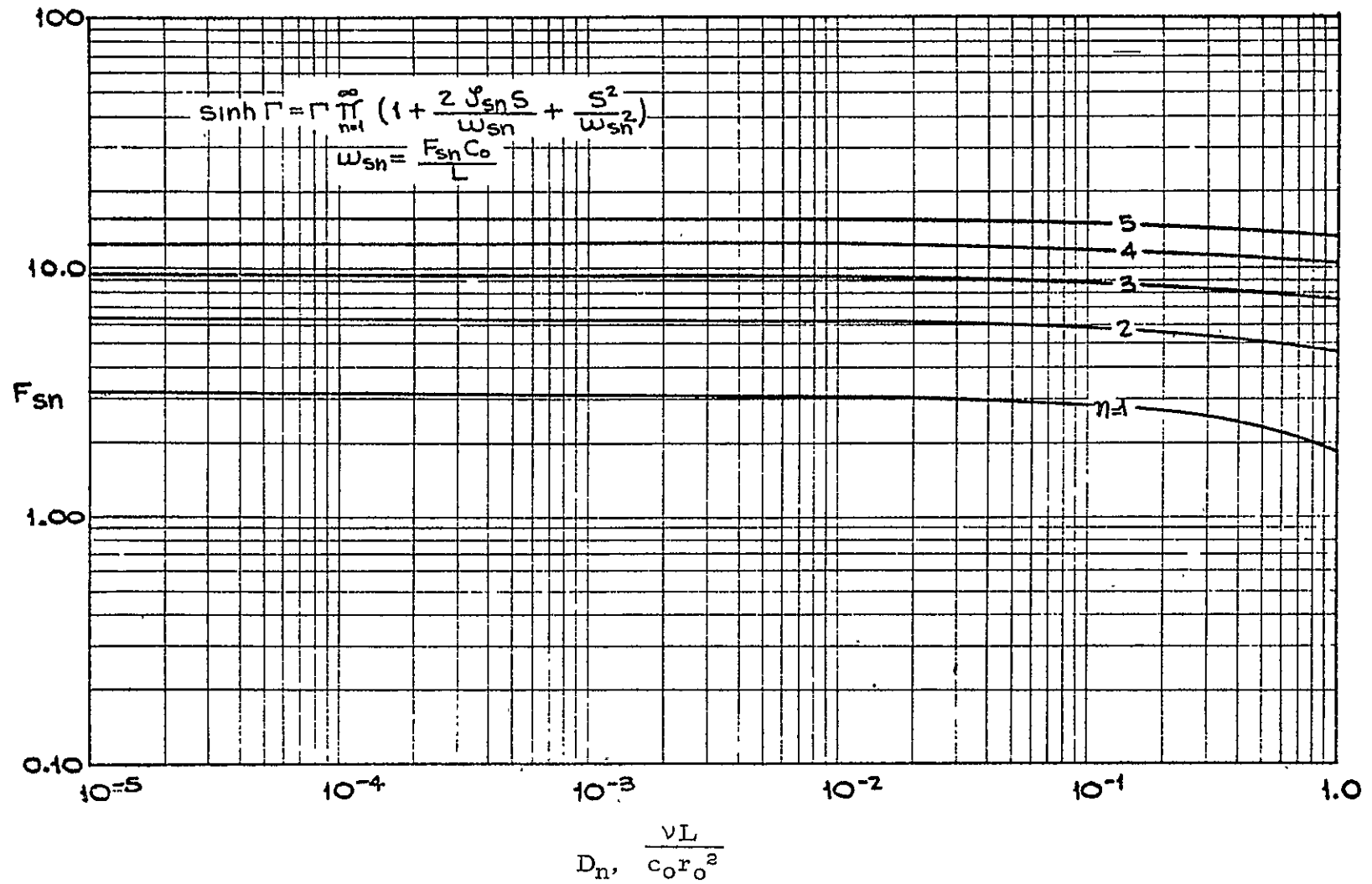
Figure A-3. Variation of the Approximate Model Parameter
F_{sn} With Axial Damping Number

$$\sinh \Gamma = \Gamma \prod_{n=1}^{\infty} \left(1 + \frac{2 \zeta_{sn} S}{\omega_{sn}} + \frac{S^2}{\omega_{sn}^2} \right)$$
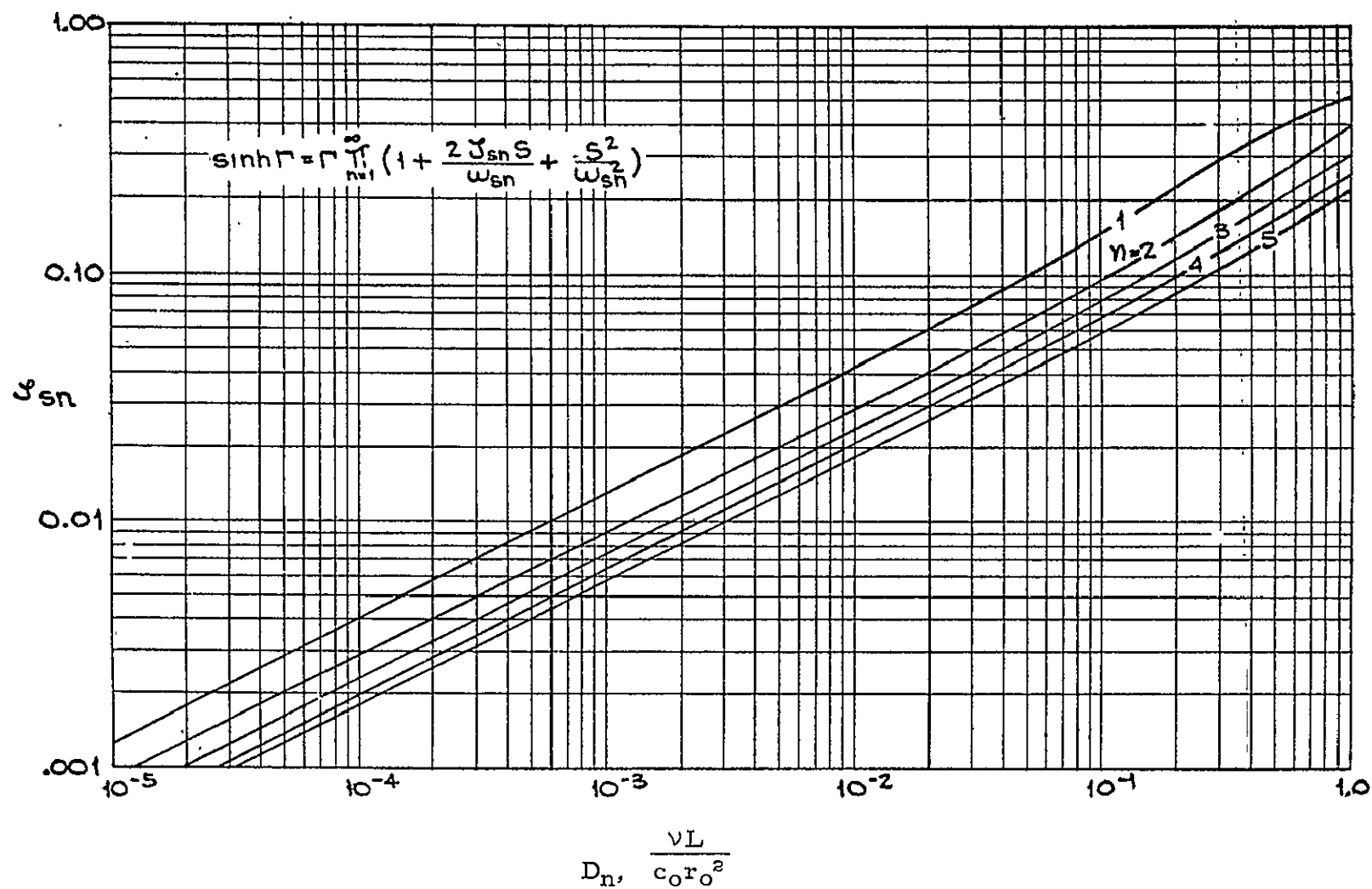
Figure A-4. Variation of the Approximate Model Parameter ζ_{sn} With Axial Damping Number

obtain the real time solution. For example, consider a transfer function in which a one-term approximation for the hyperbolic functions produces

$$\frac{P(s)}{\rho_o c_o V_o} = \frac{1}{44} \frac{1}{\left(1 + \frac{.176}{66} s + \frac{s^2}{66^2}\right)}$$ (A. 3)

Standard inversion pair yields

$$\frac{p(t)}{\rho_o c_o V_o} = 1.5 e^{-5.8t} \sin(66t)$$ (A. 4)

As a second example, consider a transfer function of the type

$$P(s) = -Z_c(s) \tanh \Gamma(s) V(s)$$ (A. 5)

A one-term approximation in the model yields

$$\left(1 + \frac{2\zeta_{co} s}{\omega_{co}} + \frac{s^2}{\omega_{co}^2}\right) P(s) = -\rho_o c_o \left(\frac{sL}{c_o}\right) V(s)$$ (A. 6)

Interpreting the Laplace operator as a time derivative, the following equation is obtained:

$$\left(1 + \frac{2\zeta_{co}}{\omega_{co}} \frac{d}{dt} + \frac{1}{\omega_{co}^2} \frac{d^2}{dt^2}\right) p(t) = -\rho_o L \frac{dv(t)}{dt}$$ (A. 7)

With a second equation relating pressure and flow velocity, a standard numerical integration easily can be obtained on the computer.

The accuracy of this model is summarized below:

(1) One term of the model well approximates the hyperbolic operators up to the first critical frequency.

(2) Two terms improve the approximation up to the first critical point and roughly (not well) approximate the hyperbolic operators up beyond the second critical frequency. The use of more terms would improve the results near the second critical frequency.

(3) A one-term approximation for the hyperbolic function is generally adequate for most engineering problems.

A-7

APPENDIX   B

SPEED OF SOUND IN A LIQUID CONTAINING

A HOMOGENEOUS DISTRIBUTION OF BUBBLES

Single-Component, Two-Phase Mixture in Equilibrium

The speed of sound in a pure, two-phase substance can be expressed by the standard form

$$a^2 = g_0 \left(\frac{\partial p}{\partial \rho}\right)_s \qquad (B.1)$$

or, in terms of specific volume rather than density,

$$a^2 = -g_0 v^2 \left(\frac{\partial p}{\partial v}\right)_s \qquad (B.2)$$

Following the approach of Gouse and Brown[8], it can be shown that the partial derivative in Equation (B.2) can be expanded such that

$$a^2 = g_0 v^2 \left(\frac{\partial s}{\partial v}\right)_p \left(\frac{\partial s}{\partial v}\right)_T \left(\frac{\partial T}{\partial s}\right)_v \qquad (B.3)$$

Since constant pressure and temperature lines are coincident in the two-phase region beneath the vapor dome,

$$\left(\frac{\partial s}{\partial v}\right)_p = \left(\frac{\partial s}{\partial v}\right)_T \qquad (B.4)$$

or in finite difference form

$$\left(\frac{\partial s}{\partial v}\right)_p = \frac{s_g - s_f}{v_g - v_f} \qquad (B.5)$$

The subscripts, f and g, refer to the saturated liquid and vapor state, respectively. Substituting Equations (B.4) and (B.5) into Equation (B.6)

$$a^2 = g_0 v^2 \left(\frac{s_g - s_f}{v_g - v_f}\right)^2 \left(\frac{\partial T}{\partial s}\right)_v \qquad (B.6)$$

Equation (B.6) can be developed into a form that is suitable for use with a standard temperature-entropy chart. The quality of a two-phase state, χ, is defined as

$$\chi = M_v / (M_\ell + M_v) \qquad (B.7)$$

and the specific volume for such a state can be written in terms of quality as

$$v = v_f + \chi(v_g - v_f) \tag{B.8}$$

Substituting this expression into Equation (B.6), the speed of sound can be written as a function of quality

$$a^2 = g_o \left[\frac{v_f}{v_g - v_f} + \chi \right]^2 (s_g - s_f)^2 \left(\frac{\partial T}{\partial s} \right)_v \tag{B.9}$$

In finite difference form, the speed of sound in a single-component, two-phase mixture in thermodynamic equilibrium becomes

$$a = \left(\frac{v_f}{v_g - v_f} + \chi \right) (s_g - s_f) \left[g_o \left(\frac{\Delta T}{\Delta s} \right)_v \right]^{\frac{1}{2}} \tag{B.10}$$

Single-Component or Two-Component, Two-Phase Mixture With Constant Quality

The above section described the acoustic velocity in an equilibrium mixture of a liquid and its vapor phase. In this section, the speed of sound is analyzed for a constant quality mixture of a liquid and a distinctly different gas, but the results also apply to single-component mixtures as long as the vaporization and condensation rates are low enough that no phase change occurs as a result of pressure disturbances (constant quality is assumed at all times). In the development of a constant quality model for the acoustic velocity in a liquid-gas mixture, the following assumptions are made:

(1) The mixture is homogeneous in phase composition.

(2) The mass of each phase remains constant.

(3) The gas behaves as a perfect gas with the appropriate equation of state and constant specific heats.

(4) The liquid compressibility is ignored.

(5) The gas and liquid phases are always at the same temperature.

The subsequent derivation is based on total volume as opposed to the specific volume approach that was utilized in the previous section. Assuming an adiabatic process,

$$c^2 = \left(\frac{dp}{d\rho} \right)_s \qquad \text{or} \qquad \frac{1}{c^2} = \left(\frac{d\rho}{dp} \right)_s \tag{B.11}$$

B-3

For a two-component mixture,

$$\rho = \frac{M_\ell + M_g}{V_\ell + V_g}$$

$$\frac{1}{c^2} = \frac{d}{dp}\left(\frac{M_\ell + M_g}{V_\ell + V_g}\right)$$

$$\frac{1}{c^2} = \left[(V_\ell + V_g)\frac{d}{dp}(M_\ell + M_g) - (M_\ell + M_g)\frac{d}{dp}(V_\ell + V_g)\right]/(V_\ell + V_g)^2$$

$$\frac{1}{c^2} = -\left(\frac{M_\ell + M_g}{V_\ell + V_g}\right)\frac{1}{V_\ell + V_g}\frac{d}{dp}(V_\ell + V_g)$$

$$\frac{1}{c^2} = -\rho\frac{1}{V_\ell + V_g}\left(\frac{d}{dp}V_\ell\left(\frac{M_\ell}{M_\ell}\right) + \frac{d}{dp}V_g\left(\frac{M_g}{M_g}\right)\right)$$

$$\frac{1}{c^2} = -\rho\frac{M_\ell}{V_\ell + V_g}\frac{d}{dp}\left(\frac{1}{\rho_\ell}\right) - \rho\frac{M_g}{V_\ell + V_g}\frac{d}{dp}\left(\frac{1}{\rho_g}\right)$$

$$\frac{1}{c^2} = -\rho\left[\frac{M_\ell}{V_\ell + V_g}\left(-\frac{1}{\rho_\ell^2}\right)\left(\frac{d\rho_\ell}{dp}\right)_s + \frac{M_g}{V_\ell + V_g}\left(-\frac{1}{\rho_g^2}\right)\left(\frac{d\rho_g}{dp}\right)_s\right] \qquad \text{(B.12)}$$

$$\frac{1}{c^2} = \rho\left[\frac{M_\ell}{V_\ell + V_g}\frac{1}{\rho_\ell^2}\frac{1}{c_\ell^2} + \frac{M_g}{V_\ell + V_g}\frac{1}{\rho_g^2}\frac{1}{c_g^2}\right] \qquad \text{(B.13)}$$

From the definition for density,

$$V = M/\rho \qquad \text{(B.14)}$$

$$V_\ell + V_g = \frac{M_\ell}{\rho_\ell} + \frac{M_g}{\rho_g} = \frac{M_\ell\rho_g + M_g\rho_\ell}{\rho_\ell\rho_g} \qquad \text{(B.15)}$$

The mass ratio, Φ, is now defined as the mass of vapor/mass of liquid.

$$\Phi = M_g/M_\ell \qquad \text{(B.16)}$$

Substituting the mass ratio into Equation (B.15),

$$V_\ell + V_g = \frac{M_\ell(\rho_g + \Phi\rho_\ell)}{\rho_g\rho_\ell} \qquad \text{(B.17)}$$

B-4

Thus, the speed of sound in a constant quality mixture becomes

$$\frac{1}{c^2} = \rho \left[\frac{\rho_g}{\rho_g + \Phi \rho_\ell} \frac{1}{\rho \ell} \frac{1}{c_\ell^2} + \frac{\Phi \rho_\ell}{\rho_\ell + \Phi \rho_g} \frac{1}{\rho_g} \frac{1}{c_g^2} \right] \qquad (B.18)$$

As mentioned in Section III, the isothermal velocity of sound might be more appropriate for two-component, two-phase mixtures rather than the adiabatic (isentropic) velocity of sound.

Plesset and Hsieh[10] have shown that bubble dynamics are governed by an isothermal process at low excitation frequencies and an adiabatic process at higher frequencies, providing there is a uniform temperature distribution within the gas bubbles. However, this sharp division of thermodynamic behavior is not necessarily the case because the heat conduction rate of the gas is considerably smaller than that in the liquid. The liquid has a large specific heat and thermal conductivity, and behaves as a heat reservoir. Consequently, in the liquid adjacent to the gas-liquid interface, there are no changes in the gas temperature during compression. In the center of the bubble away from a substance having a high specific heat, the gas follows the adiabatic equation of state. Therefore, the overall bubble follows a polytropic process. However, for very small bubbles, the heat diffusion into the liquid is so rapid that temperature changes in the bubble can not take place, and the process is essentially isothermal.

For this reason, the propagation of sound in a liquid with a homogeneous distribution of bubbles (basic assumption No. 1) indicates a speed in agreement with isothermal speed of sound. To compute the isothermal speed of sound in the mixture, the acoustic velocity of the gas in Equation (B.13) should be changed to the isothermal value, or

$$c_g = \sqrt{g_0 \gamma RT} \qquad (B.19)$$

where $\gamma = 1.0$ rather than 1.4.

APPENDIX   C

PARALLEL LINES

Consider the assemblage of parallel lines shown in Figure C-1. Although this configuration is not used frequently in propellant feed systems, the pressure-flow relationships for this component have been developed and included in the computer code for application in special situations. Assuming that flow losses due to elbow resistance are negligible, a standard four-terminal pressure-flow equation can be written for the i-th line. For this particular problem, however, it is more convenient to express that pressure-flow equation as

$$Q_{1_i} = Z_{c_i}^{-1} A_i (P_1 \coth \Gamma_i - P_2 \operatorname{csch} \Gamma_i)$$

$$Q_{2_i} = Z_{c_i}^{-1} A_i (P_1 \operatorname{csch} \Gamma_i - P_2 \coth \Gamma_i) \tag{C.1}$$

The terminal pressures, P_1 and P_2, are common to all line segments. The continuity equation requires that

$$\sum_{i=1}^{n} Q_{1_i} = Q_1 \qquad \text{and} \qquad \sum_{i=1}^{n} Q_{2_i} = Q_2 \tag{C.2}$$

Summing Equations (C.1) and utilizing Equations (C.2) yields

$$Q_1 = P_1 \sum_{i=1}^{n} Z_{c_i}^{-1} A_i \coth \Gamma_i - P_2 \sum_{i=1}^{n} Z_{c_i}^{-1} A_i \operatorname{csch} \Gamma_i$$

$$Q_2 = P_1 \sum_{i=1}^{n} Z_{c_i}^{-1} A_i \operatorname{csch} \Gamma_i - P_2 \sum_{i=1}^{n} Z_{c_i}^{-1} A_i \coth \Gamma_i \tag{C.3}$$

Equations (C.3) can be easily rearranged into the standard form

$$\begin{bmatrix} P_2 \\ Q_2 \end{bmatrix} = \begin{bmatrix} b_{11} & b_{12} \\ b_{21} & b_{22} \end{bmatrix} \begin{bmatrix} P_1 \\ Q_1 \end{bmatrix} \tag{C.4}$$

where
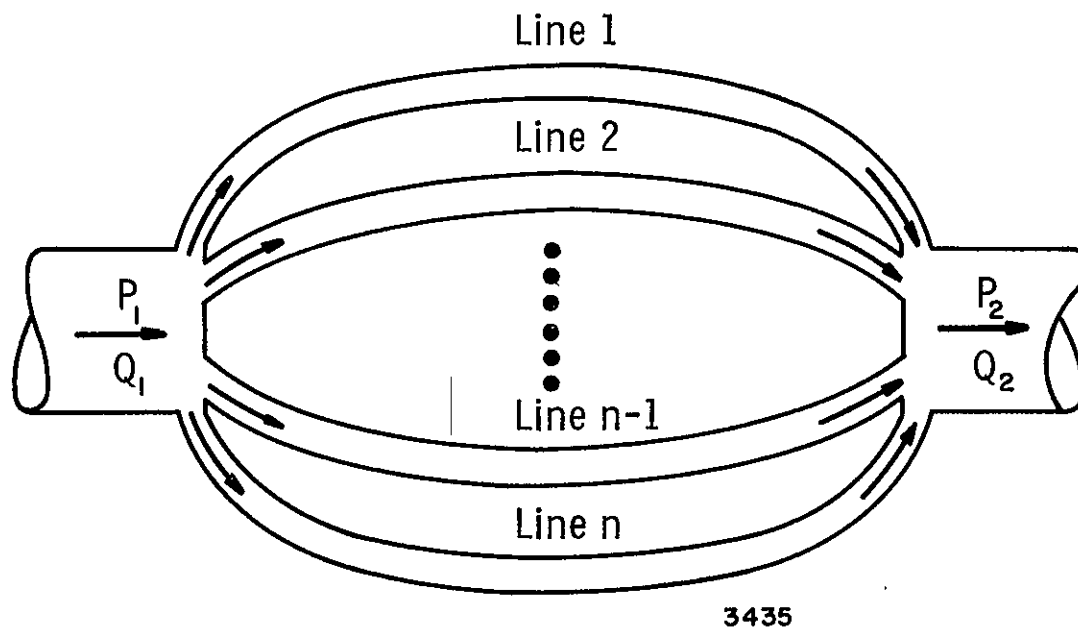
Figure C-1. Parallel Line Model

$$b_{11} = b_{22} = \frac{\sum\limits_{i=1}^{n} Z_{c_i}^{-1} A_i \coth \Gamma_i}{\sum\limits_{i=1}^{n} Z_{c_i}^{-1} A_i \operatorname{csch} \Gamma_i}$$

$$b_{12} = - \frac{1}{\sum\limits_{i=1}^{n} Z_{c_i}^{-1} A_i \operatorname{csch} \Gamma_i}$$

$$b_{21} = \sum\limits_{i=1}^{n} Z_{c_i}^{-1} A_i \operatorname{csch} \Gamma_i - \frac{\left(\sum\limits_{i=1}^{n} Z_{c_i}^{-1} A_i \coth \Gamma_i\right)^2}{\sum\limits_{i=1}^{n} Z_{c_i}^{-1} A_i \operatorname{csch} \Gamma_i}$$

The line length that appears in the expression for the propagation operator is taken to be the developed length measured along the pipe centerline.

APPENDIX D

USER'S MANUAL FOR GENERALIZED
FEEDLINE PROGRAM

D. 1   Program Organization

This manual describes the mechanics of the Generalized Feedline Computer Code. It is assumed that the user has had previous experience in FORTRAN IV coding.

The FORTRAN IV source deck is composed of a main or controller program, individual subroutines for each line component and several special purpose subroutines which either perform specific mathematical operations or serve as function evaluators. The subroutine approach was chosen because of its distinct advantages in the areas of program debugging, modification and expansion. Using the Control Data Corporation 6400 system, the source deck is compiled each time the program is submitted to the terminal for execution, thus eliminating tape handling. The function of each routine is presented below in the order in which it will appear in the FORTRAN listing which is included in the next section.

Controller:

The controller program performs the following functions:

(1) Read-in of all pertinent data for a particular line configuration;

(2) Execute the calling of subroutines in the proper sequence;

(3) Evaluate the magnitude of the transfer function at each frequency;

(4) Increment frequency, the independent variable, within a prescribed range;

(5) Perform all output operations.

Subroutine ONE: Calculates matrix elements for a straight duct of finite length and constant cross-sectional area having no external excitation.

Subroutine TWO: Calculates matrix elements for a single cavitation bubble including the effects of radiation, thermal and viscous damping.

Subroutine THREE: Calculates the matrix elements of a pressure-volume compensator (PVC) joint including the effects of internal friction.

Subroutine FOUR: ·Establishes the continuity requirements for
                       a side branch pulser.

Subroutine FIVE: Calculates the matrix elements for a straight
                       line which undergoes rigid body motion as a
                       result of an external velocity excitation.

Subroutine SIX: Calculates the matrix elements for several
                       lines in parallel all of which have a common
                       entrance-exit point.

Subroutine SEVEN: Calculates the matrix elements for a bellows
                       with gas trap liner. Relative motion between
                       the ends of the bellows is permitted.

Subroutine EIGHT: Calculates the matrix elements for a line with
                       mounting stiffness having a structural accelera-
                       tion applied to the viscoelastic support.

Subroutine NINE: Calculates the matrix elements for a line
                       undergoing forced changes in length.

Subroutine TEN: Calculates matrix elements for a line with
                       mounting stiffness using the impedance method.

Subroutine ELEVEN: Calculates the matrix elements for a com-
                       plex side branch with laminar flow.

Subroutine TWELVE
     to   FIFTEEN: Available for future expansion.

Subroutine SPEED: Calculates the speed of sound in a pure liquid
                       or a liquid with a homogeneous distribution of
                       an ullage gas. A mixture of a liquid and its
                       own vapor may also be considered. However,
                       in the latter case, the results are not precise
                       because the theoretical model does not in-
                       clude the thermodynamic effect of phase change
                       at the bubble surface. Finally, the speed of
                       sound may be corrected for wall elasticity.

Subroutine DMAT: Calculates the resultant matrix $\underline{D}$ in
                       Equation (122).

Subroutine BMAT: Calculates the resultant matrix $\underline{B}$ in
                       Equation (123).

Subroutine J1ORJ10: · Evaluates Bessel functions $J_1(Z)$ and $J_0(Z)$ for complex Z. Series expansion is used for moderate values of the argument; an asymptotic approximation is used for large arguments.

D. 2   Program Listing

This section contains a listing of the program source deck. Program control cards, which are described in Section D. 4, are applicable to CDC 6000 series computer systems.

D. 3   Program Input Package

Due to the generalized nature of this computer program, the length of the input package is variable and is directly related to the number of components in the feedline model. The first card in the package is always an alphanumeric header card on which the user can punch pertinent information such as run number, configuration number, etc., to be printed as the first line of program output. Fifty-five (55) Holerith fields have been allocated for the information on the header card. The actual data input is a combination of integer or floating point information. Integer data conforms to a (24I3) format, while the floating point data is read in with a (6E12.6) format. The following data must be supplied in the order and with the units shown:

CARD 1   Header card

CARD 2   NELM, dimensionless   Designates the number of components in the line.

            JBNUM, dimensionless   Number of matrices that must be summed to arrive at matrix B, Equation (123).

            NGAS, dimensionless   Indicates presence (NGAS = 1) or absence (NGAS = 0) of dissolved gases in propellant.

            NELAST, dimensionless   Includes (NELAST = 1) or excludes (NELAST = 0) line elasticity effects in speed of sound calculation.

            NEXCITE, dimensionless   Element type producing the primary line excitation.

```
      PROGRAM CONTROL(INPUT,OUTPUT,TAPE 60=INPUT)
C     NELM=NUMBER OF DISCRETE ELEMENTS IN THE FEEDLINE,I.E., LINES,
C       BELLOWS, PVC JOINTS,ETC.
C     NELM INTEGER CONSTANTS ARE READ IN AND DESCRIBE THE TYPE OF
C       ELEMENTS IN THE ORDER THEY APPEAR IN THE LINE BEGINNING AT THE
C       OUTPUT OF THE FUEL TANK AND TERMINATING WITH THE COMBINED INPUT
C       IMPEDANCE TO THE TURBOPUMP,INJECTOR AND ENGINE. FOR EXAMPLE,
C       ITYPE(J)=M, J=ELEMENT NUMBER, M=ELEMENT TYPE
C       M=1 SIMPLE LINE WITH NO EXTERNAL EXCITATION
C       M=2 CAVITATION BUBBLE
C       M=3 PRESSURE VOLUME COMPENSATOR
C       M=4 SIDE BRANCH PULSER
C       M=5 RIGID BODY MOTION OF A SIMPLE LINE,VELOCITY EXCITATION
C       M=6 NPAR LINES IN PARALLEL WITH A COMMON INPUT-OUTPUT POINT
C       M=7 BELLOWS WITH RELATIVE MOTION BETWEEN THE ENDS
C       M=8 LINE WITH MOUNTING STIFFNESS(OPTION 1)
C       M=9 FORCED CHANGES IN LINE LENGTH
C       M=10 LINE WITH MOUTING STIFFNESS(OPTION 2)
C       M=11 COMPLEX SIDE BRANCH
C       M=12
C       M=13
C       M=14
C       M=15
C     JBNUM=NUMBER OF MATRICES THAT MUST BE SUMMED TO CONSTRUCT MATRIX B
C       B=B(1)+B(2)+......+B(JBNUM)
C     JTERM(J) IS THE NUMBER OF SUBMATRICES IN B(J)
C     K(J,M) IS AN ARRAY THAT DESCRIBES THE TYPE OF MATRICES THAT ARE TO
C       BE MULTIPLIED TOGETHER TO CONSTRUCT THE COMPONENTS OF MATRIX B.
C       M TAKES ON VALUES FROM 1 THROUGH JTERM(J)
C       FOR EXAMPLE, IF B(2)=D5*D4*C3 THEN K(2,1)=5,K(2,2)=4,K(2,3)=3
C     NGAS=0, NO DISSOLVED GASES IN THE PROPELLANT
C     NGAS=1, DISSOLVED GASES IN PROPELLANT WITH GAS-TO-LIQUID MASS
C       FRACTION,PHI
C     NELAST=0, SPEED OF SOUND IN PROPELLANT IS BASED ON AN INFINITELY
C       RIGID TRANSMISSION LINE
C     NELAST=1, SPEED OF SOUND IN PROPELLANT REFLECTS LINE ELASTICITY
C       (WALL MODULUS EWALL AND WALL THICKNESS HWALL)
C     NEXCITE=NELM PRODUCING THE PRIMARY LINE EXCITATION
C     BRCOMP=COMPLIANCE OF SIDE BRANCH ELEMENT
C     BRL=LENGTH OF SIDE BRANCH ELEMENT IN FEET
C     BDIAM=DIAMETER OF SIDE BRANCH ELEMENT IN INCHES
C     BRR=RESISTANCE OF SIDE BRANCH ELEMENT
C     * * * * * * * * * * * * * * * * * * * * * * * * * * * * * * * * *
      COMPLEX ETA,ENUM,DENOM,TRANS,B,D,XI,ARG,RJ,GAMMA,ZC,COSHG,SINHG,DD
     1,CC,TCOTH,TCSCH,BB,Z1,Z2,X1,X2,X3,X4,QUADRAT,ALPHAP,BETAP,ALPHADP,
     2BETADP,GOFS,SLCW,COSHCW,SINHCW,COEFF,ALPHA1,ALPHA2
      COMPLEX ZSTRUCT,ALPHA,BETA
      DIMENSION ITYPE(15),JTERM(15),K(15,15),EL(15),RADIUS(15),RBUB(15),
     1FPVC(15),AKBPVC(15),AKCPVC(15),PARLEN(15,5),PARRAD(15,5),FREQ(200)
      DIMENSION B(2,1),D(2,2),SIZE(200),SIZEDB(200),ANGLE(200),FBEL(15),
     1COMPLY(15),AKBEL(15),BSIGN(10),DAMPER(15),SPRINGK(15)
      DIMENSION DD(2,2,15),CC(2,1,15),BB(2,1,15),RADSEC(200),AREA(15)
      COMMON PI,RADIUS,OMEGA,ENU,ETA,EL,CO,RHOO,THERMK,RBUB,CPCV,PO,VISC
     1,FPVC,AKBPVC,AKCPVC,NPAR,PARRAD,PARLEN,BULKMOD,RHOLIQ,NGAS,GASMW
      COMMON GAMGAS,G,TO,PHI,COMPLY,NELAST,EWALL,HWALL,NELM,JBNUM,JTERM,
     1K,DD,CC,D,B,BB,CP,J,AREA,VMEAN,FBEL,AKBEL,BSIGN,DAMPER,SPRINGK
      COMMON G1,G2,RHOWALL,ZX,ZY
```

```
      COMMON BRCOMP,BRL,BRDIAM
C     * * * * * * * * * * * * * * * * * * * * * * * * * * * * * * * *
    1 READ 1000
      IF(EOF,60)5,10
    5 STOP
   10 CONTINUE
      READ 1005,NELM,JBNUM,NGAS,NELAST,NEXCITE
      READ 1005,(ITYPE(J),J=1,NELM)
      READ 1005,(JTERM(J),J=1,JBNUM)
      DO 15 J=1,JBNUM
      KOUNT=JTERM(J)
   15 READ 1005,(K(J,M),M=1,KOUNT)
      READ 1020,(BSIGN(J),J=1,JBNUM)
      READ 1020,HERTZI,DELHZ1,F1LIM,DELHZ2,HERTZF
      READ 1020,SIGN,TERMZ,RHOLIQ,THERMK,PO,TO
      READ 1020,EWALL,HWALL,ZINPUT,CPCV,BULKMOD,PHI
      READ 1020,VISC,GASMW,GAMGAS,CP,VMEAN
C     LOOP FOR READ-IN OF LINE ELEMENT DATA
      PI=3.1415927
      DO 95 J=1,NELM
      INDEX=ITYPE(J)
      GO TO (20,25,30,35,40,45,50,55,60,65,70,75,80,85,90),INDEX
   20 READ 1020,EL(J),RADIUS(J)
      AREA(J)=PI*RADIUS(J)**2/144.
      AREA1=AREA(J)
      RAD1=RADIUS(J)/12.
      GO TO 95
   25 READ 1020,RBUB(J),RADIUS(J)
      GO TO 95
   30 READ 1020, FPVC(J),AKBPVC(J),AKCPVC(J)
      GO TO 95
   35 GO TO 95
   40 READ 1020,EL(J),RADIUS(J)
      AREA(J)=PI*RADIUS(J)**2/144.
      GO TO 95
   45 READ 1005,NPAR
      READ 1020,(PARLEN(J,I),PARRAD(J,I),I=1,NPAR)
      GO TO 95
   50 READ 1020,FBEL(J),COMPLY(J),AKBEL(J)
      GO TO 95
   55 READ 1020,EL(J),RADIUS(J),DAMPER(J),SPRINGK(J)
      AREA(J)=PI*RADIUS(J)**2/144.
      GO TO 95
   60 READ 1020,EL(J),RADIUS(J),G1,G2,RHOWALL
      AREA(J)=PI*RADIUS(J)**2/144.
      GO TO 95
   65 READ 1020,EL(J),RADIUS(J),ZX,ZY
      AREA(J)=PI*RADIUS(J)**2/144.
      GO TO 95
   70 READ 1020,BRL,BRDIAM,BRCOMP
      GO TO 95
   75 READ 1000
      GO TO 95
   80 READ 1000
      GO TO 95
   85 READ 1000
      GO TO 95
   90 READ 1000
```

```
   95 CONTINUE
C     * * * * * * * * * * * * * * * * * * * * * * * * * * * * * * *
      G=32.174049
      ETA=(0.,1.)
      IFREQ=1
      FREQ(IFREQ)=HERTZI
C     CALCULATION OF MATRIX ELEMENTS
   99 OMEGA=2.*PI*FREQ(IFREQ)
      DO 175 J=1,NELM
      INDEX=ITYPE(J)
      GO TO (100,105,110,115,120,125,130,135,140,145,150,155,160,165,170
     1),INDEX
  100 CALL ONE
      GO TO 175
  105 CALL TWO
      GO TO 175
  110 CALL THREE
      GO TO 175
  115 CALL FOUR
      GO TO 175
  120 CALL FIVE
      GO TO 175
  125 CALL SIX
      GO TO 175
  130 CALL SEVEN
      GO TO 175
  135 CALL EIGHT
      GO TO 175
  140 CALL NINE
      GO TO 175
  145 CALL TEN
      GO TO 175
  150 CALL ELEVEN
      GO TO 175
  155 CALL TWELVE
      GO TO 175
  160 CALL THIRTEN
      GO TO 175
  165 CALL FOURTEN
      GO TO 175
  170 CALL FIVETEN
  175 CONTINUE
C     * * * * * * * * * * * * * * * * * * * * * * * * * * * * * * *
      CALL DMAT
      CALL BMAT
      ENUM=B(1,1)*(D(2,1)*ZINPUT+D(2,2))-B(2,1)*(D(1,1)*ZINPUT+D(1,2))
      DENOM=D(2,1)*ZINPUT+D(2,2)-(D(1,1)*ZINPUT+D(1,2))/TERMZ
      TRANS=SIGN*ENUM/DENOM
      SIZE(IFREQ)=CABS(TRANS)
      IF(NEXCITE.EQ.4)GO TO 176
      IF(NEXCITE.EQ.5)GO TO 177
      IF(NEXCITE.EQ.7)GO TO 177
      IF(NEXCITE.EQ.9)GO TO 177
      IF(NEXCITE.EQ.8)GO TO 178
  176 SIZEDB(IFREQ)=20.*ALOG10(SIZE(IFREQ)*AREA1/SQRT(RHOLIQ*BULKMOD))
      GO TO 179
  177 SIZEDB(IFREQ)=20.*ALOG10(SIZE(IFREQ)/SQRT(RHOLIQ*BULKMOD))
      GO TO 179
```

```
 178 SIZEDB(IFREQ)=20.*ALOG10(SIZE(IFREQ)/(RHOLIQ*RAD1))
 179 CONTINUE
     ANGLE(IFREQ)=ATAN2(AIMAG(TRANS),REAL(TRANS))*57.29578
 180 ANGLE(IFREQ)=ANGLE(IFREQ)-180.
 185 RADSEC(IFREQ)=OMEGA
     IF(FREQ(IFREQ).LT.HERTZF) GO TO 190
     GO TO 205
 190 IFREQ=IFREQ+1
     IF(FREQ(IFREQ-1)-F1LIM)195,195,200
 195 FREQ(IFREQ)=FREQ(IFREQ-1)+DELHZ1
     IFINAL=IFREQ
     GO TO 99
 200 FREQ(IFREQ)=FREQ(IFREQ-1)+DELHZ2
     IFINAL=IFREQ
     GO TO 99
 205 PRINT 1000
     PRINT 1025
     PRINT 1030
     DO 250 I=1,IFINAL
 250 PRINT 1040,RADSEC(I),FREQ(I),SIZE(I),SIZEDB(I),ANGLE(I)
     GO TO 1
C    * * * * * * * * * * * * * * * * * * * * * * * * * * * * * * *
1000 FORMAT(55H1                                                    )
1005 FORMAT(24I3)
1020 FORMAT(6E12.6)
1025 FORMAT(1H0,39X,15HNON-DIMENSIONAL,5X,5HPHASE)
1030 FORMAT(14H OMEGA-RAD/SEC,4X,7HFREQ-HZ,4X,9HTRANS-P/K,6X,8HTRANS-DB
    1,6X,9HANGLE-DEG)
1040 FORMAT(1X,F9.1,F15.1,F13.3,F14.2,F15.1)
1050 FORMAT(1H1,E14.6,6E15.6)
     END
```

```
SUBROUTINE ONE
THIS SUBROUTINE CALCULATES THE ELEMENTS OF THE TRANSFER MATRIX FOR
A STRAIGHT LINE OF LENGTH L WITHOUT EXTERNAL EXCITATION
 COMPLEX ETA,ENUM,DENOM,TRANS,B,D,XI,ARG,RJ,GAMMA,ZC,COSHG,SINHG,DD
1,CC,TCOTH,TCSCH,BB,Z1,Z2,X1,X2,X3,X4,QUADRAT,ALPHAP,BETAP,ALPHADP,
2BETADP,GOFS,SLCW,COSHCW,SINHCW,COEFF,ALPHA1,ALPHA2
 COMPLEX ZSTRUCT,ALPHA,BETA
 DIMENSION ITYPE(15),JTERM(15),K(15,15),EL(15),RADIUS(15),RBUB(15),
1FPVC(15),AKBPVC(15),AKCPVC(15),PARLEN(15,5),PARRAD(15,5),FREQ(200)
 DIMENSION B(2,1),D(2,2),SIZE(200),SIZEDB(200),ANGLE(200),FBEL(15),
1COMPLY(15),AKBEL(15),BSIGN(10),DAMPER(15),SPRINGK(15)
 DIMENSION DD(2,2,15),CC(2,1,15),BB(2,1,15),RADSEC(200),AREA(15)
 COMMON PI,RADIUS,OMEGA,ENU,ETA,EL,CO,RHOO,THERMK,RBUB,CPCV,PO,VISC
1,FPVC,AKBPVC,AKCPVC,NPAR,PARRAD,PARLEN,BULKMOD,RHOLIQ,NGAS,GASMW
 COMMON GAMGAS,G,TO,PHI,COMPLY,NELAST,EWALL,HWALL,NELM,JBNUM,JTERM,
1K,DD,CC,D,B,BB,CP,J,AREA,VMEAN,FBEL,AKBEL,BSIGN,DAMPER,SPRINGK
 COMMON G1,G2,RHOWALL,ZX,ZY
 CALL SPEED
 REYNOLD=VMEAN*2.*RADIUS(J)/(ENU*12.)
 RT=144.*(2.*ENU*0.0055*REYNOLD**0.85)/(RADIUS(J)**2)
 Z1=(OMEGA*EL(J)*ETA)/CO
 Z2=CSQRT((1.,0.)+RT/(OMEGA*ETA))
 XI=SQRT(OMEGA/ENU)*CSQRT(-ETA)
 ARG=XI*RADIUS(J)/12.
 CALL J1ORJ0(ARG,RJ)
 GAMMA=ETA*OMEGA*EL(J)/(CO*CSQRT((1.,0.)-2.*RJ/ARG))+REAL(Z1*Z2)
 ZC=RHOO*CO/(CSQRT((1.,0.)-2.*RJ/ARG))
 COSHG=(CEXP(GAMMA)+CEXP(-GAMMA))/2.
 SINHG=(CEXP(GAMMA)-CEXP(-GAMMA))/2.
 DD(1,1,J)=COSHG
 DD(1,2,J)=-ZC*SINHG/AREA(J)
 DD(2,1,J)=-AREA(J)*SINHG/ZC
 DD(2,2,J)=COSHG
 RETURN
 END
```

```
      SUBROUTINE TWO
      THIS SUBROUTINE CALCULATES THE COMPLIANCE OF AND TRANSFER MATRIX
      ACROSS A SINGLE BUBBLE
      CPCV=RATIO OF SPECIFIC HEATS FOR THE GAS IN THE BUBBLE
      CP=SPECIFIC HEAT AT CONSTANT PRESSURE FOR THE GAS IN THE BUBBLE
      COMPLEX ETA,ENUM,DENOM,TRANS,B,D,XI,ARG,RJ,GAMMA,ZC,COSHG,SINHG,DD
     1,CC,TCOTH,TCSCH,BB,Z1,Z2,X1,X2,X3,X4,QUADRAT,ALPHAP,BETAP,ALPHADP,
     2BETADP,GOFS,SLCW,COSHCW,SINHCW,COEFF,ALPHA1,ALPHA2
      COMPLEX ZSTRUCT,ALPHA,BETA
      DIMENSION ITYPE(15),JTERM(15),K(15,15),EL(15),RADIUS(15),RBUB(15),
     1FPVC(15),AKBPVC(15),AKCPVC(15),PARLEN(15,5),PARRAD(15,5),FREQ(200)
      DIMENSION B(2,1),D(2,2),SIZE(200),SIZEDB(200),ANGLE(200),FBEL(15),
     1COMPLY(15),AKBEL(15),BSIGN(10),DAMPER(15),SPRINGK(15)
      DIMENSION DD(2,2,15),CC(2,1,15),BB(2,1,15),RADSEC(200),AREA(15)
      COMMON PI,RADIUS,OMEGA,ENU,ETA,EL,CO,RHOO,THERMK,RBUB,CPCV,PO,VISC
     1,FPVC,AKBPVC,AKCPVC,NPAR,PARRAD,PARLEN,BULKMOD,RHOLIQ,NGAS,GASMW
      COMMON GAMGAS,G,TO,PHI,COMPLY,NELAST,EWALL,HWALL,NELM,JBNUM,JTERM,
     1K,DD,CC,D,B,BB,CP,J,AREA,VMEAN,FBEL,AKBEL,BSIGN,DAMPER,SPRINGK
      COMMON G1,G2,RHOWALL,ZX,ZY
      GASCON=778.*CP*(1.-1./CPCV)
      GASDEN=144.*PO/(GASCON*G*(TO+460.))
      DTHERM=THERMK/(GASDEN*CP*G)
      PRO=SQRT(OMEGA*3600./(2.*DTHERM))*RBUB(J)/12.
      IF(PRO .GT. 35.)20,10
   10 T1=(SINH(2.*PRO)+SIN(2.*PRO))/(COSH(2.*PRO)-COS(2.*PRO))
      T2=(SINH(2.*PRO)-SIN(2.*PRO))/(COSH(2.*PRO)-COS(2.*PRO))
      T3=2.*PRO/(3.*(CPCV-1.))
      T4=(T1-1./PRO)/(T3+T2)
      POLY=CPCV/((1.+T2/T3)*(1.+T4**2))
      GO TO 30
   20 POLY=CPCV
   30 BUBVOL=4.*PI*RBUB(J)**3/(3.*1728.)
      CALL SPEED
      SPRING=POLY*PO*144./BUBVOL
      AMASS2=RHOO/(4.*PI*RBUB(J)/12.)
      IF(PRO.GT.35.)50,40
   40 BTHERM=T4*SPRING/OMEGA
      GO TO 60
   50 BTHERM=3.*(CPCV-1.)*SPRING/(2.*PRO*OMEGA)
   60 BRAD=AMASS2*RBUB(J)*(OMEGA**2)/(12.*CO)
      BVIS=1728.*VISC/(PI*RBUB(J)**3)
      BDAMP=BTHERM+BRAD+BVIS
      DD(1,1,J)=(1.,0.)
      DD(1,2,J)=(0.,0.)
      DD(2,1,J)=-ETA*OMEGA/(-AMASS2*OMEGA**2+ETA*BDAMP*OMEGA+SPRING)
      DD(2,2,J)=(1.,0.)
      RETURN
      END
```

```
SUBROUTINE THREE
THIS SUBROUTINE CALCULATES THE TRANSFER MATRIX FOR A PRESSURE-
VOLUME COMPENSATOR(PVC JOINT)
COMPLEX ETA,ENUM,DENOM,TRANS,B,D,XI,ARG,RJ,GAMMA,ZC,COSHG,SINHG,DD
1,CC,TCOTH,TCSCH,BB,Z1,Z2,X1,X2,X3,X4,QUADRAT,ALPHAP,BETAP,ALPHADP,
2BETADP,GOFS,SLCW,COSHCW,SINHCW,COEFF,ALPHA1,ALPHA2
COMPLEX ZSTRUCT,ALPHA,BETA
DIMENSION ITYPE(15),JTERM(15),K(15,15),EL(15),RADIUS(15),RBUB(15),
1FPVC(15),AKBPVC(15),AKCPVC(15),PARLEN(15,5),PARRAD(15,5),FREQ(200)
DIMENSION B(2,1),D(2,2),SIZE(200),SIZEDB(200),ANGLE(200),FBEL(15),
1COMPLY(15),AKBEL(15),BSIGN(10),DAMPER(15),SPRINGK(15)
DIMENSION DD(2,2,15),CC(2,1,15),BB(2,1,15),RADSEC(200),AREA(15)
COMMON PI,RADIUS,OMEGA,ENU,ETA,EL,CO,RHOO,THERMK,RBUB,CPCV,PO,VISC
1,FPVC,AKBPVC,AKCPVC,NPAR,PARRAD,PARLEN,BULKMOD,RHOLIQ,NGAS,GASMW
COMMON GAMGAS,G,TO,PHI,COMPLY,NELAST,EWALL,HWALL,NELM,JBNUM,JTERM,
1K,DD,CC,D,B,BB,CP,J,AREA,VMEAN,FBEL,AKBEL,BSIGN,DAMPER,SPRINGK
COMMON G1,G2,RHOWALL,ZX,ZY
FRICT=FPVC(J)
AKB=AKBPVC(J)
AKC=AKCPVC(J)
AKPVC=AKB-AKC
DD(1,1,J)=FRICT
DD(1,2,J)=(0.,0.)
DD(2,1,J)=(0.,0.)
DD(2,2,J)=(1.,0.)
CC(1,1,J)=(0.,0.)
CC(2,1,J)=AKPVC
RETURN
END
```

```
      SUBROUTINE FOUR
C     THIS SUBROUTINE CALCULATES THE ELEMENTS OF THE TRANSFER MATRIX FOR
C     A SIDE BRANCH PULSER
      COMPLEX ETA,ENUM,DENOM,TRANS,B,D,XI,ARG,RJ,GAMMA,ZC,COSHG,SINHG,DD
     1,CC,TCOTH,TCSCH,BB,Z1,Z2,X1,X2,X3,X4,QUADRAT,ALPHAP,BETAP,ALPHADP,
     2BETADP,GOFS,SLCW,COSHCW,SINHCW,COEFF,ALPHA1,ALPHA2
      COMPLEX ZSTRUCT,ALPHA,BETA
      DIMENSION ITYPE(15),JTERM(15),K(15,15),EL(15),RADIUS(15),RBUB(15),
     1FPVC(15),AKBPVC(15),AKCPVC(15),PARLEN(15,5),PARRAD(15,5),FREQ(200)
      DIMENSION B(2,1),D(2,2),SIZE(200),SIZEDB(200),ANGLE(200),FBEL(15),
     1COMPLY(15),AKBEL(15),BSIGN(10),DAMPER(15),SPRINGK(15)
      DIMENSION DD(2,2,15),CC(2,1,15),BB(2,1,15),RADSEC(200),AREA(15)
      COMMON PI,RADIUS,OMEGA,ENU,ETA,EL,CO,RHO0,THERMK,RBUB,CPCV,PO,VISC
     1,FPVC,AKBPVC,AKCPVC,NPAR,PARRAD,PARLEN,BULKMOD,RHOLIQ,NGAS,GASMW
      COMMON GAMGAS,G,TO,PHI,COMPLY,NELAST,EWALL,HWALL,NELM,JBNUM,JTERM,
     1K,DD,CC,D,B,BB,CP,J,AREA,VMEAN,FBEL,AKBEL,BSIGN,DAMPER,SPRINGK
      COMMON G1,G2,RHOWALL,ZX,ZY
      DD(1,1,J)=(1.,0.)
      DD(1,2,J)=(0.,0.)
      DD(2,1,J)=(0.,0.)
      DD(2,2,J)=(1.,0.)
      CC(1,1,J)=(0.,0.)
      CC(2,1,J)=(1.,0.)
      RETURN
      END
```

C3

```
      SUBROUTINE FIVE
C     THIS SUBROUTINE CALCULATES THE ELEMENTS OF THE TRANSFER MATRICES
C     FOR THE LONGITUDINAL RIGID BODY MOTION OF A SIMPLE LINE OF LENGTH
C     L. THE MOTION IS A RESULT OF VELOCITY EXCITATION.
      COMPLEX ETA,ENUM,DENOM,TRANS,B,D,XI,ARG,RJ,GAMMA,ZC,COSHG,SINHG,DD
     1,CC,TCOTH,TCSCH,BB,Z1,Z2,X1,X2,X3,X4,QUADRAT,ALPHAP,BETAP,ALPHADP,
     2BETADP,GOFS,SLCW,COSHCW,SINHCW,COEFF,ALPHA1,ALPHA2
      COMPLEX ZSTRUCT,ALPHA,BETA
      DIMENSION ITYPE(15),JTERM(15),K(15,15),EL(15),RADIUS(15),RBUB(15),
     1FPVC(15),AKBPVC(15),AKCPVC(15),PARLEN(15,5),PARRAD(15,5),FREQ(200)
      DIMENSION B(2,1),D(2,2),SIZE(200),SIZEDB(200),ANGLE(200),FBEL(15),
     1COMPLY(15),AKBEL(15),BSIGN(10),DAMPER(15),SPRINGK(15)
      DIMENSION DD(2,2,15),CC(2,1,15),BB(2,1,15),RADSEC(200),AREA(15)
      COMMON PI,RADIUS,OMEGA,ENU,ETA,EL,CO,RHOO,THERMK,RBUB,CPCV,PO,VISC
     1,FPVC,AKBPVC,AKCPVC,NPAR,PARRAD,PARLEN,BULKMOD,RHOLIQ,NGAS,GASMW
      COMMON GAMGAS,G,TO,PHI,COMPLY,NELAST,EWALL,HWALL,NELM,JBNUM,JTERM,
     1K,DD,CC,D,B,BB,CP,J,AREA,VMEAN,FBEL,AKBEL,BSIGN,DAMPER,SPRINGK
      COMMON G1,G2,RHOWALL,ZX,ZY
      CALL SPEED
      REYNOLD=VMEAN*2.*RADIUS(J)/(ENU*12.)
      RT=144.*(2.*ENU*0.0055*REYNOLD**0.85)/(RADIUS(J)**2)
      Z1=(OMEGA*EL(J)*ETA)/CO
      Z2=CSQRT((1.,0.)+RT/(OMEGA*ETA))
      XI=SQRT(OMEGA/ENU)*CSQRT(-ETA)
      ARG=XI*RADIUS(J)/12.
      CALL J1ORJ0(ARG,RJ)
      GAMMA=ETA*OMEGA*EL(J)/(CO*CSQRT((1.,0.)-2.*RJ/ARG))+REAL(Z1*Z2)
      ZC=RHOO*CO/(CSQRT((1.,0.)-2.*RJ/ARG))
      COSHG=(CEXP(GAMMA)+CEXP(-GAMMA))/2.
      SINHG=(CEXP(GAMMA)-CEXP(-GAMMA))/2.
      DD(1,1,J)=COSHG
      DD(1,2,J)=-ZC*SINHG/AREA(J)
      DD(2,1,J)=-AREA(J)*SINHG/ZC
      DD(2,2,J)=COSHG
      CC(1,1,J)=ZC*SINHG
      CC(2,1,J)=AREA(J)*((1.,0.)-COSHG)
      RETURN
      END
```

```
SUBROUTINE SIX
THIS SUBROUTINE CALCULATES THE ELEMENTS OF THE TRANSFER MATRIX FOR
AN ARBITRARY NUMBER OF LINES IN PARALLEL ALL OF WHICH EMANATE FROM
AND CONVERGE ON COMMON INPUT-OUTPUT POINTS.
      COMPLEX ETA,ENUM,DENOM,TRANS,B,D,XI,ARG,RJ,GAMMA,ZC,COSHG,SINHG,DD
     1,CC,TCOTH,TCSCH,BB,Z1,Z2,X1,X2,X3,X4,QUADRAT,ALPHAP,BETAP,ALPHADP,
     2BETADP,GOFS,SLCW,COSHCW,SINHCW,COEFF,ALPHA1,ALPHA2
      COMPLEX ZSTRUCT,ALPHA,BETA
      DIMENSION ITYPE(15),JTERM(15),K(15,15),EL(15),RADIUS(15),RBUB(15),
     1FPVC(15),AKBPVC(15),AKCPVC(15),PARLEN(15,5),PARRAD(15,5),FREQ(200)
      DIMENSION B(2,1),D(2,2),SIZE(200),SIZEDB(200),ANGLE(200),FBEL(15),
     1COMPLY(15),AKBEL(15),BSIGN(10),DAMPER(15),SPRINGK(15)
      DIMENSION DD(2,2,15),CC(2,1,15),BB(2,1,15),RADSEC(200),AREA(15)
      COMMON PI,RADIUS,OMEGA,ENU,ETA,EL,CO,RHOO,THERMK,RBUB,CPCV,PO,VISC
     1,FPVC,AKBPVC,AKCPVC,NPAR,PARRAD,PARLEN,BULKMOD,RHOLIQ,NGAS,GASMW
      COMMON GAMGAS,G,TO,PHI,COMPLY,NELAST,EWALL,HWALL,NELM,JBNUM,JTERM,
     1K,DD,CC,D,B,BB,CP,J,AREA,VMEAN,FBEL,AKBEL,BSIGN,DAMPER,SPRINGK
      COMMON G1,G2,RHOWALL,ZX,ZY
      DO 5 I=1,NPAR
      CALL SPEED
      CO=CO/SQRT(1.+BULKMOD*2.*PARRAD(J,I)/(144.*EWALL*HWALL))
      SQFT=PI*PARRAD(J,I)**2/144.
      XI=SQRT(OMEGA/ENU)*CSQRT(-ETA)
      ARG=XI*PARRAD(J,I)/12.
      CALL J1ORJO(ARG,RJ)
      GAMMA=ETA*OMEGA*PARLEN(J,I)/(CO*CSQRT((1.,0.)-2.*RJ/ARG))
      ZC=RHOO*CO/(CSQRT((1.,0.)-2.*RJ/ARG))
      COSHG=(CEXP(GAMMA)+CEXP(-GAMMA))/2.
      SINHG=(CEXP(GAMMA)-CEXP(-GAMMA))/2.
      TCOTH=TCOTH+SQFT*COSHG/(SINHG*ZC)
    5 TCSCH=TCSCH+SQFT/(ZC*SINHG)
      DD(1,1,J)=TCOTH/TCSCH
      DD(1,2,J)=-1./TCSCH
      DD(2,1,J)=TCSCH-TCOTH**2/TCSCH
      DD(2,2,J)=TCOTH/TCSCH
      RETURN
      END
```

```
SUBROUTINE SEVEN
THIS SUBROUTINE CALCULATES THE ELEMENTS OF THE TRANSFER MATRIX FOR
A BELLOWS WITH A LUMPED COMPLIANCE REPRESENTING TRAPPED GAS UNDER
THE LINER PLUS A PERIODIC VOLUMETRIC CHANGE DUE TO RELATIVE MOTION
OF THE ENDS OF THE BELLOWS
COMPLEX ETA,ENUM,DENOM,TRANS,B,D,XI,ARG,RJ,GAMMA,ZC,COSHG,SINHG,DD
1,CC,TCOTH,TCSCH,BB,Z1,Z2,X1,X2,X3,X4,QUADRAT,ALPHAP,BETAP,ALPHADP,
2BETADP,GOFS,SLCW,COSHCW,SINHCW,COEFF,ALPHA1,ALPHA2
COMPLEX ZSTRUCT,ALPHA,BETA
DIMENSION ITYPE(15),JTERM(15),K(15,15),EL(15),RADIUS(15),RBUB(15),
1FPVC(15),AKBPVC(15),AKCPVC(15),PARLEN(15,5),PARRAD(15,5),FREQ(200)
DIMENSION B(2,1),D(2,2),SIZE(200),SIZEDB(200),ANGLE(200),FBEL(15),
1COMPLY(15),AKBEL(15),BSIGN(10),DAMPER(15),SPRINGK(15)
DIMENSION DD(2,2,15),CC(2,1,15),BB(2,1,15),RADSEC(200),AREA(15)
COMMON PI,RADIUS,OMEGA,ENU,ETA,EL,CO,RHOO,THERMK,RBUB,CPCV,PO,VISC
1,FPVC,AKBPVC,AKCPVC,NPAR,PARRAD,PARLEN,BULKMOD,RHOLIQ,NGAS,GASMW
COMMON GAMGAS,G,TO,PHI,COMPLY,NELAST,EWALL,HWALL,NELM,JBNUM,JTERM,
1K,DD,CC,D,B,BB,CP,J,AREA,VMEAN,FBEL,AKBEL,BSIGN,DAMPER,SPRINGK
COMMON G1,G2,RHOWALL,ZX,ZY
FRICT=FBEL(J)
C=COMPLY(J)
AKB=AKBEL(J)
DD(1,1,J)=FRICT
DD(1,2,J)=(0.,0.)
DD(2,1,J)=-C*ETA*OMEGA
DD(2,2,J)=(1.,0.)
CC(1,1,J)=(0.,0.)
CC(2,1,J)=AKB
RETURN
END
```

```
SUBROUTINE EIGHT
THIS SUBROUTINE CALCULATES THE ELEMENTS OF THE TRANSFER MATRICES
FOR THE AXIAL MOTION OF A VERTICAL LINE WITH MOUNTING STIFFNESS
ON THE TWO ADJACENT HORIZONTAL LINES. THE TWO STIFFNESS TERMS ARE
LUMPED INTO ONE EFFECTIVE SPRING IN PARALLEL WITH ONE EFFECTIVE
VISCOUS DAMPER. THE FORCING FUNCTION IS AN ACCELERATION APPLIED
TO THE SPRING-DAMPER SUPPORT PLUS A PASSIVE INERTIAL LOADING
COMPLEX ETA,ENUM,DENOM,TRANS,B,D,XI,ARG,RJ,GAMMA,ZC,COSHG,SINHG,DD
1,CC,TCOTH,TCSCH,BB,Z1,Z2,X1,X2,X3,X4,QUADRAT,ALPHAP,BETAP,ALPHADP,
2BETADP,GOFS,SLCW,COSHCW,SINHCW,COEFF,ALPHA1,ALPHA2
COMPLEX ZSTRUCT,ALPHA,BETA
DIMENSION ITYPE(15),JTERM(15),K(15,15),EL(15),RADIUS(15),RBUB(15),
1FPVC(15),AKBPVC(15),AKCPVC(15),PARLEN(15,5),PARRAD(15,5),FREQ(200)
DIMENSION B(2,1),D(2,2),SIZE(200),SIZEDB(200),ANGLE(200),FBEL(15),
1COMPLY(15),AKBEL(15),BSIGN(10),DAMPER(15),SPRINGK(15)
DIMENSION DD(2,2,15),CC(2,1,15),BB(2,1,15),RADSEC(200),AREA(15)
COMMON PI,RADIUS,OMEGA,ENU,ETA,EL,CO,RHOO,THERMK,RBUB,CPCV,PO,VISC
1,FPVC,AKBPVC,AKCPVC,NPAR,PARRAD,PARLEN,BULKMOD,RHOLIQ,NGAS,GASMW
COMMON GAMGAS,G,TO,PHI,COMPLY,NELAST,EWALL,HWALL,NELM,JBNUM,JTERM,
1K,DD,CC,D,B,BB,CP,J,AREA,VMEAN,FBEL,AKBEL,BSIGN,DAMPER,SPRINGK
COMMON G1,G2,RHOWALL,ZX,ZY
CALL SPEED
REYNOLD=VMEAN*2.*RADIUS(J)/(ENU*12.)
RT=144.*(2.*ENU*0.0055*REYNOLD**0.85)/(RADIUS(J)**2)
Z1=(OMEGA*EL(J)*ETA)/CO
Z2=CSQRT((1.,0.)+RT/(OMEGA*ETA))
XI=SQRT(OMEGA/ENU)*CSQRT(-ETA)
ARG=XI*RADIUS(J)/12.
CALL J1ORJ0(ARG,RJ)
GAMMA=ETA*OMEGA*EL(J)/(CO*CSQRT((1.,0.)-2.*RJ/ARG))+REAL(Z1*Z2)
ZC=RHOO*CO/(CSQRT((1.,0.)-2.*RJ/ARG))
COSHG=(CEXP(GAMMA)+CEXP(-GAMMA))/2.
SINHG=(CEXP(GAMMA)-CEXP(-GAMMA))/2.
AMASS=RHOO*(AREA(J-1)*EL(J-1)+AREA(J+1)*EL(J+1))
QUADRAT=-AMASS*OMEGA**2+ETA*OMEGA*DAMPER(J)+SPRINGK(J)
ALPHAP=(ETA*OMEGA*DAMPER(J)+SPRINGK(J))*ZC*SINHG/(QUADRAT*ETA*OMEG
1A)
BETAP=AREA(J)*ETA*OMEGA*ZC*SINHG/QUADRAT
ALPHADP=(ETA*OMEGA*DAMPER(J)+SPRINGK(J))*AREA(J)*((1.,0.)-COSHG)/(
1ETA*OMEGA*QUADRAT)
BETADP=(AREA(J)**2)*ETA*OMEGA*((1.,0.)-COSHG)/QUADRAT
DD(1,1,J)=(COSHG+BETAP)/(1.+BETAP)
DD(1,2,J)=-ZC*SINHG/(AREA(J)*(1.+BETAP))
DD(2,1,J)=-AREA(J)*SINHG/ZC+BETADP*((1.,0.)-COSHG)/(1.+BETAP)
DD(2,2,J)=COSHG+BETADP*ZC*SINHG/(AREA(J)*(1.+BETAP))
CC(1,1,J)=ALPHAP/(1.+BETAP)
CC(2,1,J)=ALPHADP/(1.+BETAP)
RETURN
END
```

```
      SUBROUTINE NINE
      THIS SUBROUTINE CALCULATES THE ELEMENTS OF THE TRANSFER MATRIX
      FOR A LINE WITH FORCED CHANGES IN LINE LENGTH
      COMPLEX ETA,ENUM,DENOM,TRANS,B,D,XI,ARG,RJ,GAMMA,ZC,COSHG,SINHG,DD
     1,CC,TCOTH,TCSCH,BB,Z1,Z2,X1,X2,X3,X4,QUADRAT,ALPHAP,BETAP,ALPHADP,
     2BETADP,GOFS,SLCW,COSHCW,SINHCW,COEFF,ALPHA1,ALPHA2
      COMPLEX ZSTRUCT,ALPHA,BETA
      DIMENSION ITYPE(15),JTERM(15),K(15,15),EL(15),RADIUS(15),RBUB(15),
     1FPVC(15),AKBPVC(15),AKCPVC(15),PARLEN(15,5),PARRAD(15,5),FREQ(200)
      DIMENSION B(2,1),D(2,2),SIZE(200),SIZEDB(200),ANGLE(200),FBEL(15),
     1COMPLY(15),AKBEL(15),BSIGN(10),DAMPER(15),SPRINGK(15)
      DIMENSION DD(2,2,15),CC(2,1,15),BB(2,1,15),RADSEC(200),AREA(15)
      COMMON PI,RADIUS,OMEGA,ENU,ETA,EL,CO,RHOO,THERMK,RBUB,CPCV,PO,VISC
     1,FPVC,AKBPVC,AKCPVC,NPAR,PARRAD,PARLEN,BULKMOD,RHOLIQ,NGAS,GASMW
      COMMON GAMGAS,G,TO,PHI,COMPLY,NELAST,EWALL,HWALL,NELM,JBNUM,JTERM,
     1K,DD,CC,D,B,BB,CP,J,AREA,VMEAN,FBEL,AKBEL,BSIGN,DAMPER,SPRINGK
      COMMON G1,G2,RHOWALL,ZX,ZY
      GOFS=G1+G2*ETA
      CW=SQRT((EWALL*G)/(RHOWALL*12.))
      CALL SPEED
      REYNOLD=VMEAN*2.*RADIUS(J)/(ENU*12.)
      RT=144.*(2.*ENU*0.0055*REYNOLD**0.85)/(RADIUS(J)**2)
      Z1=(OMEGA*EL(J)*ETA)/CO
      Z2=CSQRT((1.,0.)+RT/(OMEGA*ETA))
      XI=SQRT(OMEGA/ENU)*CSQRT(-ETA)
      ARG=XI*RADIUS(J)/12.
      CALL J1ORJ0(ARG,RJ)
      GAMMA=ETA*OMEGA*EL(J)/(CO*CSQRT((1.,0.)-2.*RJ/ARG))+REAL(Z1*Z2)
      ZC=RHOO*CO/(CSQRT((1.,0.)-2.*RJ/ARG))
      COSHG=(CEXP(GAMMA)+CEXP(-GAMMA))/2.
      SINHG=(CEXP(GAMMA)-CEXP(-GAMMA))/2.
      DD(1,1,J)=COSHG
      DD(1,2,J)=-ZC*SINHG/AREA(J)
      DD(2,1,J)=-AREA(J)*SINHG/ZC
      DD(2,2,J)=COSHG
      SLCW=ETA*OMEGA*EL(J)/CW
      COSHCW=(CEXP(SLCW)+CEXP(-SLCW))/2.
      SINHCW=(CEXP(SLCW)-CEXP(-SLCW))/2.
      COEFF=(-OMEGA**2/CO**2-(GAMMA/EL(J))**2)/(-OMEGA**2/CW**2-(GAMMA/E
     1L(J))**2)
      ALPHA1=(RHOO*CO**2/(ETA*OMEGA))*((ETA*OMEGA*SINHCW/CW-GAMMA*SINHG/
     1EL(J))+(GOFS-COSHCW)*(COSHCW-COSHG)*ETA*OMEGA/(CW*SINHCW))
      ALPHA2=-((COSHCW-COSHG)+(GOFS-COSHCW)*(SINHCW-ETA*OMEGA*EL(J)*SINH
     1G/(CW*GAMMA))/SINHCW)
      CC(1,1,J)=COEFF*ALPHA1
      CC(2,1,J)=COEFF*ALPHA2*AREA(J)
      RETURN
      END
```

```
SUBROUTINE TEN
THIS SUBROUTINE CALCULATES THE ELEMENTS OF THE TRANSFER MATRIX
FOR THE AXIAL MOTION OF A VERTICAL LINE WITH MOUNTING STIFFNESS.
THE STIFFNESS IS REPRESENTED BY THE IMPEDANCE PRESENTED TO THE
LINE BY THE VEHICLE STRUCTURE.
THIS SUBROUTINE CAN BE USED ONLY WHEN ANOTHER SOURCE OF EXCITATION
IS PRESENT IN THE FEEDLINE, I.E. PULSER OR VERTICAL LINE VELOCITY
EXCITATION. THE FUNCTIONAL FORM OF THE STRUCTURAL IMPEDANCE IS
THAT OF AN EQUIVALENT SPRING AND DASHPOT IN PARALLEL.
ZX AND ZY ARE THE REAL AND IMAGINARY PARTS OF ZSTRUCT.
   COMPLEX ETA,ENUM,DENOM,TRANS,B,D,XI,ARG,RJ,GAMMA,ZC,COSHG,SINHG,DD
  1,CC,TCOTH,TCSCH,BB,Z1,Z2,X1,X2,X3,X4,QUADRAT,ALPHAP,BETAP,ALPHADP,
  2BETADP,GOFS,SLCW,COSHCW,SINHCW,COEFF,ALPHA1,ALPHA2
   COMPLEX ZSTRUCT,ALPHA,BETA
   DIMENSION ITYPE(15),JTERM(15),K(15,15),EL(15),RADIUS(15),RBUB(15),
  1FPVC(15),AKBPVC(15),AKCPVC(15),PARLEN(15,5),PARRAD(15,5),FREQ(200)
   DIMENSION B(2,1),D(2,2),SIZE(200),SIZEDB(200),ANGLE(200),FBEL(15),
  1COMPLY(15),AKBEL(15),BSIGN(10),DAMPER(15),SPRINGK(15)
   DIMENSION DD(2,2,15),CC(2,1,15),BB(2,1,15),RADSEC(200),AREA(15)
   COMMON PI,RADIUS,OMEGA,ENU,ETA,EL,CO,RHOO,THERMK,RBUB,CPCV,PO,VISC
  1,FPVC,AKBPVC,AKCPVC,NPAR,PARRAD,PARLEN,BULKMOD,RHOLIQ,NGAS,GASMW
   COMMON GAMGAS,G,TO,PHI,COMPLY,NELAST,EWALL,HWALL,NELM,JBNUM,JTERM,
  1K,DD,CC,D,B,BB,CP,J,AREA,VMEAN,FBEL,AKBEL,BSIGN,DAMPER,SPRINGK
   COMMON G1,G2,RHOWALL,ZX,ZY
   CALL SPEED
   REYNOLD=VMEAN*2.*RADIUS(J)/(ENU*12.)
   RT=144.*(2.*ENU*0.0055*REYNOLD**0.85)/(RADIUS(J)**2)
   Z1=(OMEGA*EL(J)*ETA)/CO
   Z2=CSQRT((1.,0.)+RT/(OMEGA*ETA))
   XI=SQRT(OMEGA/ENU)*CSQRT(-ETA)
   ARG=XI*RADIUS(J)/12.
   CALL J1ORJ0(ARG,RJ)
   GAMMA=ETA*OMEGA*EL(J)/(CO*CSQRT((1.,0.)-2.*RJ/ARG))+REAL(Z1*Z2)
   ZC=RHOO*CO/(CSQRT((1.,0.)-2.*RJ/ARG))
   COSHG=(CEXP(GAMMA)+CEXP(-GAMMA))/2.
   SINHG=(CEXP(GAMMA)-CEXP(-GAMMA))/2.
   AMASS=RHOO*(AREA(J-1)*EL(J-1)+AREA(J+1)*EL(J+1))
   ZSTRUCT=ZX-ETA*ZY/OMEGA
   ALPHA=AREA(J)*ZC*SINHG/(ZSTRUCT+AMASS*ETA*OMEGA)
   BETA=(1.-COSHG)*(AREA(J)**2)/(ZSTRUCT+AMASS*ETA*OMEGA)
   DD(1,1,J)=(COSHG+ALPHA)/(1.+ALPHA)
   DD(1,2,J)=-ZC*SINHG/(AREA(J)*(1.+ALPHA))
   DD(2,1,J)=-AREA(J)*SINHG/ZC+BETA*(1.-COSHG)/(1.+ALPHA)
   DD(2,2,J)=COSHG+ZC*SINHG*BETA/(AREA(J)*(1.+ALPHA))
   RETURN
   END
```

```
      SUBROUTINE ELEVEN
C     THIS SUBROUTINE CALCULATES THE ELEMENTS OF THE TRANSFER
C     MATRIX FOR A COMPLEX SIDE BRANCH. THIS MODEL ASSUMES A
C     LAMINAR FLOW IN THE SIDE BRANCH.
      COMPLEX ETA,ENUM,DENOM,TRANS,B,D,XI,ARG,RJ,GAMMA,ZC,COSHG,SINHG,DD
     1,CC,TCOTH,TCSCH,BB,Z1,Z2,X1,X2,X3,X4,QUADRAT,ALPHAP,BETAP,ALPHADP,
     2BETADP,GOFS,SLCW,COSHCW,SINHCW,COEFF,ALPHA1,ALPHA2
      COMPLEX ZSTRUCT,ALPHA,BETA
      DIMENSION ITYPE(15),JTERM(15),K(15,15),EL(15),RADIUS(15),RBUB(15),
     1FPVC(15),AKBPVC(15),AKCPVC(15),PARLEN(15,5),PARRAD(15,5),FREQ(200)
      DIMENSION B(2,1),D(2,2),SIZE(200),SIZEDB(200),ANGLE(200),FBEL(15),
     1COMPLY(15),AKBEL(15),BSIGN(10),DAMPER(15),SPRINGK(15)
      DIMENSION DD(2,2,15),CC(2,1,15),BB(2,1,15),RADSEC(200),AREA(15)
      COMMON PI,RADIUS,OMEGA,ENU,ETA,EL,CO,RHOO,THERMK,RBUB,CPCV,PO,VISC
     1,FPVC,AKBPVC,AKCPVC,NPAR,PARRAD,PARLEN,BULKMOD,RHOLIQ,NGAS,GASMW
      COMMON GAMGAS,G,TO,PHI,COMPLY,NELAST,EWALL,HWALL,NELM,JBNUM,JTERM,
     1K,DD,CC,D,B,BB,CP,J,AREA,VMEAN,FBEL,AKBEL,BSIGN,DAMPER,SPRINGK
      COMMON G1,G2,RHOWALL,ZX,ZY
      COMMON BRCOMP,BRL,BRDIAM
      COMPLEX S
      S=ETA*OMEGA
   10 CALL SPEED
      AREAB=(PI/4.)*(BRDIAM/12.)**2
      BRI=RHOO*BRL/AREAB
      BRR=128.*VISC*BRL/(PI*(BRDIAM/12.)**4.)
      DD(1,1,J)=(1.,0.)
      DD(1,2,J)=(0.,0.)
      DD(2,1,J)=-S*BRCOMP/(BRI*BRCOMP*S**2+BRR*BRCOMP*S +1.)
      DD(2,2,J)=(1.,0.)
      RETURN
      END
```

```fortran
      SUBROUTINE SPEED
C     THIS SUBROUTINE CALCULATES THE SPEED OF SOUND FOR THE FLUID IN THE
C     FEEDLINE.  THIS FLUID MAY BE A LIQUID OR A HOMOGENEOUS MIXTURE OF
C     A LIQUID AND AN ULLAGE GAS
      COMPLEX ETA,ENUM,DENOM,TRANS,B,D,XI,ARG,RJ,GAMMA,ZC,COSHG,SINHG,DD
     1,CC,TCOTH,TCSCH,BB,Z1,Z2,X1,X2,X3,X4,QUADRAT,ALPHAP,BETAP,ALPHADP,
     2BETADP,GOFS,SLCW,COSHCW,SINHCW,COEFF,ALPHA1,ALPHA2
      COMPLEX ZSTRUCT,ALPHA,BETA
      DIMENSION ITYPE(15),JTERM(15),K(15,15),EL(15),RADIUS(15),RBUB(15),
     1FPVC(15),AKBPVC(15),AKCPVC(15),PARLEN(15,5),PARRAD(15,5),FREQ(200)
      DIMENSION B(2,1),D(2,2),SIZE(200),SIZEDB(200),ANGLE(200),FBEL(15),
     1COMPLY(15),AKBEL(15),BSIGN(10),DAMPER(15),SPRINGK(15)
      DIMENSION DD(2,2,15),CC(2,1,15),BB(2,1,15),RADSEC(200),AREA(15)
      COMMON PI,RADIUS,OMEGA,ENU,ETA,EL,CO,RHOO,THERMK,RBUB,CPCV,PO,VISC
     1,FPVC,AKBPVC,AKCPVC,NPAR,PARRAD,PARLEN,BULKMOD,RHOLIQ,NGAS,GASMW
      COMMON GAMGAS,G,TO,PHI,COMPLY,NELAST,EWALL,HWALL,NELM,JBNUM,JTERM,
     1K,DD,CC,D,B,BB,CP,J,AREA,VMEAN,FBEL,AKBEL,BSIGN,DAMPER,SPRINGK
      COMMON G1,G2,RHOWALL,ZX,ZY
      CLIQUID=SQRT(BULKMOD/RHOLIQ)
      IF(NGAS.EQ.1)10,20
   10 RHOGAS=144.*PO*GASMW/(1545.*(TO+460.)*G)
      CGAS=SQRT(GAMGAS*G*1545.*(TO+460.)/GASMW)
      E1=RHOGAS+PHI*RHOLIQ
      E2=RHOGAS/(RHOLIQ*CLIQUID**2*E1)+(PHI*RHOLIQ)/(E1*RHOGAS*CGAS**2)
      E3=(1.+PHI)*RHOGAS*RHOLIQ
      CO=SQRT(E1/(E2*E3))
      RHOO=E3/E1
      ENU=VISC/RHOO
      GO TO 30
   20 CO=CLIQUID
      RHOO=RHOLIQ
      ENU=VISC/RHOO
   30 IF(NELAST.EQ.1)40,50
   40 CO=CO/SQRT(1.+CO**2*RHOO*2.*(RADIUS(J)+HWALL)/(144.*EWALL*HWALL))
   50 RETURN
      END
```

```
      SUBROUTINE DMAT
C THIS SUBROUTINE CALCULATES MATRIX D IN THE EXPRESSION P=DQ+VB
      COMPLEX ETA,ENUM,DENOM,TRANS,B,D,XI,ARG,RJ,GAMMA,ZC,COSHG,SINHG,DD
     1,CC,TCOTH,TCSCH,BB,Z1,Z2,X1,X2,X3,X4,QUADRAT,ALPHAP,BETAP,ALPHADP,
     2BETADP,GOFS,SLCW,COSHCW,SINHCW,COEFF,ALPHA1,ALPHA2
      COMPLEX ZSTRUCT,ALPHA,BETA
      DIMENSION ITYPE(15),JTERM(15),K(15,15),EL(15),RADIUS(15),RBUB(15),
     1FPVC(15),AKBPVC(15),AKCPVC(15),PARLEN(15,5),PARRAD(15,5),FREQ(200)
      DIMENSION B(2,1),D(2,2),SIZE(200),SIZEDB(200),ANGLE(200),FBEL(15),
     1COMPLY(15),AKBEL(15),BSIGN(10),DAMPER(15),SPRINGK(15)
      DIMENSION DD(2,2,15),CC(2,1,15),BB(2,1,15),RADSEC(200),AREA(15)
      COMMON PI,RADIUS,OMEGA,ENU,ETA,EL,CO,RHOO,THERMK,RBUB,CPCV,PO,VISC
     1,FPVC,AKBPVC,AKCPVC,NPAR,PARRAD,PARLEN,BULKMOD,RHOLIQ,NGAS,GASMW
      COMMON GAMGAS,G,TO,PHI,COMPLY,NELAST,EWALL,HWALL,NELM,JBNUM,JTERM,
     1K,DD,CC,D,B,BB,CP,J,AREA,VMEAN,FBEL,AKBEL,BSIGN,DAMPER,SPRINGK
      COMMON G1,G2,RHOWALL,ZX,ZY
      DO 10 M=1,2
      DO 10 N=1,2
   10 D(M,N)=DD(M,N,1)
      IF(NELM-1)50,20,30
   20 RETURN
   30 DO 40 J=2,NELM
      X1=DD(1,1,J)*D(1,1)+DD(1,2,J)*D(2,1)
      X2=DD(1,1,J)*D(1,2)+DD(1,2,J)*D(2,2)
      X3=DD(2,1,J)*D(1,1)+DD(2,2,J)*D(2,1)
      X4=DD(2,1,J)*D(1,2)+DD(2,2,J)*D(2,2)
      D(1,1)=X1
      D(1,2)=X2
      D(2,1)=X3
   40 D(2,2)=X4
      RETURN
   50 PRINT 60
      CALL EXTT
   60 FORMAT(28HOERROR IN NELM SPECIFICATION)
      END
```

```
      SUBROUTINE BMAT
C THIS SUBROUTINE CALCULATES MATRIX B IN THE EXPRESSION P=DQ+VB
      COMPLEX ETA,ENUM,DENOM,TRANS,B,D,XI,ARG,RJ,GAMMA,ZC,COSHG,SINHG,DD
     1,CC,TCOTH,TCSCH,BB,Z1,Z2,X1,X2,X3,X4,QUADRAT,ALPHAP,BETAP,ALPHADP,
     2BETADP,GOFS,SLCW,COSHCW,SINHCW,COEFF,ALPHA1,ALPHA2
      COMPLEX ZSTRUCT,ALPHA,BETA
      DIMENSION ITYPE(15),JTERM(15),K(15,15),EL(15),RADIUS(15),RBUB(15),
     1FPVC(15),AKBPVC(15),AKCPVC(15),PARLEN(15,5),PARRAD(15,5),FREQ(200)
      DIMENSION B(2,1),D(2,2),SIZE(200),SIZEDB(200),ANGLE(200),FBEL(15),
     1COMPLY(15),AKBEL(15),BSIGN(10),DAMPER(15),SPRINGK(15)
      DIMENSION DD(2,2,15),CC(2,1,15),BB(2,1,15),RADSEC(200),AREA(15)
      COMMON P1,RADIUS,OMEGA,ENU,ETA,EL,CO,RHOO,THERMK,RBUB,CPCV,PO,VISC
     1,FPVC,AKBPVC,AKCPVC,NPAR,PARRAD,PARLEN,BULKMOD,RHOLIQ,NGAS,GASMW
      COMMON GAMGAS,G,TO,PHI,COMPLY,NELAST,EWALL,HWALL,NELM,JBNUM,JTERM,
     1K,DD,CC,D,B,BB,CP,J,AREA,VMEAN,FBEL,AKBEL,BSIGN,DAMPER,SPRINGK
      COMMON G1,G2,RHOWALL,ZX,ZY
      DO 100 I=1,JBNUM
      KOUNT=JTERM(I)
      L=K(I,KOUNT)
      DO 100 J=1,KOUNT
      IF(J-1)5,5,15
    5 DO 10 M=1,2
   10 BB(M,1,I)=CC(M,1,L)
      GO TO 100
   15 L=K(I,KOUNT-J+1)
      X1=DD(1,1,L)*BB(1,1,I)+DD(1,2,L)*BB(2,1,I)
      X2=DD(2,1,L)*BB(1,1,I)+DD(2,2,L)*BB(2,1,I)
      BB(1,1,I)=X1
      BB(2,1,I)=X2
  100 CONTINUE
      B(1,1)=BSIGN(1)*BB(1,1,1)
      B(2,1)=BSIGN(1)*BB(2,1,1)
  110 DO 200 M=1,2
      DO 200 I=2,JBNUM
  200 B(M,1)=B(M,1)+BSIGN(I)*BB(M,1,I)
  210 RETURN
      END
```

```
      SUBROUTINE J1ORJO(Z,RJ)
      CALCULATION OF JO(Z) AND J1(Z)  Z-COMPLEX
      COMPLEX Z,J1,JO,TERMO,TERM1,Z1,Z2,PO,QO,P1,Q1,PHO,PH1,FZ1,FZ2,RJ
      X=REAL(Z)
      Y=AIMAG(Z)
      R=CABS(Z)
      IF(R-18.)100,100,110
100   TERM1=Z/2.
      J1=Z/2.
      JO=(1.,0.)
      TERMO=(1.,0.)
      A=1.
      AM=15.+R
101   TERMO=TERMO*(-(Z/2.)**2)/A**2
      JO=JO+TERMO
      TERM1=TERM1*(-(Z/2.)**2)/((A+1.)*A)
      J1=J1+TERM1
      A=A+1.
      IF(A-AM)101,101,115
110   IF(X)111,112,112
111   Z1=-Z
      GO TO 113
112   Z1=Z
113   PI=3.1415926
      Z2=8.*Z1
      IF(CABS(Z2)-5000.)120,120,121
120   PO=(1.,0.)-4.5/Z2**2+3675./(8.*Z2**4)
      QO=-1./Z2+37.5/Z2**3-59535./(8.*Z2**5)
      P1=(1.,0.)+7.5/Z2**2-4725./(8.*Z2**4)
      Q1=3./Z2-52.5/Z2**3+72765./(8.*Z2**5)
      GO TO 122
121   PO=(1.,0.)-4.5/Z2**2
      QO=-1./Z2
      P1=(1.,0.)+7.5/Z2**2
      Q1=3./Z2
122   PHO=Z1-PI/4.
      PH1=Z1-.75*PI
      FZ1=2./(PI*Z1)
      FZ2=CSQRT(FZ1)
      AZ1=AIMAG(Z1)
      IF(ABS(AZ1)-50.)116,116,117
116   JO=FZ2*(PO*CCOS(PHO)-QO*CSIN(PHO))
      J1=FZ2*(P1*CCOS(PH1)-Q1*CSIN(PH1))
      IF(X)114,115,115
114   J1=-J1
115   RJ=J1/JO
      GO TO 119
117   SIN=Y/ABS(Y)
      RJ=(SIN*(0.,1.)*P1+Q1)/(PO-SIN*(0.,1.)*QO)
119   RETURN
      END
```

CARD 3	ITYPE (J), J = 1, NELM dimensionless	A sequence of dimensionless numbers that describes the type of elements in the line in the order in which they appear beginning with the element attached to the fuel tank outlet. See the first page of program listing for an expanded definition.
CARD 4	JTERM (J), J = 1, JBNUM dimensionless	The number of submatrices in B (J). For example, in Equation (125), JBNUM = 3, JTERM (1) = 2, JTERM (2) = 3 and JTERM (3) = 4.
CARD 5 6 · · · · 4 + BJNUM	K (J, M), dimensionless	An array that fixes the order of matrix multiplication in B(J). For example, in Equation (125), B(3) = $\underline{D}_5\underline{D}_4\underline{D}_3\underline{C}_2$. Then K(3,1) = 5, K(3,2) = 4, K(3,3) = 3 and K(3,4) = 2.
CARD (5 + JBNUM)	BSIGN (J), dimensionless	Floating point array that defines the algebraic sign preceding each B(J). Again in Equation (125), BSIGN(1) = +1.0, BSIGN(2) = -1.0 and BSIGN(3) = -1.0.
CARD (6 + JBNUM)	HERTZI, Hz	The initial frequency where response calculations begin.
	DELHZ1, Hz	Frequency step size for frequencies between HERTZI and F1LIM.
	F1LIM, Hz	Frequency break-point which defines the boundary between regions of different grid size.
	DELHZ2, Hz	Frequency step size for frequencies beyond F1LIM.
	HERTZF, Hz	The final frequency to be evaluated.

CARD (7 + JBNUM)	SIGN, dimensionless	Algebraic sign preceding the parameter K in Equation (121).
	TERMZ, lb-sec/ft^5	Terminal impedance of the line which reflects the combined effect of the turbopump-injector-engine combination. In its present form, TERMZ is a scalar resistance.
	RHOLIQ, lb-sec^2/ft^4	Liquid propellant density.
	THERMK, Btu/(hr-ft-$^\circ$R)	Thermal conductivity of the gas inside large bubbles.
	P0, psia	Mean propellant pressure.
	T0, $^\circ$F	Mean propellant temperature.
CARD (8 + JBNUM)	EWALL, lb/in.^{2}	Wall modulus of elasticity.
	HWALL, in.	Wall thickness.
	ZINPUT, lb-sec/ft^5	Scalar flow impedance at the propellant tank outlet.
	CPCV, dimensionless	The ratio of specific heats for the gas in the cavitation bubble at the propellant temperature.
	BULKMOD, lb/ft^2	Bulk modulus of the propellant.
	PHI, dimensionless	Vapor-liquid mass ratio for the bulk propellant flow.
CARD (9 + JBNUM)	VISC, lb-sec/ft^2	Propellant dynamic viscosity.
	GASMW, dimensionless	Molecular weight of dissolved vapor or ullage gas for use in speed of sound calculation.
	GAMGAS, dimensionless	Ratio of specific heats for the gas whose molecular weight is GASMW.

	CP, Btu/lb-°R	Specific heat at constant pressure for the gas in the cavitation bubble.
	VMEAN, ft/sec	Mean propellant feed velocity.

The sequence and number of the remaining input cards cannot be stated a priori since they depend on the component structure of the feedline. However, the input for each line component appears sequentially in the same order as the components in the line beginning with the component attached to the fuel outlet. Listed below are the inputs for each class of component.

Simple line:	EL, ft	Line length.
	RADIUS, in.	Line radius as measured to the inner surface.
Cavitation bubble:	RBUB, in.	Bubble radius.
	RADIUS, in.	Internal radius of the line surrounding the bubble.
Pressure-volume compensator:	FPVC, dimensionless	Friction factor expressed as the fraction of the inlet pressure remaining at the outlet.
	AKBPVC, ft^2 AKCPVC, ft^2	Volume change constants for compensator.
Side branch pulser:		No input required.
Line with velocity excitation:	EL, ft RADIUS, in.	Same as simple line. Same as simple line.
Parallel lines:	NPAR, dimensionless PARLEN, ft PARRAD, in.	The number of parallel lines. Line length. Line radius.
Bellows with relative motion:	FBEL, dimensionless COMPLY, ft^5/lb AKBEL, ft^2	Bellows friction factor, same definition as FPVC Compliance of bellows. Volume change constant. If there is no relative motion, AKBEL = 0.

Line with mounting stiffness (discrete parameter):	EL, ft	Line length.
	RADIUS, in.	Line radius.
	DAMPER, lb-sec/ft	Coefficient of viscous damping.
	SPRINGK,lb/ft	Spring constant.
Forced changes in line length:	EL, ft	Line length.
	RADIUS, in.	Line radius.
	G1, G2	Real and imaginary parts of G(s).
	RHOWALL, lb/in^3	Wall density.
Line with mounting stiffness (impedance technique):	EL, ft	Line length.
	RADIUS, in.	Line radius.
	ZX, ZY	Components of structural impedance.
Complex side branch:	BRL, ft	Branch line length.
	BRDIAM, in.	Branch radius.
	BRCOMP, ft^5/lb	Compliance of the complex side branch.

D. 4. Deck Structure for a Normal Compliation and Multiple Execution on the CDC 6400 Digital Computer

Deck structure for multiple production runs is shown on the following page.

The anticipated run time, core memory and output linage information indicated on the first two control cards are for illustration purposes only. Typically, the combined central processor/ print processor time for compilation, execution and listing of one run is approximately 25 seconds. In the case of production runs, time-line charges can be improved by inserting a NOLIST card in front of the PROGRAM CONTROL card which will delete the source program listing from the output.

6
7
8
9

DATA DECK # 2

DATA DECK # 1

7
8
9

SOURCE DECK

PROGRAM CONTROL (INPUT,
OUTPUT, TAPE 60*INPUT)

7
8
9

DMP.

EXIT.

LGO.

REDUCE.

SETINDF.

RUN (S , , , , , , 4000)

FREQY., T43, CM25000, P2, 4421
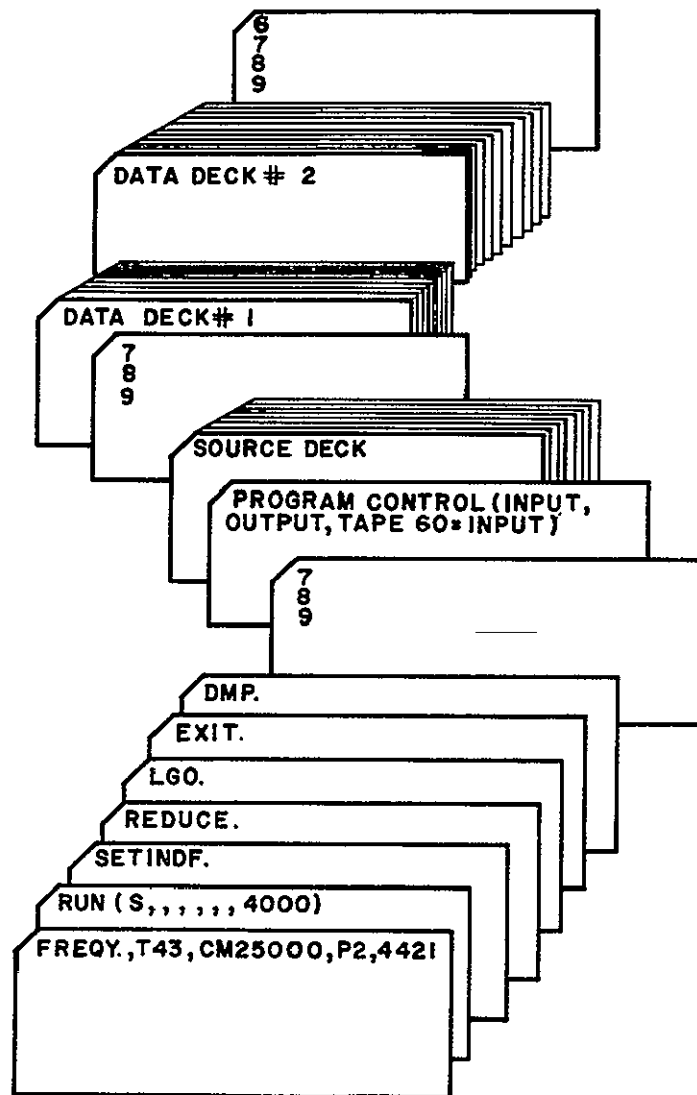
3450

H.5. <u>Computer Symbol List</u>

In order to facilitate program changes by the user, a correspondence list of the symbols used in the program is given below. The quantities on the left are the FORTRAN alphanumeric symbols in the program; on the right is the corresponding item from the analysis. Dummy variables, which are frequently used to facilitate programming of long equations, have been omitted.

TERMZ	--	Z_t	EL -- L
RHOLIQ	--	ρ_ℓ	RBUB -- R_o
(Mass density of propellant; liquid phase)			PARLEN --. L_P
THERMK	--	k	PARRAD -- r_P
PO	--	p_o	FBEL .-- $F(\rho V_x^2, G)_{BEL}$
TO	--	T_o	COMPLY -- C
EWALL	--	E_t	AKBEL -- $K_{B,BEL}$
HWALL	--	h	FPVC -- $F(\rho V_x^2, G)_{PVC}$
ZINPUT	--	Z_i	AKBPVC -- $K_{B,PVC}$
CPCV	--	C_p/C_v	ACKPVC -- $K_{C,PVC}$
BULKMOD	--	χ	DAMPER -- b
PHI	--	Φ	SPRINGK -- k
VISC	--	μ	OMEGA -- ω
GASMW	--	MW	ENU .-- ν
GAMGAS	--	γ	REYNOLD -- N_R
CP	--	C_P	RT -- R_t
VMEAN	--	v_o	ETA -- $(+i)$
RADIUS	--	r_o	XI -- ξ

J1ORJ0	--	J_1/J_0	RHOGAS	--	ρ_g
GAMMA	--	Γ	CGAS	--	c_g
ZC	--	Z_c	RHO0	--	ρ_0
COSHG	--	$\cosh \Gamma$	ENU	--	ν
SINHG	--	$\sinh \Gamma$	PR0	--	$\Phi_1 R_0$
AREA	--	A	DTHERM	--	D_1
AMASS	--	$m_1 + m_3$	BTHERM	--	b_{th}
ALPHAP	--	α'	BVIS	--	b_{VISC}
BETAP	--	β'	BRAD	--	b_{RAD}
ALPHADP	--	α''	POLY	--	η
BETADP	--	β''	VBUB	--	V_{BUB}
CW	--	c_w	SPRING	--	$\eta P_0/V_{BUB}$
GOFS	--	$G(s)$	ZSTRUCT	--	$Z_s = Z_x - iZ_y/\omega$
RHOWALL	--	ρ_t	AREAB	--	A_b
SLCW	--	sL/c_w	BRI	--	I
COSHCW	--	$\cosh(sL/c_w)$	BRCOMP	--	C
SINHCW	--	$\sinh(sL/c_w)$	BRR	--	R
ALPHA1	--	α_1	BRL	--	L_b
ALPHA2	--	α_2	BRDIAM	--	d_b
CLIQUID	--	c_ℓ			

D. 6.   Example Problems

This section contains five example problems which will acquaint the user with the mechanics of program setup and execution. The development of each problem follows the same general format: statement of the physical problem, generation of the system matrix equation, presentation of critical input data and a computer listing and graphical representation of the configuration response. In all cases, only a portion of the output is shown since the remaining calculations follow the same format through termination of execution.

Problem No. 1:

The first feedline example, shown in Figure D-1, consists of a rigid length of line, a sidebranch pulser and a cavitation bubble in series with the fuel tank and a scalar terminal impedance, R. The perturbation pressure at Station 1 is assumed to be negligible. This assumption is for illustration purposes only, since the computer program accepts an arbitrary scalar input impedance at Station 1. The physical distance between Stations 2 and 4 is assumed to be small compared to the total line length, L. It is required that the perturbation pressure at Station 4 be determined for oscillatory pulser inputs, Q_d. The first step is to set up the station numbers, component numbers and component matrix equations in the Laplace domain as indicated in the illustration. Note that the subscripts on pressure and flow perturbations correspond to a particular station number, whereas the subscripts on matrices $\underline{D}_i$ and $\underline{C}_i$ refer to a specific component number. Beginning with the matrix equation for component number 3, successive substitution of the remaining expressions yields the overall line equation:

$$\begin{bmatrix} P_4 \\ P_4/R \end{bmatrix} = \underline{D}_3\ \underline{D}_2\ \underline{D}_1 \begin{bmatrix} 0 \\ Q_1 \end{bmatrix} + Q_d(s)\ (+\underline{D}_3\ \underline{C}_2) \tag{D.1}$$

The fundamental operations involved in the derivation of this system equation are common to the setup of all problems, and the user is required to perform these steps in order to execute the program.

At this point, the user would make the following general observations regarding the program input:

(1)   NELM = 3   The number of components in the line.

(2)   NEXCITE = 4   Element number providing the excitation.

Station No.	Component No.	Component Matrix Equation

1

$$\begin{bmatrix} P_2 \\ Q_2 \end{bmatrix} = \underline{D}_1 \begin{bmatrix} Z_i \, Q_1 \\ Q_1 \end{bmatrix}$$

L = 30 ft.

①

2

②

$$\begin{bmatrix} P_3 \\ Q_3 \end{bmatrix} = \underline{D}_2 \begin{bmatrix} P_2 \\ Q_2 \end{bmatrix} + Q_d \, \underline{C}_2$$

③

3

4

$$\begin{bmatrix} P_4 \\ Q_4 \end{bmatrix} = \underline{D}_3 \begin{bmatrix} P_3 \\ Q_3 \end{bmatrix}$$

$$Q_4 = P_4 / R$$

3446

R
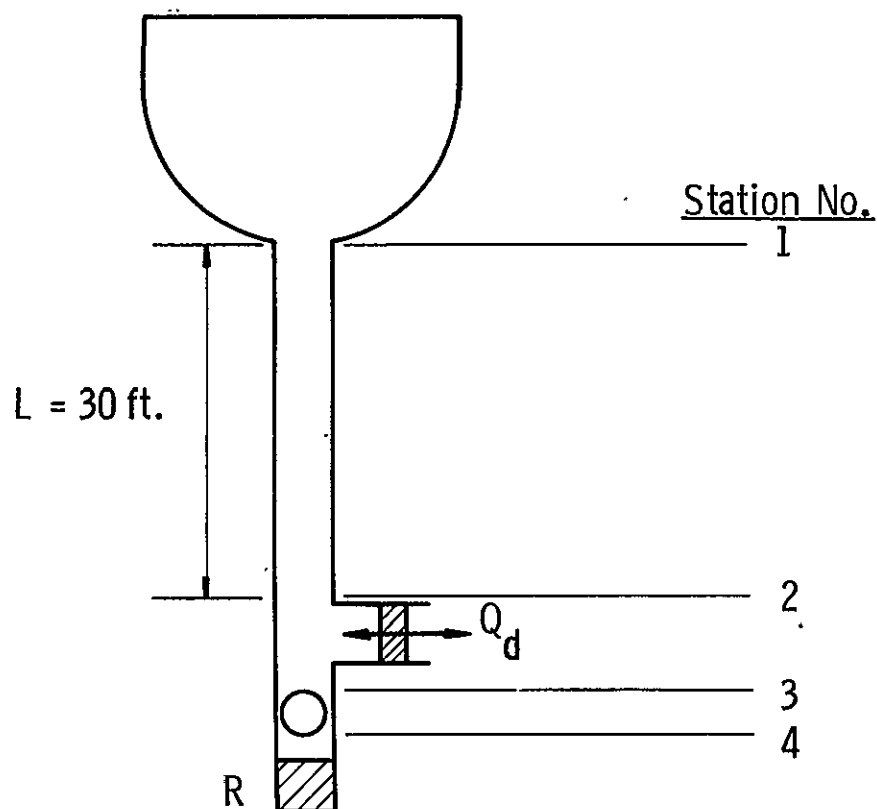
Mean Flow Velocity = 50 ft./sec.
Bubble Radius = 1.2 in.
Line Radius = 4.0 in.

Figure D-1. Line Model For Example Problem No. 1

(2) $B = \underline{D}_3 \, \underline{C}_2$ Therefore, JBNUM = 1

JTERM(1) = 2 (two sub-
matrices in $\underline{B}_1 = \underline{B}$)

K(1,1) = 3

K(1,2) = 2

(3) ITYPE (1) = 1 ITYPE(J) indicates the type of compo-
nent corresponding to component

ITYPE (2) = 4 number J. Refer to comment cards on
first page program listing.

ITYPE (3) = 2

(4) SIGN = +1.0 The algebraic sign preceding the exci-
tation, Q_d, in Equation (D.1).

(5) BSIGN (J) = 1.0, J = JBUM = 1. BSIGN (J) is the algebraic
sign preceding the Jth term in $\underline{B} = \underline{B}_1 + \underline{B}_2 + \ldots$. The
usefulness of this input will be demonstrated later in a
more complex example.

In this example, we will assume that the propellant does not contain
any dissolved gases, and the calculated speed of sound in the pro-
pellant will reflect wall elasticity effects.

Using typical values for the physical parameters associated
with the line and the propellant, a complete input package would take
the form shown in the following listing. At this point, the reader
should thoroughly review the setup instructions listed at the begin-
ning of the PROGRAM CONTROL. These instructions pertain to
program inputs between statement numbers 10 and 15, and they indi-
cate the flow of calculations within the program. Note that, when a
pulser is involved in the feedline, no input is required for its des-
cription (see statement number 35).

The computer inputs and outputs for this problem are shown
on the following page. The column labeled TRANS is the magnitude
of P_4 / Q_d. Due to the flexibility of the computer code, the transfer
function is not normalized. The reader may wish to normalize the
output, and, in this event, a suitable normalization factor would be
the characteristic line impedance, $Z_c = \rho_0 c_0$. The response magni-
tude for this configuration is presented in Figure D-2.

EXAMPLE PROBLEM NO. 1
```
    3   1   0   1   4
    1   4   2
    2
    3   2
 +.100000+01
 +.100000+01  +.500000+00  +.600000+02  +.500000+00  +.600000+02
 +.100000+01  +.461000+05  +.220000+01  +.460000-02  +.347000+02  -.298000+03
 +.300000+08  +.660000-01  +.000000+00  +.140000+01  +.199000+08  +.000000+00
 +.408000-05  +.000000+00  +.000000+00  +.224000+00  +.500000+02
 +.300000+02  +.400000+01
 +.120000+01  +.400000+01
```

OUTPUT

OMEGA-RAD/SEC	FREQ-HZ	TRANS-P/K	NON-DIMENSIONAL TRANS-DB	PHASE ANGLE-DEG
6.3	1.0	1197.728	-23.99	-92.9
9.4	1.5	1809.636	-20.40	-93.2
12.6	2.0	2438.836	-17.81	-93.8
15.7	2.5	3091.948	-15.75	-94.5
18.8	3.0	3776.372	-14.01	-95.2
22.0	3.5	4500.573	-12.49	-96.1
25.1	4.0	5274.435	-11.11	-97.0
28.3	4.5	6109.728	-9.83	-98.0
31.4	5.0	7020.705	-8.63	-99.2
34.6	5.5	8024.905	-7.47	-100.4
37.7	6.0	9144.224	-6.33	-101.9
40.8	6.5	10406.364	-5.21	-103.5
44.0	7.0	11846.773	-4.08	-105.3
47.1	7.5	13511.200	-2.94	-107.5
50.3	8.0	15458.904	-1.77	-110.1
53.4	8.5	17766.119	-.56	-113.2
56.5	9.0	20528.217	.69	-117.0
59.7	9.5	23855.386	2.00	-121.8
62.8	10.0	27847.643	3.34	-128.0
66.0	10.5	32515.468	4.69	-135.9
69.1	11.0	37590.935	5.95	-146.1
72.3	11.5	42239.563	6.96	-158.7
75.4	12.0	45045.750	7.52	-173.2
78.5	12.5	44918.265	7.49	-188.2
81.7	13.0	42195.753	6.95	-201.6
84.8	13.5	38205.405	6.09	-212.7
88.0	14.0	34073.188	5.09	-221.4
91.1	14.5	30335.271	4.08	-228.1
94.2	15.0	27134.204	3.12	-233.3
97.4	15.5	24444.038	2.21	-237.5
100.5	16.0	22188.596	1.37	-240.8
103.7	16.5	20288.054	.59	-243.5
106.8	17.0	18673.392	-.13	-245.7
110.0	17.5	17288.818	-.80	-247.6
113.1	18.0	16090.349	-1.42	-249.3
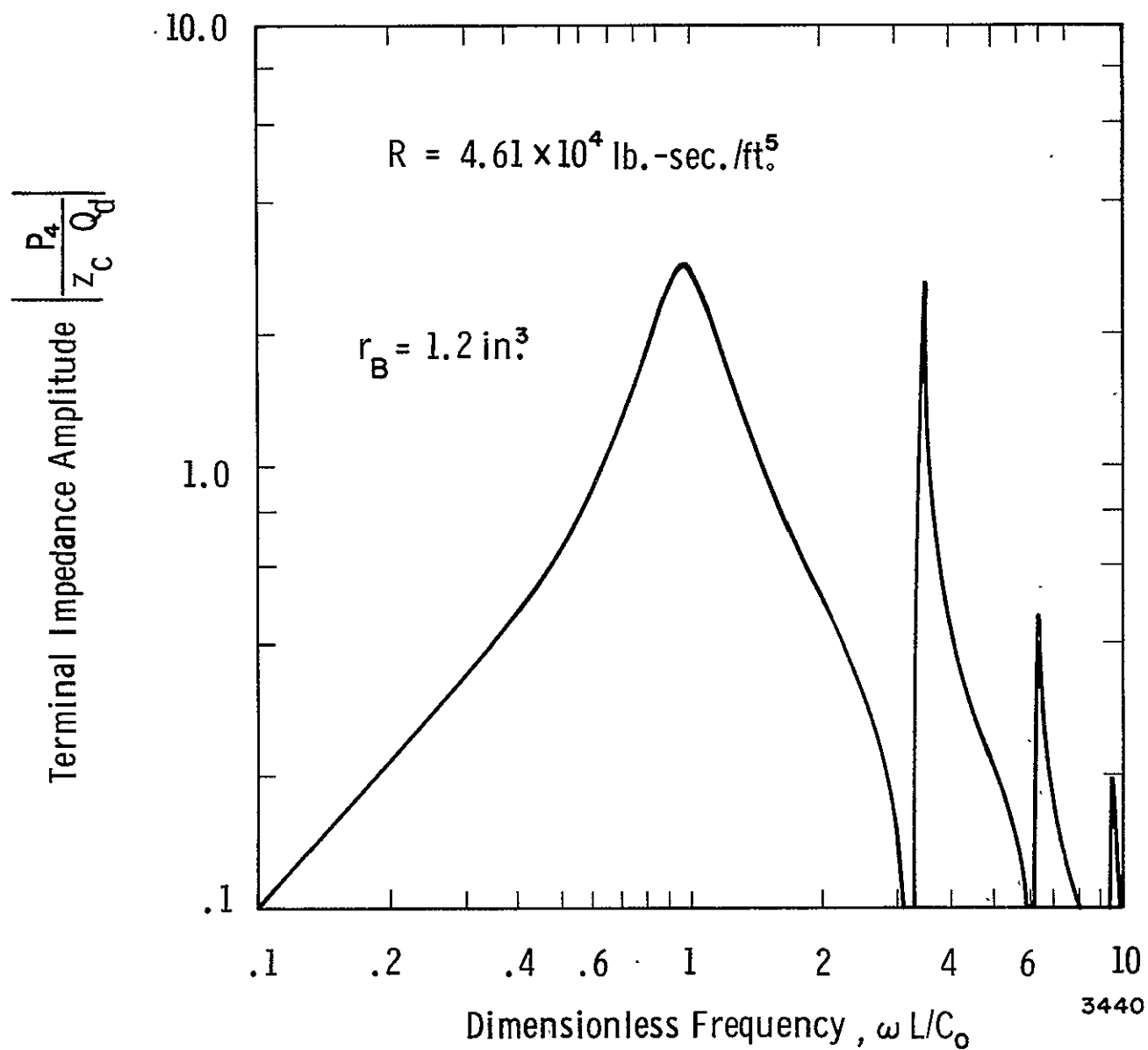
Figure D-2. Frequency Response For The Feedline In
Example Problem No. 1

Problem No. 2:

In this example, the feedline configuration consists of a large cavitation bubble situated in the line midway between the fuel tank outlet and the terminal impedance, R. As shown in Figure D-3, the entire line is acted upon by a structural velocity, $V_\ell(s)$. For analysis purposes, it is assumed that bubble acceleration effects are negligible, and that the bubble diameter is small compared to the total line length, $L_1 + L_3$. Proceeding as in Problem No. 1 with the assumption of zero tank exit pressure perturbation, the following system equation is obtained:

$$\begin{bmatrix} P_4 \\ P_4/R \end{bmatrix} = \underline{D}_3 \underline{D}_2 \underline{D}_1 \begin{bmatrix} 0 \\ Q_1 \end{bmatrix} - V_\ell(s) \begin{bmatrix} \underline{D}_3 \underline{D}_2 \underline{C}_1 + \underline{C}_3 \end{bmatrix} \qquad (D.2)$$

Note that in this and the preceding example, the number of line components is the same. However, the present configuration results in a more complex functional representation of matrix $\underline{B}$:

$$\underline{B} = \underline{D}_3 \underline{D}_2 \underline{C}_1 + \underline{C}_3 = \underline{B}_1 + \underline{B}_2 \qquad (D.3)$$

The following deductions can be made.

(1) NELM = 3   The number of elements in the line.

(2) JBNUM = 2   The number of B_i's that must be summed to form B.

(3) JTERM(1) = 3   The number of matrices that comprise
     JTERM(2) = 1 $\underline{B}_1$ and $\underline{B}_2$, respectively.

(4) K(1,1) = 3   Two-dimensional integer array desig-
     K(1,2) = 2   nating the ordered subscripts of the
     K(1,3) = 1   matrices that comprise $\underline{B}_1$ and $\underline{B}_2$.
     K(2,1) = 3

(5) ITYPE(1) = 5   Integers describing the type of compo-
     ITYPE(2) = 2   nent located in the Jth component
     ITYPE(3) = 5   position.
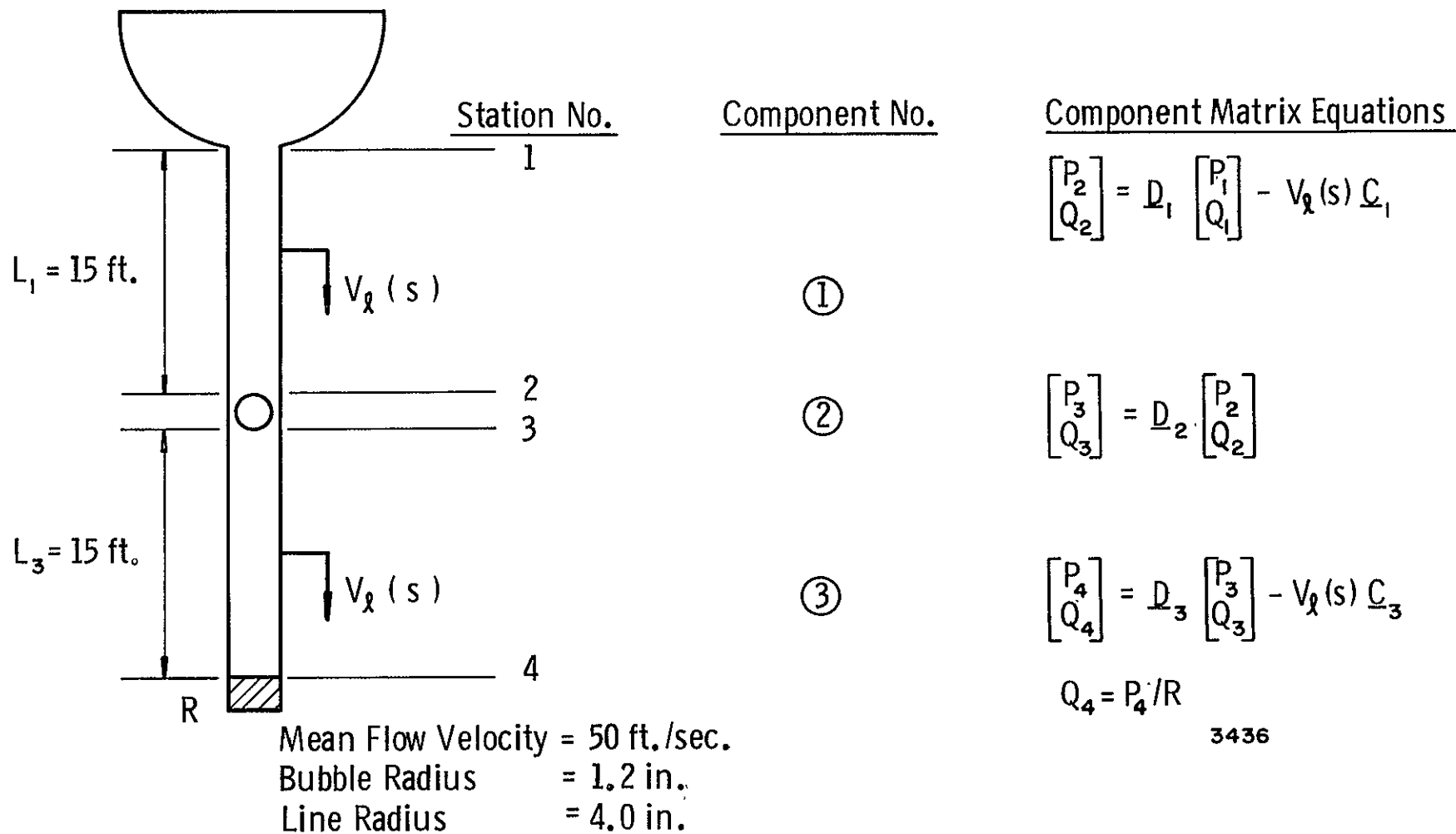
Figure D-3. Line Model For Example Problem No. 2

(6) BSIGN (1) = +1.0   The algebraic sign preceding the
     BSIGN (2) = +1.0   submatrices, $\underline{B}_1$.

(7) SIGN = -1.0   The algebraic sign preceding the
                         excitation, V_ℓ.

The complete input package, followed by the program output is
shown on the following page. The transfer function, which is the
ratio of P_4 and V_ℓ, may be normalized with respect to the pro-
duct of the acoustic impedance, Z_c, and the line cross-sectional
area, A, as shown in the response plot of Figure D-4. Note that,
in this example, both line segments have the same cross-sectional
area; however, this is not a prerequisite.

<u>INPUT</u>

EXAMPLE PROBLEM NO. 2
```
  3  2  0  1  5
  5  2  5
  3  0
  3  2  1
  3
 +.100000+01 +.100000+01
 +.100000+01 +.500000+00 +.600000+02 +.500000+00 +.600000+02
 -.100000+01 +.461000+05 +.220000+01 +.460000-02 +.347000+02 -.298000+03
 +.300000+08 +.660000-01 +.000000+00 +.140000+01 +.199000+08 +.000000+00
 +.408000-05 +.000000+00 +.000000+00 +.224000+00 +.500000+02
 +.150000+02 +.400000+01
 +.120000+01 +.400000+01
 +.150000+02 +.400000+01
```

<u>OUTPUT</u>

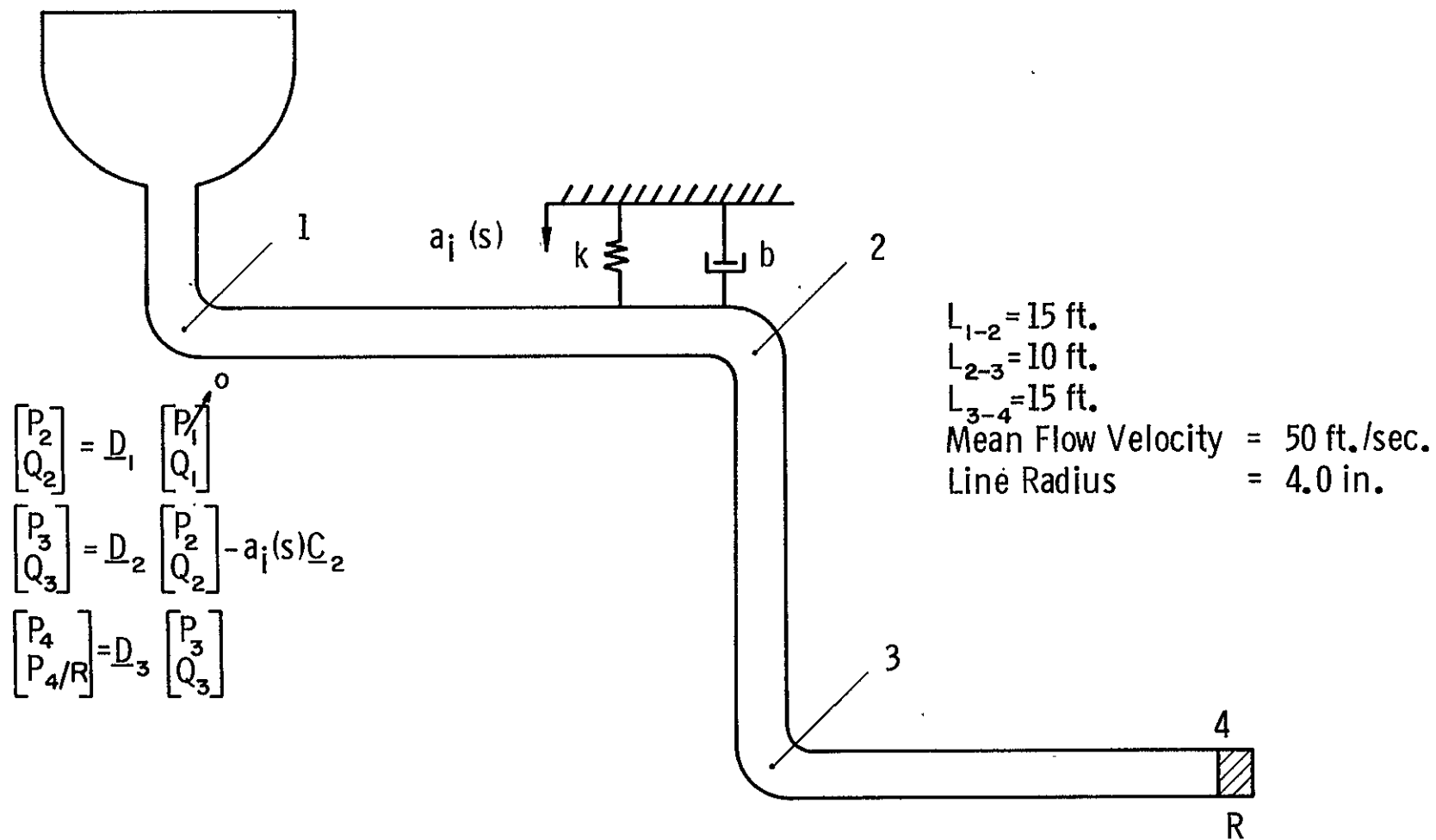| OMEGA-RAD/SEC	FREQ-HZ	TRANS-P/K	NON-DIMENSIONAL TRANS-DB	PHASE ANGLE-DEG
6.3	1.0	416.682	-24.02	-272.8
9.4	1.5	626.900	-20.47	-273.2
12.6	2.0	839.826	-17.93	-273.7
15.7	2.5	1056.454	-15.94	-274.4
18.8	3.0	1277.856	-14.28	-275.1
22.0	3.5	1505.200	-12.86	-275.8
25.1	4.0	1739.787	-11.60	-276.6
28.3	4.5	1983.077	-10.47	-277.5
31.4	5.0	2236.741	-9.42	-278.3
34.6	5.5	2502.710	-8.44	-279.3
37.7	6.0	2783.243	-7.52	-280.3
40.8	6.5	3081.011	-6.64	-281.4
44.0	7.0	3399.212	-5.79	-282.5
47.1	7.5	3741.710	-4.95	-283.8
50.3	8.0	4113.225	-4.13	-285.1
53.4	8.5	4519.572	-3.31	-286.6
56.5	9.0	4967.987	-2.49	-288.3
59.7	9.5	5467.531	-1.66	-290.2
62.8	10.0	6029.613	-.81	-292.4
66.0	10.5	6668.586	.07	-294.9
69.1	11.0	7402.340	.97	-297.8
72.3	11.5	8252.522	1.92	-301.3
75.4	12.0	9243.426	2.90	-305.6
78.5	12.5	10397.067	3.93	-310.9
81.7	13.0	11718.694	4.96	-317.6
84.8	13.5	13161.998	5.97	-326.1
88.0	14.0	14564.733	6.85	-336.7
91.1	14.5	15588.090	7.44	-349.5
94.2	15.0	15803.520	7.56	-3.9
97.4	15.5	15024.751	7.12	-18.3
100.5	16.0	13518.973	6.21	-31.2
103.7	16.5	11747.600	4.99	-41.9
106.8	17.0	10038.740	3.62	-50.4
110.0	17.5	8528.551	2.20	-57.1
113.1	18.0	7239.188	.78	-62.5
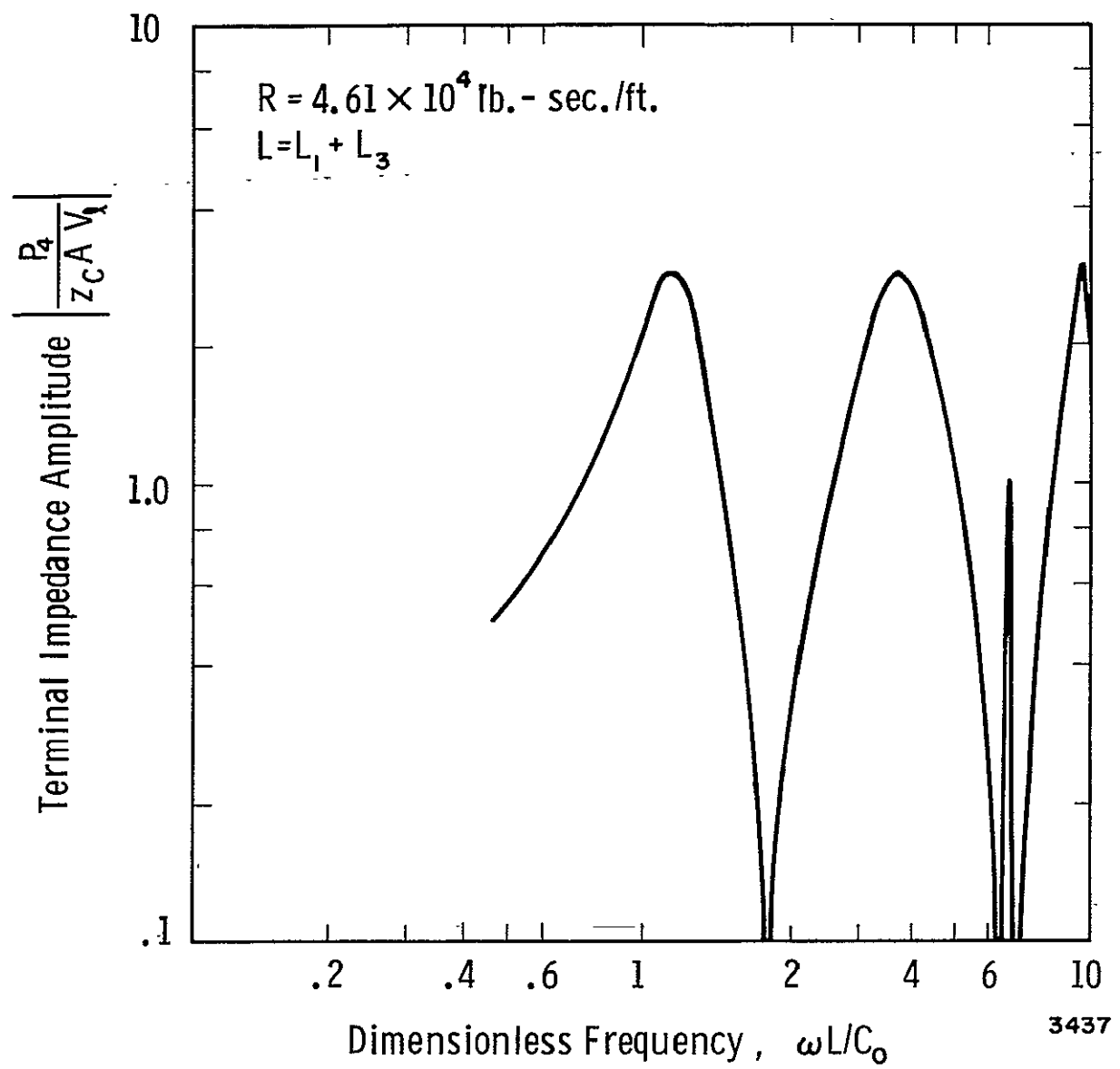
Figure D-4. Frequency Response Of The Feedline In Example
Problem No. 2

Problem No. 3:

Setup procedures for the feedline example shown in Figure D-5 parallel quite closely the procedures used in Problem No. 1. The basic difference is in the matrix representation of the center component, which reflects a structural acceleration input to the line through a viscoelastic mounting element. The functional form of the system equation,

$$
\begin{bmatrix} \dot{P}_4 \\ P_4/R \end{bmatrix} = \underline{D}_3\,\underline{D}_2\,\underline{D}_1 \begin{bmatrix} 0_1 \\ Q_1 \end{bmatrix} - a_1(s)\,\underline{D}_3\,\underline{C}_2 \tag{D.4}
$$

is virtually identical to Problem No. 1. Despite this apparent redundancy, this problem affords the opportunity to incorporate a previously unused subroutine, Subroutine EIGHT, into the analysis.

Since most vehicles employ lightly damped structures, a rather large amplification factor, Q, was assumed in order to size the spring constant and damping coefficient. By definition,

$$
\hat{Q} = \frac{1}{2\zeta} = \sqrt{\frac{km}{b}} \; .
$$

The mass term is taken to be the combined fluid mass contained in the horizontal limbs of the feedline. For the line dimensions shown in Figure D-5 and $\hat{Q} = 100$, k and b were taken to be 88×10^4 lb/ft and 45.2 lb-sec/ft, respectively.

For this problem,

(1) ITYPE(1) = 1;

ITYPE(2) = 8;

ITYPE(3) = 1;

(2) SIGN = -1.0

Input values for items (1), (2) and (5) in Problem No. 1 apply also to this example. The response magnitude, normalized with respect to LOX density and a characteristic length, is shown in Figure D-6.

<u>INPUT</u>

EXAMPLE PROBLEM NO. 3
```
   3   1   0   1   8
   1   8   1
   2
   3   2
 +.100000+01
 +.100000+01  +.500000+00  +.600000+02  +.500000+00  +.600000+02
 -.100000+01  +.461000+05  +.220000+01  +.000000+00  +.347000+02  -.298000+03
 +.300000+08  +.660000-01  +.000000+00  +.000000+00  +.199000+08  +.000000+00
 +.408000-05  +.000100+00  +.000000+00  +.000000+00  +.500000+02
 +.150000+02  +.400000+01
 +.100000+02  +.400000+01  +.452000+02  +.880000+06
 +.150000+02  +.400000+01
```

<u>OUTPUT</u>

OMEGA-RAD/SEC	FREQ-HZ	TRANS-P/K	NON-DIMENSIONAL TRANS-DB	PHASE ANGLE-DEG
6.3	1.0	22.146	29.60	-3.3
9.4	1.5	22.269	29.65	-3.9
12.6	2.0	22.453	29.72	-4.7
15.7	2.5	22.699	29.81	-5.6
18.8	3.0	23.007	29.93	-6.6
22.0	3.5	23.382	30.07	-7.7
25.1	4.0	23.827	30.24	-8.7
28.3	4.5	24.347	30.42	-9.9
31.4	5.0	24.951	30.64	-11.1
34.6	5.5	25.646	30.87	-12.4
37.7	6.0	26.442	31.14	-13.8
40.8	6.5	27.350	31.43	-15.3
44.0	7.0	28.384	31.76	-16.9
47.1	7.5	29.561	32.11	-18.6
50.3	8.0	30.900	32.49	-20.5
53.4	8.5	32.423	32.91	-22.6
56.5	9.0	34.155	33.36	-24.9
59.7	9.5	36.124	33.85	-27.5
62.8	10.0	38.361	34.37	-30.4
66.0	10.5	40.895	34.93	-33.7
69.1	11.0	43.748	35.51	-37.5
72.3	11.5	46.929	36.12	-41.8
75.4	12.0	50.410	36.74	-46.8
78.5	12.5	54.107	37.36	-52.6
81.7	13.0	57.839	37.94	-59.3
84.8	13.5	61.306	38.44	-66.9
88.0	14.0	64.087	38.83	-75.3
91.1	14.5	65.735	39.05	-84.3
94.2	15.0	65.928	39.08	-93.7
97.4	15.5	64.626	38.90	-102.8
100.5	16.0	62.096	38.56	-111.4
103.7	16.5	58.775	38.08	-119.2
106.8	17.0	55.105	37.52	-126.2
110.0	17.5	51.423	36.92	-132.2
113.1	18.0	47.941	36.31	-137.4

$$\begin{bmatrix} P_2 \\ Q_2 \end{bmatrix} = \underline{D}_1 \begin{bmatrix} P_1 \\ Q_1 \end{bmatrix}$$

$$\begin{bmatrix} P_3 \\ Q_3 \end{bmatrix} = \underline{D}_2 \begin{bmatrix} P_2 \\ Q_2 \end{bmatrix} - a_i(s)\underline{C}_2$$

$$\begin{bmatrix} P_4 \\ P_4/R \end{bmatrix} = \underline{D}_3 \begin{bmatrix} P_3 \\ Q_3 \end{bmatrix}$$

$L_{1-2} = 15$ ft.
$L_{2-3} = 10$ ft.
$L_{3-4} = 15$ ft.
Mean Flow Velocity = 50 ft./sec.
Line Radius = 4.0 in.

The line length from Station 1 to the tank exit is assumed to be negligible. Tank exit conditions exist at Station 1.

3448

Figure D-5. Line Model For Example Problem No. 3
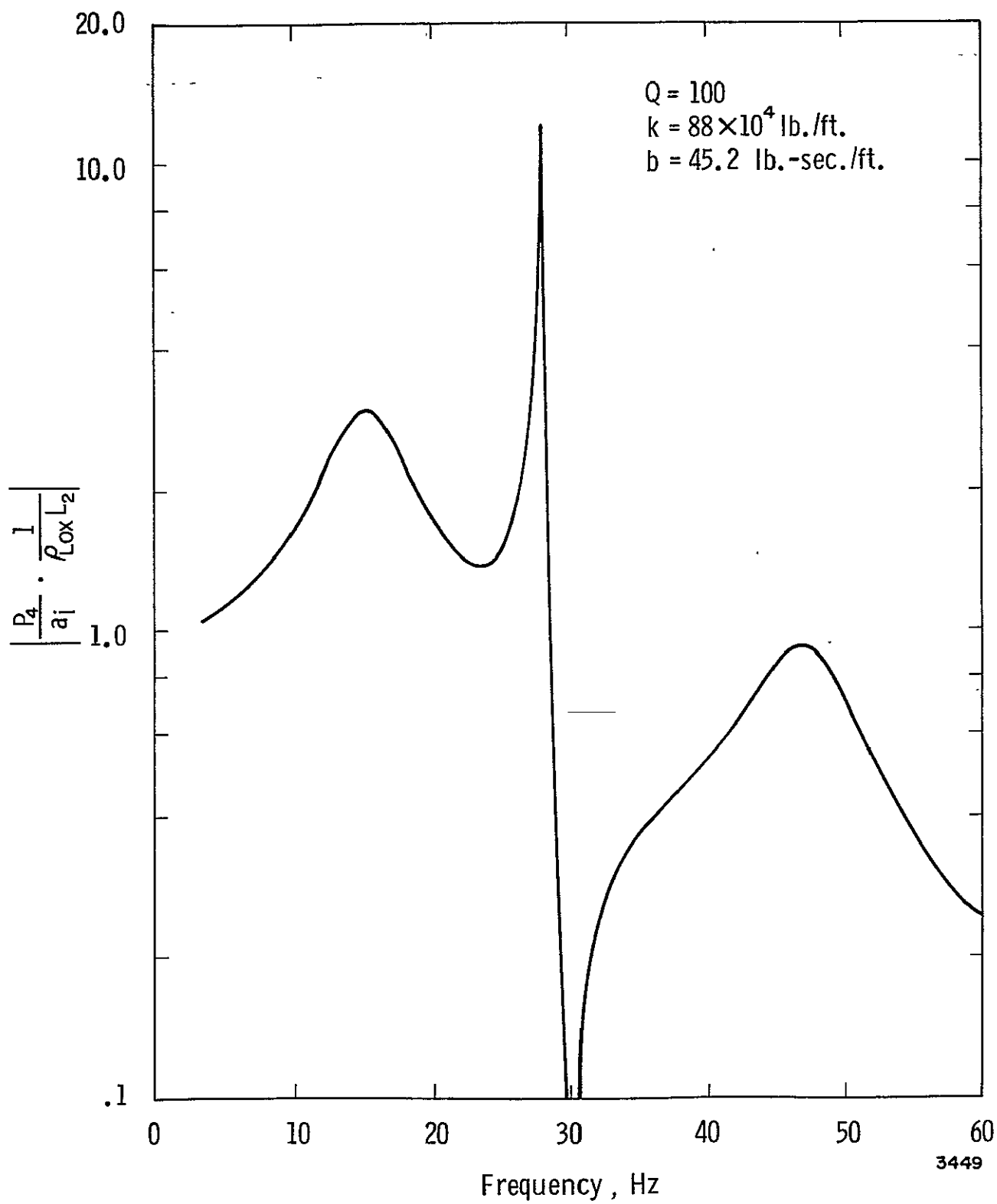
Figure D-6. Frequency Response Of The Feedline In Example
Problem No. 3

Problem No. 4:

In this fourth example, shown in Figure D-7, an externally excited segment of line is coupled at its extremities to the remainder of the line through two flexible bellows. This problem was discussed briefly in Section VI.

Initially, the user would set up the physical problem exactly as shown in Figure D-7. Note that the functional form of the bellows equations differs only in the algebraic sign of the excitation term, which reflects the fact that one bellows is compressed while the other is expanded. The response of the turbopump inlet pressure, P_6, in the presence of the velocity excitation, V_ℓ, is to be determined. The component equations are combined manually to produce the system equation:

$$\begin{bmatrix} P_6 \\ P_6/Z_t \end{bmatrix} = D_5 D_4 D_3 D_2 D_1 \begin{bmatrix} Z_i Q_1 \\ Q_1 \end{bmatrix} + V_\ell \left(D_5 C_4 - D_5 D_4 C_3 - D_5 D_4 D_3 C_2 \right) \tag{D.5}$$

Observe that this system equation is more complex than the system equations in the previous examples. The following information is immediately available from the system equation:

(1) NELM = 5

(2) JBNUM = 3; therefore JTERM (1) = 2

JTERM (2) = 3

JTERM (3) = 4

and

K (1,1) = 5

K (1,2) = 4

K (2,1) = 5

K (2,2) = 4

K (2,3) = 3

K (3,1) = 5

K (3,2) = 4

K (3,3) = 3

K (3,4) = 2
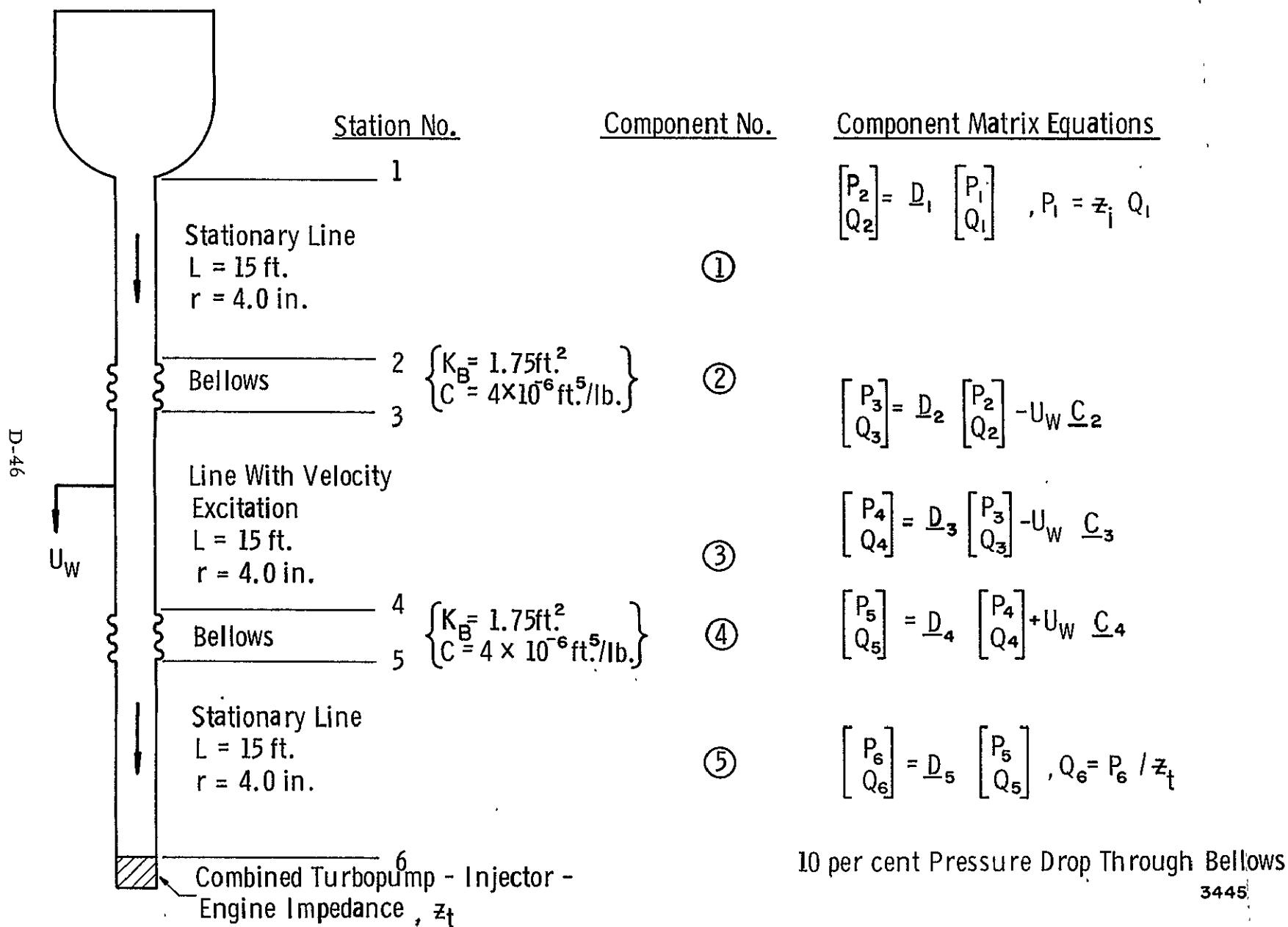
Figure D-7. Line Model for Example Problem No.

Station No.

1

Stationary Line
L = 15 ft.
r = 4.0 in.

2 $\left\{ \begin{array}{l} K_B = 1.75 ft.^2 \\ C = 4 \times 10^{-6} ft.^5/lb. \end{array} \right\}$

Bellows

3

Line With Velocity
Excitation
L = 15 ft.
r = 4.0 in.

4 $\left\{ \begin{array}{l} K_B = 1.75 ft.^2 \\ C = 4 \times 10^{-6} ft.^5/lb. \end{array} \right\}$

Bellows

5

Stationary Line
L = 15 ft.
r = 4.0 in.

6

Combined Turbopump – Injector –
Engine Impedance , z_t

Component No.

①

②

③

④

⑤

Component Matrix Equations

$$\begin{bmatrix} P_2 \\ Q_2 \end{bmatrix} = \underline{D}_1 \begin{bmatrix} P_1 \\ Q_1 \end{bmatrix} \quad , P_1 = z_i \, Q_1$$

$$\begin{bmatrix} P_3 \\ Q_3 \end{bmatrix} = \underline{D}_2 \begin{bmatrix} P_2 \\ Q_2 \end{bmatrix} - U_W \underline{C}_2$$

$$\begin{bmatrix} P_4 \\ Q_4 \end{bmatrix} = \underline{D}_3 \begin{bmatrix} P_3 \\ Q_3 \end{bmatrix} - U_W \underline{C}_3$$

$$\begin{bmatrix} P_5 \\ Q_5 \end{bmatrix} = \underline{D}_4 \begin{bmatrix} P_4 \\ Q_4 \end{bmatrix} + U_W \underline{C}_4$$

$$\begin{bmatrix} P_6 \\ Q_6 \end{bmatrix} = \underline{D}_5 \begin{bmatrix} P_5 \\ Q_5 \end{bmatrix} \quad , Q_6 = P_6 / z_t$$

10 per cent Pressure Drop Through Bellows

3445

(3) BSIGN (1) = +1.0

BSIGN (2) = -1.0

BSIGN (3) = -1.0

(4) ITYPE (1) = 1

ITYPE (2) = 7

ITYPE (3) = 5

ITYPE (4) = 7

ITYPE (5) = 1

(5) SIGN = +1.0

For computational purposes, it is assumed that $Z_i = 0$ and $Z_t = R$. In addition, there are no dissolved gases in the propellant (NGAS = 0). Wall elasticity is to be reflected in the speed of sound calculations (NELAST = 1). The entire input package is listed on the following page. At this point, the reader should make the correspondence between each numerical input quantity and the FORTRAN statement governing that input. The response magnitude, shown in the output listing, was normalized manually, and the resultant response is illustrated in Figure D-8.

INPUT

EXAMPLE PROBLEM NO. 4

```
 5    3    6    1    5
 1    7    6    2    4
 2    4    4
 5    4
 5    4    3
 5    4    3    2
+.100002+01  -.100000+01  -.100000+01
+.100000+03  +.500000+00  +.600000+02  +.500000+00  +.600000+02
+.100000+01  +.461000+05  +.220000+01  +.000000+00  +.347000+02  -.292000+03
+.300000+06  +.660400-01  +.000000+00  +.000000+00  +.199000+08  +.901000+00
+.408000-05  +.000000+00  +.000000+00  +.000000+00  +.500000+02
+.150000+02  +.460000+01
+.900000+00  +.400000-05  +.175000+01
+.150000+02  +.400000+01
+.900000+00  +.400000-05  +.175000+01
+.150000+02  +.400000+01
```

OUTPUT

| OMEGA-RAD/SEC	FREQ-HZ	TRANS-P/K	NON-DIMENSIONAL TRANS-DB	PHASE ANGLE-DEG
6.3	1.0	775.523	-18.62	-93.5
9.4	1.5	1214.547	-14.72	-94.2
12.6	2.0	1729.378	-11.65	-95.3
15.7	2.5	2376.194	-8.90	-96.9
18.8	3.0	3264.015	-6.14	-99.0
22.0	3.5	4644.356	-3.07	-102.3
25.1	4.0	7257.886	.80	-108.7
28.3	4.5	14214.916	6.64	-127.1
31.4	5.0	22266.064	10.54	-204.9
34.6	5.5	9176.650	2.84	-249.0
37.7	6.0	4807.562	-2.77	-259.6
40.8	6.5	2801.231	-7.47	-264.1
44.0	7.0	1554.485	-12.58	-266.6
47.1	7.5	611.527	-20.68	-267.2
50.3	8.0	215.462	-29.75	-97.4
53.4	8.5	1025.212	-16.20	-93.7
56.5	9.0	1903.656	-10.82	-94.3
59.7	9.5	2942.767	-7.04	-95.3
62.8	10.0	4281.699	-3.78	-96.4
66.0	10.5	6177.855	-.60	-97.8
69.1	11.0	9209.054	2.87	-99.7
72.3	11.5	15048.200	7.14	-102.8
75.4	12.0	31348.314	13.51	-110.5
78.5	12.5	130410.719	25.89	-179.5
81.7	13.0	38101.154	15.21	-261.0
84.8	13.5	20414.111	9.79	-269.4
88.0	14.0	14332.930	6.71	-272.6
91.1	14.5	11267.839	4.62	-274.5
94.2	15.0	9418.832	3.07	-275.9
97.4	15.5	8180.467	1.84	-276.9
100.5	16.0	7292.480	.84	-277.9
103.7	16.5	6624.534	.01	-278.7
106.8	17.0	6104.130	-.70	-279.5
110.0	17.5	5687.711	-1.31	-280.3
113.1	18.0	5347.520	-1.85	-281.0
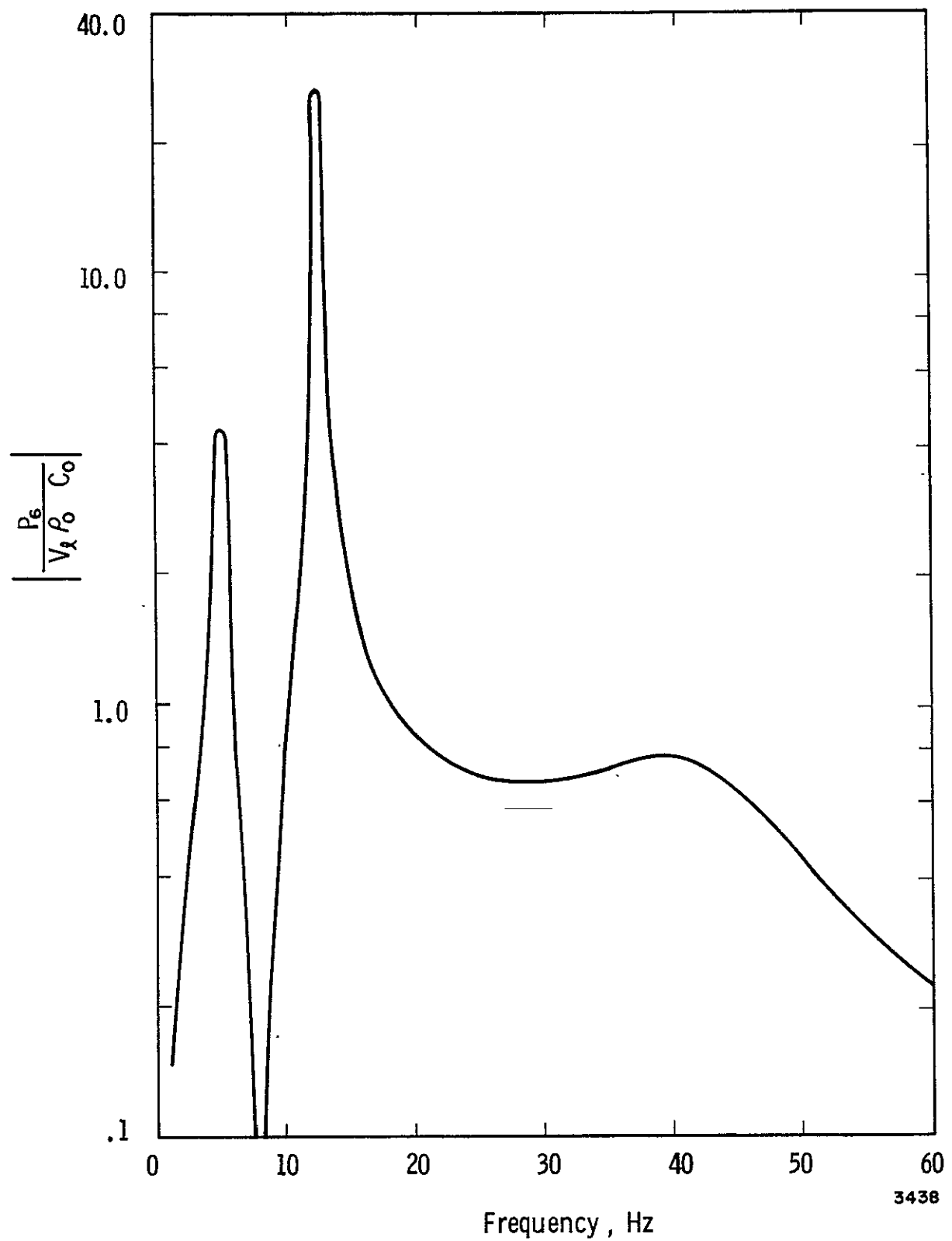
Figure D-8. Frequency Response Of the Feedline In
Example Problem No. 4

3438

Problem No. 5:

    As depicted in Figure D-9, the vertical segment of the pro-
pellant feedline is undergoing forced changes in line length. The
structural forces applied at Stations 2 and 3 produce measurable
velocities which, in general, differ in magnitude and/or phase.
Normally, these velocities can be related through a transfer func-
tion, $G(s)$. This function has been assigned a simple complex
variable form in the computer code: $G = G_1 + iG_2$. The user may
wish to alter this form to include a specific type of frequency
dependence based on experimental observations of velocity excited
lines. Such a program modification can easily be accomplished.

    The length changes imposed on the vertical line segment do
not influence the pressure-flow relationships of the horizontal seg-
ment.

    As in the preceding examples, the first step is to describe
each component by the appropriate matrix expression. The matrix
equations can then be combined to yield the overall line equation
which, for this example, is

$$\begin{bmatrix} P_3 \\ P_3/R \end{bmatrix} = \underline{D}_2\,\underline{D}_1 \begin{bmatrix} P_1 \\ Q_1 \end{bmatrix} - V_2\,\underline{C}_2 \qquad (D.6)$$

The effect of the structural velocity at Station 3 is contained in the
column matrix, $\underline{C}_2$. In computing the response of P_3 to changes
in line length, the perturbation pressure at the exit to the fuel tank,
P_1, has been assumed to be negligible.

    At this point, the reader should have no difficulty in con-
structing a data input package for this problem. For example, the
input listing may take the form shown below in which the function, G,
was taken to be

$$\frac{1}{\sqrt{2}} + i\,\frac{1}{\sqrt{2}} \;.$$

The computer input and corresponding output for this package, is
shown on the following page. The modulus of the transfer function
relating P_3 and V_2 is shown in Figure D-10

INPUT

EXAMPLE PROBLEM NO. 5
```
  2  1  0  1  9
  1  9
  1
  2
+.100000+01
+.100000+01 +.500000+00 +.600000+02 +.500000+00 +.600000+02
-.100000+01 +.461000+05 +.220000+01 +.000000+00 +.347000+02 -.258000+03
+.300000+08 +.660000-01 +.000000+00 +.000000+00 +.199000+08 +.000000+00
+.408000-05 +.000000+00 +.000000+00 +.000000+00 +.500000+02
+.100000+02 +.400000+01
+.300000+02 +.400000+01 +.707000+00 +.707000+00 +.280000+00
```

OUTPUT

OMEGA-RAD/SEC	FREQ-HZ	TRANS-P/K	NON-DIMENSIONAL TRANS-DB	PHASE ANGLE-DEG
6.3	1.0	17.367	-51.62	-157.2
9.4	1.5	17.631	-51.49	-157.4
12.6	2.0	17.888	-51.36	-157.9
15.7	2.5	18.150	-51.24	-158.5
18.8	3.0	18.424	-51.10	-159.1
22.0	3.5	18.716	-50.97	-159.9
25.1	4.0	19.030	-50.82	-160.8
28.3	4.5	19.369	-50.67	-161.7
31.4	5.0	19.738	-50.51	-162.8
34.6	5.5	20.140	-50.33	-163.9
37.7	6.0	20.579	-50.14	-165.2
40.8	6.5	21.060	-49.94	-166.6
44.0	7.0	21.587	-49.73	-168.1
47.1	7.5	22.167	-49.50	-169.7
50.3	8.0	22.806	-49.25	-171.6
53.4	8.5	23.509	-48.99	-173.6
56.5	9.0	24.282	-48.71	-175.9
59.7	9.5	25.134	-48.41	-178.5
62.8	10.0	26.066	-48.09	-181.4
66.0	10.5	27.083	-47.76	-184.6
69.1	11.0	28.178	-47.41	-188.4
72.3	11.5	29.336	-47.06	-192.7
75.4	12.0	30.525	-46.72	-197.7
78.5	12.5	31.681	-46.40	-203.4
81.7	13.0	32.703	-46.12	-210.0
84.8	13.5	33.442	-45.93	-217.5
88.0	14.0	33.714	-45.86	-225.8
91.1	14.5	33.335	-45.95	-234.9
94.2	15.0	32.193	-46.26	-244.4
97.4	15.5	30.314	-46.78	-254.1
100.5	16.0	27.863	-47.51	-263.4
103.7	16.5	25.087	-48.42	-272.2
106.8	17.0	22.228	-49.47	-280.4
110.0	17.5	19.466	-50.63	-287.8
113.1	18.0	16.906	-51.85	-294.7

$$\begin{bmatrix} P_2 \\ Q_2 \end{bmatrix} = \underline{D}_1 \begin{bmatrix} P_1 \\ Q_1 \end{bmatrix}$$

$$\begin{bmatrix} P_3 \\ Q_3 \end{bmatrix} = \underline{D}_2 \begin{bmatrix} P_2 \\ Q_2 \end{bmatrix} - V_2 \underline{C}_2$$

$$Q_3 = P_3/R$$

$L_{1-2} = 10$ ft.
$L_{2-3} = 30$ ft.
Mean Flow Velocity $= 50$ ft./sec.
Line Radius $\qquad = 4.0$ in.

V_2

2

1

3

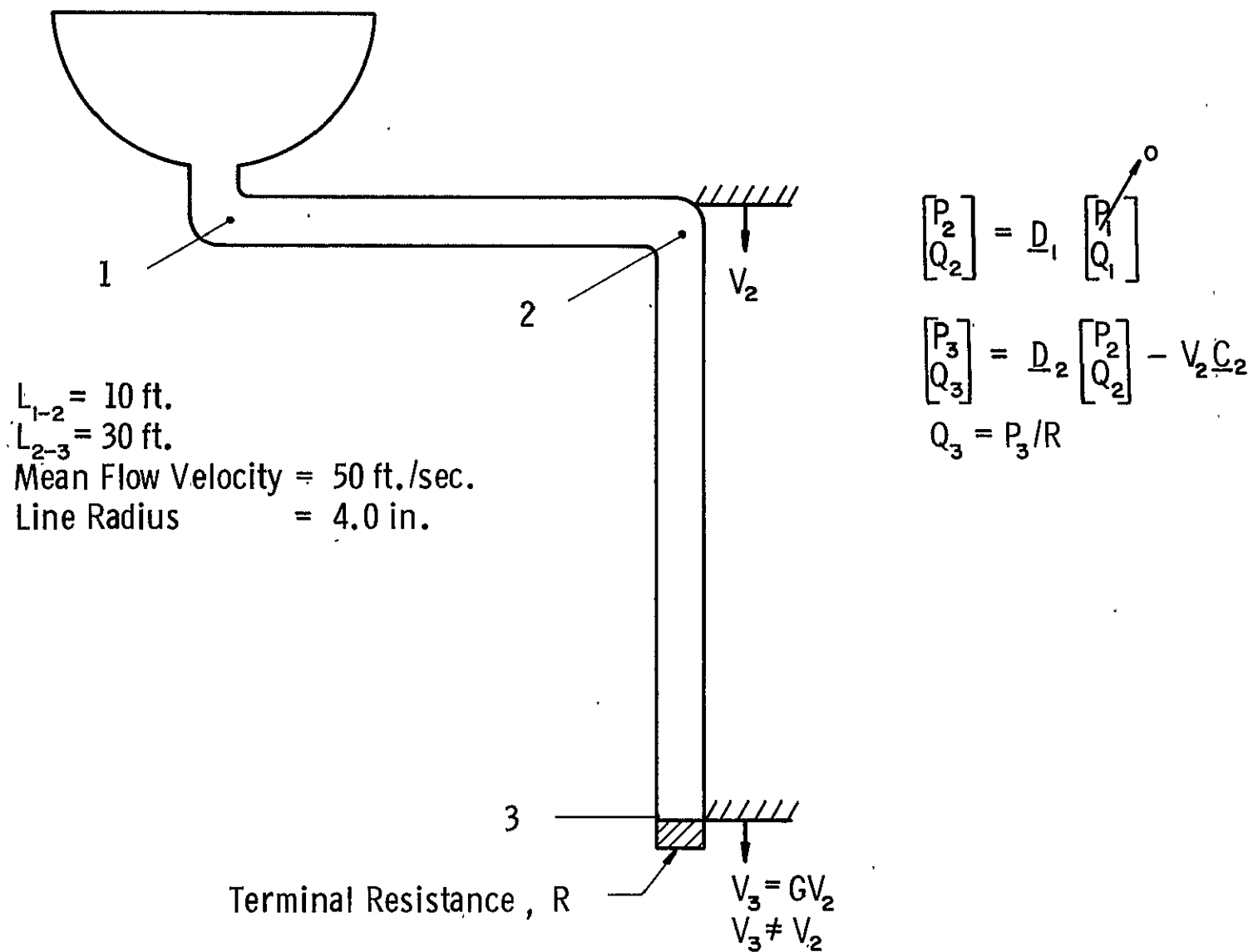Terminal Resistance , R

$V_3 = GV_2$
$V_3 \neq V_2$

3451

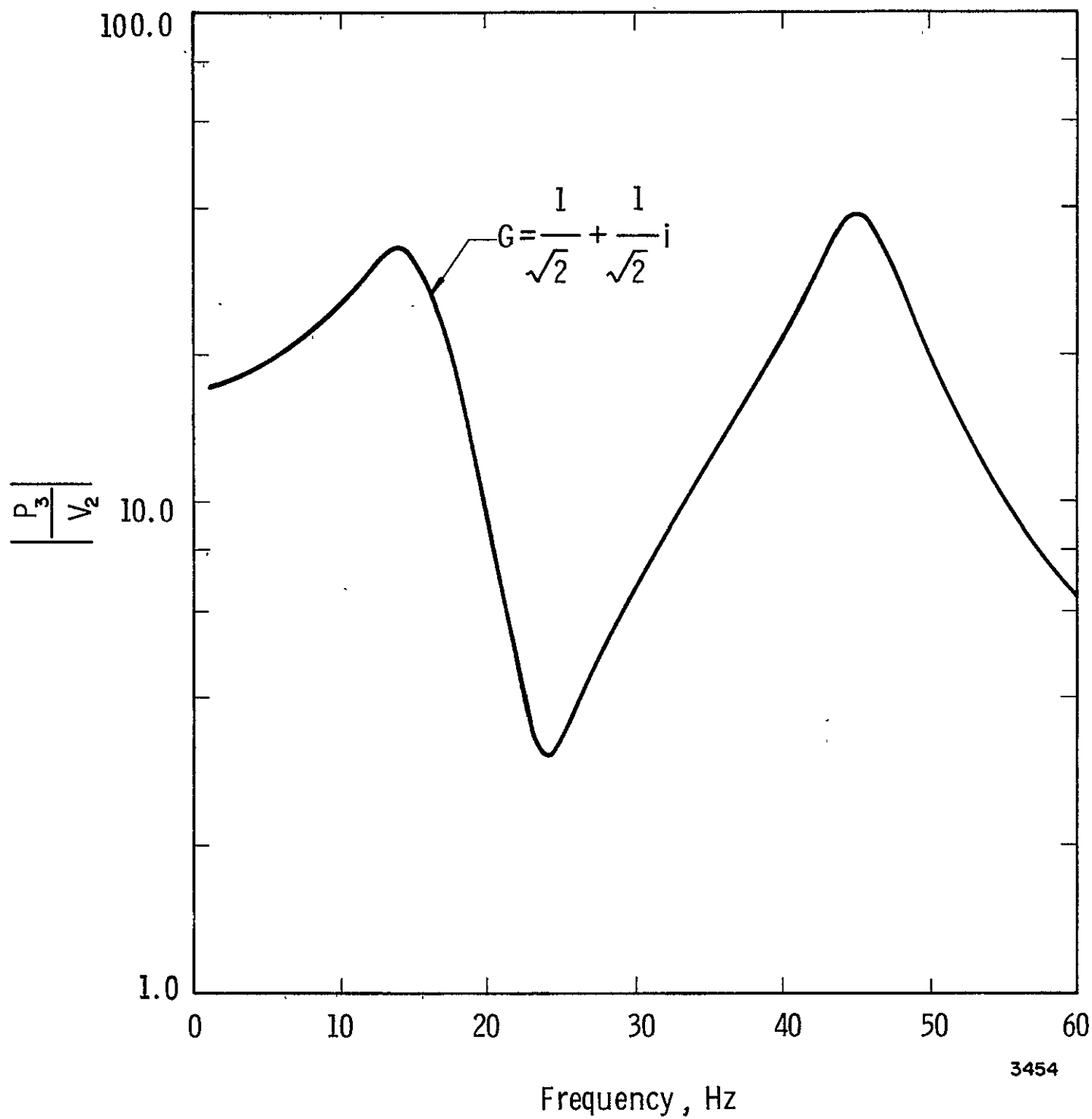Figure D-9.   Line Model For Example Problem No. 5

Figure D-10. Frequency Response Of The Feedline In Example
Problem No. 5

THE FOLLOWING PAGES ARE DUPLICATES OF

ILLUSTRATIONS APPEARING ELSEWHERE IN THIS

REPORT.　THEY HAVE BEEN REPRODUCED HERE BY

A DIFFERENT METHOD TO PROVIDE BETTER DETAIL